

UC San Diego

UC San Diego Electronic Theses and Dissertations

Title

Conversion of Metal Chelators to Selective and Potent Inhibitors of New Delhi Metallo-beta-lactamase

Permalink

<https://escholarship.org/uc/item/8xk949p6>

Author

Chen, Allie Yingyao

Publication Date

2020

Peer reviewed|Thesis/dissertation

UNIVERSITY OF CALIFORNIA SAN DIEGO

Conversion of Metal Chelators to Selective and Potent Inhibitors
of New Delhi Metallo-beta-lactamase

A dissertation submitted in partial satisfaction of the requirements for the degree Doctor
of Philosophy

in

Chemistry

by

Allie Yingyao Chen

Committee in charge:

Professor Seth M. Cohen, Chair
Professor Michael D. Burkart, Co-Chair
Professor Bradley S. Moore
Professor Joseph M. O'Connor
Professor Faik Akif Tezcan

2020

The Dissertation of Allie Yingyao Chen is approved, and it is acceptable in quality and form for publication on microfilm and electronically:

Co-Chair

Chair

University of California San Diego

2020

DEDICATION

To my family - thank you & I love you.

TABLE OF CONTENTS

Signature Page.....	iii
Dedication.....	iv
Table of Contents.....	v
List of Symbols and Abbreviations.....	ix
List of Figures.....	xiii
List of Schemes.....	xvi
List of Tables.....	xviii
Acknowledgements.....	xx
Vita.....	xxiii
Abstract of the Dissertation.....	xxiv
Chapter 1. Introduction.....	1
1.1 Targeting Metalloenzymes for Therapeutic Intervention.....	2
1.2 Fragment-Based Drug Discovery Approach for the Development of Metalloenzyme Inhibitors.....	7
1.3 Introduction to New Delhi Metallo- β -lactamase-1.....	11
1.4 Outlook.....	16
1.5 Acknowledgements.....	17
1.6 References.....	18
Chapter 2. Dipicolinic Acid Derivatives as Inhibitors of NDM-1.....	23
2.1 Introduction.....	24
2.2 Results and Discussion.....	26

2.2.1 MBP Library Screen and Selection of DPA as Lead Fragment.....	26
2.2.2 Design and Synthesis of DPA Derivatives (Sublibrary 1 – Sublibrary 3).....	30
2.2.3 In Vitro Activity of DPA Derivatives as Inhibitors of NDM-1.....	35
2.2.4 Investigation of Inhibitor Selectivity.....	43
2.2.5 Determination of Mode of Inhibition.....	45
2.2.6 Microdilution Broth Minimum Inhibitory Concentrations (MICs).....	57
2.3 Conclusion.....	60
2.4 Experimental.....	62
2.5 Acknowledgements.....	87
2.6 References.....	88
Chapter 3. Investigation of DPA Isosteres for the Inhibition of MBLs.....	93
3.1 Introduction.....	94
3.2 Results and Discussion.....	96
3.2.1 DPA Isostere Design and Synthesis (Sublibrary 4).....	96
3.2.2 Evaluation of DPA Isosteres Against MBLs.....	100
3.2.3 DPA Isostere pK_a Analysis	102
3.2.4 Mechanism of Isostere Inhibition.....	104
3.2.5 Derivatization of Isostere 49 (Sublibrary 5).....	108
3.3 Discussion.....	115
3.4 Conclusion.....	118
3.5 Experimental.....	119
3.6 Acknowledgements.....	141

3.7 References.....	142
Chapter 4. Iminodiacetic Acid as a Metal-binding Pharmacophore for New Delhi Metallo- β-lactamase Inhibitor Development.....	145
4.1 Introduction.....	146
4.2 Results and Discussion.....	148
4.2.1 IDA MBP Design and Verification.....	148
4.2.2 IDA Derivative Synthesis and Inhibitory Activity (Sublibrary 6 – Sublibrary 7)....	153
4.2.3 Thermal Shift Assay.....	157
4.2.4. Native State Electrospray Ionization Mass Spectrometry.....	159
4.3 Conclusion.....	165
4.4 Experimental.....	166
4.5 Acknowledgements.....	188
4.6 References.....	189
Chapter 5. Alternative DPA Libraries and the Future of NDM-1 Inhibitor Development.....	192
5.1 Introduction.....	193
5.2. <i>meta</i> -Substituted DPA Derivatives (Sublibrary 8).....	195
5.2.1. Synthesis and Evaluation of Sublibrary 8.....	197
5.2.2 Discussion.....	200
5.2.3. Experimental.....	201
5.3 Tetrazole DPA Derivatives (Sublibrary 9).....	213
5.3.1 Synthesis and Evaluation of Sublibrary 9.....	214

5.3.2 Discussion.....	216
5.3.3 Experimental.....	217
5.4 Alternative Isosteres for Inhibitor Development (Sublibrary 10).....	220
5.4.1 Synthesis and Evaluation of Sublibrary 10.....	222
5.4.2. Discussion.....	225
5.4.3. Experimental.....	226
5.5 Synthesis and Evaluation of Aspergillomarasmine A.....	231
5.5.1. Synthesis and Evaluation of AMA.....	233
5.5.2 Discussion.....	235
5.5.3 Experimental.....	236
5.6 Outlook and Perspective on Future NDM-1 Inhibitor Development.....	242
5.7 References.....	246

LIST OF SYMBOLS AND ABBREVIATIONS

AMA	Aspergillomarasmine A
ATP	Adenosine Triphosphate
BBL	B β -Lactamase
BLA	Biologic License Application
Bn	Benzyl
C	Celsius
CDC	Centers for Disease Control and Prevention
CHAPS	3-((3-Cholamidopropyl) Dimethylammonio)-1-propanesulfonate
CuAAC	Copper-catalyzed Azide-alkyne Cycloaddition
DCC	<i>N,N'</i> -Dicyclohexylcarbodiimide
DCU	Dicyclohexylurea
DMF	<i>N,N'</i> -Dimethylformamide
DMSO	Dimethyl Sulfoxide
DPA	Dipicolinic Acid
EDC	1-Ethyl-3-(3-dimethylaminopropyl)carbodiimide
EDTA	Ethylenediaminetetraacetic Acid
EPR	Electron Paramagnetic Resonance
ESBL	Extended Spectrum β -Lactamases
EtOAc	Ethyl Acetate
FBDD	Fragment-based Drug Discovery
FDA	Food and Drug Administration

GHz	Gigahertz
Glo1	Glyoxalase 1
h	Hour
hCAII	Human Carbonic Anhydrase II
HDAC	Histone Deacetylase
HEPES	4-(2-Hydroxyethyl)-1-piperazineethanesulfonic Acid
HOBT	Hydroxybenzotriazole
HPLC	High-performance Liquid Chromatography
HTS	High-throughput Screening
IDA	Iminodiacetic acid
IMP	IMiPenemase
K	Kelvin
kHz	Kilohertz
LasB	<i>Pseudomonas Aeruginosa</i> Elastase
LE	Ligand Efficiency
LLE	Lipophilic Ligand Efficiency
MBI	Metal-binding Isostere
MBL	Metallo- β -Lactamase
MBP	Metal-binding Pharmacophore
MeOH	Methanol
MHz	Megahertz
MIC	Minimum Inhibitory Concentration

min	Minute
mL	Milliliter
μM	Micromolar
mM	Millimolar
mmol	Millimoles
MMP	Matrix Metalloproteinases
MOE	Molecular Operating Environment
MS	Mass Spectrometry
μs	Microsecond
ms	Miliseconds
mW	Milliwatts
NDM	New Delhi Metallo- β -lactamase
ng	Nanogram
nm	Nanometer
nM	Nanomolar
NMEs	New Molecular Entities
NMR	Nuclear Magnetic Resonance
NSA	([1,1'-Biphenyl]-4-ylsulfonyl)-D-phenylalanine
PBP	Penicillin-binding Protein
PDB	Protein Data Bank
PK	Pharmacokinetic
pM	Picomolar

ppm	Parts Per Million
RO3	Rule of Three
s	Second
SAR	Structure-activity Relationship
SBL	Serine- β -Lactamase
TEA	Triethyl Amine
TFA	Trifluoroacetic Acid
THF	Tetrahydrofuran
TLC	Thin Layer Chromatography
VIM	Verona Integron-encoded Metallo- β -lactamase
X-Phos	2-Dicyclohexylphosphino-2',4',6'-triisopropylbiphenyl

LIST OF FIGURES

Figure 1-1. FDA-approved metalloenzyme inhibitors between 2013 and 2017 with MBP motifs shown in red.....	6
Figure 1-2. Representative compounds in the MBP fragment library.....	10
Figure 1-3. <i>Top:</i> NDM-1 hydrolysis of β -lactam drug; <i>Bottom:</i> Structure of NDM-1 with the di-Zn(II) active site, L3, L5, and L10 labeled (adapted from PDB 4EYB). Figure generated via Pymol.....	13
Figure 1-4. Examples of current NDM-1 inhibitors reported in literature.....	15
Figure 2-1. Z' Factor determination using the substrate chromacef. Absorbance values for positive (■) controls and negative (●) controls. Solid lines are the mean values for each set, dashed lines are fixed at $\pm 3\sigma$	28
Figure 2-2. Chemical illustration of the predicted mode of binding of DPA with the di-Zn(II) active site with L3 and L10 outlined. Zn(II) and hydroxide ion are represented as orange and blue spheres, respectively.....	31
Figure 2-3. Example IC ₅₀ determinations for DPA (●, 410 nM) and 36 (■, 80 nM) utilizing fluorocillin substrate.....	41
Figure 2-4. IC ₅₀ variation with excess exogenous Zn(II). IC ₅₀ values for inhibition of NDM-1 by DPA (●, 3 replicates), or 36 (▲, 4 replicates) were determined at varying concentrations of exogenous ZnSO ₄ using fluorocillin as the reporter substrate and NDM-1 (final concentration at 0.025 nM).....	41
Figure 2-5. 300 MHz ¹ H NMR titrations of di-Co(II) NDM-1 with (A) DPA and (B) 36 . Resonances assigned to Zn ₁ ligands (black squares), Zn ₂ ligands (gray squares) and a ternary complex formation (red squares) are marked.....	47
Figure 2-6. Control titrations. 300 MHz ¹ H NMR spectra of di-Co(II) NDM-1 titrated with (A) L-captopril and (B) EDTA.....	48
Figure 2-7. 300 MHz ¹ H NMR of various combinations of CoCl ₂ and the compounds under study in the absence of NDM-1.....	48
Figure 2-8. X-band EPR spectroscopy of di-Co(II) NDM-1 (black) and di-Co(II) NDM-1 with 1 equivalent of added DPA (blue) and 36 (red). Inset: Expansion of the low-field region of the perpendicular mode spectra.....	50

Figure 2-9. UV-vis spectroscopy of di-Co(II) NDM-1 (black lines) and di-Co(II) NDM-1 (300 μ M) with (A) EDTA and (B) L-captopril as control, and 1 – 2 equivalents of added (C) **DPA**, and (D) **36**.....52

Figure 2-10. (A) Control optical spectra of a buffered Co(II) solution, in the presence of the various inhibitors under study; (B) Full spectra for the titration of Co(II) with **36**.....53

Figure 2-11. Metal content of NDM-1 (8 μ M) after dialysis with various concentrations of EDTA, L-captopril, **DPA**, and **36** in 50 mM HEPES, pH 7.5, buffer.....54

Figure 2-12. (A) Relative intrinsic tryptophan fluorescence emission versus concentration of inhibitor; (B) Relative intrinsic tryptophan fluorescence emission versus concentration of **36**, L-captopril and EDTA. The concentration of NDM-1 was 2 μ M, L-tryptophan was 2 μ M and the buffer for both studies was 50 mM HEPES, pH 7.5.....56

Figure 2-13. HEK293 cells cultured in the presence of vehicle-only or **36** showed no statistical difference in cell viability at concentrations of **36** up to 400 μ M, the highest concentration used in MIC determinations. Much higher concentrations (4 mM) of **36** cause some cell toxicity that is statistically significant.....59

Figure 2-14. HEK293 cells cultured in the presence of 0.4 to 400 μ M **36** showed similar morphology to those grown with addition of a vehicle (DMSO) only control. Morphological changes typical of apoptosis were apparent with treatments of a high concentration (4 mM) of **36**.....59

Figure 3-1. **DPA** and Sublibrary 4 (compounds **48** – **57**) reported in this chapter.....97

Figure 3-2. The pK_a ionization graphs of selected inhibitors.....103

Figure 3-3. Zn(II) content of NDM-1 (8 μ M) upon incubation with increasing concentrations of captopril, **DPA**, and **48** – **51** (16 μ M – 128 μ M).....105

Figure 3-4. (A) UV-Vis spectrum of di-Co(II) NDM-1 with captopril and EDTA; (B) UV-Vis spectrum of di-Co(II) NDM-1 with **DPA** and isosteres **48** – **51**..107

Figure 3-5. *Top:* Inhibitor **49** complexed with IMP-1 (PDB 5HH4).¹⁶ Figure was rendered with Pymol. *Bottom:* Chemical representation of the predicted binding of **49** with the NDM-1 active site. Zn(II) ions are shown as orange spheres and bridging hydroxide is shown as a red sphere.....109

Figure 3-6. Zn(II) content of NDM-1 (8 μ M) upon incubation with increasing concentrations of **65b**, **65i**, and EDTA (16 μ M – 128 μ M).....114

Figure 4-1. NDM-1 inhibitors and hydrolyzed penicillin bearing the IDA motif.....147

Figure 4-2. Control spectra of A) NDM-1 and B) NDM-1 incubated with DPA	160
Figure 4-3. Control spectra of A) VIM-2 and B) VIM-2 incubated with DPA	163
Figure 4-4. Spectra of NDM-1 incubated with A) 77 , B) 89d , C) 89d , D) 89e , and E) 89f	162
Figure 4-5. Control spectra of A) VIM-2 and B) VIM-2 incubated with DPA	163
Figure 4-6. Spectra of VIM-2 incubated with A) 77 , B) 89d , C) 89d , D) 89e , and E) 89f	165
Figure 5-1. The NDM active site pockets available for inhibitor development (standard BBL numbering).....	194
Figure 5-2. Cyclic boronate inhibitors previously reported against MBLs.....	196
Figure 5-3. Substitution of the phenyl ring with a tetrazole heterocycle for NDM-1 inhibitor development.....	213
Figure 5-4. Derivatives of 51 that were screened against NDM-1.....	220
Figure 5-5. MBI library screened against NDM-1 in an attempt to discover new isostere leads.....	221
Figure 5-6. Percent Inhibition of MBIs and Sublibrary 10 at 100 μ M against NDM-1 with substrate meropenem. ^[a]	224
Figure 5-7. Predicted AMA chelation (<i>left</i>) in comparison with known EDTA chelation (<i>right</i>).....	231

LIST OF SCHEMES

Scheme 2-1. Synthetic route for Sublibrary 1 (compounds **3 – 20**). Reagents and conditions: (a) MeOH, H₂SO₄ (cat.), 75 °C, 24 h, 100%; (b) MeOH, KOH, 0 °C, 4 h, 81%; (c) EDC, HOBT, corresponding amine H₂NR, 18 h; then 3:1 1M NaOH: THF, 30 min – 1 h, 4M HCl, 34 – 87%.....33

Scheme 2-2. Synthetic route for Sublibrary 2 (compounds **22 – 30**). Reagents and conditions: (a) 10:1 1M NaOH: THF, 70 °C, 3 h, 80%; (b) corresponding amine, H₂O, microwave at 160 °C, 30 min, 10 – 80%.....33

Scheme 2-3. Synthetic route for Sublibrary 3 (compounds **33 – 47**). Reagents and conditions: (a) MeOH, H₂SO₄ (cat.), 75 °C, 24 h, 88%; (b) tetrabutylammonium bromide, P₄O₁₀, toluene, 100 °C, 3 h, 92%; (c) Pd(PPh₃)₄, K₃PO₄/CH₃CO₂K, 1,4-dioxane, 85 °C, overnight; then 4:1 1M NaOH:THF, H₂SO₄, 22 – 84%.....34

Scheme 3-1. Synthesis of isosteres **48, 51, 56, and 57**. Reagents and conditions: (a) Pd₂(dba)₃, Pd(dppf)Cl₂, diethylphosphate, triethylamine, toluene, 90 °C, 20 h; then 6M HCl, 100 °C, 20 h; *two steps* 19%; (b) CuCN, pyridine, 116 °C, 4 h, 21%; (c) NaN₃, NH₄Cl, DMF, 130 °C, 20 h; then 2M HCl, 25 °C.....98

Scheme 3-2. Synthesis of isosteres **49, 50, 52, 53, and 55**. Reagents and conditions: (a) PBr₃, CHCl₃, 0 °C, 3 h, 70%; (b) P(OEt)₃, toluene, 140 °C, 2 h, 80%; (c) 6M HCl, 100 °C, 27 h, 98%; (d) KCN, THF, 50 °C, 19 h, 49%; (e) 12M HCl, 100 °C, 12 h, then 1M NaOH, 60 °C, 6 h, 30%; (f) Na₂SO₃, H₂O, then 4M HCl, 100 °C, 16 h.....99

Scheme 3-3. Synthesis of isostere **54**. Reagents and conditions: (a) Methanesulfonyl chloride, triethylamine, CH₂Cl₂, 0 °C, 16 h; then 1M NaOH:THF, r.t., 16 h; *two steps* 12.4%.....99

Scheme 3-4. Synthesis of Sublibrary 5 (compounds **65a – 65m**). Reagents and conditions: (a) MeOH, H₂SO₄ (cat.), 70 °C, overnight, 60%; (b) P₄O₁₀, tetrabutylammonium bromide, toluene, 100 °C, 3 h, 75%; (c) NaBH₄, MeOH/CH₂Cl₂, 0 °C, 1 h, 80%; (d) PBr₃, CHCl₃, 0 °C, 1 h, 68%; (e) P(OEt)₃, toluene.....111

Scheme 4-1. Synthesis of **79a** and **79b**. Reagents and conditions: *tert*-butyl acrylate, TEA, EtOH, 65 °C, 16 h, 43 – 90%; (b) TFA:CH₂Cl₂, 25 °C, 16 h, ~99%.....152

Scheme 4-2. Synthesis of **IDA** inhibitors **81** and **83**. Reagents and conditions: (a) diethyl (2-bromoethyl)phosphonate, K₂CO₃, KI, ACN, 82 °C, 16 h, 40%; (b) HCl, 100 °C, 16 h, 99%; (c) 2-bromocetonitrile, K₂CO₃, KI, ACN, 25 °C, 16 h, 74%; (d) NaN₃, NH₄Cl, DMF, 110 °C, 16 h; then 1:1:1 MeOH:THF:1M NaOH, 60 °C, 16 h; *two steps* 19%....152

Scheme 4-3. Synthesis of **85a – 85d**. Reagents and conditions: (a) *tert*-butyl 2-bromoacetate, TEA, DMF, 0 – 25 °C, 16 h, 40 – 54%; (b) TFA, CH₂Cl₂, 25 °C, 16 h, ~99%.....152

Scheme 4-4. Synthesis of **IDA** inhibitors Sublibrary 6 (compounds **87a – 87n**) and Sublibrary 7 (compounds **89a – 89h**). Reagents and conditions: (a) *tert*-butyl 2-bromoacetate, KHCO₃, THF, 25 °C, 16 h, 25 – 98%; (b) TFA, CH₂Cl₂, 25 °C, 16 h or (c) MeOH:THF:1M NaOH, 100 °C, 16 h, 29 – 100%.....153

Scheme 5-1. Synthetic procedures for Sublibrary 8 (compounds **95a – 95j**). Reagents and conditions: (a) di-*tert*-butyl dicarbonate, CH₂Cl₂, 25 °C, 3 h, 36%; (b) KMnO₄, H₂O, 70 – 90 °C, 10 h; then (c) MeOH, H₂SO₄ (cat.), 70 °C, 24 h; *two steps* 48%; (d) Pd₂(dba)₃ (cat.), Cs₂CO₃.....198

Scheme 5-2. Synthetic route for compounds in Sublibrary 9 (compounds **97a – 97g**). Reagents and conditions: (a) **96** (cat.), MeOH, corresponding alkyne, 25 °C, 16 h; (b) 3:1 1M NaOH:THF, 25 °C, 16 h; then 4M HCl to pH 4; *two steps*: 48 – 79%.....214

Scheme 5-3. Synthetic procedures for Sublibrary 10 (compounds **51a – 51d**). Reagents and conditions: (a) Pd(Ph₃)₄, ZnCN₂, DMF, 80 °C, 16 h, 51 – 84%; (b) NaN₃, NH₄Cl, 120 °C, 2.5 – 16 h, then 3:1 mL 1M NaOH:THF, 25 °C, 16 h; *two steps*: 32 – 92%.....223

Scheme 5-4. Synthesis of LLL-AMA according to reported procedures.¹⁵ Reagents and conditions: (a) MsCl, TEA, THF, 65 °C, 46 h, 76%; (b) TFA, 0°C, 30 min; *o*-NsCl, 25 °C, 24 h, 70%; (c) L-aspartic acid di-*tert*-butyl ester, THF, 25 °C, 16 h, 72%; (d) PhSH, DIPEA, ACN, 25 °C, 2.5 h, 83%.....234

LIST OF TABLES

Table 1-1. List of metalloenzymes targeted for therapeutic intervention.....	5
Table 2-1. List of MBP primary screening hits against MBLs. Percent inhibition values were obtained via monitoring the MBL-catalyzed hydrolysis of substrate chromacef....	29
Table 2-2. Inhibitory activity of Sublibrary 1 (compounds 3 – 20) against NDM-1. Inhibition values were obtained via monitoring the NDM-1-catalyzed hydrolysis of substrate chromacef.....	38
Table 2-3. Inhibitory activity of Sublibrary 2 (compounds 21 – 30) against NDM-1. Inhibition values were obtained via monitoring the NDM-1-catalyzed hydrolysis of substrate chromacef.....	39
Table 2-4. Inhibitory activity of Sublibrary 3 (compounds 33 – 47) against NDM-1. Inhibition values were obtained via monitoring the NDM-1-catalyzed hydrolysis of substrate chromacef and fluorocillin (bold typeface).....	40
Table 2-5. Inhibitory activity of DPA and 36 against B1 MBLs. Inhibition values were obtained via monitoring the MBL-catalyzed hydrolysis of substrate fluorocillin.....	44
Table 2-6. Percent inhibition of 36 (at 10 μ M) against Zn(II)-metalloenzymes.....	44
Table 2-7. Microdilution broth MICs of clinical <i>E. coli</i> isolates expressing <i>bla</i> _{NDM-1} . All strains possess <i>bla</i> _{CTX-M-15} and <i>bla</i> _{CMY-2} except for <i>E. coli</i> Ah8.74 which possesses only <i>bla</i> _{NDM-1}	58
Table 2-8. Microdilution broth MICs of clinical <i>K. pneumoniae</i> isolates expressing <i>bla</i> _{NDM-1} . Strains Cm1.62 and Cm1.63 possess <i>bla</i> _{CTX-M-15} and <i>bla</i> _{CMY-2} . Strain Pd1.48 possesses <i>bla</i> _{SHV-12} and <i>bla</i> _{CTX-M-15} . Strains Pd1.49, Pd1.50, Pd1.53, Pd1.54, and Pd1.55 possess <i>bla</i> _{CTX-M-15}	58
Table 3-1. Inhibitory activity of DPA isosteres against NDM-1. Inhibition values were obtained via monitoring the NDM-1-catalyzed hydrolysis of substrate meropenem. ^[a]	101
Table 3-2. Inhibitory activity of DPA isosteres against B1 MBLs. Inhibition values were obtained via monitoring the MBL-catalyzed hydrolysis of substrate fluorocillin. ^[a]	101
Table 3-3. The <i>pK</i> _a values of selected inhibitors in this study. ^[a]	102

Table 3-4. Inhibitory activity of Sublibrary 5 (compounds 65a – 65m) against NDM-1. Inhibition values were obtained via monitoring the MBL-catalyzed hydrolysis of substrate meropenem. ^[a]	113
Table 3-5. Inhibitory activity of Sublibrary 5 (compounds 65a – 65m) against IMP-1. Inhibition values were obtained via monitoring the MBL-catalyzed hydrolysis of substrate meropenem. ^[a]	114
Table 4-1. Percent inhibition of MBPs and IDA derivatives (at 200 μ M) against NDM-1. Percent inhibition values were obtained via monitoring the MBL-catalyzed hydrolysis of substrate meropenem.....	149
Table 4-2. Percent inhibition of IDA MBP derivatives at 250 μ M against NDM-1. Percent inhibition values were obtained via monitoring the MBL-catalyzed hydrolysis of substrate meropenem. ^[a]	151
Table 4-3. Inhibitory activity of Sublibrary 6 (compounds 87a – 87n) against NDM-1.....	154
Table 4-4. Inhibitory activity of Sublibrary 7 (compounds 89a – 89h) against NDM-1.....	156
Table 4-5. Protein thermal shift of compounds against NDM-1.....	158
Table 4-6. Summary of the native MS experimental results for NDM-1. ^[a]	162
Table 4-7. Summary of the native MS experimental results for VIM-2. ^[a]	164
Table 5-1. Inhibitory activity of Sublibrary 8 (compounds 95a – 95j) against NDM-1. Inhibition values were obtained via monitoring the MBL-catalyzed hydrolysis of substrate meropenem.....	199
Table 5-2. Inhibitory activity against NDM-1 of Sublibrary 9 (97a – 97g). ^[a]	215
Table 5-3. Inhibitory activity of compounds 51 , 51a – 51b , MBI-1 and MBI-20 against NDM-1. Inhibition values were obtained via monitoring the MBL-catalyzed hydrolysis of substrate meropenem.....	224
Table 5-4. AMA and EDTA screened against a panel of Zn(II)-dependent metalloenzymes.....	234

ACKNOWLEDGEMENTS

To my parents, Juyuan Chen and Huilan Liang, thank you for your unconditional love and support. Thank you for always giving me the freedom to chase my dreams while keeping me grounded. To my sisters, Abby and Amanda “Nini” Chen, both of you inspire me in unimaginable ways. I have learned so much from both of you, and love you with all my heart. To my doggo, Creamy “Beanie”, thank you for the endless cuddles and long walks on the beach.

I want to thank Professor Seth M. Cohen for allowing me to be part of your lab. You have not only been a great PI, but also a mentor and a friend. I appreciate your patience and honesty throughout my graduate career. Thank you to all former and current Cohen lab members. Special thanks to Dr. David Puerta and Professor Yao Chen for being great mentors during my first year of graduate school. I would also like to thank my “bruh” Dr. Christian Perez. You have not only been an amazing mentor, but also a best friend who is always down for some happy hour, gossip, and life advice. Big thank you to Stephanie Duggan and Dr. Jennifer Bartoli – I’ll always cherish our time in lab jamming to acoustic covers and coffee dates. Special thanks to Dr. Kathleen Prosser, Professor Christine Morrison, Sergio Alaya, and Kyle Barcus - y’all rock.

During my graduate studies, I have had the honor of working with the best collaborators. I would like to thank Professor Walter Fast and Dr. Pei W. Thomas for your help, guidance, and contributions to my projects. I appreciate your availability to always discuss scientific ideas with me. I would also like to thank Professor Michael Crowder, Professor David Tierney, Professor Robert Bonomo and Professor Richard

Page and their laboratory members for assistance in my projects. Thank you to Dr. Yongxuan Su and Dr. Anthony Mrse for your assistance.

Lastly, I would like to thank my friends and colleges. Graduate school is hard, but you guys have made it so much more fun and enjoyable. Thank you for always having my back and putting up with me: Dr. Woojoo Eunice Kim, Jon Sauer, Naneki Collins, Yanice Benitez, Brock Mitts, Peter Glatt, Warren Chan, Kyle Bentz, Matt Nattikia, Myles Drance, Jeff Mindrebo, and Ben Dick.

Chapter 1, in part, is adapted and revised from the materials published in the following papers: Allie Y. Chen, Rebecca N. Adamek, Benjamin L. Dick, Cy V. Credille, Christine N. Morrison, Seth M. Cohen, “Targeting Metalloenzymes for Therapeutic Intervention”, *Chem. Rev.* **2019**, *119*, 1323-1455, and Allie Y. Chen, Pei W. Thomas, Zishuo Cheng, Nasa Y. Xu, David L. Tierney, Michael W. Crowder, Walter Fast, Seth M. Cohen, “Investigation of Dipicolinic Acid Isosteres for the Inhibition of Metallo- β -Lactamases”, *ChemMedChem*, **2019**, *14*, 1271-1282. The permission to reproduce materials is granted by American Chemical Society and John Wiley and Sons. The dissertation author was the primary researcher for the data presented. The co-authors listed in these publications also participated in the research.

Chapter 2, in part, is adapted and revised from the materials published in the following paper: Allie Y. Chen, Pei W. Thomas, Alesha C. Stewart, Alexander Bergstrom, Zishuo Cheng, Callie Miller, Christopher R. Bethel, Steven H. Marshall, Cy V. Credille, Christopher L. Riley, Richard C. Page, Robert A. Bonomo, Michael W. Crowder, David L. Tierney, Walter Fast, Seth M. Cohen, “Dipicolinic Acid Derivatives as

Inhibitors of New Delhi Metallo- β -lactamase-1” *J. Med. Chem.* **2017**, *60*, 7267-7283.

The dissertation author was the primary researcher and author. The permission to reproduce this paper was granted by the American Chemical Society. The co-authors listed in these publications also participated in the research.

Texts, schemes, and figures in Chapter 3 have been adapted from the materials published in the following paper: Allie Y. Chen, Pei W. Thomas, Zishuo Cheng, Nasa Y. Xu, David L. Tierney, Michael W. Crowder, Walter Fast, Seth M. Cohen, “Investigation of Dipicolinic Acid Isosteres for the Inhibition of Metallo- β -Lactamases” *ChemMedChem*, **2019**, *14*, 1271-1282. The dissertation author was the primary researcher and author, and gratefully acknowledges the contributions of all co-authors. The permission to reproduce this paper was granted by the John Wiley and Sons.

Chapter 4 highlights the work of a publication currently in preparation. The manuscript in preparation is authored by the following: Allie Y. Chen, Caitlyn Thomas, Pei W. Thomas, Walter Fast, Michael W. Crowder and Seth M. Cohen with a planned title of “Iminodiacetic Acid as a Metal-binding Pharmacophore for New Delhi Metallo- β -lactamase Inhibitor Development.” The dissertation author was the primary researcher for the data presented. The co-authors listed in these publications also participated in the research.

VITA

EDUCATION

University of California San Diego Ph.D., Chemistry	2020
University of California San Diego M.S., Chemistry	2016
University of California Irvine B.S., Chemistry	2014

PUBLICATIONS

1. **Chen, A. Y.**; Thomas, C.; Thomas, P.W.; Fast, W.; Crowder, M.W.; Cohen, S.M. "Iminodiacetic Acid as a Metal-binding Pharmacophore for New Delhi Metallo- β -lactamase Inhibitor Development" *manuscript in preparation*, **2020**
2. **Chen, A.Y.**; Thomas, P.W.; Cheng, Z.; Xu, N.Y.; Tierney, D.L.; Crowder, M.W.; Fast, W.; Cohen, S.M. "Investigation of Dipicolinic Acid Isosteres for the Inhibition of Metallo- β -Lactamases" *ChemMedChem*, **2019**, *14*.
3. **Chen, A.Y.**; Adamek, R.N.; Dick, B.L.; Credille, C.V.; Morrison, C.N.; Cohen, S.M. "Targeting Metalloenzymes for Therapeutic Intervention" *Chem. Rev.* **2019**, *119*, 1323-1455.
4. **Chen, A.Y.**; Thomas, P.W.; Stewart, A.C.; Bergstrom, A.; Cheng, Z.; Miller, C.; Bethel, C.R.; Marshall, S.H.; Credille, C.V.; Riley, C.L; Page, R.C.; Bonomo, R.A.; Crowder, M.W.; Tierney, D.L.; Fast, W.; and Cohen, S.M. "Dipicolinic Acid Derivatives as Inhibitors of New Delhi Metallo- β -lactamase-1" *J. Med. Chem.* **2017**, *60*, 7267–7283.

ABSTRACT OF THE DISSERTATION

Conversion of Metal Chelators to Selective and Potent Inhibitors
of New Delhi Metallo-beta-lactamase

by

Allie Yingyao Chen

Doctor of Philosophy in Chemistry

University of California San Diego, 2020

Professor Seth M. Cohen, Chair

Professor Michael D. Burkart, Co-Chair

Metalloproteins are essential to a wide range of biological functions including nucleic acid modification, protein degradation, and many others. Metalloproteins that utilize a metal ion to facilitate catalysis are known as metalloenzymes. Due to their role

discovery of novel New Delhi Metallo- β -lactamase-1 (NDM-1) inhibitors. NDM-1 is a metalloenzyme that hydrolyzes β -lactam containing antibiotics and contributes to the heightened threat of antibiotic resistance. NDM-1 Inhibitor development presented in this dissertation will focus on the conversion of traditional metal chelating fragments to compounds which form stable protein:inhibitor ternary complexes. Chapter 1 describes the current landscape of metalloenzyme inhibitors and relevant background information of NDM-1. Chapter 2 details the discovery of dipicolinic acid (DPA) as a lead fragment and the hit-to-lead development of DPA derivatives as inhibitors for NDM-1. The development of DPA isosteres and investigation in the relationship of observed inhibition value versus mechanism of action is presented in Chapter 3. The investigation of an alternative MBP, iminodiacetic acid (IDA), into a second class of novel NDM-1 inhibitors is described in Chapter 4. Chapter 5 includes a description of alternative synthesized libraries and perspective on the future of NDM inhibitor development. Together these chapters demonstrate the utility of fragment-based drug discovery and metal-binding pharmacophores for the development of novel and potent NDM-1 inhibitors.

Chapter 1. Introduction

1.1 Targeting Metalloenzymes for Therapeutic Intervention

Proteins that utilize one or more metal ions to function are referred to as metalloproteins. The role of metal ion(s) in metalloproteins falls into two broad categories: structural and functional. Structural metal ions are required for proper folding of a protein, with a canonical example being the Zn(II) finger proteins.¹ Functional metal ions are at the active site of metalloproteins and carry out a diverse range of processes such as electron transfer, substrate recognition/binding, and catalysis that together serve a wide variety of biological functions. When the functional metal ion(s) serves to promote catalysis, the metalloprotein can be categorized as a metalloenzyme.

An early review by Solomon in 1996 stated that 52% of all proteins in the Protein Data Bank (PDB) included a metal ion.² A 2008 study using the Metal MACiE database suggested ~40% of enzymes with known structures were metal-dependent.³ Another review by Robinson in 2009 cited that nearly one-half of all enzymes require a metal ion for proper function.⁴ Collectively, the literature suggests that the number of enzymes that can be categorized as metalloenzymes is between 40% and 50%. The ubiquitous roles of metalloenzymes in biology result in metalloenzymes being a key factor in the propagation of many diseases. This can be due to the overexpression, enhanced activation, or misregulation of an endogenous metalloenzyme. The misregulation of metalloenzymes has been associated with many diseases ranging from diabetes, cancer, depression, anxiety, and pathogenic infections.⁵ Some clinically relevant metalloenzyme targets, along with their metal co-factor and indication, are highlighted in

Table 1-1. An extensive overview of clinically relevant metalloenzyme targets and their drug discovery efforts are described elsewhere.⁵ Metalloenzymes that are validated targets or where the biological role of the metalloenzyme supports the case for therapeutic intervention are of greatest interest for the development of metalloenzyme inhibitors.

From 2013 to 2017, there were a total of 181 drugs that were approved by the U.S. Food and Drug Administration (FDA), of which 137 are new molecular entities (NMEs) and 44 are biologics license applications (BLAs). Interestingly, of the 137 NMEs, only 13 target metalloenzymes (representing ~7% of the FDA-approved drugs, Figure 1-1). Notably, an additional 17 NMEs are kinase inhibitors which contain Mg(II) ions that act as a co-substrate with ATP; however, these inhibitors (like other reported kinase inhibitors) do not engage in Mg(II) binding.⁶⁻⁷ This discrepancy between the number of potential metalloenzyme targets and the number of developed FDA-approved drugs indicates an area of untapped potential for the development of metal-binding inhibitors against therapeutic targets.

The majority of clinically relevant and literature published metalloenzyme inhibitors are small molecules that contain two substituents: a metal-binding pharmacophore (MBP) and a backbone. The MBP is a functional group that serves as an “anchor” to the metalloenzyme active site metal ion(s) (primary coordination sphere), and the backbone forms interactions with amino acid residues in the active site pocket (secondary coordination sphere). While the backbone component of most metalloenzyme inhibitors has been extensively explored and is the focus of structure-

activity relationship (SAR) efforts, research regarding the MBP has been limited. This is demonstrated by the nearly singular reliance on the hydroxamic acid MBP (also referred to as the “silver bullet”).⁸ Other frequently used MBPs include carboxylic acids, thiols, and phosphates.⁵ Although these MBPs are capable of forming coordination bonds with active site metal(s), they often do not possess optimal pharmacokinetic (PK) properties (such as metabolic stability and oral bioavailability) and can be a liability in drug design and development.⁹⁻¹⁵

Table 1-1. List of metalloenzymes targeted for therapeutic intervention.

Enzyme	Metal Ion	Disease/Condition
Angiotensin Converting Enzyme	Zn(II)	Hypertension
Carbonic Anhydrase (CA)	Zn(II)	Glaucoma
Anthrax Lethal Factor	Zn(II)	Anthrax infection
Catechol- <i>O</i> -Methyltransferase	Mg(II)	Parkinson's disease
Farnesyl Transferase	Zn(II)	Cancer
Glyoxalase 1 (Glo1)	Zn(II)	Cancer
Matrix Metalloproteinase	Zn(II)	Cancer, arthritis, inflammation
Methionine Aminopeptidase	Mn(II)	Cancer
Neprilysin	Zn(II)	Hypertension
Rpn11	Zn(II)	Cancer
HIV Integrase	Mg(II)	Human Immunodeficiency Virus
Histone Demethylase	Fe(II)	Cancer
Influenza Endonuclease	Mn(II)	Influenza Virus
<i>Pseudomonas Aeruginosa</i> Elastase	Zn(II)	<i>P. aureginosa</i> infection
Metallo- β -Lactamases	Zn(II)	Bacterial infections

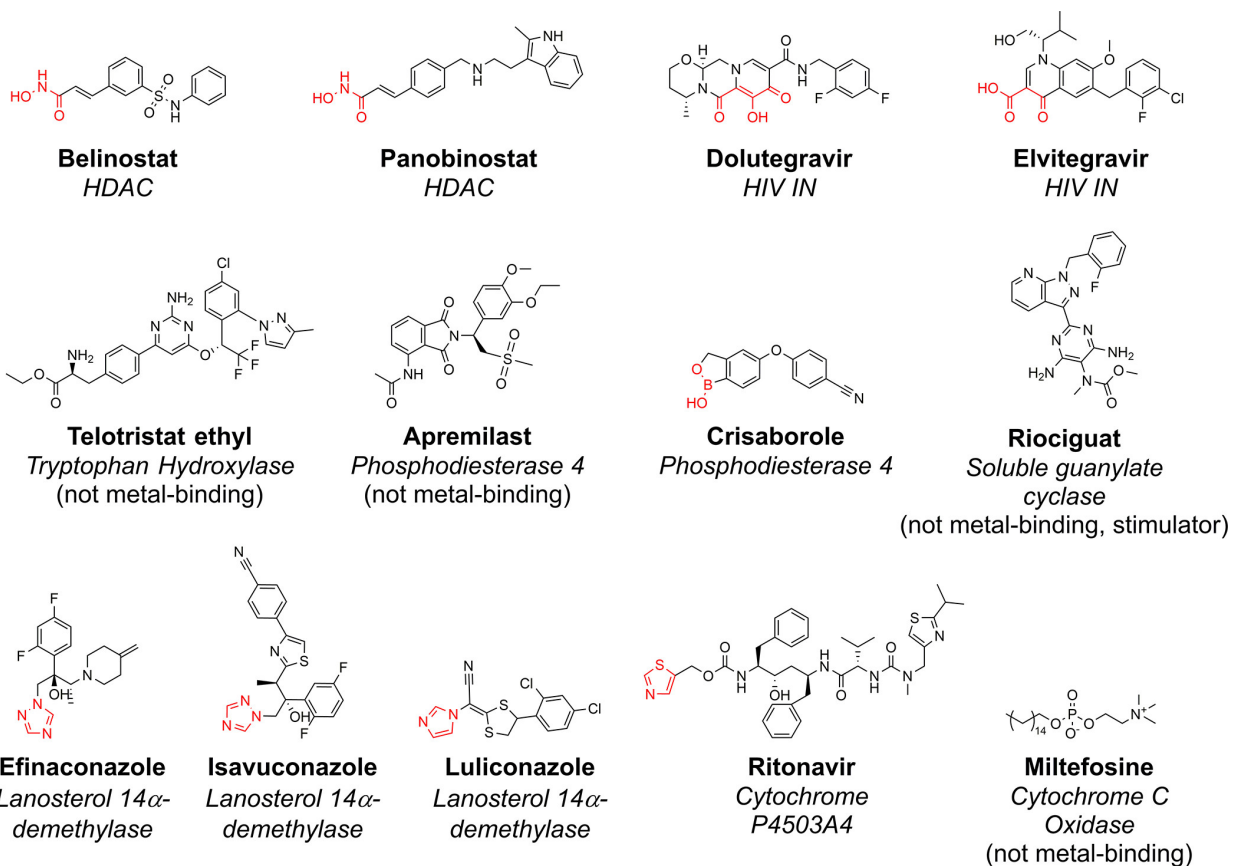


Figure 1-1. FDA-approved metalloenzyme inhibitors between 2013 and 2017 with MBP motifs shown in red.

1.2 A Fragment-Based Drug Discovery Approach for the Development of Metalloenzyme Inhibitors

In the last two decades, fragment-based drug discovery (FBDD) has been proven a successful alternative/complementary approach to traditional drug discovery methods such as high-throughput screening (HTS), combinatorial chemistry, computer-aided design, and de novo design.¹⁶⁻¹⁹ Compared to traditional HTS (which utilizes large libraries of up to millions of compounds), FBDD utilizes smaller and more focused libraries of simpler compounds. Due to the limited number of interactions small fragments can make with the protein, higher equilibrium dissociation constants (K_D in the micro to the low-millimolar range)²⁰ for compounds in FBDD libraries are observed compared to that of HTS libraries. Although these fragment hits are weak, they are considered to be "high-quality" interactions as they must overcome a substantial entropic barrier to binding relative to their size.²¹ The FBDD hits can be derivatized to yield more potent leads. This hit-to-lead development is not easily achieved with leads discovered from HTS screens, as those are often fully elaborated compounds. A set of guidelines utilized to generate FBDD libraries includes the "rule of three" (RO3). The RO3 describes desirable physiochemical and PK properties for the fragments in the FBDD libraries and includes the following criteria: molecular weight <300 amu, $cLogP \leq 3$, hydrogen bond donors ≤ 3 and hydrogen bond acceptors ≤ 3 .²¹ Upon the identification of fragment hits, biophysical characterization and/or structural determination can be used to understand the mode of binding. This is followed by subsequent rounds of hit-to-lead optimization to yield full-length inhibitors.

Although FBDD provides many advantages over HTS, some challenges must be overcome, including the identification of proper screening methods and transforming hits to lead drugs.²¹ Due to the inherent low affinity (high K_D) of the fragment to the target protein, identified hits can vary depending on the screening technique used; thus, chemists must carefully evaluate the method for their FBDD campaign.²² For instance, in ligand-observed nuclear magnetic resonance (NMR), only 5% of the fragment needs to interact with the protein to be detected as an NMR hit, while in X-ray crystallography, at least 70% occupancy of the active site is required to be considered a hit. It is proposed that of all the techniques used to identify fragment hits (surface plasmon resonance, calorimetry, mass spectrometry, bioassays, NMR, etc.), X-ray crystallography is the most successful method with near-absence of false positives and ability to detect most weakly binding fragments.²¹ To address the ladder challenge of transforming fragment hits to useful lead drugs, additional guidelines such as physicochemical properties (cLogP and cLogD), efficiency metrics (ligand efficiency, LE, and lipophilic ligand efficiency, LLE), fragment growth vectors and potential for new interactions, and synthetic accessibility are also taken into consideration.²¹

A common strategy for developing metalloenzyme inhibitors is by designing a compound that incorporates a MBP, typically the aforementioned hydroxamic acid, to serve as an “anchor” via coordination to the active-site metal ion(s). Through coordination, the compound blocks natural substrate turnover and effectively inhibits catalysis via a competitive mechanism of action. The application of FBDD using a MBP fragment library for the discovery of metalloenzyme inhibitors represents a unique

opportunity. Compared to FBDD of non-metalloenzyme inhibitors where the site of fragment binding can be ambiguous and would need further validation, MBPs bind at the active site metal ion(s). This eliminates the need for sophisticated biophysical methods (X-ray crystallography) to detect the location of inhibitor binding. In addition, taking advantage of the presence of metal in the protein, additional techniques such as X-ray absorption spectroscopy, electron paramagnetic resonance (EPR) spectroscopy, Mössbauer spectroscopy, and bioinorganic complexes are also available to guide inhibitor development.

The Cohen lab has assembled a novel MBP fragment library (~320 MBPs) containing several classes of metal-binding groups (salicylic acids, hydroxyl pyrones, hydroxypyridinones, hydroxyquinolones, among others, Figure 1-2). The MBP library can be screened against metalloenzyme targets of interest to yield fragment hits. The fragments are then derivatized via “fragment-growth” and “fragment-merge” strategies to generate full-length inhibitors. The implementation of a MBP library for FBDD has led to the discovery of novel inhibitors for several metalloenzymes, including *Pseudomonas Aeruginosa* elastase (LasB),²³ human carbonic anhydrase II (hCAII),²⁴ glyoxalase 1 (Glo1),²⁵ proteasome subunit Rpn11,²⁶⁻²⁷ and influenza endonuclease.²⁸ The focus of this dissertation is the utilization of the MBP library for FBDD of inhibitors against New Delhi Metallo- β -lactamase (NDM).

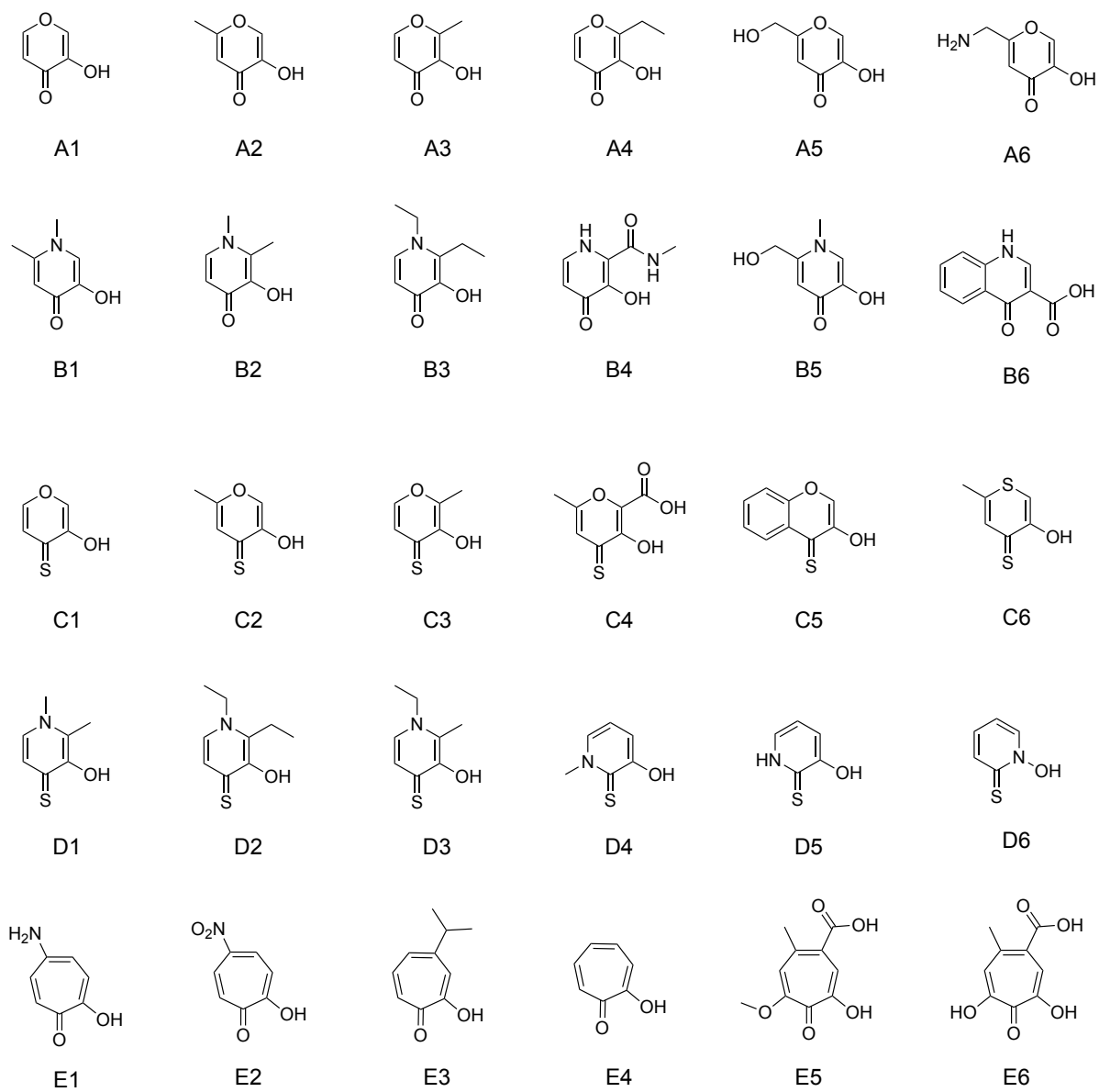


Figure 1-2. Representative compounds in the MBP fragment library.

1.3 Introduction to New Delhi Metallo- β -lactamase-1

β -Lactam-containing antibiotics have been one of the most successful and popular classes of antibiotics for combating a wide range of Gram-positive and -negative bacterial infections. Unsurprisingly, since the introduction of β -lactam containing antibiotics (beginning with penicillin in the 1940s), the widespread use of this class of antibiotics has led to the emergence of various resistance mechanisms. A 2019 report by the Centers for Disease Control and Prevention (CDC) estimates that >2.8 million antibiotic-resistance infections occur in the United States each year, with >35,000 of those resulting in death.²⁹ Resistance mechanisms that bacteria employ include mutation of penicillin-binding proteins (PBPs), modification of outer membrane proteins, production of efflux pumps, expression of β -lactamases, and others.³⁰⁻³¹ β -Lactamases utilize either an active site serine residue (Ambler classes A, C, and D, also known as serine- β -lactamases, SBLs) or Zn(II) metal ion(s) (Ambler class B, also known as metallo- β -lactamases, MBLs) to facilitate the hydrolysis of the β -lactam ring of the target antibiotic and render the drug ineffective.^{30, 32} A dedicated β -lactamase database provides an up-to-date compilation of the biochemical and structural data of all MBLs (<http://www.bldb.eu/>).³³ First observed in 1966 by Sabath and Abraham (merely two decades after the introduction of penicillin), there are now >80 reported unique MBL families.^{32, 34} MBLs have become one of the most problematic bacterial resistance mechanisms due to their wide substrate profile, with the ability to hydrolyze virtually all clinically used bicyclic β -lactam antibiotics.³⁵⁻³⁶

MBLs are divided into B1, B2, and B3 subclasses depending on sequence identity and the number of Zn(II) ion(s) (either one or two) in the active site. Description of subclasses and their mechanism of action are reviewed elsewhere.³⁵⁻³⁸ Commonly observed and clinically relevant members of the MBLs belong to subclass B1, of which New Delhi Metallo- β -lactamase (NDM) is a prominent representative.³⁹ NDM bears a di-Zn(II) active site, with Zn₁ ligated by His116, His118, His196, and a bridging hydroxide (in a tetrahedral coordination geometry), and Zn₂ ligated by Asp120, Cys221, His263, the bridging hydroxide, and an apical H₂O (in a trigonal bipyramidal coordination geometry, standard BBL numbering, Figure 1-3).⁴⁰ The active site is flanked between two flexible loops (L3 and L10), allowing the protein to accommodate a wide range of antibiotic substrates.⁴¹⁻⁴² The three loops (L3, L5 and L10) of NDM have been the primary focus for inhibitor development and will be discussed further in this dissertation. Plasmids that carry the *bla*_{NDM}-gene are capable of undergoing horizontal gene transfer between different species of microorganisms, leading to an increase in the prevalence of *bla*_{NDM}-bearing pathogens.⁴³⁻⁴⁴ Additionally, the threat of NDM is exacerbated (compared to the two other most prevalent members of the B1 MBLs, IMiPenemase, IMP, and Verona Integron-encoded Metallo- β -lactamase, VIM) by the ability of NDM to membrane anchor, leading to higher protein stability and secretion.⁴⁵⁻⁴⁶ Resistance to a broad spectrum of β -lactams and the high horizontal gene transfer ability have allowed for rapid propagation from nosocomial infections to infections within the general population.⁴⁷⁻⁴⁹ Furthermore, *bla*_{NDM} is often carried on plasmids containing other genes that encode various resistance factors (including macrolides,

aminoglycosides, rifampicin, and sulfamethoxazole),⁴³ resulting in bacterial infections that are resistant to many different classes of antimicrobials.

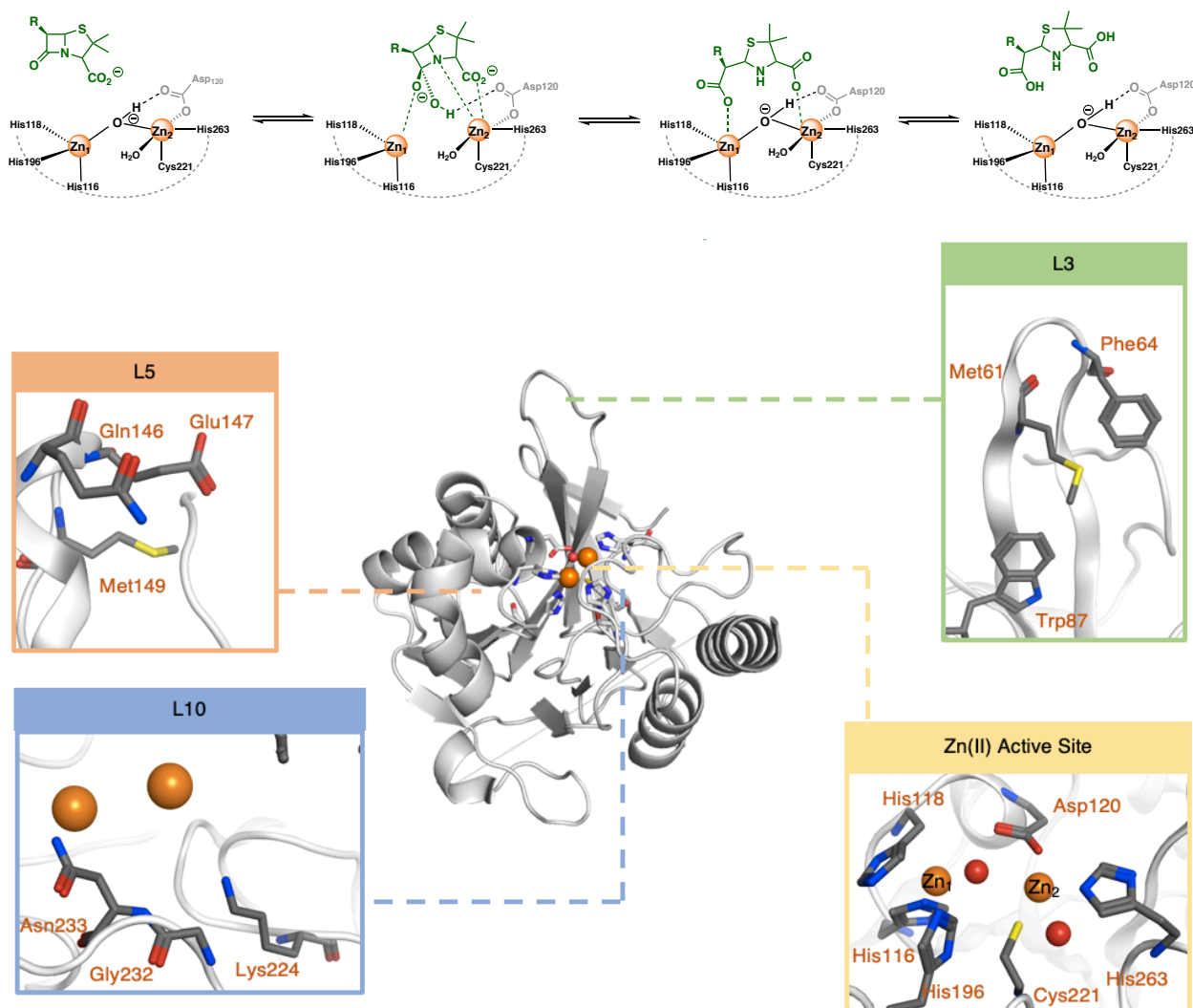


Figure 1-3. *Top:* NDM-1 hydrolysis of β -lactam drug; *Bottom:* Structure of NDM-1 with the di-Zn(II) active site, L3, L5, and L10 labeled (adapted from PDB 4EYB). Figure generated via Pymol.

Ten years since the first report of NDM-1 there are now >24 NDM variants identified.^{33, 50-51} Variants have evolved to exhibit an increase in thermal stability, Zn(II) affinity, and mononuclear Zn(II) activity.⁵²⁻⁵⁴ Unfortunately, even with the rapid spread of the *bla*_{NDM-1} gene and the evolution of NDM variants, little advancement has been made in inhibitor development. Currently, there are >500 inhibitors reported in the literature (representative structures are shown in Figure 1-4),⁵⁵ but many of these inhibitors share similar structural features and only one has advanced to clinical trials. VNRX-5133 (VenatoRx Pharmaceuticals) has been reported as a broad spectrum β -lactamase inhibitor and is currently in phase III clinical trials.⁵⁶ Through X-ray crystallography, it was discovered that upon NDM-1 binding, the acylamino oxygen of VNRX-5133 cyclizes onto the boron of the bicyclic core, providing insight for the future development of these tetrahedral (sp^3) boron species inhibitors. The flexible active site of NDM-1, the diversity of related MBLs, a lack of understanding for inhibition mechanisms, and misinterpretation of structural data have all contributed to a delay in inhibitor development.⁵⁷⁻⁵⁸ To combat this class of resistance mechanism, additional potent inhibitors with well-studied mechanism of action is of urgent need.

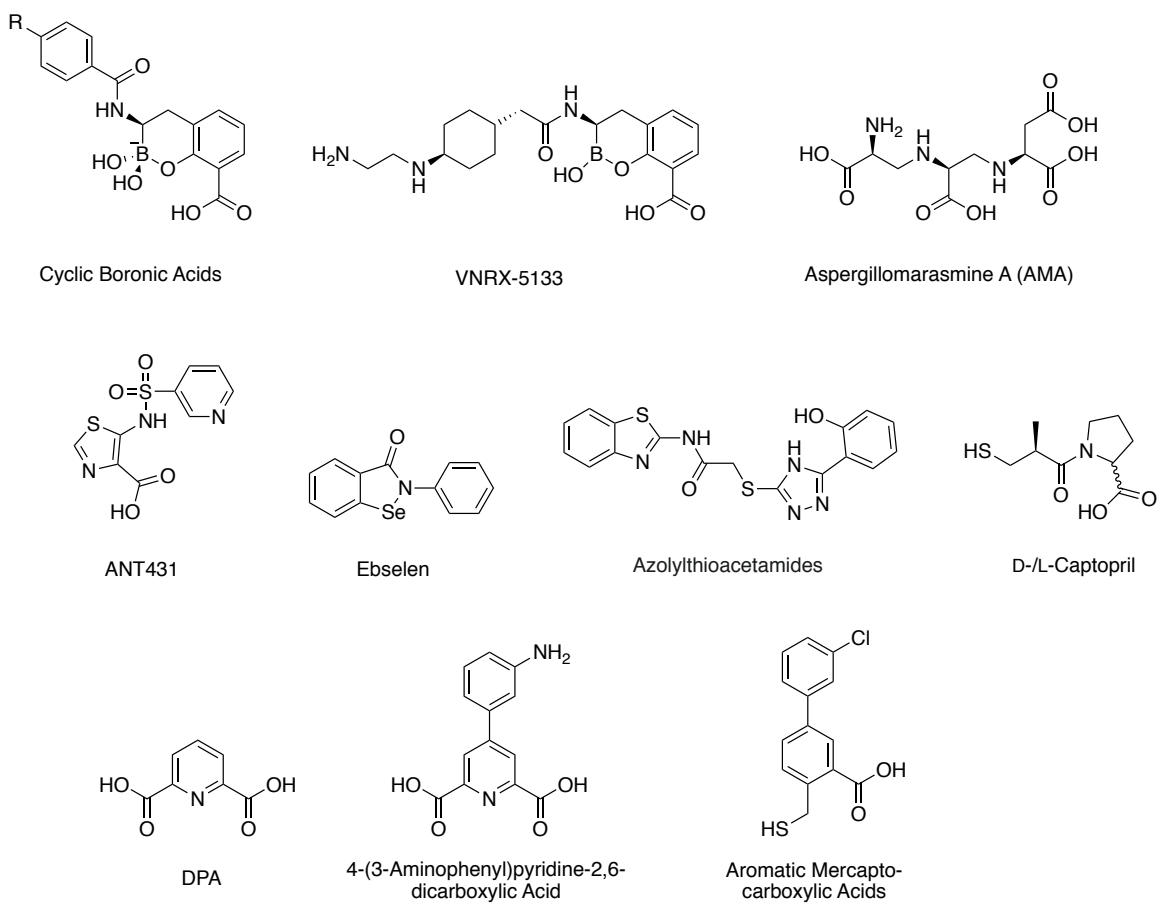


Figure 1-4. Examples of current NDM-1 inhibitors reported in literature.

1.4 Outlook

Metalloenzymes play a central role in the propagation of many diseases. The overexpression, enhanced activation, or misregulation of an endogenous metalloenzyme has been associated with diabetes, cancer, depression, anxiety, and pathogenic infections. The development of novel therapeutics that target specific metalloenzymes in these diseased states is of great need. Traditional metalloenzyme inhibitor design has focused on a handful of MBPs (hydroxamic acids, thiols, and carboxylic acids) which do not bear the best PK properties and may become a liability in later drug development. The utilization of a MBP library for FBDD provides a unique opportunity in metalloenzyme inhibitor design by expanding the scope of MBPs available for hit-to-lead development.

This dissertation will focus on leveraging the MBP library for the FBDD of NDM-1 inhibitors, with an emphasis on the conversion of routine metal chelators into selective and potent inhibitors. The discovery and subsequent hit-to-lead optimization of dipicolinic acid (**DPA**) to yield a potent and selective inhibitor of NDM-1 is presented in Chapter 2. Chapter 3 describes the development of **DPA** isosteres and the investigation of how isosteric replacement influences both potency and mechanism of action. The development of a second MBP, iminodiacetic acid (**IDA**), into a novel class of NDM-1 inhibitors is described in Chapter 4. Chapter 5 details additional inhibitor libraries and provides an outlook on future NDM inhibitor development.

1.5 Acknowledgements

Chapter 1, in part, is adapted and revised from the materials published in the following papers: Allie Y. Chen, Rebecca N. Adamek, Benjamin L. Dick, Cy V. Credille, Christine N. Morrison, Seth M. Cohen, “Targeting Metalloenzymes for Therapeutic Intervention”, *Chem. Rev.* **2019**, *119*, 1323-1455, and Allie Y. Chen, Pei W. Thomas, Zishuo Cheng, Nasa Y. Xu, David L. Tierney, Michael W. Crowder, Walter Fast, Seth M. Cohen, “Investigation of Dipicolinic Acid Isosteres for the Inhibition of Metallo- β -Lactamases”, *ChemMedChem*, **2019**, *14*, 1271-1282. The permission to reproduce materials is granted by American Chemical Society and John Wiley and Sons. The dissertation author was the primary researcher for the data presented. The co-authors listed in these publications also participated in the research.

1.6 References

1. Cassandri, M.; Smirnov, A.; Novelli, F.; Pitolli, C.; Agostini, M.; Malewicz, M.; Melino, G.; Raschella, G., Zinc-finger Proteins in Health and Disease. *Cell Death Discov.* **2017**, *3*, 17071.
2. Solomon, E. I.; Sundaram, U. M.; Machonkin, T. E., Multicopper Oxidases and Oxygenases. *Chem. Rev.* **1996**, *96* (7), 2563-2606.
3. Andreini, C.; Bertini, I.; Cavallaro, G.; Holliday, G. L.; Thornton, J. M., Metal Ions in Biological Catalysis: from Enzyme Databases to General Principles. *J. Biol. Inorg. Chem.* **2008**, *13* (8), 1205-1218.
4. Waldron, K. J.; Rutherford, J. C.; Ford, D.; Robinson, N. J., Metalloproteins and Metal Sensing. *Nature* **2009**, *460* (7257), 823-830.
5. Chen, A. Y.; Adamek, R. N.; Dick, B. L.; Credille, C. V.; Morrison, C. N.; Cohen, S. M., Targeting Metalloenzymes for Therapeutic Intervention. *Chem Rev* **2019**, *119* (2), 1323-1455.
6. Knape, M. J.; Ballez, M.; Burghardt, N. C.; Zimmermann, B.; Bertinetti, D.; Kornev, A. P.; Herberg, F. W., Divalent Metal Ions Control Activity and Inhibition of Protein Kinases. *Metallomics* **2017**, *9* (11), 1576-1584.
7. Ferguson, F. M.; Gray, N. S., Kinase Inhibitors: the Road Ahead. *Nat. Rev. Drug Discov* **2018**, *17* (5), 353-377.
8. Cohen, S. M., A Bioinorganic Approach to Fragment-Based Drug Discovery Targeting Metalloenzymes. *Acc. Chem. Res.* **2017**, *50* (8), 2007-2016.
9. Ballatore, C.; Huryn, D. M.; Smith, A. B., 3rd, Carboxylic Acid (Bio)isosteres in Drug Design. *ChemMedChem* **2013**, *8* (3), 385-395.
10. Lassalas, P.; Gay, B.; Lasfargeas, C.; James, M. J.; Tran, V.; Vijayendran, K. G.; Brunden, K. R.; Kozlowski, M. C.; Thomas, C. J.; Smith, A. B., 3rd; Huryn, D. M.; Ballatore, C., Structure Property Relationships of Carboxylic Acid Isosteres. *J. Med. Chem.* **2016**, *59* (7), 3183-3203.
11. Lassila, T.; Hokkanen, J.; Aatsinki, S. M.; Mattila, S.; Turpeinen, M.; Tolonen, A., Toxicity of Carboxylic Acid-Containing Drugs: The Role of Acyl Migration and CoA Conjugation Investigated. *Chem. Res. Toxicol.* **2015**, *28* (12), 2292-2303.
12. Sawamura, R.; Okudaira, N.; Watanabe, K.; Murai, T.; Kobayashi, Y.; Tachibana, M.; Ohnuki, T.; Masuda, K.; Honma, H.; Kurihara, A.; Okazaki, O., Predictability of Idiosyncratic Drug Toxicity Risk for Carboxylic Acid-containing Drugs Based on the Chemical Stability of Acyl Glucuronide. *Drug Metab. Dispos.* **2010**, *38* (10), 1857-1864.

13. Shen, S.; Kozikowski, A. P., Why Hydroxamates May Not Be the Best Histone Deacetylase Inhibitors--What Some May Have Forgotten or Would Rather Forget? *ChemMedChem* **2016**, *11* (1), 15-21.
14. Munday, R., Toxicity of Thiols and Disulphides: Involvement of Free-radical Species. *Free Radic. Biol. Med.* **1989**, *7* (6), 659-673.
15. Elliott, T. S.; Slowey, A.; Ye, Y.; Conway, S. J., The Use of Phosphate Bioisosteres in Medicinal Chemistry and Chemical Biology. *MedChemComm* **2012**, *3* (7), 735-751.
16. Erlanson, D. A.; McDowell, R. S.; O'Brien, T., Fragment-based Drug Discovery. *J. Med. Chem.* **2004**, *47* (14), 3463-3482.
17. Rees, D. C.; Congreve, M.; Murray, C. W.; Carr, R., Fragment-based Lead Discovery. *Nat. Rev. Drug Discov.* **2004**, *3* (8), 660-672.
18. Joseph-McCarthy, D.; Campbell, A. J.; Kern, G.; Moustakas, D., Fragment-Based Lead Discovery and Design. *J. Chem. Inf. Model.* **2014**, *54* (3), 693-704.
19. Congreve, M.; Chessari, G.; Tisi, D.; Woodhead, A. J., Recent developments in fragment-based drug discovery. *J. Med. Chem.* **2008**, *51* (13), 3661-3680.
20. Lamoree, B.; Hubbard, R. E., Current Perspectives in Fragment-based Lead Discovery (FBLD). *Essays Biochem.* **2017**, *61* (5), 453-464.
21. Jhoti, H.; Williams, G.; Rees, D. C.; Murray, C. W., The 'Rule of Three' for Fragment-Based Drug Discovery: Where are We Now? *Nat. Rev. Drug Discov.* **2013**, *12* (8), 644.
22. Robson-Tull, J., Biophysical Screening in Fragment-based Drug Design: a Brief Overview. *Biosci. Horiz.* **2019**, *11*.
23. Garner, A. L.; Struss, A. K.; Fullagar, J. L.; Agrawal, A.; Moreno, A. Y.; Cohen, S. M.; Janda, K. D., 3-Hydroxy-1-alkyl-2-methylpyridine-4(1H)-thiones: Inhibition of the *Pseudomonas aeruginosa* Virulence Factor LasB. *ACS Med. Chem. Lett.* **2012**, *3* (8), 668-672.
24. Martin, D. P.; Cohen, S. M., Nucleophile Recognition as an Alternative Inhibition Mode for Benzoic Acid Based Carbonic Anhydrase Inhibitors. *Chem. Commun.* **2012**, *48* (43), 5259-5261.
25. Perez, C.; Barkley-Levenson, A. M.; Dick, B. L.; Glatt, P. F.; Martinez, Y.; Siegel, D.; Momper, J. D.; Palmer, A. A.; Cohen, S. M., Metal-Binding Pharmacophore Library Yields the Discovery of a Glyoxalase 1 Inhibitor. *J. Med. Chem.* **2019**, *62* (3), 1609-1625.

26. Perez, C.; Li, J.; Parlati, F.; Rouffet, M.; Ma, Y.; Mackinnon, A. L.; Chou, T. F.; Deshaies, R. J.; Cohen, S. M., Discovery of an Inhibitor of the Proteasome Subunit Rpn11. *J. Med. Chem.* **2017**, *60* (4), 1343-1361.
27. Li, J.; Yakushi, T.; Parlati, F.; Mackinnon, A. L.; Perez, C.; Ma, Y.; Carter, K. P.; Colayco, S.; Magnuson, G.; Brown, B.; Nguyen, K.; Vasile, S.; Suyama, E.; Smith, L. H.; Sergienko, E.; Pinkerton, A. B.; Chung, T. D. Y.; Palmer, A. E.; Pass, I.; Hess, S.; Cohen, S. M.; Deshaies, R. J., Capzimin is a Potent and Specific Inhibitor of Proteasome Isopeptidase Rpn11. *Nat. Chem. Biol.* **2017**, *13* (5), 486-493.
28. Credille, C. V.; Chen, Y.; Cohen, S. M., Fragment-Based Identification of Influenza Endonuclease Inhibitors. *J. Med. Chem.* **2016**, *59* (13), 6444-6454.
29. *Antibiotic Resistance Threats in the United States, 2019 (2019 AR Threats Report)*; Centers for Disease Control and Prevention 2019; p 148.
30. Bonomo, R. A., beta-Lactamases: A Focus on Current Challenges. *Cold Spring Harbor Perspect. Med.* **2017**, *7*.
31. Fisher, J. F.; Meroueh, S. O.; Mobashery, S., Bacterial Resistance to beta-Lactam Antibiotics: Compelling Opportunism, Compelling Opportunity. *Chem. Rev.* **2005**, *105*, 395-424.
32. Bush, K.; Jacoby, G. A., Updated Functional Classification of beta-Lactamases. *Antimicrob. Agents Chemother.* **2010**, *54*, 969-976.
33. Naas, T.; Oueslati, S.; Bonnin, R. A.; Dabos, M. L.; Zavala, A.; Dortet, L.; Retailliau, P.; Iorga, B. I., beta-Lactamase Database (BLDB) - Structure and Function. *J. Enzyme Inhib. Med. Chem.* **2017**, *32*, 917-919.
34. Sabath, L. D.; Abraham, E. P., Zinc as a Cofactor for Cephalosporinase from *Bacillus cereus* 569. *Biochem. J.* **1966**, *98*, 11-13.
35. Meini, M. R.; Llarrull, L. I.; Vila, A. J., Overcoming Differences: The Catalytic Mechanism of Metallo-beta-Lactamases. *FEBS Lett.* **2015**, *589*, 3419-3432.
36. Mojica, M. F.; Bonomo, R. A.; Fast, W., B1-Metallo-beta-Lactamases: Where Do We Stand? *Curr. Drug Targets* **2016**, *17*, 1029-1050.
37. Drawz, S. M.; Bonomo, R. A., Three Decades of beta-Lactamase Inhibitors. *Clin. Microbiol. Rev.* **2010**, *23*, 160-201.
38. Crowder, M. W.; Spencer, J.; Vila, A. J., Metallo-beta-Lactamases: Novel Weaponry for Antibiotic Resistance in Bacteria. *Acc. Chem. Res.* **2006**, *39*, 721-728.
39. Nordmann, P.; Naas, T.; Poirel, L., Global Spread of Carbapenemase-producing Enterobacteriaceae. *Emerging Infect. Dis.* **2011**, *17*, 1791-1798.

40. Kang, J. S.; Zhang, A. L.; Faheem, M.; Zhang, C. J.; Ai, N.; Buynak, J. D.; Welsh, W. J.; Oelschlaeger, P., Virtual Screening and Experimental Testing of B1 Metallo-beta-lactamase Inhibitors. *J. Chem. Inf. Model.* **2018**, *58*, 1902-1914.
41. Sun, Z.; Hu, L.; Sankaran, B.; Prasad, B. V. V.; Palzkill, T., Differential Active Site Requirements for NDM-1 beta-Lactamase Hydrolysis of Carbapenem versus Penicillin and Cephalosporin Antibiotics. *Nat. Commun.* **2018**, *9*, 4524.
42. Zhang, H.; Hao, Q., Crystal Structure of NDM-1 Reveals a Common beta-Lactam Hydrolysis Mechanism. *FASEB J.* **2011**, *25*, 2574-2582.
43. Yong, D.; Toleman, M. A.; Giske, C. G.; Cho, H. S.; Sundman, K.; Lee, K.; Walsh, T. R., Characterization of a New Metallo-beta-lactamase Gene, bla(NDM-1), and a Novel Erythromycin Esterase gene Carried on a Unique Genetic Structure in *Klebsiella pneumoniae* Sequence Type 14 from India. *Antimicrob. Agents Chemother.* **2009**, *53*, 5046-5054.
44. Zou, D.; Huang, Y.; Liu, W.; Yang, Z.; Dong, D.; Huang, S.; He, X.; Ao, D.; Liu, N.; Wang, S.; Wang, Y.; Tong, Y.; Yuan, J.; Huang, L., Complete Sequences of Two Novel blaNDM-1-Harboring Plasmids from Two *Acinetobacter towneri* Isolates in China Associated with the Acquisition of Tn125. *Sci. Rep.* **2017**, *7*, 9405.
45. Gonzalez, L. J.; Bahr, G.; Nakashige, T. G.; Nolan, E. M.; Bonomo, R. A.; Vila, A. J., Membrane Anchoring Stabilizes and Favors Secretion of New Delhi Metallo-beta-Lactamase. *Nat. Chem. Biol.* **2016**, *12*, 516-522.
46. King, D.; Strynadka, N., Crystal Structure of New Delhi Metallo-beta-lactamase Reveals Molecular Basis for Antibiotic Resistance. *Protein Sci.* **2011**, *20*, 1484-1491.
47. Walsh, T. R., Emerging Carbapenemases: a Global Perspective. *Int. J. Antimicrob. Agents* **2010**, *36*, S8-S14.
48. Nordmann, P.; Poirel, L.; Toleman, M. A.; Walsh, T. R., Does Broad-spectrum beta-Lactam Resistance due to NDM-1 Herald the End of the Antibiotic era for Treatment of Infections Caused by Gram-negative Bacteria? *J. Antimicrob. Chemother.* **2011**, *66*, 689-692.
49. Kumarasamy, K. K.; Toleman, M. A.; Walsh, T. R.; Bagaria, J.; Butt, F.; Balakrishnan, R.; Chaudhary, U.; Doumith, M.; Giske, C. G.; Irfan, S.; Krishnan, P.; Kumar, A. V.; Maharjan, S.; Mushtaq, S.; Noorie, T.; Paterson, D. L.; Pearson, A.; Perry, C.; Pike, R.; Rao, B.; Ray, U.; Sarma, J. B.; Sharma, M.; Sheridan, E.; Thirunarayan, M. A.; Turton, J.; Upadhyay, S.; Warner, M.; Welfare, W.; Livermore, D. M.; Woodford, N., Emergence of a New Antibiotic Resistance Mechanism in India, Pakistan, and the UK: a Molecular, Biological, and Epidemiological Study. *Lancet Infect. Dis.* **2010**, *10*, 597-602.
50. Yong, D.; Toleman, M. A.; Giske, C. G.; Cho, H. S.; Sundman, K.; Lee, K.; Walsh, T. R., Characterization of a new metallo-beta-lactamase gene, bla(NDM-1), and a novel erythromycin esterase gene carried on a unique genetic structure in *Klebsiella*

pneumoniae sequence type 14 from India. *Antimicrob Agents Chemother* **2009**, *53* (12), 5046-5054.

51. Liu, L.; Feng, Y.; McNally, A.; Zong, Z., blaNDM-21, a New Variant of blaNDM in an Escherichia Coli Clinical Isolate Carrying blaCTX-M-55 and rmtB. *J. Antimicrob. Chemother.* **2018**, *73*, 2336-2339.

52. Cheng, Z.; Thomas, P. W.; Ju, L.; Bergstrom, A.; Mason, K.; Clayton, D.; Miller, C.; Bethel, C. R.; VanPelt, J.; Tierney, D. L.; Page, R. C.; Bonomo, R. A.; Fast, W.; Crowder, M. W., Evolution of New Delhi Metallo-beta-Lactamase (NDM) in the Clinic: Effects of NDM Mutations on Stability, Zinc Affinity, and Mono-Zinc Activity. *J. Biol. Chem.* **2018**, *293*, 12606-12618.

53. Stewart, A. C.; Bethel, C. R.; VanPelt, J.; Bergstrom, A.; Cheng, Z.; Miller, C. G.; Williams, C.; Poth, R.; Morris, M.; Lahey, O.; Nix, J. C.; Tierney, D. L.; Page, R. C.; Crowder, M. W.; Bonomo, R. A.; Fast, W., Clinical Variants of New Delhi Metallo-beta-Lactamase Are Evolving To Overcome Zinc Scarcity. *ACS Infect. Dis.* **2017**, *3*, 927-940.

54. Bahr, G.; Vitor-Horen, L.; Bethel, C. R.; Bonomo, R. A.; Gonzalez, L. J.; Vila, A. J., Clinical Evolution of New Delhi Metallo-beta-Lactamase (NDM) Optimizes Resistance under Zn(II) Deprivation. *Antimicrob. Agents Chemother.* **2018**, *62* (1), e01849-e01817.

55. Linciano, P.; Cendron, L.; Gianquinto, E.; Spyraakis, F.; Tondi, D., Ten Years with New Delhi Metallo-beta-Lactamase-1 (NDM-1): From Structural Insights to Inhibitor Design. *ACS Infect. Dis.* **2018**.

56. Krajnc, A.; Brem, J.; Hinchliffe, P.; Calvopina, K.; Panduwawala, T.; Lang, P. A.; Kamps, J.; Tyrell, J. M.; Widlake, E.; Seward, B. G.; Walsh, T. R.; Spencer, J.; Schofield, C. J., Bicyclic Boronate VNRX-5133 Inhibits Metallo- and Serine-beta-Lactamases. *J Med Chem* **2019**.

57. Ju, L. C.; Cheng, Z.; Fast, W.; Bonomo, R. A.; Crowder, M. W., The Continuing Challenge of Metallo-beta-Lactamase Inhibition: Mechanism Matters. *Trends Pharmacol. Sci.* **2018**, *39*, 635-647.

58. Raczynska, J. E.; Shabalin, I. G.; Minor, W.; Wlodawer, A.; Jaskolski, M., A Close Look onto Structural Models and Primary Ligands of Metallo-beta-Lactamases. *Drug Resist. Updates* **2018**, *40*, 1-12.

Chapter 2. Dipicolinic Acid Derivatives as Inhibitors of NDM-1

2.1 Introduction

Antibiotic-resistance in pathogenic bacteria has become a critical public health threat.¹ A major mechanism of antibiotic resistance is microbial degradation of drugs by enzymes such as MBLs. MBLs with the greatest clinical impact are found in the B1 subfamily, with the most prevalent members being NDM, VIM, and IMP. NDM, the newest member of the trio, has been the focus of recent inhibitor development due to its carriage on easily transmissible plasmids and its emergence in community-acquired infections.²⁻⁵ This chapter will describe the utilization of FBDD for the design, synthesis, and evaluation of a novel class of NDM-1 inhibitors. A focused library of MBPs enabled a systematic search of compounds that target the di-Zn(II) site of B1 MBLs. SAR analysis and optimization of primary hit dipicolinic acid (**DPA**) led to the discovery of **36** with an $IC_{50} = 80$ nM, putting it on par with the most potent NDM-1 inhibitors known.⁶⁻⁷ Compound **36** showed increased inhibition against IMP-1 and VIM-2 when compared to **DPA** and no significant inhibition against several other Zn(II)-dependent metalloenzymes. The interaction of **36** with the active site of di-Zn(II) or di-Co(II) metalloforms of NDM-1 was characterized via ¹H NMR spectroscopy, electron paramagnetic resonance (EPR) spectroscopy, equilibrium dialysis, intrinsic tryptophan fluorescence quenching, and UV-vis spectroscopy. As inhibition of **36** was improved, a metal ion stripping mechanism was replaced in favor of a ternary NDM-1:Zn(II):**36** complex mechanism of action. Microdilution broth studies performed with clinical *E. coli* and *K. pneumoniae* strains harboring *bla*_{NDM-1} reveal that coadministration with **36** significantly reduced the minimum inhibitory concentration (MIC) values of imipenem.

Furthermore, no toxicity was observed for **36** in mammalian cell culture. This work provides a roadmap for the transformation of MBPs into selective and effective NDM-1 inhibitors.

2.2 Results and Discussion

2.2.1 MBP Library Screen and Selection of DPA as Lead Fragment

The extreme sequence diversity found within the family of MBL proteins complicates the design of a single compound to serve as an effective broad-spectrum MBL inhibitor. Even within the B1 subclass of MBLs, which contains the most clinically relevant targets, sequence identity is low. Pairwise protein sequence alignments between all combinations of the three MBLs tested here (NDM-1, IMP-1, and VIM-2) have identities of only ~30%.⁸⁻⁹ This diversity is also present at the active site where very few residues are essential for catalysis due to a mechanism that relies mostly on substrate interactions with the di-Zn(II) site.⁸ However, this same property makes the di-Zn(II) active site an attractive target for inhibition by MBPs. The search for MBL inhibitors through a systematic exploration of chemical space by screening the MBP library against three representative B1 MBLs, NDM-1, IMP-1, and VIM-2 is described. Several MBPs fragments were identified as attractive leads for MBL inhibitor development.

A 96-well plate, continuous assay was optimized for the hydrolysis of the colorimetric β -lactam substrate chromacef by NDM-1 (substrate concentration of $3 \times K_M$), IMP-1 (substrate concentration of K_M), and VIM-2 (substrate concentration of K_M). The substrate concentrations were kept close to K_M values to better detect competitive inhibitors, yet high enough to allow for maintenance of linear initial rates.¹⁰ The assays showed good discrimination between positive (enzyme added) and negative (enzyme omitted) samples, with Z' factors of 0.7, 0.7, and 0.8 for NDM-1, IMP-1, and VIM-2,

respectively (Figure 2-1).¹¹ Each fragment in the MBP library was screened at a concentration of 50 μ M against each of the three MBL enzymes, and the resulting percent inhibition was measured. The activity of MBPs ranged from 0% to 100% inhibition, with an average of ~27% inhibition for the entire library screened against all three enzymes. Using a cutoff of >60% inhibition, six compounds remained as hits (Table 2-1).

One primary hit, 1,10-phenanthroline, is a known metal stripping agent and was omitted. Another hit, 2-(pyridine-2-yl)-4,5-dihydrothiazole, was disregarded because mass spectrometry indicated the stock solution of the MBP had degraded. The remaining five primary hits consisted of 3-hydroxypyridine-2(1*H*)-thione, which shares some structural similarities to the known MBL inhibitor thiomaltol (which was also a hit),¹² two 8-hydroxyquinoline compounds (shown to inhibit a different di-Zn(II) enzyme),¹³ and **DPA**. **DPA** was selected as the initial scaffold for further optimization because previous reports described dicarboxylate compounds and 2-carboxypyridines as inhibitors of other MBLs.^{8, 14} Furthermore, **DPA** bears resemblance to the core of a hydrolyzed cephalosporin, mimicking both the carboxylate formed upon β -lactam hydrolysis and the leaving group nitrogen. The IC_{50} of **DPA** was first determined via colorimetric assay to be 520 nM.

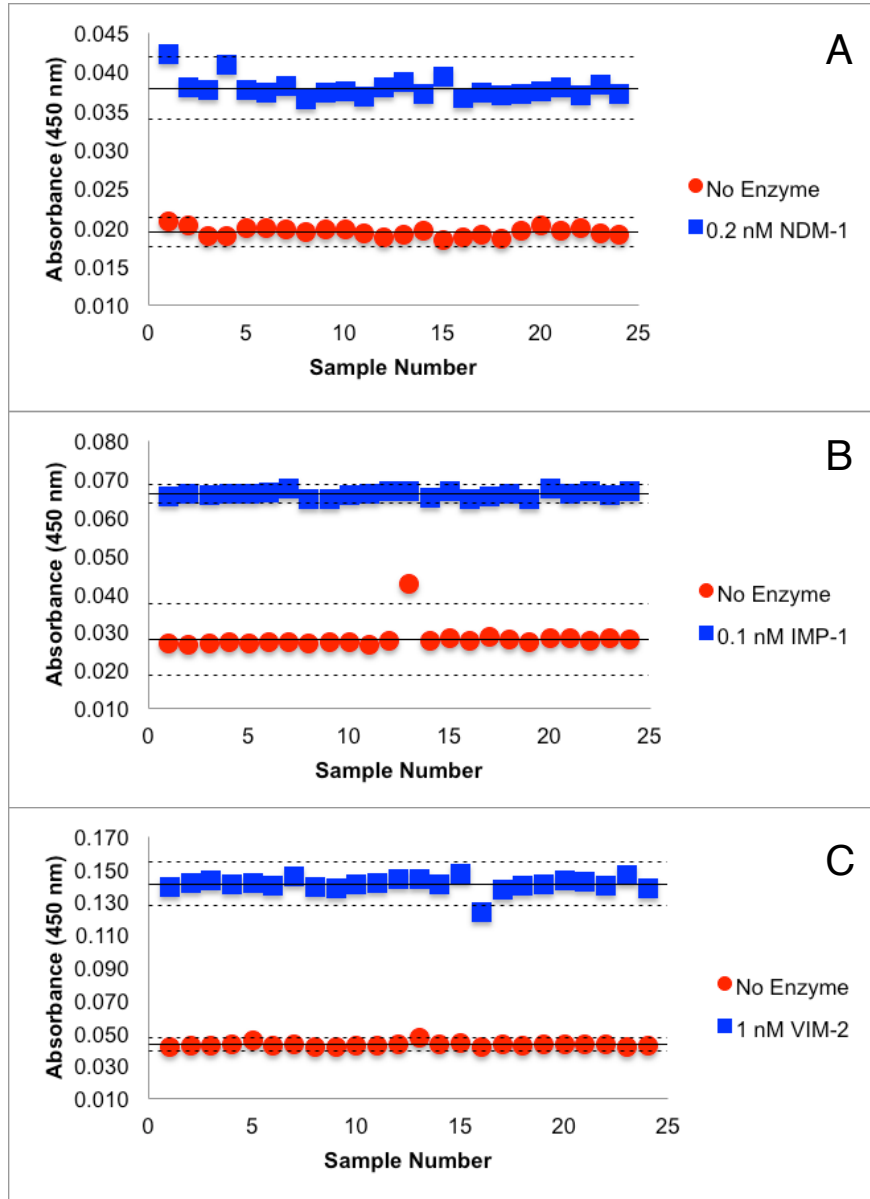
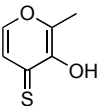
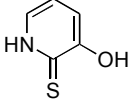
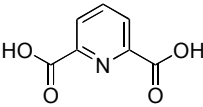
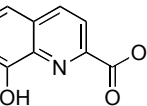
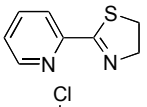
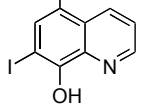
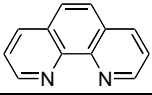


Figure 2-1. Z' Factor determination using the substrate chromacef. Absorbance values for positive (■) controls and negative (●) controls. Solid lines are the mean values for each set, dashed lines are fixed at $\pm 3\sigma$.

Table 2-1. List of MBP primary screening hits against MBLs. Percent inhibition values were obtained via monitoring the MBL-catalyzed hydrolysis of substrate chromacef.

Compound		NDM-1	VIM-2	IMP-1
thiomaltol		70	2	54
3-hydroxypyridine-2(1H)-thione		76	85	104
DPA				
8-hydroxyquinoline-2-carboxylic acid		106	104	99
2-(pyridine-2-yl)-4,5-dihydrothiazole		98	103	99
2-(pyridine-2-yl)-4,5-dihydrothiazole		61	85	96
5-chloro-7-iodoquinolin-8-ol		106	96	142
1,10-phenanthroline		90	103	90

2.2.2 Design and Synthesis of DPA Derivatives (Sublibrary 1 – Sublibrary 3)

To augment the inherent affinity of **DPA** for the di-Zn(II) component of MBLs, we sought to design **DPA**-based inhibitors of NDM-1 that focus on increasing the binding interactions with protein residues surrounding the active-site Zn(II) ions, namely residues on L3 and L10. The L3 mobile β -hairpin loop allows for the accommodation of a wide range of antibiotic substrates, plays a role in the accumulation of catalytic reaction intermediates, and presents a hydrophobic surface as one wall of the active site.¹⁵ L3 moves over the di-Zn(II) ions and back to the original position on the millisecond timescale upon substrate hydrolysis, making it an attractive active site to probe.¹⁶ The other loop that flanks the di-Zn(II) active site, L10, is a conserved loop that provides potential binding partners: Lys224, Gly232, and Asn233 (standard BBL numbering, Figure 2-2).¹⁷ The two sides of L3 and L10 form a shallow, relatively featureless hydrophobic channel. L5, a loop that runs perpendicular to the L3 and L10, is also of interest for inhibitor development. On the basis of the structure of the coordination complex of **DPA** with free Zn(II)¹⁸ and hydrolyzed antibiotic cefuroxime complexed with NDM-1 (PDB 5O2E),¹⁹ a similar coordination at the active site of NDM-1 was assumed to guide inhibitor optimization. The design and synthesis of subsequent sublibraries aimed to improve interactions with amino acid residues of L3 and L10.

The first of three sublibraries (Sublibrary 1) contained compounds with substituents designed to extend into the hydrophobic channel, as well as to determine the necessity of both carboxylate groups on the **DPA** fragment for inhibition. These substitutions were introduced through the conversion of one of the carboxylate groups

of **DPA** to various amide substituents via standard peptide coupling procedures (compounds **3** – **20**, Scheme 2-1). The carboxylic acids of **DPA** were first esterified to give the dimethyl ester derivative **1**. One of the esters were hydrolyzed with KOH at 0 °C to obtain the monomethyl ester product (**2**). Coupling **2** with primary amines by 1-ethyl-3-(3-dimethylaminopropyl)-carbodiimide (EDC) and hydroxybenzotriazole (HOBT) afford the desired amide derivatives. Finally, hydrolysis of the methyl ester in 1M NaOH:THF produced the monocarboxylic acid **DPA** derivatives that comprise sublibrary 1 (compounds **3** – **20**).

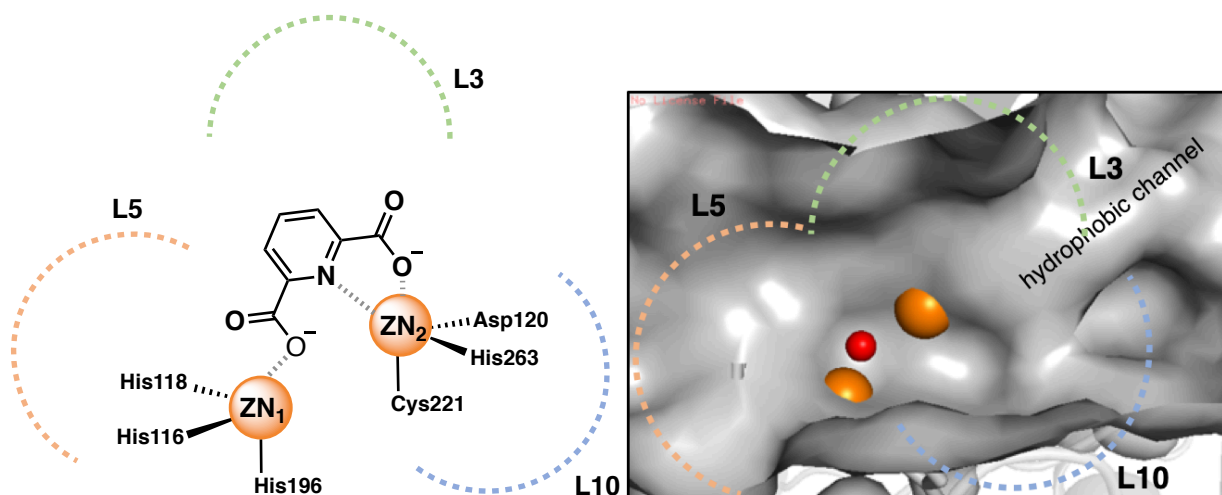
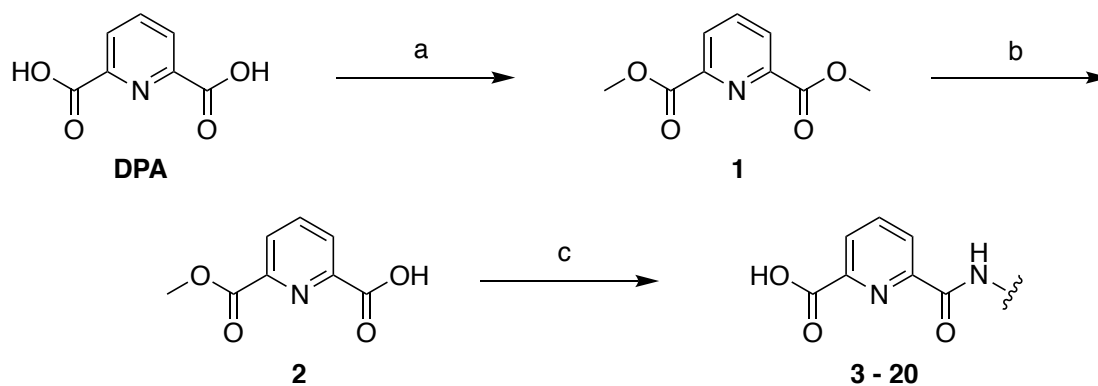


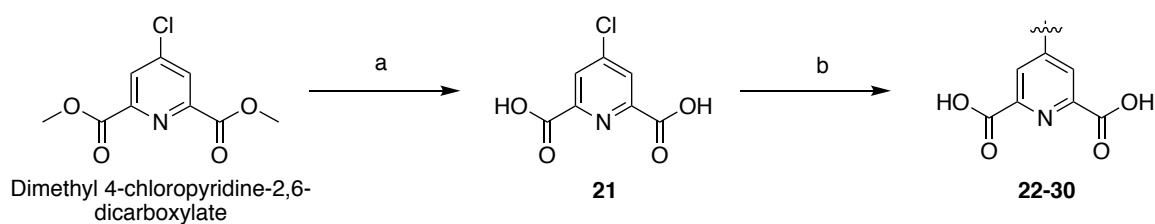
Figure 2-2. Chemical illustration of the predicted mode of binding of **DPA** with the di-Zn(II) active site with L3, L5 and L10 outlined. Zn(II) and hydroxide ion are represented as orange and red spheres, respectively.

Sublibrary 2 (compounds **22** – **30**) consisted of **DPA** derivatives with substituents at the 4-position of the pyridine ring connected through an amine linker (Scheme 2-2). This sublibrary was designed to determine what substituents could be tolerated in the active site pocket below the β -hairpin loop. Compounds **22** – **30** were synthesized starting from dimethyl 4-chloropyridine-2,6-dicarboxylate followed by saponification in a

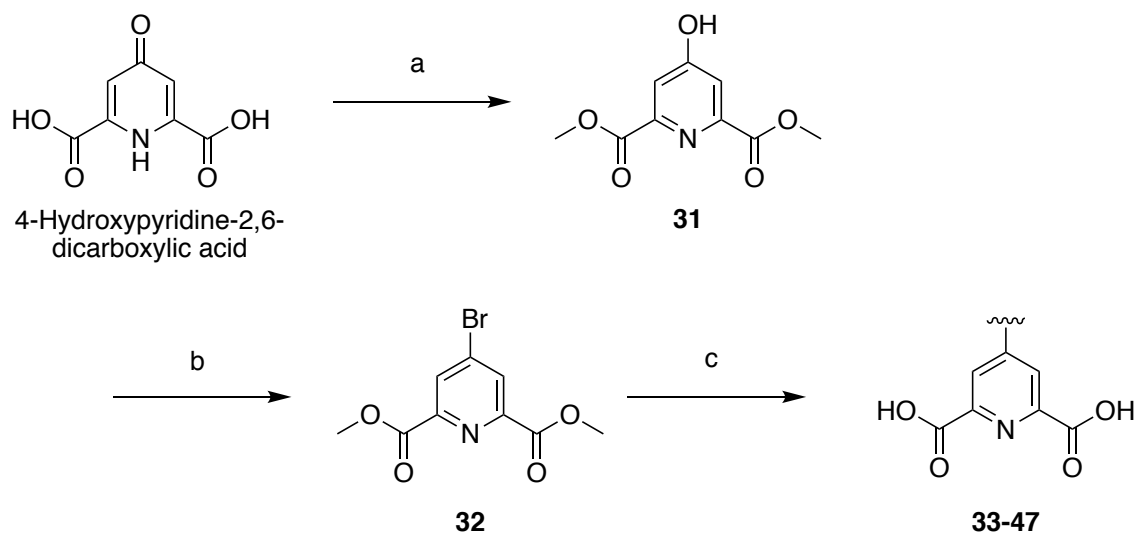
1M NaOH:THF solution to afford **21**. Next, **21** was heated using a microwave reactor in the presence of the corresponding amine to generate compounds **22** – **30**. Lastly, Sublibrary 3 (compounds **33** – **47**) also contained **DPA** derivatives with substituents at the 4-position but incorporated a series of substituted aryl substituents to enhance possible hydrophobic interactions at the base of the L3 β -hairpin loop and included substitutions to make possible hydrogen-bonding interactions with nearby L10 residues. In this sublibrary, instead of an amine linker, the aryl substituents are attached through a direct carbon–carbon bond formed via Palladium-catalyzed Suzuki cross-coupling (Scheme 2-3). 4-Hydroxypyridine-2,6-dicarboxylic acid was esterified to **31** by heating to reflux in MeOH with catalytic H_2SO_4 . Next, **31** was converted into the bromide derivative **32** using tetrabutylammonium bromide and P_4O_{10} . Compounds **33–47** were then synthesized via Suzuki cross-coupling procedures utilizing $\text{Pd}(\text{PPh}_3)_4$ and $\text{K}_3\text{PO}_4/\text{CH}_3\text{CO}_2\text{K}$, with the final compounds obtained by saponification with 1M NaOH:THF.



Scheme 2-1. Synthetic route for Sublibrary 1 (compounds **3 – 20**). Reagents and conditions: (a) MeOH, H₂SO₄ (cat.), 75 °C, 24 h, 100%; (b) MeOH, KOH, 0 °C, 4 h, 81%; (c) EDC, HOBT, corresponding amine H₂NR, 18 h; then 3:1 1M NaOH: THF, 30 min – 1 h, 4M HCl, 34 – 87%.



Scheme 2-2. Synthetic route for Sublibrary 2 (compounds **22 – 30**). Reagents and conditions: (a) 10:1 1M NaOH: THF, 70 °C, 3 h, 80%; (b) corresponding amine, H₂O, microwave at 160 °C, 30 min, 10 – 80%.



Scheme 2-3. Synthetic route for Sublibrary 3 (compounds **33** – **47**). Reagents and conditions: (a) MeOH, H₂SO₄ (cat.), 75 °C, 24 h, 88%; (b) tetrabutylammonium bromide, P₄O₁₀, toluene, 100 °C, 3 h, 92%; (c) Pd(PPh₃)₄, K₃PO₄/CH₃CO₂K, 1,4-dioxane, 85 °C, overnight; then 4:1 1M NaOH:THF, H₂SO₄, 22 – 84%.

2.2.3 In Vitro Activity of DPA Derivatives as Inhibitors of NDM-1

An initial ranking of NDM-1 inhibition by **DPA** derivatives in Sublibraries 1 – 3 was first completed by determining the IC_{50} values using the colorimetric substrate chromacef. Chromacef, at a concentration of $3 \times K_M$, allowed for linear hydrolysis rates over the assay duration. A secondary assay, using the fluorescent substrate fluorocillin,²⁰⁻²¹ was then used to verify the ranking of the most potent compounds (Sublibrary 3). The K_M of fluorocillin was determined to be $0.46 \pm 0.06 \mu M$. By use of a concentration less than K_M , the fluorescent substrate allowed for increased signal response, a longer linear portion of the kinetic assay, and minimized substrate perturbation of IC_{50} values for competitive inhibitors. The addition of a fluorescence-based assay also provides an orthogonal method to verify inhibition. False positives in the screen arising from compounds with absorbance at wavelengths similar to the product detected in the absorbance-based assay would not interfere with the excitation or emission wavelengths used in the fluorescence-based assay. IC_{50} values determined using either substrate give similar relative rankings of potency but are of different absolute magnitudes due to differing assay conditions (most significantly substrate concentration relative to K_M values).¹⁰ A summary of the inhibition data is provided in Table 2-2 – Table 2-4.

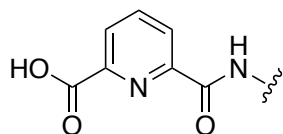
Utilizing a colorimetric assay, it was found that most of the compounds in Sublibrary 1 (**3** – **20**) showed ≥ 100 -fold loss in activity when compared to the unsubstituted **DPA** ($IC_{50} = 520 \text{ nM}$). This indicates that both carboxylate groups on **DPA** are required for inhibition. Both aromatic (**8**) and alkyl (**15**) substitutions were

detrimental; however, substituents that reintroduce a potential metal coordinating ligand or H-bonding ligand (**12** – **14**) retained some activity. **DPA** derivatized with D-valine (**14**), in comparison with **13** and **16**, suggests that a carboxylate at this position drives activity and bulky hydrophobic substitutions can also improve inhibition, albeit to a lesser degree. On the basis of this SAR, both carboxylates of the **DPA** scaffold were retained in the design of subsequent sublibraries. Compounds in Sublibrary 2 (**21** – **30**) showed a modest loss in inhibition (7- to 26-fold) relative to **DPA**, with a small dimethylamine substituent (**22**) causing the most significant loss. The addition of a hydrophobic aryl group to the nitrogen linker (as in compound **23**) significantly rescued activity and resulted in the most potent inhibitor in this series ($IC_{50} = 3.4 \mu\text{M}$). Extending the length of the linker (**23** vs **24** or **25**) reduced activity. The substitution of the aryl ring (**26** – **28**) or replacement with different heterocycles (**29** and **30**) did not result in any significant improvement. These results suggest that substitution at the 4-position with an amine linkage is not favorable (even relative to unsubstituted **DPA**), but the addition of hydrophobic substituents can rescue activity. These results are consistent with the hypothesis that substitution at this position can lead to interactions with the hydrophobic L3 adjacent to the active site. Therefore, the aryl substituent was kept in the design of the third sublibrary but a different linkage was utilized.

In contrast to the previous two sublibraries, compounds in Sublibrary 3 (**33** – **47**) showed inhibition of NDM-1 that is on the same order of magnitude as **DPA** and in some cases significantly better. Examination of the fluorescent assay results reveals that **DPA** with aryl groups containing *ortho*-substituents (**38** and **39**) showed similar or

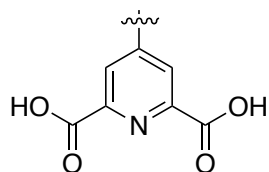
improved inhibition relative to **DPA** ($IC_{50} = 410$ nM). In general, those with *para*-substituents (**40** – **43**) showed modest changes in inhibition. The same general trend is seen with *meta*-substitutions (**34**, **35**, **37**, **44** – **47**) except for compound **36**. Compound **36** stood out in Sublibrary 3, with an IC_{50} value of 80 ± 2 nM (Figure 2-3). This compound represents a 4-fold improvement in inhibition compared to **DPA** and achieves one of the lowest IC_{50} values for NDM-1 reported to date. A comparison of **36** with **42** suggests that the increase in inhibition is not likely due to the electron-donating effects of **36** on metal binding, as a greater effect would be expected from the *para*-substituted compound. The substitution of a methoxy (**34**), alcohol (**35**), or dimethylamine (**37**) group at the same position shows a loss in activity, suggesting that specific interactions (possibly by H-bond donation) of **36** with the protein are responsible for the improved inhibition. It is proposed that aryl substituents directly linked to the 4-position of **DPA** augmented by *meta*-substituents are capable of specific protein interactions and represent an effective route for fragment growth. Notably, additional exogenous Zn(II) in the assay buffer has little impact on the IC_{50} value of **36**, suggesting a specific, direct interaction of **36** with amino acid residues in the active site of NDM-1. In contrast, exogenous Zn(II) in the assay buffer diminishes the inhibition activity of **DPA** against NDM-1, presumably due to the sequestering of the excess Zn(II) by **DPA** (Figure 2-4).

Table 2-2. Inhibitory activity of Sublibrary 1 (compounds **3** – **20**) against NDM-1. Inhibition values were obtained via monitoring the NDM-1-catalyzed hydrolysis of substrate chromacef.



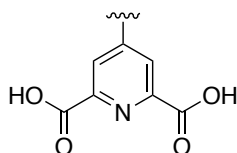
Compound	IC ₅₀ (μM)	Compound	IC ₅₀ (μM)
3	>50	12	24±1
4	>50	13	49±1
5	>50	14	22±1
6	>50	15	>50
7	>50	16	>50
8	>50	17	>50
9	>50	18	>50
10	>50	19	>50
11	>50	20	>50

Table 2-3. Inhibitory activity of Sublibrary 2 (compounds **21** – **30**) against NDM-1. Inhibition values were obtained via monitoring the NDM-1-catalyzed hydrolysis of substrate chromacef.



Compound		IC ₅₀ (μM)	Compound		IC ₅₀ (μM)
21		5.0±0.1	26		4.5±0.1
22		13.6±0.8	27		7.2±0.4
23		3.4±0.2	28		5.8±0.4
24		8.4±1.1	29		5.2±0.1
25		9.1±0.2	30		4.9±0.1

Table 2-4. Inhibitory activity of Sublibrary 3 (compounds **33** – **47**) against NDM-1. Inhibition values were obtained via monitoring the NDM-1-catalyzed hydrolysis of substrate chromacef and fluorocillin (**bold typeface**).



Compound	IC ₅₀ (μM)	Compound	IC ₅₀ (μM)
DPA	0.52 ± 0.04 0.41 ± 0.02	40	0.43 ± 0.02 0.38 ± 0.02
33	0.99 ± 0.02	41	0.66 ± 0.03 0.39 ± 0.02
34	0.80 ± 0.02 1.07 ± 0.07	42	1.03 ± 0.01 0.54 ± 0.02
35	0.60 ± 0.03 0.43 ± 0.01	43	0.57 ± 0.02 0.19 ± 0.01
36	0.32 ± 0.01 0.08 ± 0.002	44	0.89 ± 0.03 0.20 ± 0.08
37	0.82 ± 0.01 0.43 ± 0.01	45	0.99 ± 0.04 0.93 ± 0.02
38	0.50 ± 0.02 0.50 ± 0.01	46	0.86 ± 0.02 0.13 ± 0.01
39	0.52 ± 0.02 0.13 ± 0.01	47	0.86 ± 0.02 0.59 ± 0.06

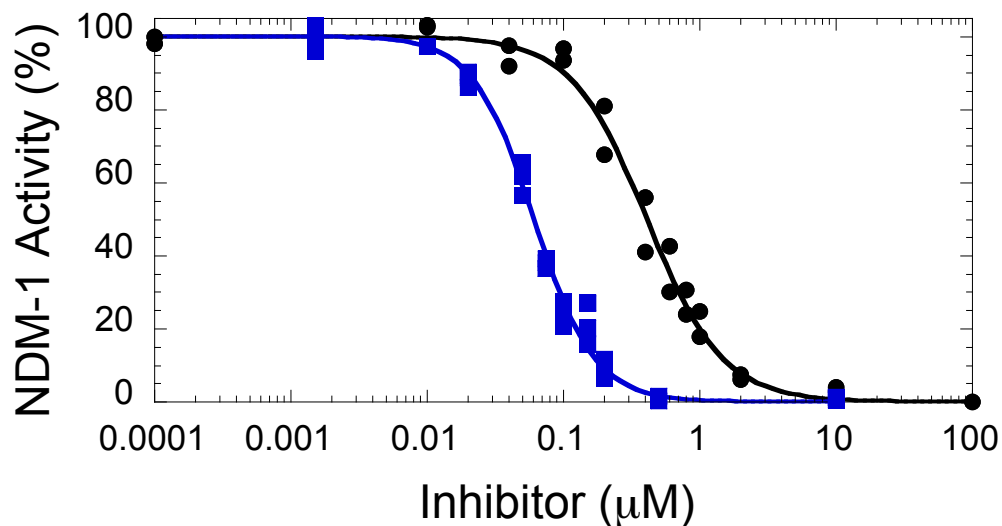


Figure 2-3. Example IC_{50} determinations for **DPA** (●, 410 nM) and **36** (■, 80 nM) utilizing fluorocillin substrate.

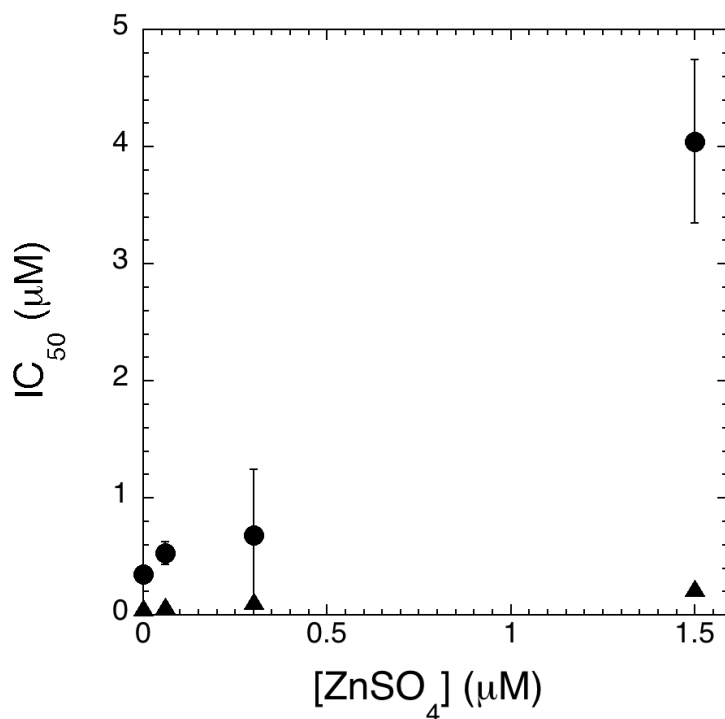


Figure 2-4. IC_{50} variation with excess exogenous Zn(II). IC_{50} values for inhibition of NDM-1 by **DPA** (●, 3 replicates), or **36** (▲, 4 replicates) were determined at varying concentrations of exogenous $ZnSO_4$ using fluorocillin as the reporter substrate and NDM-1 (final concentration at 0.025 nM).

In comparison with the most potent NDM-1 inhibitor reported at the time of publication, a diamino-substituted cyclic boronate inhibitor ($IC_{50} = 4 \text{ nM}$),⁶ **36** is a smaller, achiral compound with a higher LE (0.5 versus 0.4 (kcal/mol)/non-H atom).²² Furthermore, a review profiling 3,200 antibacterial project compounds with whole-cell activity found that active compounds against Gram-negative bacteria have an average of calculated LogD (cLogD pH 7.4) of <10 .²³ The cLogD_{7.4} of **36** (−5.19 to −4.48) falls into the typical hydrophobic region of such antibacterial drugs. Structural determination of the ternary complex between **36** with NDM-1 will be required to reveal the precise active site interactions, but molecular modeling suggests that placement of the **DPA** scaffold at the di-Zn(II) active site may position the 4-aryl substituent near the hydrophobic base of the active-site β -hairpin loop L3 and situate the meta-substituent close to L10.

2.2.4 Investigation of Inhibitor Selectivity

To determine the selectivity of **36** for MBLs, compound **36** was screened against two other B1 MBLs and a panel of other clinically relevant Zn(II)-dependent metalloenzymes. Despite the sequence diversity among B1 MBLs, the elaboration of **DPA** to **36** resulted in the enhancement of potency for inhibition against both VIM-2 and IMP-1 (Table 2-5). Next, inhibitor **36** was screened against a panel of Zn(II)-dependent metalloenzymes including histone deacetylases (HDACs),²⁴ matrix metalloproteinases (MMPs),²⁵ and human carbonic anhydrase (hCAII)²⁶ (Table 2-6). Screening protocols followed previously published procedures²⁷⁻²⁸ and values are reported as percent inhibition. At a concentration of 10 μ M (significantly higher than the IC₅₀ value against NDM-1), compound **36** showed some inhibition against MMP-2 and MMP-12 but did not show inhibition against HDAC-1, HDAC6, and hCAII. Testing **36** at higher concentrations (50 – 100 μ M) resulted in some inhibition of these metalloenzymes; however, the inhibition values were <50% (data not shown). On the basis of the data obtained, compound **36** is between 100- and 1000-fold more selective for NDM-1 than for MMPs, between 500- and 1000-fold more selective for HDACs, and at least 500-fold more selective than for hCAII. Overall, **36** has strong activity against MBLs (NDM-1, IMP-1, VIM-2) and no significant inhibition of other Zn(II)-dependent metalloenzymes (at concentrations of \leq 10 μ M). This data demonstrates the potential for **36** to be broad-spectrum MBL inhibitor that does not exhibit off-target inhibition.

Table 2-5. Inhibitory activity of **DPA** and **36** against B1 MBLs. Inhibition values were obtained via monitoring the MBL-catalyzed hydrolysis of substrate fluorocillin.

Compound	IC ₅₀ (μM)		
	NDM-1	VIM-2	IMP-1
DPA	0.41±0.02	1.66±0.03	3.03±0.04
36	0.080±0.002	0.21±0.01	0.24±0.01

Table 2-6. Percent inhibition of **36** (at 10 μM) against Zn(II)-metalloenzymes.

Compound	MMP-2	MMP-12	HDAC-1	HDAC-6	hCAII
36	<6	48±8	no inhibition	no inhibition	no inhibition

2.2.5 Determination of Mode of Inhibition

¹H NMR Spectroscopy. In previous work, we examined a series of M_{1,2}(II)-substituted analogs of NDM-1 (M_{1,2} = Co, Cd, Zn) by ¹H NMR.²⁹⁻³⁰ Comparing the CoCd and ZnCo analogs of NDM-1, we assigned several resonances in the rich spectrum displayed by the di-Co(II) enzyme (shown at the bottom of each panel in Figure 2-5). The solvent exchangeable resonances at 78, 73, and 65 ppm are ascribed to the three Co(II)-coordinated histidines at the Zn₁ site, while the peak at 107 ppm is assigned to the NH proton from His263 coordinated to Co(II) in the Zn₂ site. The sharp resonance at 47 ppm can be attributed to the β-CH₂ pair of Asp120, coordinated to Co(II) at the Zn₂ site, while the poorly resolved doublet near 170 ppm arises from β-CH₂ protons of the Co(II)-bound cysteine at the same site. In addition, several poorly resolved resonances attributed to secondary interactions between Co(II) in the Zn₂ site and distant residues in the substrate-binding pocket are seen in the range from +40 to -80 ppm.

With a paramagnet in both sites and the ability to attribute many of the signals to either the Zn₁ or Zn₂ site, we used these signatures to examine the metal-binding properties of the individual inhibitors. di-Co(II) NDM-1 was titrated with increasing molar equivalents of **DPA** and **36** (Figure 2-5), along with a known competitive inhibitor (L-captopril)³¹ and a known chelator ethylenediaminetetraacetic acid (EDTA) as controls (Figure 2-6). Each titration was compared to control spectra from an aqueous solution of the inhibitor and Co(II), in the absence of protein (Figure 2-7). The NDM-1 titrations with L-captopril and EDTA gave results as expected, with L-captopril forming a ternary

complex (Figure 2-6A) and EDTA (Figure 2-6B) indiscriminately removing metal. The titration with **DPA** (Figure 2-5A) shows evidence of metal removal at 1 equivalent, with the appearance of four very sharp, intense resonances at 102, 91, 37, and 30 ppm, consistent with the formation of the $\text{Co}(\text{DPA})_n$ adducts seen in control spectra. However, the rest of the spectrum is largely unaffected, suggesting that **DPA** indiscriminately removes metal ions, and shows no changes that can be attributed to an NDM-1:Co(II):**DPA** ternary complex. Additional added **DPA** simply resulted in the removal of both metal ions in the NDM-1 active site and further loss in signal intensity. Titration of di-Co(II) NDM-1 with the **DPA** derivative **36** (Figure 2-5B) shows some evidence for metal ion removal; however, unlike **DPA**, **36** also shows evidence of a ternary complex formation. The addition of 1 equivalent of **36** led to a set of sharp resonances that indicate $\text{Co}(\text{36})_n$ formation. Although it is not possible to directly compare the intensity of these sharp lines to the broader lines of the Co(II) ligand protons, the relative intensity of these lines to those from $\text{Co}(\text{DPA})_n$ at 1 equivalent of added **DPA** is significantly lower. Meanwhile, at least two new resonances (red markers at ~125 and ~30 ppm) attributed to an NDM-1:Co(II):**36** ternary complex appears. At 2 equivalents of **36**, substantial metal removal is apparent, evidenced by a loss of intensity particularly from the Zn_2 site ligands, suggesting **36** shows some preference for the formation of a ternary complex.

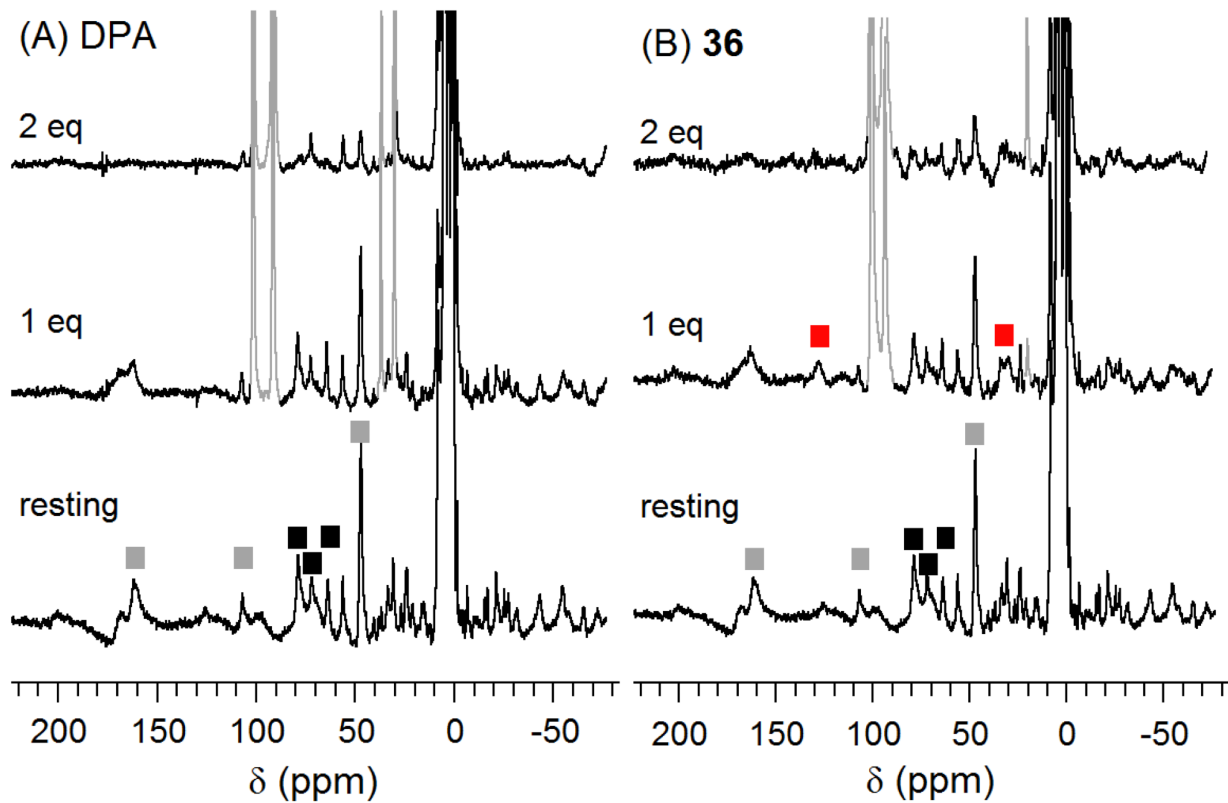


Figure 2-5. 300 MHz ¹H NMR titrations of di-Co(II) NDM-1 with (A) **DPA** and (B) **36**. Resonances assigned to Zn₁ ligands (black squares), Zn₂ ligands (gray squares) and a ternary complex formation (red squares) are marked.

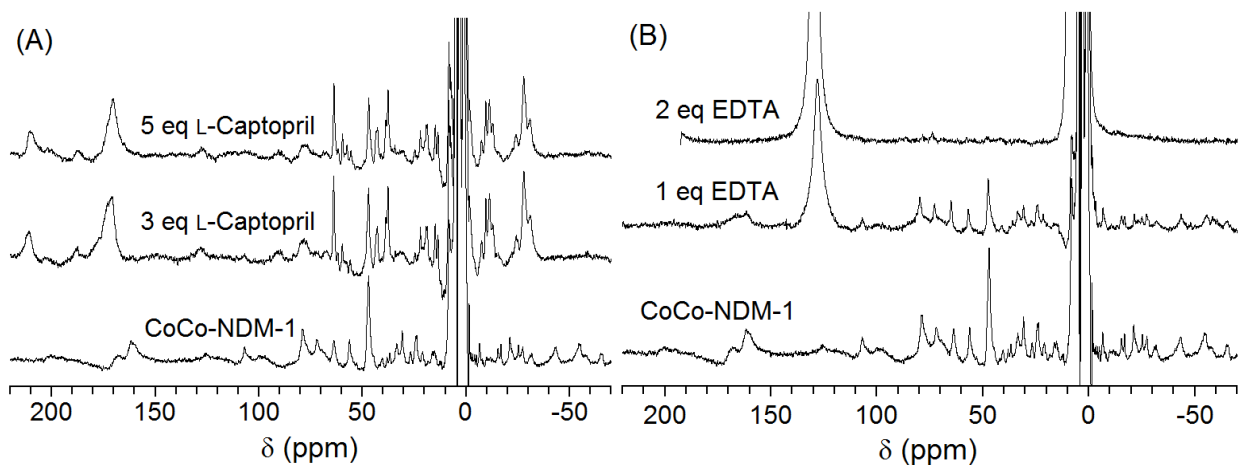


Figure 2-6. Control titrations. 300 MHz ^1H NMR spectra of di-Co(II) NDM-1 titrated with (A) L-captopril and (B) EDTA.

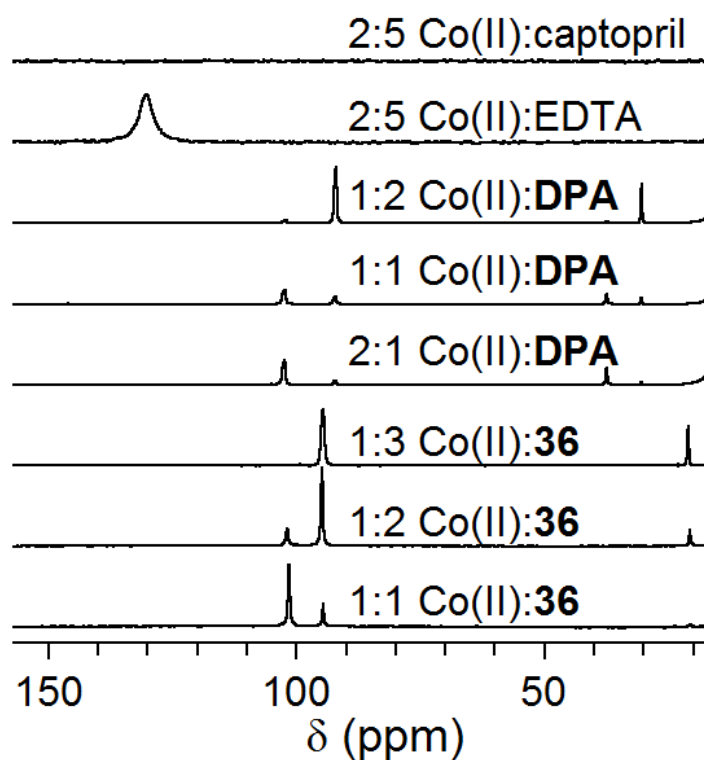


Figure 2-7. 300 MHz ^1H NMR of various combinations of CoCl_2 and the compounds under study in the absence of NDM-1.

EPR Spectroscopy. To gain a better understanding of the ternary complex formed, we turned to EPR spectroscopy. As can be seen in Figure 2-8, the addition of 1 equivalent of **DPA** and **36** (similar to L-captopril, data not shown) led to minimal perturbation of the spectra, aside from minor modulation of the line shapes, when compared to the resting di-Co(II) NDM-1 spectra. The reason for small perturbations produced by L-captopril in the EPR spectra of NDM-1 is unknown but consistent with similar previous findings.³² This suggests the electronic structure of the Co(II) ions, and their physical structures, by extension, are largely unchanged. However, as shown in the inset, the addition of **36** led to a new feature near 600 G, which has been seen in EPR studies of MBLs in the presence of substrates during turnover.³³ This feature, indicative of a more tightly coupled di-Co(II) site, is suggestive of an additional bridging species, arising from the weak ferromagnetic coupling of the Co(II) ions. This can be more readily seen in the parallel mode spectra, which shows a deep negative feature (~800 G) that appears on the addition of 1 equivalent of **DPA** and **36**. These data indicate not only the formation of a ternary complex but also bridging binding modes for both **DPA** and the synthesized inhibitor.

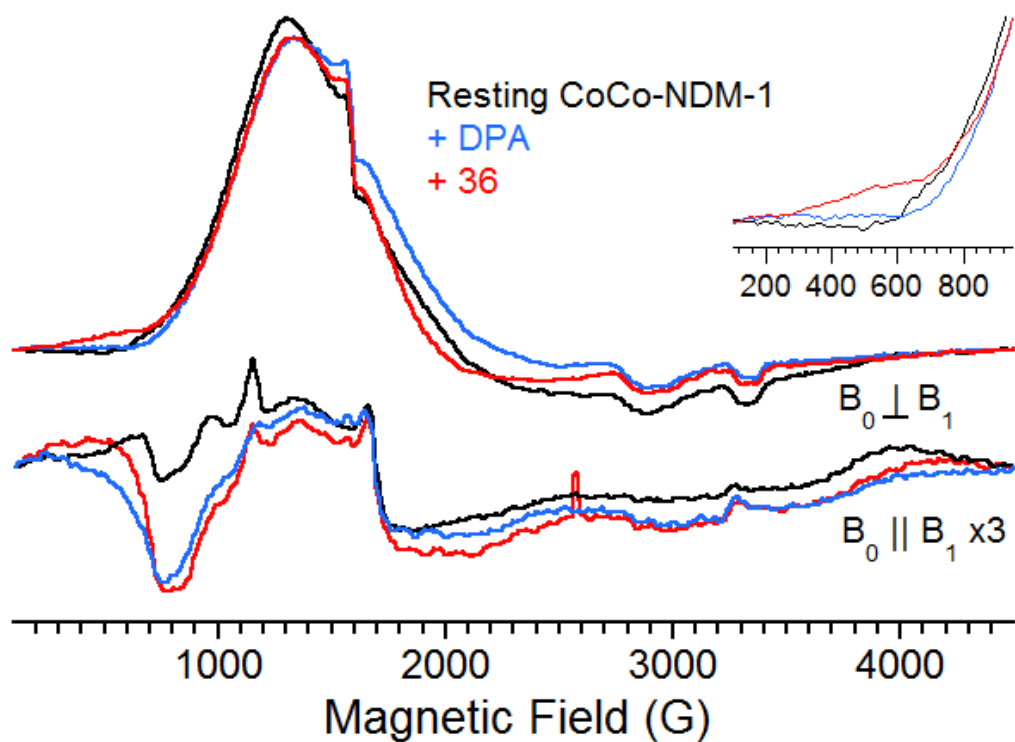


Figure 2-8. X-band EPR spectroscopy of di-Co(II) NDM-1 (black) and di-Co(II) NDM-1 with 1 equivalent of added **DPA** (blue) and **36** (red). Inset: Expansion of the low-field region of the perpendicular mode spectra.

UV-Visible Spectroscopy. Previously, UV-vis spectroscopy has been used to probe Co(II) binding to NDM-1. The optical spectrum of di-Co(II) NDM-1 presented here (Figure 2-9A) is identical to that previously published, with ligand field transitions in the 500–700 nm region²⁹ from protein-bound high-spin Co(II) (the small absorbance at 420 nm has previously been attributed to the presence of Co(III)).³⁴ Control spectra from buffered solutions of Co(II) in the presence of 2 equivalents of EDTA, captopril, **DPA**, or **36** (Figure 2-10) showed minimal absorbance in the ligand field region suggesting that the presence or absence of the ligand field bands can serve as a marker for protein-bound Co(II). Titration of di-Co(II)NDM-1 with 1 equivalent of EDTA results in a small reduction of the intensities of all four ligand field transitions, suggesting removal of small amounts of Co(II). A second equivalent of EDTA results in complete loss of the ligand field transitions, indicating that EDTA fully removed Co(II) from the active site of NDM-1 (Figure 2-9A). Conversely, the titration of di-Co(II) NDM-1 with competitive inhibitor L-captopril (Figure 2-9B) results in a change in the shape of the ligand field bands but no loss in intensity. While the inclusion of a second sulfur atom in the ligand set will surely complicate the interpretation of the captopril spectra, the retention of d–d band intensity strongly suggests the formation of an NDM-1:Co(II):captopril ternary complex.

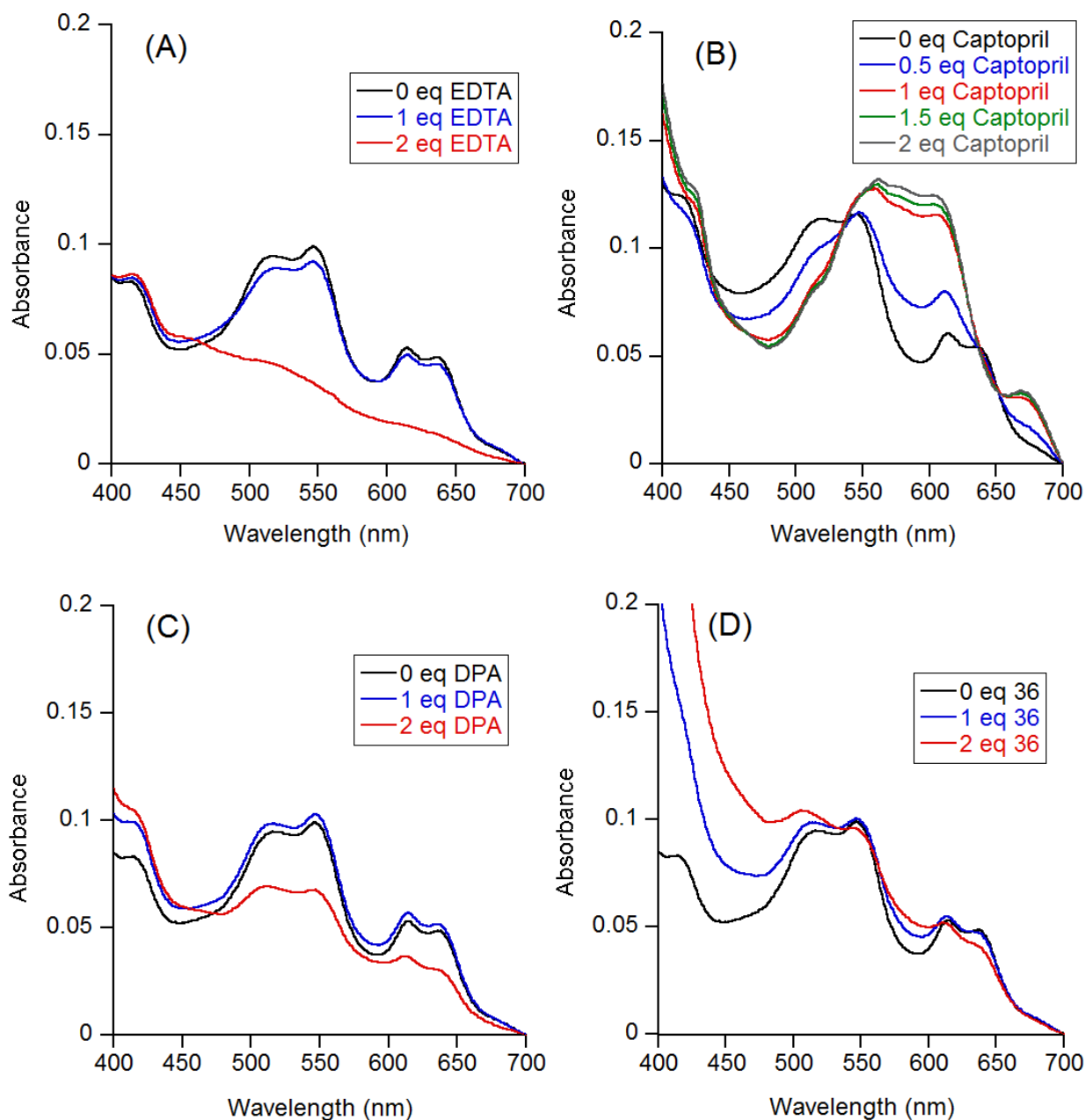


Figure 2-9. UV-vis spectroscopy of di-Co(II) NDM-1 (black lines) and di-Co(II) NDM-1 (300 μ M) with (A) EDTA and (B) L-captopril as control, and 1 – 2 equivalents of added (C) **DPA**, and (D) **36**.

Titration of di-Co(II) NDM-1 with **DPA** was similar to that with EDTA, with the addition of the first equivalent of **DPA** resulting in a reduction in the ligand field intensity (Figure 2-9C), and a more dramatic reduction at 2 equivalents of **DPA**. While these

data indicate that Co(II) is being removed from the active site, the retention of some ligand field intensity at 2 equivalents of **DPA** shows that **DPA** does not bind Co(II) as tightly as EDTA.³⁵ Meanwhile, titration of di-Co(II) NDM-1 with **36** (Figure 2-9D) up to 2 equivalents shows minimal loss of d-d band intensity, suggesting minimal removal of the active site metal ion. The only perturbation produced by **36** is a strong charge-transfer transition at ~320 nm (an internal π - π^* transition of **36**) that alters the background associated with the ligand field region.

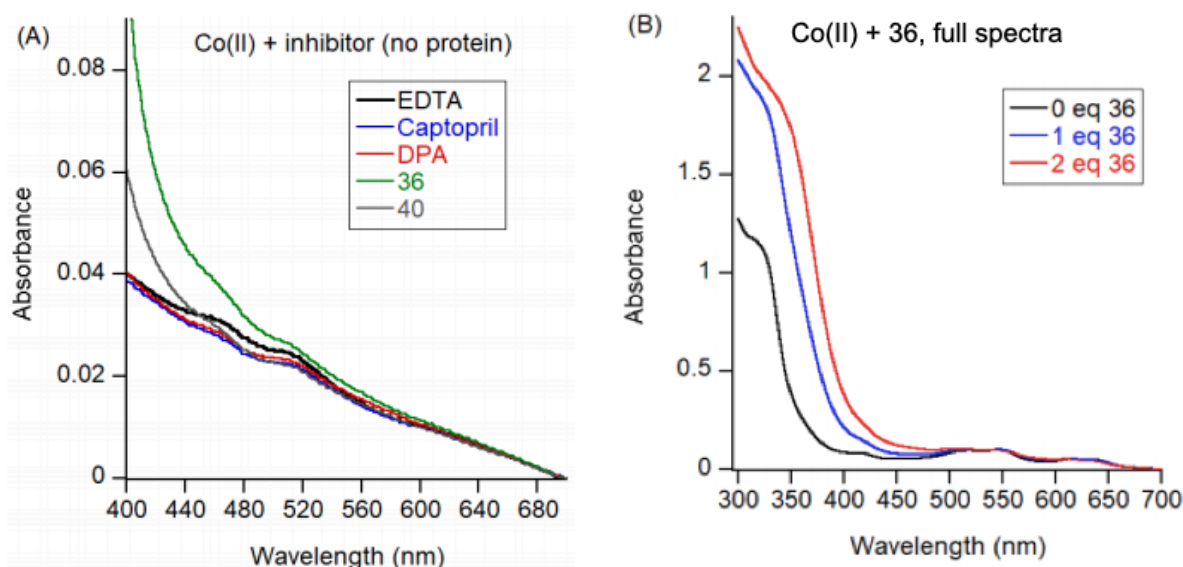


Figure 2-10. (A) Control optical spectra of a buffered Co(II) solution, in the presence of the various inhibitors under study; (B) Full spectra for the titration of Co(II) with **36**.

Equilibrium Dialysis. To be certain the mode of inhibition determined above is representative of the di-Zn(II) enzymes, equilibrium dialysis studies were conducted. Not surprisingly, the Zn(II) content of NDM-1 was significantly reduced when incubated with the metal chelator EDTA, while the Zn(II) content did not change upon incubation with L-captopril (Figure 2-11). Incubation of NDM-1 with **DPA** resulted in a significant loss in Zn(II) content albeit not as much as EDTA at similar concentrations. Unlike **DPA** or EDTA, **36** behaves more like L-captopril. At low concentrations of **36**, incubation with NDM-1 resulted in no significant removal of Zn(II); only upon exposure to higher concentrations of these compounds (~24 μM , about 240-fold greater than the IC_{50} value) was 10–20% of the Zn(II) removed from NDM-1. This result further supports that the mode of inhibition exhibited by **36** is through the formation of a NDM-1:Zn(II):**36** ternary complex rather than metal stripping, even at micromolar concentrations.

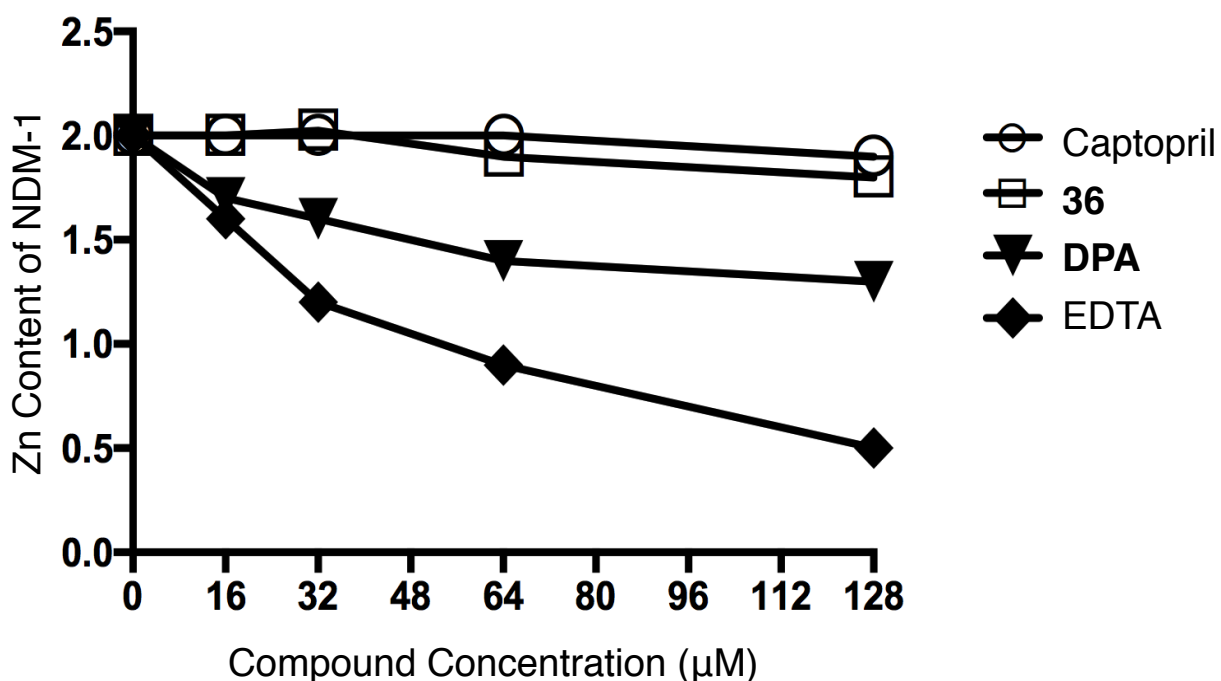


Figure 2-11. Metal content of NDM-1 (8 μM) after dialysis with various concentrations of EDTA, L-captopril, **DPA**, and **36** in 50 mM HEPES, pH 7.5, buffer.

Tryptophan Fluorescence. Previously, stopped-flow fluorescence studies were used to probe the kinetic mechanism of NDM-1.²⁹⁻³⁰ These studies revealed that the binding of the substrate results in a rapid decrease in fluorescence, and as the substrate is hydrolyzed and the product is released, there is a rate-limiting return of fluorescence intensity. We attributed these fluorescence properties to Trp87 (standard BBL numbering, Trp93 in NDM numbering), which is 5.7 Å from the Zn(II) binding site. As before, we utilized EDTA and L-captopril as controls to evaluate how a metal chelator versus a competitive inhibitor affects the fluorescence properties of NDM-1. Incubation of 2 μM NDM-1 with up to 32 μM EDTA resulted in <10% quenching of intrinsic tryptophan fluorescence (Figure 2-12A). Conversely, incubation of NDM-1 with up to 32 μM L-captopril resulted in a 10% increase in fluorescence, indicating a different binding mode for this compound. The increase in fluorescence is likely due to the interaction of C3 and C5 in L-captopril with Trp87.³¹

Incubation of NDM-1 with **DPA** resulted in a 20% quenching of tryptophan fluorescence emission (at 32 μM **DPA** where 20% of the Zn(II) was removed, as shown in Figure 2-11). In contrast, incubation of NDM-1 with **36** resulted in a 50–60% quenching of the intrinsic tryptophan fluorescence (Figure 2-12A). Due to the aromatic ring in **36**, we attribute the quenching of fluorescence to be due to the binding of these compounds to the metal center, resulting in a change in the fluorescence properties of Trp87. In support of this hypothesis, a control titration of L-tryptophan with EDTA, L-captopril, and **36** was performed. The titration of L-tryptophan with EDTA and L-captopril results in no change in the fluorescence emission of tryptophan, while titration with **36**

results in a 50% reduction of fluorescence emission (Figure 2-12B). The results from fluorescence titrations are consistent with those from previous analysis, which indicate compound **36** is binding in the active site, forming a ternary NDM-1:Zn(II):**36** complex.

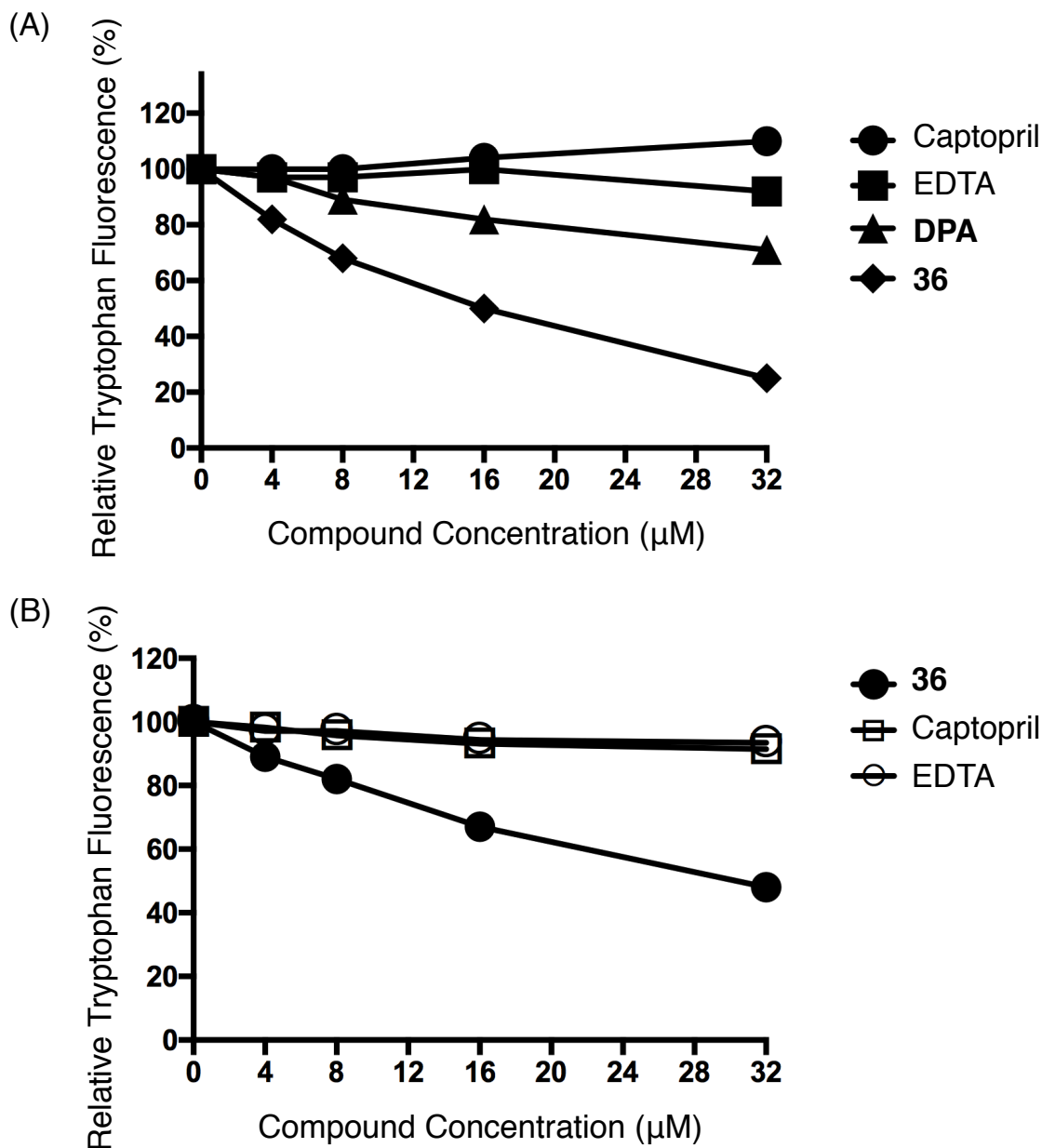


Figure 2-12. (A) Relative intrinsic tryptophan fluorescence emission versus concentration of inhibitor; (B) Relative intrinsic tryptophan fluorescence emission versus concentration of **36**, L-captopril and EDTA. The concentration of NDM-1 was 2 μM, L-tryptophan was 2 μM and the buffer for both studies was 50 mM HEPES, pH 7.5.

2.2.6 Microdilution Broth Minimum Inhibitory Concentrations (MICs)

Microdilution broth MICs were next performed on *E. coli* and *K. pneumoniae* clinical isolates expressing *bla*_{NDM-1}³⁶ using imipenem and compound **36** (Table 2-7 and Table 2-8). The MICs of imipenem alone were 4 – 16 mg/L. Notably, the addition of compound **36** at 100 mg/L significantly lowered the imipenem MICs (0.5 – 1 mg/L). For all *E. coli* and *K. pneumoniae* strains, no effect on growth was observed with compound **36** alone, indicating a lack of toxicity at these concentrations. Even though standard CLSI guidelines have not yet been established for this imipenem:**36** combination, the reduction in MICs from 8 – 16 mg/L to 0.5 – 1 mg/L for the clinical strains would represent a reduction in MICs from “resistant” to “susceptible” range. These results serve as an important proof of concept that these exploratory scaffolds are critical starting points for novel design strategies. Noteworthy, the β -lactam resistance profile in the selected strains is mediated by both extended-spectrum β -lactamases (ESBLs) (*bla*_{CTX-M-15}) and plasmid-mediated AmpCs (*bla*_{CMY-2}). A therapeutic combination of imipenem and **36** able to overcome the complex background of a MBL, ESBL, and plasmid-mediated AmpC is notable. Furthermore, growth and morphology of cultured human HEK293 cells were not adversely affected by **36** at concentrations relevant to the MIC studies (Figure 2-13 and Figure 2-14).

Table 2-7. Microdilution broth MICs of clinical *E. coli* Isolates Expressing *bla*_{NDM-1}. All strains possess *bla*_{CTX-M-15} and *bla*_{CMY-2} except for *E. coli* Ah8.74 which possesses only *bla*_{NDM-1}.

<i>E. coli</i> Isolates	MICs (mg/L)	
	Imipenem	Imipenem + 36
Ch8.68	16	1
Ch8.69	4	0.5
Ch8.70	16	0.5
Ah8.71	16	1
Ch8.72	16	0.5
Ah8.73	16	0.5
Ah8.74	8	0.5
Ah8.75	16	0.5

Table 2-8. Microdilution broth MICs of clinical *K. pneumoniae* isolates expressing *bla*_{NDM-1}. Strains Cm1.62 and Cm1.63 possess *bla*_{CTX-M-15} and *bla*_{CMY-2}. Strain Pd1.48 possesses *bla*_{SHV-12} and *bla*_{CTX-M-15}. Strains Pd1.49, Pd1.50, Pd1.53, Pd1.54, and Pd1.55 possess *bla*_{CTX-M-15}.

<i>K. pneumoniae</i> Isolates	MICs (mg/L)	
	Imipenem	Imipenem + 36
Pd1.48	8	0.5
Pd1.49	4	1
Pd1.50	8	0.5
Pd1.53	8	0.5
Pd1.54	8	0.5
Pd1.55	8	0.5
Cm1.62	16	1
Cm1.63	8	1

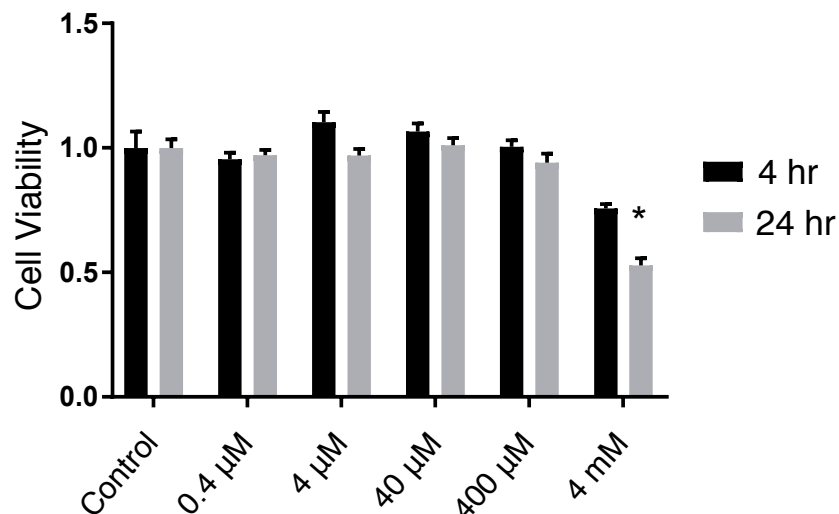


Figure 2-13. HEK293 cells cultured in the presence of vehicle-only or **36** showed no statistical difference in cell viability at concentrations of **36** up to 400 μM, the highest concentration used in MIC determinations. Much higher concentrations (4 mM) of **36** cause some cell toxicity that is statistically significant (*represents a p-value <.001 when compared to control values).

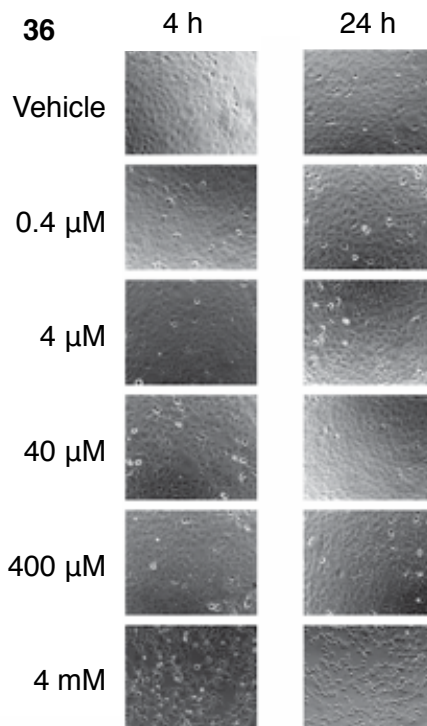


Figure 2-14. HEK293 cells cultured in the presence of 0.4 to 400 μM **36** showed similar morphology to those grown with addition of a vehicle (DMSO) only control. Morphological changes typical of apoptosis were apparent with treatments of a high concentration (4 mM) of **36**, which is 10-fold higher than the concentration used in MIC determinations.

2.3 Conclusion

A FBDD strategy was applied to design potent inhibitors of the most clinically relevant MBLs. Previously, fragment-based approaches have been used for MBL inhibitor discovery.³⁷⁻³⁹ Here, the use of a small MBP fragment library enabled a systematic search for metal-directed inhibitors and identification of the scaffold **DPA**, which shares structural aspects of a hydrolyzed β -lactam product. Through the synthesis and screening of three sublibraries, 4-(3-aminophenyl)pyridine-2,6-dicarboxylic acid (**36**) was identified as a broad spectrum potent inhibitor of NDM-1, IMP-1, and VIM-2, arguably the most clinically important MBLs, with no significant inhibition of other Zn(II)-dependent metalloenzymes. A focus on screening metal-binding fragments to target the most conserved feature of MBLs and the criteria of inhibiting three different MBLs in the primary screen may have contributed to the success of this strategy in developing a potent pan-MBL inhibitor. Detailed spectroscopic characterization (¹H NMR, EPR, equilibrium dialysis, intrinsic tryptophan fluorescence emission, and UV-Vis) of the enzyme, inhibitor, metal:**36**, and the enzyme:metal:**36** ternary complexes reveal that optimization of IC₅₀ values correlated with a tighter formation of the ternary NDM-1:Zn(II):**36** complex. This work serves as a roadmap for converting a hit with metal-stripping tendencies into a potent metalloprotein-binding ligand. Microdilution broth MICs performed on a panel of highly-resistant clinical *E. coli* and *K. pneumoniae* strains harboring *bla*_{NDM-1} reveal that in all cases, **36** reduced imipenem MICs to a “susceptible” range and did not exhibit cytotoxicity against bacterial cells or human HEK293 cells. Compound **36** represents a

new type of non-toxic, potent, pan-MBL inhibitor that is effective against clinical strains of carbapenem-resistant Enterobacteriaceae.

2.4 Experimental

All reagents and solvents were obtained from commercial sources and used without further purification. Nunc 96-well polystyrene clear flat bottom microplates, Corning black polypropylene round-bottom 96-well microplates, Costar black polystyrene round-bottom 96-well microplates, Costar clear polystyrene flat-bottom 96-well microplates, 3-((3-cholamidopropyl) dimethylammonio)-1-propanesulfonate (CHAPS), 4-(2-hydroxyethyl)-1-piperazineethanesulfonic acid (HEPES), dimethyl sulfoxide (DMSO), and ethylenediaminetetraacetic acid (EDTA) and Fluorocillin green 495/525 β -lactamase substrate, soluble product, were purchased from ThermoFisher Scientific Inc. (Fair Lawn, NJ). Chromacef was a generous gift from Dr. Larry Sutton (Benedictine College, Atchison, KS).⁴⁰ ([1,1'-Biphenyl]-4-ylsulfonyl)-D-phenylalanine (NSA) was prepared by literature methods.⁴¹ All other reagents were purchased from Sigma-Aldrich Inc. (St. Louis, MO). High-throughput screening and chromacef assays were performed on a Perkin Elmer Victor 3V 1420 Multilabel Counter plate reader. Fluorescent assays were performed on a PerkinElmer Victor ³V fluorescent plate reader. Inhibitor selectivity absorbance and fluorescence assays were performed using a BioTek Synergy HT microplate reader. Microwave reactions were performed in 10 mL microwave vials using a CEM Discover S reactor. Column chromatography was performed using a Teledyne ISCO CombiFlash Rf system with prepacked silica cartridges. All ¹H NMR spectra were recorded at ambient temperature using a 400 Varian Mercury FT-NMR instrument located in the Department of Chemistry and Biochemistry at the University of California, San Diego. Low Resolution mass

spectrometry (MS) data were obtained from the University of California San Diego Chemistry and Biochemistry Mass Spectrometry Facility. The purity of all compounds used in the assays was determined to be $\geq 95\%$ by ^1H NMR spectroscopy and high-performance liquid chromatography (HPLC).

Steady State Kinetic Parameters for Fluorocillin with NDM-1

The difference in the extinction coefficient was determined for the hydrolysis of fluorocillin. The spectra of a solution of fluorocillin (50 μM) in 50 mM HEPES, 2 mM CHAPS at pH 7.0, were recorded before and after addition of NDM-1 (18 nM). The maximum difference in absorption occurred at 490 nm, reflecting a difference in the extinction coefficient between substrate and product of $\Delta\epsilon_{490} = 6683 \text{ M}^{-1}\text{cm}^{-1}$. Using this extinction coefficient, initial rates of fluorocillin (0 – 4 μM) hydrolysis as catalyzed by NDM-1 (2 nM) in 50 mM HEPES, 2 mM CHAPS at pH 7.0, at 25 $^\circ\text{C}$, were recorded and fit to the Michaelis-Menten equation to derive K_M ($0.46 \pm 0.06 \mu\text{M}$), k_{cat} ($68 \pm 3 \text{ s}^{-1}$), and k_{cat}/K_M ($1.5 \times 10^8 \text{ M}^{-1}\text{s}^{-1}$) values.

Synthesis

Dimethyl pyridine-2,6-dicarboxylate (1). DPA (1 g, 5.98 mmol) was dissolved in MeOH (1 L) and concentrated H_2SO_4 (0.5 mL) was added dropwise to the solution. The reaction mixture was heated to reflux for 24 h and monitored via TLC. Once the reaction was completed by TLC, the solvent was removed by evaporation in vacuo to afford 1 as a white crystalline solid in 100% yield (1.16 g, 5.96 mmol). No further

purification was needed. ^1H NMR (400 MHz, DMSO- d_6): δ 8.26-8.13 (m, 3H), 3.90 (s, 6H). ESI-MS(+) calculated for $[\text{C}_9\text{H}_{10}\text{NO}_4]^+$ m/z 196.06, found m/z 196.09 $[\text{M}+\text{H}]^+$.

6-(Methoxycarbonyl)picolinic acid (2). Dimethyl pyridine-2,6-dicarboxylate (1.9 g, 9.92 mmol) was dissolved in MeOH (75 mL) and cooled to 0 °C. KOH pellets (557 mg, 9.92 mmol) were added to the solution portion-wise and stirred at 0 °C for an additional 4 h. Once the reaction was completed, the MeOH was removed by evaporation in vacuo. The white salt was washed with copious amounts of EtOAc to remove any remaining starting material. The salt was then dissolved in water (25 mL) and solution was acidified with 4M HCl to pH 2. The aqueous solution was extracted with chloroform (25 mL \times 3) and the combined organic layers were dried over MgSO_4 . MgSO_4 was removed by vacuum filtration and the organic layer was dried by evaporation in vacuo to afford 2 as a white powder in 81% yield (1.45 g, 8.00 mmol). ^1H NMR (400 MHz, DMSO- d_6): δ 8.23-8.14 (m, 3H), 3.90 (s, 3H). ESI-MS(-) calculated for $[\text{C}_8\text{H}_6\text{NO}_4]^-$ m/z 180.03, found m/z 180.09 $[\text{M}-\text{H}]^-$.

General synthetic procedures for compounds 3 – 20.

6-(Methoxycarbonyl)picolinic acid (200 mg, 1.10 mmol), EDC (1 equivalent) and HOBT (1.1 equivalents) were dissolved in dry DMF (10 mL) and the reaction mixture was stirred at room temperature for 30 min. The corresponding amine (1.1 equivalents) was then added and the reaction mixture and allowed to react at room temperature overnight. DMF was dried by evaporation in vacuo, and the reaction was taken up in

EtOAc (10 mL), and extracted with copious amounts of saturated NaHCO₃ (10 mL×3). The organic layer was dried by evaporation in vacuo and purified by EtOAc and hexane column chromatography. Hydrolysis was then performed by stirring the product in a solution of 1M NaOH (4 mL) and THF (1 mL) at room temperature. Once the hydrolysis was completed, the solution was acidified with 4M HCl to pH 4 and the precipitate was collected via vacuum filtration.

6-(Phenylcarbamoyl)picolinic acid (3). Yield: 85% (227 mg, 0.937 mmol). ¹H NMR (400 MHz, MeOD-*d*₄): δ 8.45 (d, *J*=7.6 Hz, 1H), 8.36 (d, *J*=6.8 Hz, 1H), 8.21 (m, 1H), 7.86 (d, *J*=7.6 Hz, 2H), 7.34 (t, *J*=7.6 Hz, 2H), 7.17 (t, *J*=7.2 Hz, 1H). ESI-MS(-) calculated for [C₁₃H₉N₂O₃]⁻ *m/z* 241.06, found *m/z* 241.03 [M-H]⁻.

6-(Benzylcarbamoyl)picolinic acid (4). Yield: 87% (185 mg, 0.722 mmol). ¹H NMR (400 MHz, MeOD-*d*₄): δ 8.34 (d, *J*=7.2 Hz, 1H), 8.30 (d, *J*=7.2 Hz, 1H), 8.15 (m, 1H), 7.38-7.23 (m, 5H), 4.63 (s, 2H). ESI-MS(-) calculated for [C₁₄H₁₁N₂O₃]⁻ *m/z* 255.08, found *m/z* 255.23 [M-H]⁻.

6-(Phenethylcarbamoyl)picolinic acid (5). Yield: 77% (231 mg, 0.853 mmol). ¹H NMR (400 MHz, MeOD-*d*₄): δ 8.31-8.29 (m, 2H), 8.15 (m, 1H), 7.27-7.26 (br s, 4H), 7.19 (t, *J*=4 Hz, 1H), 3.66 (t, *J*=7.6 Hz, 2H), 2.95 (t, *J*=7.6 Hz, 2H). ESI-MS(-) calculated for [C₁₅H₁₃N₂O₃]⁻ *m/z* 269.09, found *m/z* 269.13 [M-H]⁻.

6-((4-Methoxyphenyl)carbamoyl)picolinic acid (6). Yield: 79% (237 mg, 0.871 mmol). ^1H NMR (400 MHz, MeOD- d_4): δ 8.41 (d, J = 8 Hz, 1H), 8.33 (d, J = 7.6 Hz, 1H), 8.19 (m, 1H), 7.75 (d, J = 8.8 Hz, 2H), 6.94 (d, J = 8.8 Hz, 2H), 3.80 (s, 3H). ESI-MS(-) calculated for $[\text{C}_{14}\text{H}_{11}\text{N}_2\text{O}_4]^-$ m/z 271.07, found m/z 271.17 $[\text{M}-\text{H}]^-$.

6-((4-Methoxybenzyl)carbamoyl)picolinic acid (7). Yield: 81% (255 mg, 0.891 mmol). ^1H NMR (400 MHz, MeOD- d_4): δ 8.34 (d, J =8 Hz, 1H), 8.30 (d, J =7.6 Hz, 1H), 8.16 (m, 1H), 7.30 (d, J =7.6 Hz, 2H), 6.87 (d, J =8 Hz, 2H), 4.55 (s, 2H), 3.76 (s, 3H). ESI-MS(-) calculated for $[\text{C}_{15}\text{H}_{13}\text{N}_2\text{O}_4]^-$ m/z 285.08, found m/z 285.16 $[\text{M}-\text{H}]^-$.

6-((Benzo[d][1,3]dioxol-5-ylmethyl)carbamoyl)picolinic acid (8). Yield: 35% (116 mg, 0.386 mmol). ^1H NMR (400 MHz, MeOD- d_4): δ 8.33 (d, J =15.2 Hz, 1H), 8.31 (d, J =14.8 Hz, 1H), 8.16 (m, 1H), 6.88-6.75 (m, 3H), 5.91 (s, 2H), 4.53 (s, 2H). ESI-MS(-) calculated for $[\text{C}_{15}\text{H}_{11}\text{N}_2\text{O}_5]^-$ m/z 299.07, found m/z 299.04 $[\text{M}-\text{H}]^-$.

6-((Furan-2-ylmethyl)carbamoyl)picolinic acid (9). Yield: 79% (216 mg, 0.877 mmol). ^1H NMR (400 MHz, MeOD- d_4): δ 8.34-8.29 (m, 2H), 8.16 (m, 1H), 7.44 (s, 1H), 6.36-6.34 (m, 2H), 4.62 (s, 2H). ESI-MS(-) calculated for $[\text{C}_{12}\text{H}_9\text{N}_2\text{O}_4]^-$ m/z 245.06, found m/z 245.20 $[\text{M}-\text{H}]^-$.

6-((Thiophen-2-ylmethyl)carbamoyl)picolinic acid (10). Yield: 77% (223 mg, 0.850 mmol). ^1H NMR (400 MHz, MeOD- d_4): δ 8.34 (d, J =7.6 Hz, 1H), 8.30 (d, J =7.6 Hz, 1H),

8.16 (m, 1H), 7.29 (d, $J=4.8$ Hz, 1H), 7.08 (s, 1H), 6.96-6.94 (m, 1H), 4.79 (s, 2H). ESI-MS(-) calculated for $[\text{C}_{12}\text{H}_9\text{N}_2\text{O}_3\text{S}]^-$ m/z 261.03, found m/z 261.18 $[\text{M}-\text{H}]^-$.

6-((2-(Thiophen-2-yl)ethyl)carbamoyl)picolinic acid (11). Yield: 78% (231 mg, 0.836 mmol). ^1H NMR (400 MHz, MeOD- d_4): δ 8.31-8.29 (m, 2H), 8.15 (m, 1H), 7.19-7.18(m, 1H), 6.91 (br s, 2H), 3.69 (t, $J=7.2$ Hz, 2H), 3.18 (t, $J=7.2$ Hz, 2H). ESI-MS(-) calculated for $[\text{C}_{13}\text{H}_{11}\text{N}_2\text{O}_3\text{S}]^-$ m/z 275.05, found m/z 275.07 $[\text{M}-\text{H}]^-$.

6-((Thiazol-2-ylmethyl)carbamoyl)picolinic acid (12). Yield: 34% (99 mg, 0.376 mmol). ^1H NMR (400 MHz, MeOD- d_4): δ 8.36-8.32 (m, 2H), 8.19 (m, 1H), 7.73 (s, 1H), 7.53 (s, 1H), 4.95 (s, 2H). ESI-MS(-) calculated for $[\text{C}_{11}\text{H}_8\text{N}_3\text{O}_3\text{S}]^-$ m/z 262.03, found m/z 261.98 $[\text{M}-\text{H}]^-$.

6-((Carboxymethyl)carbamoyl)picolinic acid (13). Yield: 57% (141 mg, 0.627 mmol). ^1H NMR (400 MHz, MeOD- d_4): δ 8.33-8.31(m, 2H), 8.18 (m, 1H), 4.18 (s, 2H). ESI-MS(-) calculated for $[\text{C}_9\text{H}_7\text{N}_2\text{O}_5]^-$ m/z 223.04, found m/z 222.99 $[\text{M}-\text{H}]^-$, 245.13 $[\text{M}+\text{Na}-2\text{H}]^-$, 111.16 $[\text{M}-2\text{H}]^{2-}$.

(R)-6-((1-Carboxy-2-methylpropyl)carbamoyl)picolinic acid (14). Yield: 62% (182 mg, 0.684 mmol). ^1H NMR (400 MHz, MeOD- d_4): δ 8.34-8.32 (m, 2H), 8.17 (m, 1H), 4.53 (d, $J=6$ Hz, 1H), 3.30 (s, 1H), 1.07 (s, 6H). ESI-MS(-) calculated for $[\text{C}_{12}\text{H}_{13}\text{N}_2\text{O}_5]^-$ m/z 265.08, found m/z 265.04 $[\text{M}-\text{H}]^-$, 287.17 $[\text{M}+\text{Na}-2\text{H}]^-$, 303.16 $[\text{M}+\text{K}-2\text{H}]^-$.

6-(Isopropylcarbamoyl)picolinic acid (15). Yield: 74% (170 mg, 0.816 mmol). ^1H NMR (400 MHz, MeOD- d_4): δ 8.33-8.14 (m, 3H), 4.26-4.20 (m, 1H), 1.31 (s, 3H), 1.29 (s, 3H). ESI-MS(-) calculated for $[\text{C}_{10}\text{H}_{11}\text{N}_2\text{O}_3]^-$ m/z 207.08, found m/z 207.08 $[\text{M}-\text{H}]^-$.

6-(Isobutylcarbamoyl)picolinic acid (16). Yield: 71% (130 mg, 0.585 mmol). ^1H NMR (400 MHz, MeOD- d_4): δ 8.33-8.30 (m, 2H), 8.17 (m, 1H), 3.31-3.30 (m, 1H), 3.27 (s, 1H), 3.26 (s, 1H), 0.99 (s, 3H), 0.98 (s, 3H). ESI-MS(-) calculated for $[\text{C}_{11}\text{H}_{13}\text{N}_2\text{O}_3]^-$ m/z 223.11, found m/z 223.09 $[\text{M}+\text{H}]^-$.

6-(Cyclopentylcarbamoyl)picolinic acid (17). Yield: 64% (168 mg, 0.175 mmol). ^1H NMR (400 MHz, MeOD- d_4): δ 8.32-8.28 (m, 2H), 8.15 (m, 1H), 4.38-4.31 (m, 1H), 2.05 (br s, 2H), 1.82 (br s, 2H), 1.66 (br s, 4H). ESI-MS(-) calculated for $[\text{C}_{12}\text{H}_{13}\text{N}_2\text{O}_3]^-$ m/z 233.09, found m/z 233.12 $[\text{M}-\text{H}]^-$.

6-(Cyclohexylcarbamoyl)picolinic acid (18). Yield: 64% (174 mg, 0.701 mmol). ^1H NMR (400 MHz, MeOD- d_4): δ 8.33-8.29 (m, 2H), 8.17-8.13 (m, 1H), 3.98 (br s, 1H), 1.98 (br s, 2H), 1.84 (br s, 2H), 1.71 (d, $J=12$ Hz, 1H), 1.48-1.38 (m, 4H), 1.27 (br s, 1H). ESI-MS(-) calculated for $[\text{C}_{13}\text{H}_{15}\text{N}_2\text{O}_3]^-$ m/z 247.10, found m/z 247.11 $[\text{M}-\text{H}]^-$.

6-(((Tetrahydrofuran-2-yl)methyl)carbamoyl)picolinic acid (19). Yield: 44% (121 mg, 0.484 mmol). ^1H NMR (400 MHz, MeOD- d_4): δ 8.33-8.30 (m, 2H), 8.18-8.14 (m, 1H), 4.17-4.11 (m, 1H), 3.93-3.88(m, 1H), 3.79-3.74 (br s, 1H), 3.75-3.49 (m, 2H), 2.08-

1.86 (m, 3H), 1.73-1.65 (m, 1H). ESI-MS(-) calculated for $[C_{12}H_{13}N_2O_4]^-$ m/z 249.09, found m/z 249.12 $[M-H]^-$.

6-(Piperidine-1-carbonyl)picolinic acid (20). Yield: 58% (151 mg, 0.645 mmol). 1H NMR (400 MHz, MeOD- d_4): δ 8.21 (d, $J=8$ Hz, 1H), 8.12-8.08 (m, 1H), 7.74 (d, $J=7.6$ Hz, 1H), 3.74 (br s, 2H), 3.36 (t, $J=5.6$ Hz, 2H), 1.72 (br s, 4H), 1.60 (br s, 2H). ESI-MS(-) calculated for $[C_{12}H_{13}N_2O_3]^-$ m/z 233.09, found m/z 233.18 $[M-H]^-$.

4-Chloropyridine-2,6-dicarboxylic acid (21). Dimethyl 4-chloropyridine-2,6-dicarboxylate (270 mg, 1.18 mmol) was dissolved in a solution of 1M NaOH (10 mL) and THF (1 mL). The reaction mixture was stirred at 70 °C for 3 h and monitored via TLC. Upon completion of the reaction, THF was removed by evaporation in vacuo. The aqueous solution was washed with EtOAc (20 mL) to remove any remaining starting material. The aqueous phase was acidified with 4M HCl to pH 4 to obtain a yellow precipitate. The precipitate was collected via vacuum filtration and washed with copious amounts of water to afford 21 in 80% yield (190 mg, 0.94 mmol). 1H NMR (400 MHz, DMSO- d_6): δ 8.14 (s, 2H). ESI-MS(-) calculated for $[C_7H_3ClNO_4]^-$ m/z 199.97, found m/z 200.95 $[M-H]^-$.

General Synthetic Procedures for Compounds 22 – 30

In a microwave vessel, 4-chloropyridine-2,6-dicarboxylic acid (50 mg, 0.25 mmol, unless otherwise noted) and the corresponding amine (3 equivalents, unless otherwise

noted) were suspended in water (2 mL). The reaction mixture was heated via microwave irradiation for 30 min at 160 °C. The resulting solution was acidified with 4M HCl to pH 4, and the resulting precipitate was collected via vacuum filtration and washed with cold water.

4-(Dimethylamino)pyridine-2,6-dicarboxylic acid (22). 4-Chloropyridine-2,6-dicarboxylic acid (60 mg, 0.30 mmol) and dimethylamine (1.70 mL, 13.39 mmol). Yield: 64% (40 mg, 0.190 mmol). ¹H NMR (400 MHz, DMSO-*d*₆): δ 7.31 (s, 2H), 3.04 (s, 6H). ESI-MS(-) calculated for [C₉H₉N₂O₄]⁻ *m/z* 209.06, found *m/z* 208.95 [M-H]⁻.

4-(Phenylamino)pyridine-2,6-dicarboxylic acid (23). 4-Chloropyridine-2,6-dicarboxylic acid (70 mg, 0.35 mmol) and aniline (0.104 mL, 1.15 mmol). Yield: 59% (53 mg, 0.205 mmol). ¹H NMR (400 MHz, DMSO-*d*₆): δ 9.90 (s, 1H), 7.54 (s, 2H), 7.48-7.23 (m, 5H). ESI-MS(-) calculated for [C₁₃H₉N₂O₄]⁻ *m/z* 257.06, found 279.19 [M-H+Na]⁻.

4-(Benzylamino)pyridine-2,6-dicarboxylic acid (24). 4-Chloropyridine-2,6-dicarboxylic acid (54 mg, 0.27 mmol) and phenylmethanamine (100 mg, 0.94 mmol). Yield: 14% (10 mg, 0.037 mmol). ¹H NMR (400 MHz, DMSO-*d*₆): δ 8.92 (s, 1H), 7.35-7.03 (m, 7H), 4.56 (br s, 2H). ESI-MS(-) calculated for [C₁₄H₁₁N₂O₄]⁻ *m/z* 271.07, found *m/z* 270.98 [M-H]⁻.

4-(Phenethylamino)pyridine-2,6-dicarboxylic acid (25). Yield: 80% (57 mg, 0.199 mmol). ^1H NMR (400 MHz, $\text{DMSO-}d_6$): δ 7.67 (t, $J=5.6$ Hz, 1H), 7.29-7.19 (m, 7H), 3.45 (q, $J_1=6.4$ Hz, $J_2=4$ Hz, 2H), 2.85 (t, $J=6.8$ Hz, 2H). ESI-MS(-) calculated for $[\text{C}_{15}\text{H}_{13}\text{N}_2\text{O}_4]^-$ m/z 285.09, found 307.21 $[\text{M-H}+\text{Na}]^-$.

4-((4-Methoxyphenyl)amino)pyridine-2,6-dicarboxylic acid (26). Yield: 35% (25 mg, 0.087 mmol). ^1H NMR (400 MHz, $\text{MeOD-}d_4$): δ 7.47 (s, 2H), 7.27 (d, $J=8.8$ Hz, 2H), 7.05 (d, $J=8.8$ Hz, 2H), 3.84 (s, 3H). ESI-MS(-) calculated for $[\text{C}_{14}\text{H}_{11}\text{N}_2\text{O}_5]^-$ m/z 287.07, found, m/z 245.20 $[\text{M-H-CO}_2]^-$.

4-((4-Methoxybenzyl)amino)pyridine-2,6-dicarboxylic acid (27). Yield: 48% (36 mg, 0.119 mmol). ^1H NMR (400 MHz, $\text{DMSO-}d_6$): δ 8.44 (s, 1H), 7.27-6.90 (m, 6H), 4.42 (d, $J=5.6$ Hz, 2H), 2.72 (s, 3H). ESI-MS(-) calculated for $[\text{C}_{15}\text{H}_{13}\text{N}_2\text{O}_5]^-$ m/z 301.08, found m/z 300.98 $[\text{M-H}]^-$.

4-((Benzo[d][1,3]dioxol-5-ylmethyl)amino)pyridine-2,6-dicarboxylic acid (28). Yield: 29% (23 mg, 0.073 mmol). ^1H NMR (400 MHz, $\text{DMSO-}d_6$): δ 8.81 (s, 1H), 7.27 (s, 1H), 7.03 (s, 1H), 6.92-6.81 (m, 3H), 5.99 (s, 2H), 4.45 (d, $J=5.2$ Hz, 2H). ESI-MS(-) calculated for $[\text{C}_{15}\text{H}_{11}\text{N}_2\text{O}_6]^-$ m/z 315.06, found m/z 314.93 $[\text{M-H}]^-$.

4-((Thiophen-2-ylmethyl)amino)pyridine-2,6-dicarboxylic acid (29). Yield: 32% (22 mg, 0.079 mmol). ^1H NMR (400 MHz, $\text{DMSO-}d_6$): δ 8.90 (t, $J=5.6$ Hz, 1H), 7.45 (d, $J=5.2$ Hz, 1H), 7.22 (s, 2H), 7.09 (d, $J=2$ Hz, 1H), 7.00 (dd, $J_1=3.6$ Hz, $J_2=0.8$ Hz, 1H),

4.75 (d, $J=5.6$ Hz, 2H). ESI-MS(+) calculated for $[C_{12}H_{11}N_2O_4S]^+$ m/z 279.04, found m/z 279.12 $[M+H]^+$, 301.09 $[M+Na]^+$, 323.07 $[M+H+2Na]^+$.

4-((Furan-2-ylmethyl)amino)pyridine-2,6-dicarboxylic acid (30). Yield: 52% (34 mg, 0.130 mmol). 1H NMR (400 MHz, DMSO- d_6): δ 7.93 (t, $J=5.6$ Hz, 1H), 7.60 (s, 1H), 7.43 (s, 2H), 6.40 (dd, $J_1=40$ Hz, $J_2=1.2$ Hz, 1H), 6.34 (d, $J=2.5$ Hz, 1H), 4.46 (d, $J=6$ Hz, 2H). ESI-MS(-) calculated for $[C_{12}H_9N_2O_5]^-$ m/z 261.05, found m/z 261.00 $[M-H]^-$.

Dimethyl 4-hydroxypyridine-2,6-dicarboxylate (31). 4-Hydroxypyridine-2,6-dicarboxylic acid (1 g, 5.46 mmol) was dissolved in MeOH (200 mL) and concentrated H_2SO_4 (0.5 mL) was added to the reaction mixture. The reaction mixture was heated to reflux for 24 h. Once the reaction was completed by TLC, the solvent was removed by evaporation in vacuo to afford 31 as a white powder in 88% yield (1.01 g, 4.78 mmol). No further purification was required. 1H NMR (400 MHz, MeOD- d_4): δ 7.58 (s, 2H), 3.95 (s, 6H). ESI-MS(+) calculated for $[C_9H_{10}NO_5]^+$ m/z 212.05, found m/z 212.07 $[M+H]^+$.

Dimethyl 4-bromopyridine-2,6-dicarboxylate (32). Tetrabutylammonium bromide (6.92 g, 21.45 mmol) and P_4O_{10} (3.04 g, 21.45 mmol) were dissolved in dry toluene (20 mL) and the solution was heated to 100 °C for 30 min under N_2 atmosphere. Dimethyl 4-hydroxypyridine-2,6-dicarboxylate (1.51 g, 7.15 mmol) was added to the reaction mixture and set to reflux for 3 h. Once the reaction was complete, the toluene layer was

removed. Additional 10 mL of dry toluene was added to the residual brown oil, and heated to reflux for an additional 20 min. The second toluene layer was collected and the combined toluene layers were dried by evaporation in vacuo. The compound was purified by EtOAc and hexane column chromatography, eluting at 45% EtOAc to afford the title compound as white crystals in 92% yield (1.8 g, 6.57 mmol). ^1H NMR (400 MHz, DMSO- d_6): δ 8.42 (s, 2H), 3.93 (s, 6H). ESI-MS(+) calculated for $[\text{C}_9\text{H}_9\text{BrNO}_4]^+$ m/z 273.97, found m/z 273.98 $[\text{M}+\text{H}]^+$.

General synthetic procedures for compounds 33 – 47.

Dimethyl 4-bromopyridine-2,6-dicarboxylate (200 mg, 0.730 mmol, unless otherwise noted), the corresponding boronic acid (1.2 equivalents), and potassium phosphate or potassium acetate (2 equivalents), were dissolved in dry 1,4-dioxane (5 mL). The solution was purged with N_2 gas for 30 min. To this reaction suspension, $\text{Pd}(\text{Ph}_3)_4$ (0.2 equivalents) was added, and the mixture was heated to reflux at 85 °C for 16 h. The reaction mixture was then filtered through a pad of celite. The organic layer was dried by evaporation in vacuo. The product was purified by EtOAc and hexane column chromatography. Hydrolysis was performed by dissolving the product in a solution of 1M NaOH (4 mL) and THF (1 mL) at room temperature. Once the reaction was complete, THF was removed by evaporation in vacuo, and the solution was acidified with 4M HCl to pH 4. The precipitate was collected via vacuum filtration.

4-Phenylpyridine-2,6-dicarboxylic acid (33). Yield: 68% (120 mg, 0.493 mmol). ¹H NMR (400 MHz, MeOD-*d*₄): δ 8.59 (s, 2H), 7.86-7.84 (m, 2H), 7.60-7.52 (m, 3H). ESI-MS(-) calculated for [C₁₃H₈NO₄]⁻ *m/z* 242.04, found *m/z* 241.92 [M-H]⁻.

4-(3-Methoxyphenyl)pyridine-2,6-dicarboxylic acid (34). Yield: 70% (100 mg, 0.366 mmol). ¹H NMR (400 MHz, MeOD-*d*₄): δ 8.55 (s, 2H), 7.49-7.38 (m, 2H), 7.33 (s, 1H), 7.10 (d, *J*=8 Hz, 1H), 3.90 (s, 3H). ESI-MS(+) calculated for [C₁₄H₁₂NO₅]⁺ *m/z* 274.07, found *m/z* 274.13 [M+H]⁺.

4-(3-Hydroxyphenyl)pyridine-2,6-dicarboxylic acid (35). Yield: 70% (69 mg, 0.305 mmol). ¹H NMR (400 MHz, DMSO-*d*₆): δ 8.37 (s, 2H), 7.38-7.29 (m, 2H), 7.21 (s, 1H), 6.92 (d, *J*=8 Hz, 1H). ESI-MS(-) calculated for [C₁₃H₈NO₅]⁻ *m/z* 258.04, found *m/z* 258.36 [M-H]⁻.

4-(3-Aminophenyl)pyridine-2,6-dicarboxylic acid (36). Yield: 59% (67 mg, 0.259 mmol). ¹H NMR (400 MHz, MeOD-*d*₄): δ 8.36 (s, 2H), 7.21-7.17 (m, 1H), 7.07 (br s, 1H), 7.00 (d, *J*=8 Hz, 1H), 6.70 (d, *J*=8 Hz, 1H). ESI-MS(-) calculated for [C₁₃H₉N₂O₄]⁻ *m/z* 257.06, found *m/z* 257.04 [M-H]⁻.

4-(3-(Dimethylamino)phenyl)pyridine-2,6-dicarboxylic acid (37). Dimethyl 4-bromopyridine-2,6-dicarboxylate (120 mg, 0.438 mmol). Yield: 70.2% (88 mg, 0.307 mmol). ¹H NMR (400 MHz, DMSO-*d*₆): δ 8.38 (s, 2H), 7.33 (d, *J*=8.7 Hz, 1H), 7.07 (d,

$J=13.2$ Hz, 2H), 6.87 (d, $J=8.3$ Hz, 1H), 2.49 (s, 6H). ESI-MS(-) calculated for $[C_{15}H_{13}N_2O_4]^-$ m/z 285.09, found m/z 285.05 $[M-H]^-$.

4-(2-Methoxyphenyl)pyridine-2,6-dicarboxylic acid (38). Yield: 84% (100 mg, 0.366 mmol). 1H NMR (400 MHz, DMSO- d_6): δ 8.29 (s, 2H), 7.50-7.46 (m, 2H), 7.20 (d, $J=8.4$ Hz, 1H), 7.12-7.09 (m, 1H), 3.82 (s, 3H). ESI-MS(-) calculated for $[C_{14}H_{10}NO_5]^-$ m/z 272.05, found m/z 271.91 $[M-H]^-$.

4-(2-Hydroxyphenyl)pyridine-2,6-dicarboxylic acid (39). Yield: 22% (25 mg, 0.096 mmol). 1H NMR (400 MHz, DMSO- d_6): δ 8.43 (s, 2H), 7.49-7.29 (m, 2H), 7.03-6.94 (m, 2H). ESI-MS(-) calculated for $[C_{13}H_8NO_5]^-$ m/z 258.04, found m/z 257.97 $[M-H]^-$.

4-(4-Methoxyphenyl)pyridine-2,6-dicarboxylic acid (40). Yield: 57% (120 mg, 0.418 mmol). 1H NMR (400 MHz, DMSO- d_6): δ 8.37 (s, 2H), 7.89 (d, $J=8.4$ Hz, 2H), 7.10 (d, $J=8.2$ Hz, 2H), 3.83 (s, 3H). ESI-MS(-) calculated for $[C_{14}H_{11}NO_5]^-$ m/z 272.06, found m/z 271.93 $[M-H]^-$.

4-(4-Hydroxyphenyl)pyridine-2,6-dicarboxylic acid (41). Yield: 26% (50 mg, 0.192 mmol). 1H NMR (400 MHz, DMSO- d_6): δ 8.35 (s, 2H), 7.77 (s, 2H), 6.92 (d, $J=8.9$ Hz, 2H). ESI-MS(-) calculated for $[C_{13}H_8NO_5]^-$ m/z 258.04, found m/z 258.04 $[M-H]^-$.

4-(4-Aminophenyl)pyridine-2,6-dicarboxylic acid (42). Yield: 23% (44 mg, 0.170 mmol). ^1H NMR (400 MHz, DMSO- d_6): δ 8.42 (s, 2H), 7.91 (d, $J=8.2$ Hz, 2H), 7.22 (d, $J=8.1$ Hz, 2H). ESI-MS(-) calculated for $[\text{C}_{13}\text{H}_9\text{N}_2\text{O}_4]^-$ m/z 257.06, found m/z 256.98[M-H] $^-$.

4-(4-(Dimethylamino)phenyl)pyridine-2,6-dicarboxylic acid (43). Dimethyl 4-bromopyridine-2,6-dicarboxylate (120 mg, 0.438 mmol). Yield: 40% (50 mg, 0.175 mmol). ^1H NMR (400 MHz, DMSO- d_6): δ 8.39 (s, 2H), 8.02 (s, 2H), 6.86 (s, 2H). ESI-MS(-) calculated for $[\text{C}_{15}\text{H}_{13}\text{N}_2\text{O}_4]^-$ m/z 285.09, found m/z 285.04[M-H] $^-$.

4-(3-Carboxyphenyl)pyridine-2,6-dicarboxylic acid (44). Dimethyl 4-bromopyridine-2,6-dicarboxylate (120 mg, 0.438 mmol). Yield: 45% (57 mg, 0.198 mmol). ^1H NMR (400 MHz, DMSO- d_6): δ 8.47 (s, 2H), 8.34 (s, 1H), 8.17 (d, $J=7.9$ Hz, 1H), 8.09 (d, $J=7.9$ Hz, 1H), 7.70 (t, $J=7.9$ Hz, 1H). ESI-MS(-) calculated for $[\text{C}_{14}\text{H}_8\text{NO}_6]^-$ m/z 286.04, found m/z 285.89 [M-H] $^-$.

4-(3-Acetamidophenyl)pyridine-2,6-dicarboxylic acid (45). Dimethyl 4-bromopyridine-2,6-dicarboxylate (50 mg, 0.175 mmol). Yield: 57% (30 mg, 0.100 mmol). ^1H NMR (400 MHz, DMSO- d_6): δ 8.40 (s, 2H), 8.12 (s, 1H), 7.76 (d, $J=8.2$ Hz, 1H), 8.58 (d, $J=8.0$ Hz, 1H), 7.48 (s, 1H), 2.07 (s, 3H). ESI-MS(-) calculated for $[\text{C}_{15}\text{H}_{11}\text{N}_2\text{O}_5]^-$ m/z 299.07, found m/z 299.00 [M-H] $^-$.

4-(3-Benzamidophenyl)pyridine-2,6-dicarboxylic acid (46). Dimethyl 4-bromopyridine-2,6-dicarboxylate (50 mg, 0.175 mmol). Yield: 81% (51 mg, 0.141 mmol). ¹H NMR (400 MHz, DMSO-*d*₆): δ 8.43 (s, 2H), 8.31 (s, 1H), 8.05 (d, *J*=8.4 Hz, 1H), 7.99 (d, *J*=7.6 Hz, 2H), 7.66 (d, *J*=7.6 Hz, 1H), 7.61-7.57 (m, 1H), 7.54 (t, *J*=7.4 Hz, 3H). ESI-MS(-) calculated for [C₂₀H₁₃N₂O₅]⁻ *m/z* 361.08, found *m/z* 361.00 [M-H]⁻.

4-(3-(2-Phenylacetamido)phenyl)pyridine-2,6-dicarboxylic acid (47). Dimethyl 4-bromopyridine-2,6-dicarboxylate (50 mg, 0.175 mmol). Yield: 29% (19 mg, 0.050 mmol). ¹H NMR (400 MHz, DMSO-*d*₆): δ 8.37 (d, *J*=0.9 Hz, 2H), 8.12 (d, *J*=2.0 Hz, 1H), 7.77 (ddd, *J*₁=8.0, *J*₂=2.0, *J*₃=1.0 Hz, 1H), 7.59 (dt, *J*₁=7.9, *J*₂=1.3 Hz, 1H), 7.48 (t, *J*=7.9 Hz, 1H), 7.38 – 7.26 (m, 4H), 7.27 – 7.21 (m, 1H), 3.67 (s, 2H). ESI-MS(-) calculated for [C₂₁H₁₅N₂O₅]⁻ *m/z* 375.10, found *m/z* 374.99 [M-H]⁻.

Expression and Purification of MBL Metalloforms

NDM-1, IMP-1 and VIM-2 were over-expressed and purified as previously described.^{30, 42-43} The Co(II)-substituted metalloform of NDM-1 was generated using the direct addition method, as previously described.²⁹

High-Throughput Screening Assay and Z' Factor Determination

Colorimetric, 96-well plate-based assays for the activity of NDM-1, IMP-1 and VIM-2 were established using the substrate chromacef.⁴⁰ Each library compound (50 μM) or a vehicle-only control (DMSO) was incubated for 10 min with each enzyme,

NDM-1 (0.2 nM), IMP-1 (0.1 nM) or VIM-2 (1 nM), in 50 mM HEPES, 2 mM CHAPS at pH 7.0 (final assay concentrations). Each reaction was initiated upon addition, with gentle mixing, of the substrate at the following concentrations: 3 μ M for NDM-1 (which corresponds to approximately $3 \times K_M$), 7.2 μ M for IMP-1 (at K_M), and 16 μ M for VIM-2 (at K_M). In the absence of added inhibitors, the increase in absorbance due to formation of the hydrolysis product was followed continuously at 25 °C using a Perkin Elmer Victor 3V 1420 Multilabel Counter plate reader equipped with a 450 nm filter and found to be linear for ≥ 20 min. For subsequent screening, a discontinuous assay was used by treating an unmonitored 20 min reaction incubation with addition of EDTA (80 mM), followed by a 3 min incubation, and then reading the final stable absorbance value for each well as described above. The Z' factor determinations¹¹ were completed using an uninhibited control, and omitting the enzyme as the fully-inhibited control. Low resolution MS was used to analyze the six primary screen hits at the Mass Spectrometry Facility at The University of Texas at Austin.

IC₅₀ Determinations

For initial ranking of the inhibition potency of sublibrary compounds, IC₅₀ values were determined for NDM-1 (and with selected inhibitors for VIM-2 and IMP-1) using the colorimetric substrate chromacef. Stock solutions of each enzyme were diluted using HEPES buffer (50 mM) supplemented with CHAPS (2 mM) at pH 7.0. Steady-state rate parameters were determined for each enzyme in the assay buffer (50 mM HEPES, 1% DMSO at pH 7.0; for IMP-1 only, the assay buffer also contained 2mM CHAPS): NDM-1

($k_{\text{cat}} = 17 \pm 1 \text{ s}^{-1}$, $K_{\text{M}} = 0.66 \pm 0.07 \text{ }\mu\text{M}$), VIM-2 ($k_{\text{cat}} = 89 \pm 2 \text{ s}^{-1}$, $K_{\text{M}} = 10.6 \pm 0.6 \text{ }\mu\text{M}$), IMP-1 ($k_{\text{cat}} = 320 \pm 10 \text{ s}^{-1}$, $K_{\text{M}} = 7 \pm 1 \text{ }\mu\text{M}$ using $\Delta\epsilon_{442\text{nm}} = 14,5000 \text{ M}^{-1}\text{cm}^{-1}$ (Sopharma)). IC_{50} determinations were typically performed in assay buffer using NDM-1 (3 nM), VIM-2 (2 nM), or IMP-1 (0.8 nM), with approximately 20 different inhibitor concentrations. Each reaction contained the following substrate concentrations: 3 μM for NDM-1 (approximately $3 \times K_{\text{M}}$), 14 μM for VIM-2, and 7 μM for IMP-1, (approximately at their respective K_{M} values). Inhibitor and enzyme are pre-incubated for 20 min (525 μL volume in a 1 mL polystyrene cuvette) and the reaction initiated upon addition of substrate (475 μL volume) and absorbance at 442 nm followed continuously during the linear portion for approximately 0.3 min at 25 °C. Initial velocities are plotted as percent activity with uninhibited enzyme representing 100% and a no-enzyme control as 0 % and fitted to $\text{Percent Activity} = (100/((1+(\text{IC}_{50}/[\text{I}])^h))$ to obtain IC_{50} values using KaleidaGraph (Synergy, Reading, PA).

A more sensitive, continuous, fluorescent, 96-well plate-based assay with a larger signal and longer linear assay window was used to rank the potency of the more potent compounds found in sublibrary 3. Typically, inhibitor stock solutions (50 mM in DMSO) were diluted in DMSO to 5 mM and used to prepare five sub-stock solutions of each inhibitor spanning between 500 μM and 50 nM in assay buffer (50 mM HEPES, 2 mM CHAPS at pH 7.0), and then arrayed as 20 μL aliquots, with addition of assay buffer to reach a final inhibitor assay concentration between 100 μM and 1 nM, into a round-bottomed, untreated black polypropylene 96-well plate (Corning). Enzyme (NDM-1 at 41.7 μM) was added in a volume of 60 μL and incubated for 20 min after briefly

shaking. Full activity (no added inhibitor) controls were performed by substituting 20 μL of assay buffer for the inhibitor solution, and no-enzyme controls (to monitor background hydrolysis rates of substrate) were performed in a total of 80 μL assay buffer. Next, the fluorocillin substrate was added in a 20 μL aliquot (from a 433 nM stock solution prepared immediately in assay buffer prior to use) to initiate the reaction. Fluorocillin green has a difluorofluorescein core coupled to two cefalotin groups that serve as a substrate for β -lactamases and hydrolysis can be followed by monitoring changes in fluorescence at $\lambda_{\text{ex/em}}$ 495/525 nm.²⁰⁻²¹ The automatic shaking feature of the PerkinElmer Victor ³V fluorescent plate reader was used to mix the samples for 5 s and fluorescence is determined during a 1 s interval for each well and then repeated 10 times over the duration of the assay, typically 25 min, during which linear rates are observed. The rates of fluorescence increase are determined and IC_{50} values determined as described above for the chromogenic assay. Final assay concentrations were NDM-1 (25 μM), or VIM-2 (250 μM) and IMP-1 (5 μM), and fluorocillin (87 nM) in HEPES buffer (50 mM), CHAPS (2 mM in IMP-1 assays only), at pH 7.0. Periodically, selected sublibrary compounds were assayed independently in two separate laboratories (SMC, WF) to validate the rank order of compound potency.

Inhibitor Selectivity Studies

MMP-2/MMP-12 Assays.²⁷⁻²⁸ MMP-2 and -12, and OmniMMP fluorogenic substrate were purchased from Enzo Life Sciences (Farmingdale, NY, USA). The assays were carried out in black 96-well plates (Corning). Each well contained a volume of 100 μ L including buffer (50 mM HEPES, 10 mM CaCl_2 , 0.05% Brij-35, pH 7.5), human recombinant MMP (1.16 U/well of MMP-2, 0.007 U/well of MMP-12, Enzo Life Sciences), inhibitor (various concentrations, 1mM – 5 μ M), and fluorogenic OmniMMP substrate (4 μ M Mca-Pro-LeuGly-Leu-Dpa-Ala-Arg-NH₂•AcOH, Enzo Life Sciences). The enzyme and inhibitor were incubated in solution at 37 °C for 30 min, followed by the addition of the substrate to initiate the reaction. The change in fluorescence was monitored over 20 min with excitation and emission wavelengths at 320 nm and 400 nm, respectively. The negative control wells, containing no inhibitor, were arbitrarily set as 100% activity. The positive control wells, containing 200 μ M NSA, were arbitrarily set as 0% activity. MMP activity was defined as the ratio of fluorescence increase in the inhibitor wells relative to the negative control wells, expressed as a percentage. The assays were performed in triplicate.

HDAC-1/ HDAC-6 Assays. HDAC-1 and -6 were purchased from BPS Bioscience (BPS Bioscience catalog #50051 and 50006, San Diego, CA, USA) and the assay was carried out as instructed by manufacturer. The assays were carried out in black 96-well plates (Costar). Each well contained a volume of 50 μ L including buffer (25 mM Tris/HCl, 137 mM NaCl, 2.7 mM KCl, 1 mM MgCl_2 , 0.1 mg/mL BSA, pH 8.0),

HDAC (3.8 ng/well of HDAC-1, 50 ng/well of HDAC-6, BPS Bioscience, catalogue no. 50051 and no. 50006, respectively), inhibitor (various concentrations, 1 mM – 5 μ M), and HDAC substrate 3 (20 μ M, BPS Bioscience, catalogue no. 50037). Prior to adding substrate, the plate was pre-incubated for 5 min. Upon addition of substrate, the plate was incubated at 37 °C for 30 min. HDAC assay developer (50 μ L, BPS Bioscience, catalogue no. 50030) was added to each well and the plate incubated for 15 min at room temperature. The fluorescence was recorded at excitation and emission wavelengths of 360 nm and 460 nm, respectively. The negative control wells, containing no inhibitor, were arbitrarily set as 100% activity. The positive control wells, containing 200 μ M SAHA, were arbitrarily set as 0% activity. HDAC activity was defined as the ratio of fluorescence in the inhibitor wells relative to the negative control wells, expressed as a percentage. The assays were performed in triplicate.

hCAII Assays.⁴⁴ hCAII was expressed and purified as previously described.⁴⁵ Assays were carried out in clear 96-well plates (Costar). Each well contained a volume of 100 μ L including buffer (50 mM HEPES, pH = 8.0), hCAII (100 nM), inhibitor (various concentrations, 1 mM – 5 μ M), and *p*-nitrophenyl acetate (500 μ M). The enzyme and inhibitor were incubated in solution at 30 °C for 10 min prior to the addition of the *p*-nitrophenyl acetate to initiate the reaction. The change in absorbance was monitored for 15 min at 405 nm. The negative control wells, containing no inhibitor, were arbitrarily set as 100% activity. The positive control wells, containing 50 μ M benzene sulfonamide, were arbitrarily set as 0% activity. Activity was defined as the ratio of color shift in the

inhibitor wells relative to the negative control wells, expressed as a percentage. The assays were performed in triplicate.

¹H NMR Spectroscopy

Metal-free, apo-NDM-1 was concentrated to ~1 mM with an Amicon Ultra-4 Centrifugal Unit with an Ultracel-10 membrane. To the concentrated protein, 2 equivalents of CoCl₂ were added. Each NMR sample was buffered with 50 mM HEPES, 150 mM NaCl, 10% D₂O at pH 6.8. Tested compounds were dissolved in DMSO at high concentration (50 – 100 mM) so they could be titrated in ~5 μL aliquots. Spectra were collected at 292 K on a Bruker ASX300 (BBI probe) ¹H NMR operating at a frequency of 300.16 MHz. Spectra were collected using a frequency-switching method, applying a long, low power (270 ms) pulse centered at the water frequency, followed by a high power 3 μs pulse centered at 90 ppm.⁴⁶ This method allows for suppression of the water signal with enhancement of severely hyperfine shifted resonances. Spectra consisted of 30,000 transients of 16k data points over a 333 ppm spectral window (t_{aq} ~51 ms); signal averaging took ~3 h per spectrum.

EPR Spectroscopy

Samples containing 1 molar equivalent of compound of interest added to di-Co(II) NDM-1, and di-Co(II) NDM-1 in the absence of compound, included ~10 % (v/v) glycerol as glassing agent. Samples were loaded into EPR tubes, degassed by repeated evacuation/purgation with N₂, prior to data collection. Spectra were collected on a

Bruker EMX EPR spectrometer, equipped with an ER4116-DM dual mode resonator (9.37 GHz, parallel; 9.62 GHz perpendicular). The data in Figure 4 were scaled so that the x-axes matched (perpendicular mode field values were scaled by 9.37/9.62). Temperature control was accomplished using an Oxford ESR900 cryostat and temperature controller. Other spectral conditions included: microwave power = 0.2 mW; field modulation = 10 G (100 kHz); receiver gain = 10^4 ; time constant/conversion time = 41 ms.

UV-Vis Spectroscopy

Apo-NDM-1 was diluted to 300 μ M in 50 mM HEPES, pH 6.8 containing 150 mM NaCl. Two molar equivalents of CoCl_2 were added to the protein from a 50 mM stock solution. The resulting diCo(II)-substituted NDM-1 enzyme was separated into 500 μ L aliquots. To each aliquot, between 0 – 600 μ M of the compound of interest was added. The compound stock concentrations were 20 mM. L-captopril, **DPA**, and **36** stocks were dissolved in DMSO, and the EDTA stock was dissolved in water. The samples were then incubated on ice for 30 min. The samples were added to a 500 μ L quartz cuvette and UV-Vis spectra were collected on a PerkinElmer Lambda 750 UV/VIS/NIR Spectrometer measuring absorbance between 300 to 700 nm at 25 °C. A blank spectrum of 50 mM HEPES, pH 6.8 containing 150 mM NaCl was used to generate difference spectra. All data was normalized at 700 nm.

Equilibrium Dialysis

NDM-1 (final concentration 8 μM) in 5 mL of 50 mM HEPES at pH 7.5, was mixed with the compound of interest at concentrations from 0 – 128 μM . After incubation for 30 min, the solutions were dialyzed versus 500 mL of metal-free, 50 mM HEPES at pH 7.5, for 4 h (dialysis tubing MWCO 6000-8000, Fisherbrand). The Zn(II) content in the resulting NDM-1 samples was determined using Inductively Coupled Plasma with Atomic Emission Spectroscopy (ICP-AES, Perkin Elmer Optima 7300DV). The emission wavelength was set to 213.856 nm, as previously described.²⁹⁻³⁰

Fluorescence Emission Studies

NDM-1 (final concentration 2 μM) in 2 mL of 50 mM HEPES at pH 7.5, was mixed with the compound of interest at concentrations from 4 – 32 μM . After incubation for 30 min, fluorescence emission spectra of NDM-1 samples were obtained on a Perkin Elmer Luminescence spectrometer (Model LS-55), with an excitation wavelength of 280 nm and an emission spectrum from 300 to 400 nm. The relative tryptophan fluorescence intensity (at 348 nm) was calculated setting the intensity of HEPES buffer 0% and NDM-1 containing no inhibitors at 100%. L-Tryptophan (2 μM) was used in place of NDM-1 as a control.

Microdilution Broth Minimum Inhibitory Concentrations (MICs)

MICs were performed in triplicate in Mueller-Hinton broth according to CLSI guidelines.⁴⁷ Overnight cultures of *E.coli* and *K. pneumoniae* clinical isolates expressing *bla*_{NDM-1}³⁶ were inoculated into 5 mL Mueller-Hinton broth to $\text{OD}_{600} = 0.1$ and

grown to $OD_{600} = 0.224$ (approximately $1-2 \times 10^8$ CFU/mL). These cultures were diluted (3 μ L + 4997 μ L MH) and 100 μ L inoculated into each well of a 96-well plate containing 100 μ L of serial dilutions of imipenem (Fresenius Kabi, Lake Zurich, IL) with or without added compound **36** (100 mg/L). Compound **36** alone was included as a control. The plates were placed in a 37 °C incubator for 18 – 20 h and wells checked for growth.

Cytotoxicity Assay

HEK293 cells were plated at 10,000 cells/well in a clear bottom black walled 96-well plate 12 h prior to treatment with either vehicle (DMSO) or compound **36** (n=6 per treatment per time point). Cells were incubated with DMSO or **36** for 4 and 24 h in 100 μ L of Dulbecco's Modified Eagle Medium supplemented with 10% Equafetal (Atlas Biologicals) and Penicillin-Streptomycin (Sigma-Aldrich). Cell-titer blue reagent (Promega) was added after either 4 or 24 h incubation with DMSO or **36** and incubated for an additional 1 h prior to being read on a Victor3V spectrophotometer (536ex/595em). Graphs were created using GraphPad Prism and significance was calculated using an ANOVA followed by a Tukey's post-hoc analysis. A cell viability of 1.0 (100%) was defined by the vehicle only (DMSO) control.

Cell Imaging

HEK293 cells were treated as described in the cytotoxicity assay and imaged with using a NIKON EclipseTi epifluorescent microscope using 20X magnification.

2.5 Acknowledgements

Chapter 2, in part, is adapted and revised from the materials published in the following paper: Allie Y. Chen, Pei W. Thomas, Alesha C. Stewart, Alexander Bergstrom, Zishuo Cheng, Callie Miller, Christopher R. Bethel, Steven H. Marshall, Cy V. Credille, Christopher L. Riley, Richard C. Page, Robert A. Bonomo, Michael W. Crowder, David L. Tierney, Walter Fast, Seth M. Cohen, "Dipicolinic Acid Derivatives as Inhibitors of New Delhi Metallo- β -lactamase-1" *J. Med. Chem.* **2017**, *60*, 7267-7283. The dissertation author was the primary researcher and author. The permission to reproduce this paper was granted by the American Chemical Society. The co-authors listed in these publications also participated in the research.

2.6 References

1. Brown, E. D.; Wright, G. D., Antibacterial Drug Discovery in the Resistance Era. *Nature* **2016**, *529* (7586), 336-343.
2. Walsh, T. R., Emerging Carbapenemases: a Global Perspective. *Int. J. Antimicrob. Agents*. **2010**, *36* S8-14.
3. Yong, D.; Toleman, M. A.; Giske, C. G.; Cho, H. S.; Sundman, K.; Lee, K.; Walsh, T. R., Characterization of a New Metallo-beta-Lactamase Gene, bla(NDM-1), and a Novel Erythromycin Esterase Gene Carried on a Unique Genetic Structure in *Klebsiella pneumoniae* Sequence Type 14 from India. *Antimicrob. Agents Chemother.* **2009**, *53* (12), 5046-5054.
4. Nordmann, P.; Poirel, L.; Toleman, M. A.; Walsh, T. R., Does Broad-spectrum beta-Lactam Resistance Due to NDM-1 Herald the End of the Antibiotic Era for Treatment of Infections Caused by Gram-Negative Bacteria? *J. Antimicrob. Chemother.* **2011**, *66* (4), 689-692.
5. Kumarasamy, K. K.; Toleman, M. A.; Walsh, T. R.; Bagaria, J.; Butt, F.; Balakrishnan, R.; Chaudhary, U.; Doumith, M.; Giske, C. G.; Irfan, S.; Krishnan, P.; Kumar, A. V.; Maharjan, S.; Mushtaq, S.; Noorie, T.; Paterson, D. L.; Pearson, A.; Perry, C.; Pike, R.; Rao, B.; Ray, U.; Sarma, J. B.; Sharma, M.; Sheridan, E.; Thirunarayan, M. A.; Turton, J.; Upadhyay, S.; Warner, M.; Welfare, W.; Livermore, D. M.; Woodford, N., Emergence of a New Antibiotic Resistance Mechanism in India, Pakistan, and the UK: a Molecular, Biological, and Epidemiological Study. *Lancet Infect. Dis.* **2010**, *10* (9), 597-602.
6. Brem, J.; Cain, R.; Cahill, S.; McDonough, M. A.; Clifton, I. J.; Jimenez-Castellanos, J. C.; Avison, M. B.; Spencer, J.; Fishwick, C. W.; Schofield, C. J., Structural Basis of Metallo-beta-Lactamase, Serine-beta-Lactamase and Penicillin-binding Protein Inhibition by Cyclic Boronates. *Nat. Commun.* **2016**, *7*, 12406.
7. Linciano, P.; Cendron, L.; Gianquinto, E.; Spyrakis, F.; Tondi, D., Ten Years with New Delhi Metallo-beta-lactamase-1 (NDM-1): From Structural Insights to Inhibitor Design. *ACS Infect. Dis.* **2019**, *5* (1), 9-34.
8. Mojica, M. F.; Bonomo, R. A.; Fast, W., B1-Metallo-beta-Lactamases: Where Do We Stand? *Curr. Drug Targets* **2016**, *17* (9), 1029-1050.
9. Garau, G.; Garcia-Saez, I.; Bebrone, C.; Anne, C.; Mercuri, P.; Galleni, M.; Frere, J. M.; Dideberg, O., Update of the Standard Numbering Scheme for Class B beta-Lactamases. *Antimicrob. Agents Chemother.* **2004**, *48* (7), 2347-2349.
10. Copeland, R. A., Evaluation of Enzyme Inhibitors in Drug Discovery. A Guide for Medicinal Chemists and Pharmacologists. *Methods Biochem. Anal.* **2005**, *46*, 1-265.

11. Zhang, J. H.; Chung, T. D.; Oldenburg, K. R., A simple statistical parameter for use in evaluation and validation of high throughput screening assays. *J. Biomol. Screen.* **1999**, *4* (2), 67-73.
12. Schlesinger, S. R.; Bruner, B.; Farmer, P. J.; Kim, S. K., Kinetic Characterization of a Slow-binding Inhibitor of Bla₂: Thiomaltol. *J. Enzyme Inhib. Med. Chem.* **2013**, *28* (1), 137-142.
13. Hanaya, K.; Suetsugu, M.; Saijo, S.; Yamato, I.; Aoki, S., Potent Inhibition of Dinuclear Zinc(II) Peptidase, an Aminopeptidase from *Aeromonas proteolytica*, by 8-Quinololinol Derivatives: Inhibitor Design Based on Zn²⁺ Fluorophores, Kinetic, and X-Ray Crystallographic Study. *J. Biol. Inorg. Chem.* **2012**, *17* (4), 517-529.
14. Horsfall, L. E.; Garau, G.; Lienard, B. M.; Dideberg, O.; Schofield, C. J.; Frere, J. M.; Galleni, M., Competitive Inhibitors of the CphA Metallo-beta-Lactamase from *Aeromonas hydrophila*. *Antimicrob. Agents Chemother.* **2007**, *51* (6), 2136-2142.
15. Palacios, A. R.; Mojica, M. F.; Giannini, E.; Taracila, M. A.; Bethel, C. R.; Alzari, P. M.; Otero, L. H.; Klinke, S.; Llarrull, L. I.; Bonomo, R. A.; Vila, A. J., The Reaction Mechanism of Metallo-beta-Lactamases Is Tuned by the Conformation of an Active-Site Mobile Loop. *Antimicrob. Agents Chemother.* **2019**, *63* (1), e01754-01718.
16. Aitha, M.; Moller, A. J.; Sahu, I. D.; Horitani, M.; Tierney, D. L.; Crowder, M. W., Investigating the Position of the Hairpin Loop in New Delhi Metallo-beta-Lactamase, NDM-1, During Catalysis and Inhibitor Binding. *J. Inorg. Biochem.* **2016**, *156*, 35-39.
17. Sun, Z.; Hu, L.; Sankaran, B.; Prasad, B. V. V.; Palzkill, T., Differential Active Site Requirements for NDM-1 beta-Lactamase Hydrolysis of Carbapenem Versus Penicillin and Cephalosporin Antibiotics. *Nat. Commun.* **2018**, *9* (1), 4524.
18. Okabe, N.; Oya, N., Copper(II) and Zinc(II) Complexes of Pyridine-2,6-dicarboxylic Acid. *Acta Crystallogr., Sect. C: Struct. Chem.* **2000**, *56*, 305-307.
19. Raczynska, J. E.; Shabalina, I. G.; Minor, W.; Wlodawer, A.; Jaskolski, M., A Close Look onto Structural Models and Primary Ligands of Metallo-beta-Lactamases. *Drug Resist. Updat.* **2018**, *40*, 1-12.
20. Rukavishnikov, A.; Gee, K. R.; Johnson, I.; Corry, S., Fluorogenic Cephalosporin Substrates for beta-Lactamase TEM-1. *Anal. Biochem.* **2011**, *419* (1), 9-16.
21. Klingler, F. M.; Wichelhaus, T. A.; Frank, D.; Cuesta-Bernal, J.; El-Delik, J.; Muller, H. F.; Sjuts, H.; Gottig, S.; Koenigs, A.; Pos, K. M.; Pogoryelov, D.; Proschak, E., Approved Drugs Containing Thiols as Inhibitors of Metallo-beta-lactamases: Strategy To Combat Multidrug-Resistant Bacteria. *J. Med. Chem.* **2015**, *58* (8), 3626-3630.
22. Hopkins, A. L.; Groom, C. R.; Alex, A., Ligand Efficiency: a Useful Metric for Lead Selection. *Drug Discov. Today* **2004**, *9* (10), 430-431.

23. Brown, D. G.; May-Dracka, T. L.; Gagnon, M. M.; Tommasi, R., Trends and Exceptions of Physical Properties on Antibacterial Activity for Gram-positive and Gram-negative Pathogens. *J. Med. Chem.* **2014**, *57* (23), 10144-10161.
24. Gregoretto, I. V.; Lee, Y. M.; Goodson, H. V., Molecular Evolution of the Histone Deacetylase Family: Functional Implications of Phylogenetic Analysis. *J. Mol. Biol.* **2004**, *338* (1), 17-31.
25. Devel, L.; Rogakos, V.; David, A.; Makaritis, A.; Beau, F.; Cuniasse, P.; Yiotakis, A.; Dive, V., Development of Selective Inhibitors and Substrate of Matrix Metalloproteinase-12. *J. Biol. Chem.* **2006**, *281* (16), 11152-11160.
26. Sly, W. S.; Hu, P. Y., Human Carbonic Anhydrases and Carbonic Anhydrase Deficiencies. *Annu. Rev. Biochem.* **1995**, *64*, 375-401.
27. Day, J. A.; Cohen, S. M., Investigating the Selectivity of Metalloenzyme Inhibitors. *J. Med. Chem.* **2013**, *56* (20), 7997-8007.
28. Chen, Y.; Cohen, S. M., Investigating the Selectivity of Metalloenzyme Inhibitors in the Presence of Competing Metalloproteins. *ChemMedChem* **2015**, *10* (10), 1733-1738.
29. Yang, H.; Aitha, M.; Marts, A. R.; Hetrick, A.; Bennett, B.; Crowder, M. W.; Tierney, D. L., Spectroscopic and Mechanistic Studies of Heterodimetallic Forms of Metallo-beta-Lactamase NDM-1. *J. Am. Chem. Soc.* **2014**, *136* (20), 7273-7285.
30. Yang, H.; Aitha, M.; Hetrick, A. M.; Richmond, T. K.; Tierney, D. L.; Crowder, M. W., Mechanistic and Spectroscopic Studies of Metallo-beta-Lactamase NDM-1. *Biochemistry* **2012**, *51* (18), 3839-3847.
31. King, D. T.; Worrall, L. J.; Gruninger, R.; Strynadka, N. C., New Delhi Metallo-beta-Lactamase: Structural Insights into beta-Lactam Recognition and Inhibition. *J. Am. Chem. Soc.* **2012**, *134* (28), 11362-11365.
32. Selleck, C.; Larrabee, J. A.; Harmer, J.; Guddat, L. W.; Mitic, N.; Helweh, W.; Ollis, D. L.; Craig, W. R.; Tierney, D. L.; Monteiro Pedrosa, M.; Schenk, G., AIM-1: An Antibiotic-Degrading Metallohydrolase That Displays Mechanistic Flexibility. *Chemistry* **2016**, *22* (49), 17704-17714.
33. Hanson, G. B., L.J., *Metals in Biology: Applications of High-Resolution EPR to Metalloenzymes*. 2010; p 345–370.
34. Crowder, M. W.; Yang, K. W.; Carenbauer, A. L.; Periyannan, G.; Seifert, M. E.; Rude, N. E.; Walsh, T. R., The Problem of a Solvent Exposable Disulfide When Preparing Co(II)-Substituted Metallo-beta-Lactamase L1 from *Stenotrophomonas maltophilia*. *J. Biol. Inorg. Chem.* **2001**, *6* (1), 91-99.

35. Krezel, A.; Maret, W., The biological inorganic chemistry of zinc ions. *Arch Biochem Biophys* **2016**, *611*, 3-19.
36. Lascols, C.; Hackel, M.; Marshall, S. H.; Hujer, A. M.; Bouchillon, S.; Badal, R.; Hoban, D.; Bonomo, R. A., Increasing Prevalence and Dissemination of NDM-1 Metallo- β -Lactamase in India: Data from the SMART Study (2009). *J. Antimicrob. Chemother.* **2011**, *66* (9), 1992-1997.
37. Christopeit, T.; Carlsen, T. J.; Helland, R.; Leiros, H. K., Discovery of Novel Inhibitor Scaffolds Against the Metallo- β -Lactamase VIM-2 by Surface Plasmon Resonance (SPR) Based Fragment Screening. *J. Med. Chem.* **2015**, *58* (21), 8671-8682.
38. Christopeit, T.; Leiros, H. K., Fragment-based Discovery of Inhibitor Scaffolds Targeting the Metallo- β -Lactamases NDM-1 and VIM-2. *Bioorg. Med. Chem. Lett.* **2016**, *26* (8), 1973-1977.
39. Klingler, F. M.; Moser, D.; Buttner, D.; Wichelhaus, T. A.; Lohr, F.; Dotsch, V.; Proschak, E., Probing Metallo-beta-Lactamases with Molecular Fragments Identified by Consensus Docking. *Bioorg. Med. Chem. Lett.* **2015**, *25* (22), 5243-5246.
40. Yu, S.; Vosbeek, A.; Corbella, K.; Severson, J.; Schesser, J.; Sutton, L. D., A Chromogenic Cephalosporin for beta-Lactamase Inhibitor Screening Assays. *Anal. Biochem.* **2012**, *428* (2), 96-98.
41. Perez, C.; Monserrat, J. P.; Chen, Y.; Cohen, S. M., Exploring Hydrogen Peroxide Responsive Thiazolidinone-based Prodrugs. *Chem. Commun.* **2015**, *51* (33), 7116-7119.
42. Griffin, D. H.; Richmond, T. K.; Sanchez, C.; Moller, A. J.; Breece, R. M.; Tierney, D. L.; Bennett, B.; Crowder, M. W., Structural and Kinetic Studies on Metallo-beta-Lactamase IMP-1. *Biochemistry* **2011**, *50* (42), 9125-9134.
43. Aitha, M.; Marts, A. R.; Bergstrom, A.; Moller, A. J.; Moritz, L.; Turner, L.; Nix, J. C.; Bonomo, R. A.; Page, R. C.; Tierney, D. L.; Crowder, M. W., Biochemical, Mechanistic, and Spectroscopic Characterization of Metallo-beta-Lactamase VIM-2. *Biochemistry* **2014**, *53* (46), 7321-7331.
44. Martin, D. P.; Cohen, S. M., Nucleophile Recognition as an Alternative Inhibition Mode for Benzoic Acid Based Carbonic Anhydrase Inhibitors. *Chem. Commun.* **2012**, *48* (43), 5259-5261.
45. Monnard, F. W.; Heinisch, T.; Nogueira, E. S.; Schirmer, T.; Ward, T. R., Human Carbonic Anhydrase II as a Host for Piano-stool Complexes Bearing a Sulfonamide Anchor. *Chem. Commun.* **2011**, *47* (29), 8238-8240.
46. Riley, E. A.; Petros, A. K.; Smith, K. A.; Gibney, B. R.; Tierney, D. L., Frequency-switching Inversion-recovery for Severely Hyperfine-Shifted NMR: Evidence of

Asymmetric Electron Relaxation in High-spin Co(II). *Inorg. Chem.* **2006**, *45* (25), 10016-10018.

47. Methods for Dilution Antimicrobial Susceptibility Tests for Bacteria That Grow Aerobically; Approved Standard- Tenth Edition. In *CLSI M07-A10* [Online] 2 ed.; Clinical and Laboratory Standards Institute: Wayne, PA, United States, 2015.

Chapter 3. Investigation of DPA Isosteres for the Inhibition of MBLs

3.1 Introduction

There are an estimated >450 marketed drugs (including nonsteroidal anti-inflammatory drugs, antibiotics, anticoagulants, and cholesterol-lowering statins) that utilize a carboxylic acid motif.¹⁻³ The ionizable nature of the carboxylic acid under physiological conditions (pH 7.4) makes it a useful handle for generating strong inhibitor-target interactions (i.e., electrostatic and hydrogen bonds). In metalloenzyme inhibition, the carboxylic acid motif routinely participates in metal coordination, as seen in inhibitors for neutral endopeptidase, class II fructose-1,6-bisphosphate aldolase, angiotensin-converting enzyme, and many others.⁴ Despite the utility of this functional group, its practicality can be limited in drug development due to poor cell permeability, metabolic instability, and off-target effects.^{1,3} In an attempt to overcome such liabilities, medicinal chemists have often turned to the utilization of pro-drugs or isosteric replacement.¹⁻² Carboxylic acid isosteres bear similar structural and physical properties compared to carboxylic acids and are used as surrogates to improve the overall drug-likeness (i.e., increased permeability, better pharmacokinetics, and/or reduced toxicity). Recent efforts by the Cohen lab have begun to explore MBP isosteric replacement and its effect on metalloenzyme inhibition and pharmacokinetic profile.⁵⁻⁷

In Chapter 2, a FBDD approach was utilized to identify **DPA** as a lead MBP for NDM-1 inhibitor development.⁸ Derivatization of **DPA** was performed to obtain 4-(3-aminophenyl)pyridine-2,6-dicarboxylic acid (**36**) as a highly selective inhibitor for NDM-1 (IMP-1 and VIM-2) that inhibits by forming a stable NDM-1:Zn(II):**36** ternary complex. In this chapter, we further investigate the **DPA** MBP as an inhibitor for NDM-1 utilizing the concept of isosteric replacement. Ten **DPA** isosteres were designed and synthesized

as inhibitors of NDM-1 and related MBLs. A selection of carboxylic acid isostere motifs was chosen to span a range of acidity (pK_a) values and metal coordination preferences. Varying the identity of the isostere impacts both inhibition value and inhibition mechanism. Furthermore, an isostere which inhibited via a metal-stripping mechanism was derivatized and re-engineered to yield inhibitors which inhibited via the formation of a ternary complex. This study provides a roadmap for the isosteric replacement of current and future metal-binding motifs for the generation of new entities in NDM-1 inhibitor design and may be adopted for the inhibitor development of MBLs and other metalloenzymes.

3.2 Results and Discussion

3.2.1 DPA Isostere Design and Synthesis (Sublibrary 4)

The synthesis of Sublibrary 4 (**DPA** isosteres **48** – **57**, Figure 3-1) is presented in Scheme 3-1, Scheme 3-2, and Scheme 3-3. The synthesis of isosteres **48**, **51**, **56**, and **57** is summarized in Scheme 3-1. Isostere **48** was obtained from a Hirao cross-coupling reaction of commercially available methyl 6-bromopicolinate and diethylphosphate, followed by acid hydrolysis. Isostere **51** was achieved by conversion of the methyl 6-bromopicolinate to a nitrile via the Rosenmund-von Braun reaction, followed by an azide-nitrile cycloaddition. Isosteres **56** and **57** were synthesized via a Stille coupling of methyl 6-bromopicolinate with the corresponding organotin reagents, followed by saponification. Synthesis of isosteres **49**, **50**, **52**, **53**, and **55** is summarized in Scheme 3-2. Briefly, compound **58** was obtained from commercially available methyl 6-(hydroxymethyl)picolinate. Substitution of the alkyl bromide of compound **58** with various nucleophiles, followed by hydrolysis yielded isosteres **49**, **50**, **52**, **53**, and **55**. Lastly, methyl 6-aminopicolinate was treated with methanesulfonyl chloride, followed by saponification to yield isostere **54** (Scheme 3-3).

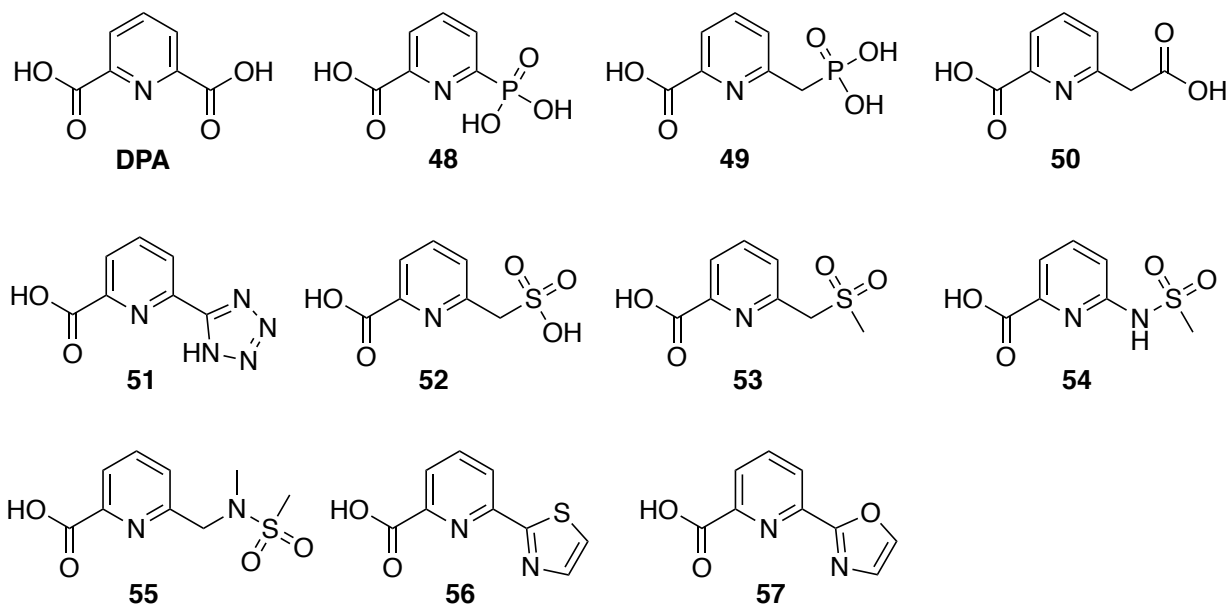
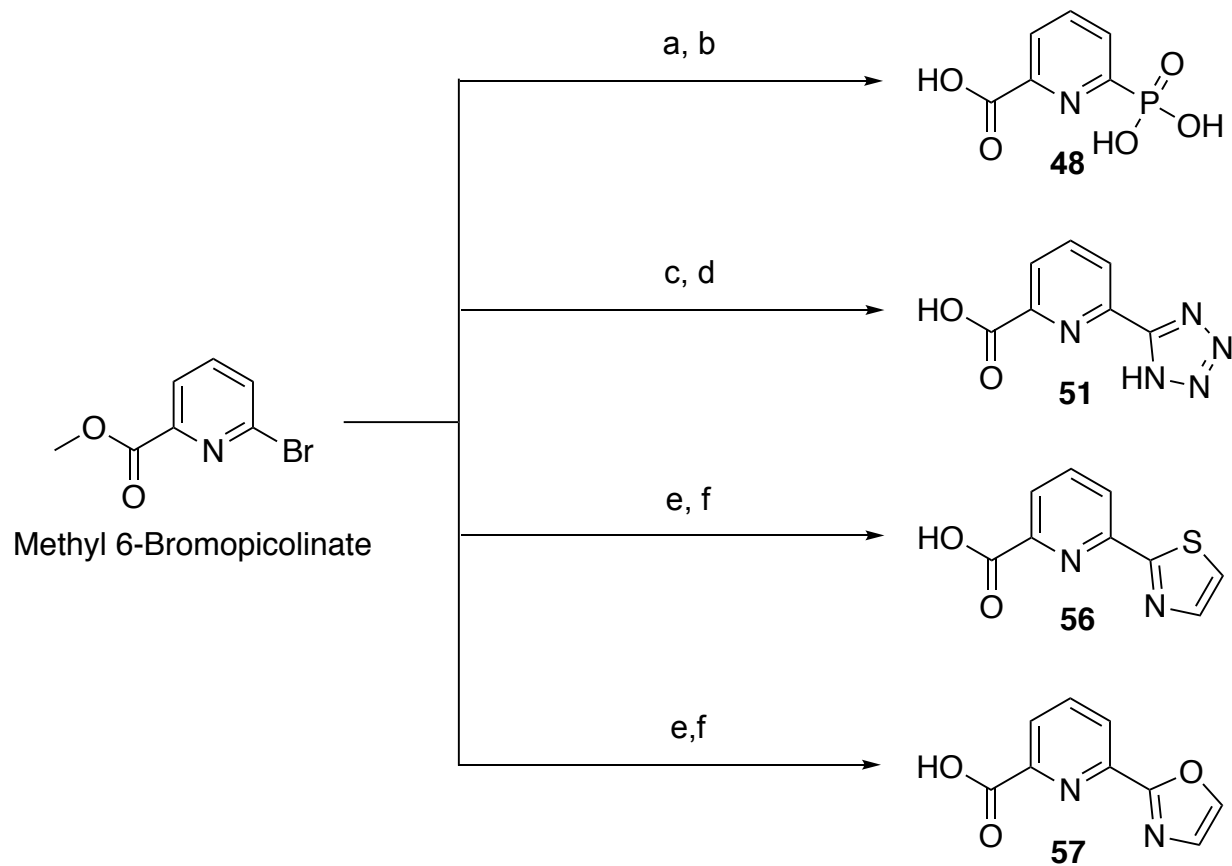
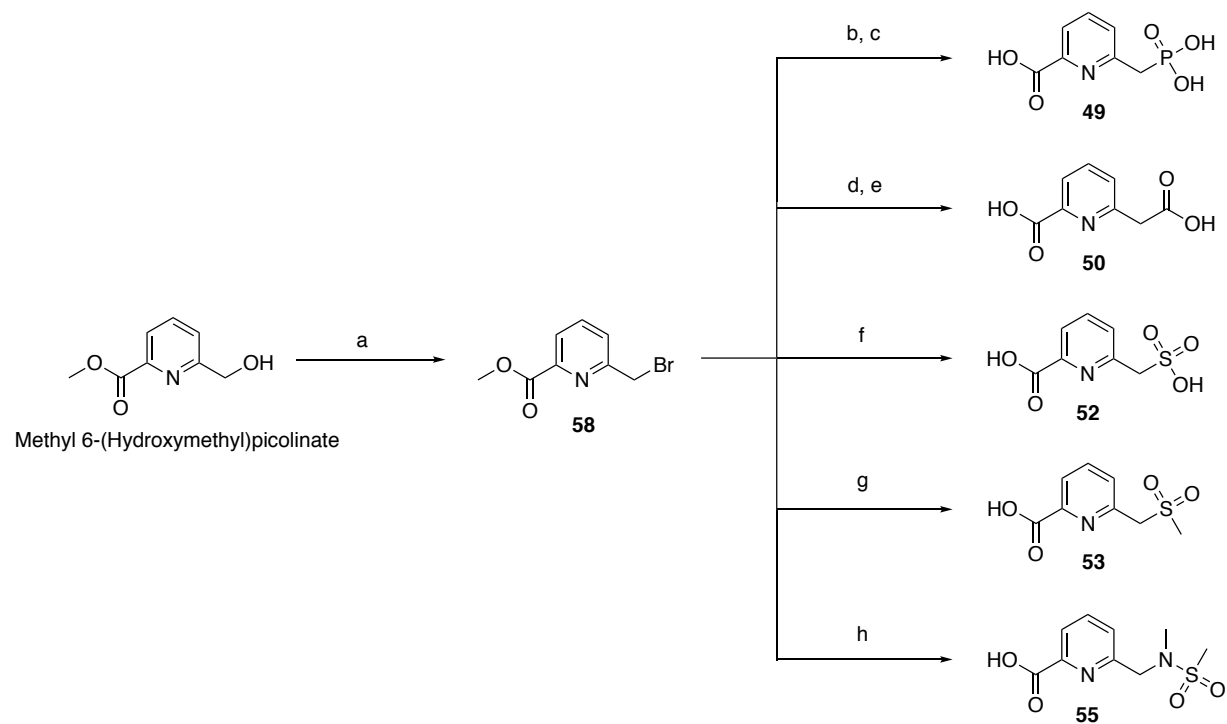


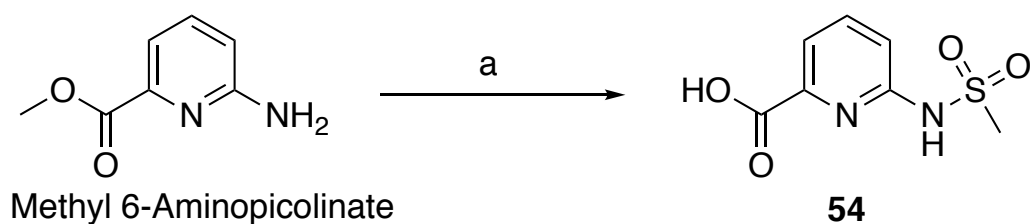
Figure 3-1. DPA and Sublibrary 4 (compounds 48 – 57) reported in this chapter.



Scheme 3-1. Synthesis of isosteres **48**, **51**, **56**, and **57**. Reagents and conditions: (a) $\text{Pd}_2(\text{dba})_3$, $\text{Pd}(\text{dppf})\text{Cl}_2$, diethylphosphate, triethylamine, toluene, 90 °C, 20 h; then 6M HCl, 100 °C, 20 h; *two steps* 19%; (b) CuCN, pyridine, 116 °C, 4 h, 21%; (c) NaN_3 , NH_4Cl , DMF, 130 °C, 20 h; then 2M HCl, 25 °C, 1 h; *two steps* 98%; (d) 2-(tributylstannyl)thiazole/ 2-(tributylstannyl)oxazole, $\text{Pd}(\text{PPh}_3)_2\text{Cl}_2$, THF, 75 °C, 18 h; then 3:1 1M NaOH:THF, 70 °C, 3 h; *two steps* 8-74%.



Scheme 3-2. Synthesis of isosteres **49**, **50**, **52**, **53**, and **55**. Reagents and conditions: (a) PBr_3 , CHCl_3 , $0\text{ }^\circ\text{C}$, 3 h, 70%; (b) $\text{P}(\text{OEt})_3$, toluene, $140\text{ }^\circ\text{C}$, 2 h, 80%; (c) 6M HCl , $100\text{ }^\circ\text{C}$, 27 h, 98%; (d) KCN , THF, $50\text{ }^\circ\text{C}$, 19 h, 49%; (e) 12M HCl , $100\text{ }^\circ\text{C}$, 12 h, then 1M NaOH , $60\text{ }^\circ\text{C}$, 6 h, 30%; (f) Na_2SO_3 , H_2O , then 4M HCl , $100\text{ }^\circ\text{C}$, 16 h; *two steps* 41%; (g) NaSO_2CH_3 , DMF, $120\text{ }^\circ\text{C}$, 2 h, then 3:1 1M NaOH :THF, $70\text{ }^\circ\text{C}$, 3 h; *two steps* 43%; (h) $\text{CH}_3\text{NHSO}_2\text{CH}_3$, K_2CO_3 , ACN, $75\text{ }^\circ\text{C}$, 25 h; then 1M NaOH , $70\text{ }^\circ\text{C}$, 3 h; *two steps* 55%.



Scheme 3-3. Synthesis of isostere **54**. Reagents and conditions: (a) Methanesulfonyl chloride, triethylamine, CH_2Cl_2 , $0\text{ }^\circ\text{C}$, 16 h; then 1M NaOH :THF, r.t., 16 h; *two steps* 12.4%.

3.2.2 Evaluation of DPA Isosteres Against MBLs

A preliminary screen of isosteres **48** – **57** was performed against NDM-1 utilizing meropenem as the substrate (at a single concentration of 180 μM , Table 3-1). Meropenem was observed to have a $K_{\text{M,NDM-1}} = 80 \pm 7 \mu\text{M}$ and $k_{\text{cat}} = 15.3 \pm 0.4 \text{ s}^{-1}$. Compounds **48** – **51** exhibited inhibition against NDM-1 with IC_{50} values ranging from 0.13 – 7.7 μM . Compounds **48** and **49** (both bearing a phosphonic acid) exhibited lower IC_{50} values (130 ± 10 and $310 \pm 10 \text{ nM}$, respectively) compared to that of **DPA** ($840 \pm 40 \text{ nM}$), while **50** and **51** revealed higher IC_{50} values (7.7 ± 0.6 and $7.0 \pm 0.5 \mu\text{M}$, respectively). Interestingly, compound **52**, which possesses a similar acidic motif as **48** and **49** (a sulfonic acid versus a phosphonic acid) showed no inhibition at concentrations up to 10 μM . Notably, all compounds where the substituted moiety was not acidic (**53** – **57**) showed no appreciable inhibition at concentrations up to 10 μM .

To determine the ability of isosteres to inhibit other B1 MBLs, the inhibition of **48** – **51** against NDM-1, IMP-1, and VIM-2 was investigated. An alternative substrate, fluorocillin ($K_{\text{M,NDM-1}} = 460 \text{ nM}$), was utilized to increase assay sensitivity.⁸⁻⁹ Lower IC_{50} values for fluorocillin compared to meropenem were expected due to using a smaller $[\text{S}]/K_{\text{M}}$ ratio in these experiments. IC_{50} values determined for NDM-1 inhibition via fluorocillin showed the same trends as with meropenem, with **48** and **49** showing the lowest IC_{50} values, followed by the parent **DPA** fragment, with **50** and **51** yielding higher IC_{50} values among these five compounds (Table 3-2). Similar trends, but with IC_{50} values about an order of magnitude higher, were observed for IMP-1 and VIM-2 as well.

Table 3-1. Inhibitory activity of **DPA** isosteres against NDM-1. Inhibition values were obtained via monitoring the NDM-1-catalyzed hydrolysis of substrate meropenem.^[a]

Compound	IC₅₀ (μM)	Compound	IC₅₀ (μM)
DPA	0.84±0.04	53	>10
48	0.31±0.01	54	>10
49	0.13±0.01	55	>10
50	7.7±0.6	56	>10
51	7.0±0.5	57	>10
52	>10		

^[a] Activity measurements were taken in triplicate using varying inhibitor concentrations that bracket each IC₅₀ value, with fitting errors listed above.

Table 3-2. Inhibitory activity of **DPA** isosteres against B1 MBLs. Inhibition values were obtained via monitoring the MBL-catalyzed hydrolysis of substrate fluorocillin.^[a]

Compound	IC₅₀ (μM)		
	NDM-1	IMP-1	VIM-2
DPA	0.33±0.04	2.54±0.04	2.34±0.04
48	0.064±0.001	0.85±0.06	0.85±0.02
49	0.068±0.002	0.63±0.01	0.62±0.01
50	2.05±0.09	59±5	35±1
51	2.19±0.13	22±1	27±2

^[a] Activity measurements were taken in triplicate using varying inhibitor concentrations that bracket each IC₅₀ value, with fitting errors listed above.

3.2.3 DPA Isostere pK_a Analysis

To validate the potential of the synthesized **DPA** isosteres in physicochemical property modulation for drug development, the pK_a values of **DPA**, **48**, **49**, and **50** were obtained via previously reported methods (Table 3-3, Figure 3-2).⁶ The selected compounds yield a wide range of acidity values, with pK_a spanning 1.68 – 7.40. Due to the selected isosteres bearing multiple microscopic protonation states (arising from the acidic isostere motifs and the basic pyridine ring), it is important to note the complexity when analyzing the obtained pK_a values. Some protonation states may be transient and the pK_a values may not be detected. Additionally, due to the instrument limit and reliability, pK_a values of < 2 should be regarded with caution. The pK_a analysis reveal the ability of selected isosteres to access a broad range of acidity values and demonstrate the potential to modulate physicochemical properties in future drug development.

Table 3-3. The pK_a values of selected inhibitors in this study.^[a]

	DPA	48	49	50
pK_{a1}	4.53	1.68	5.03	2.66
pK_{a2}	–	3.65	7.40	5.54
pK_{a3}	–	7.05	–	–

^[a] All values from these experiments yielded standard deviations < 0.03 .

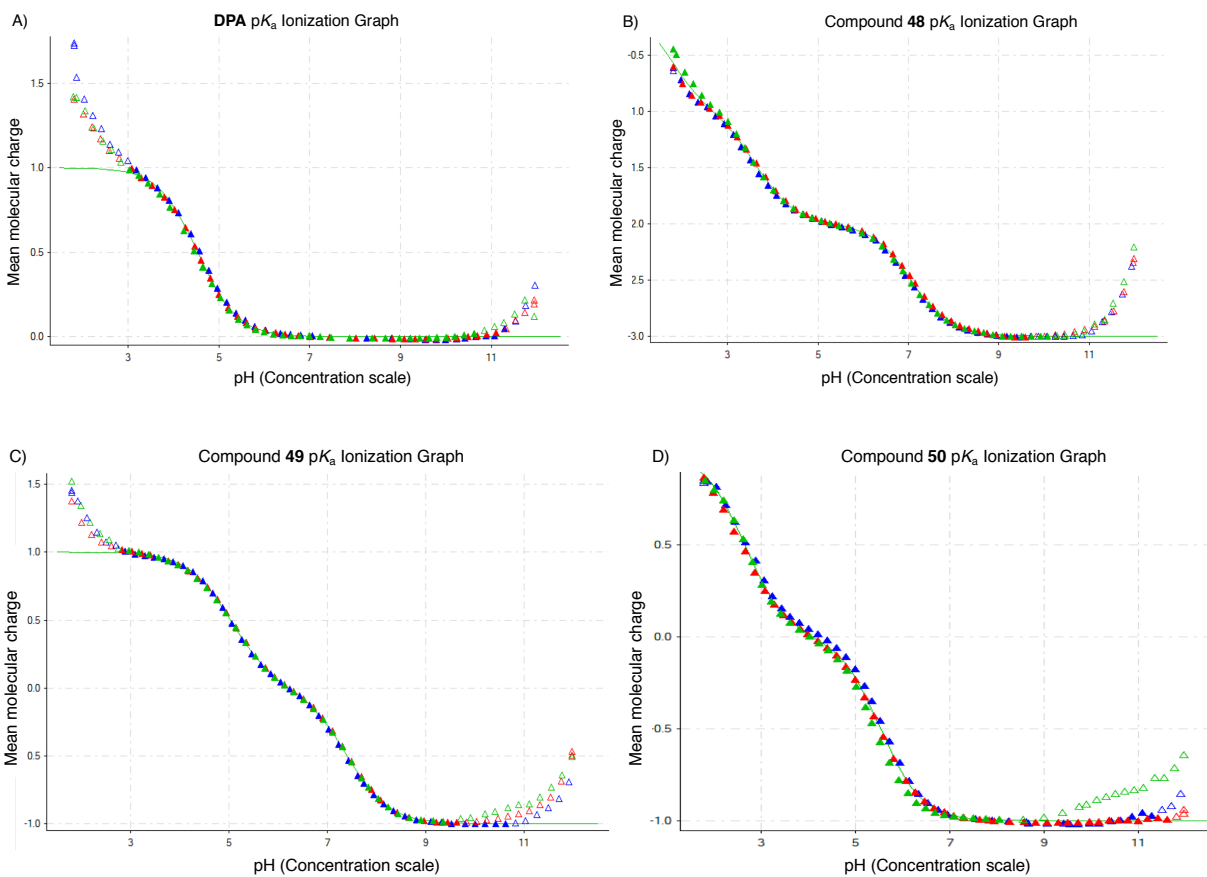


Figure 3-2. The pK_a ionization graphs of selected inhibitors.

3.2.4 Mechanism of Isostere Inhibition

Equilibrium Dialysis. Equilibrium dialysis experiments were performed to give insight into the inhibition mechanism (metal stripping versus ternary complex formation) of **DPA** and the active isosteres. After protein purification, NDM-1 was exchanged into ammonium acetate buffer to facilitate the use of ICP-AES in determining metal content. Metal analyses of the resulting protein showed that the enzyme binds ~1.7 equivalents of Zn(II) (Figure 3-3). While holoNDM-1 is expected to bind 2 equivalents of Zn(II), previous studies have shown that Zn₂ binds more weakly than Zn₁, resulting in a protein that contains less than the full complement of two Zn(II) ions.¹⁰⁻¹¹ As previously reported, incubation of NDM-1 with captopril, a known competitive inhibitor,¹² did not show any evidence of Zn(II) removal. In contrast, the Zn(II) content of NDM-1 was significantly reduced when incubated with **DPA**.⁸ Isosteres **48** – **51** exhibited different levels of Zn(II) removal from NDM-1. Compounds **50** and **51** behaved more like captopril, removing only small amounts of Zn(II) from NDM-1 even at concentrations up to 128 μM. Conversely, compounds **48** and **49** removed more Zn(II) from NDM-1 than the parent **DPA**.

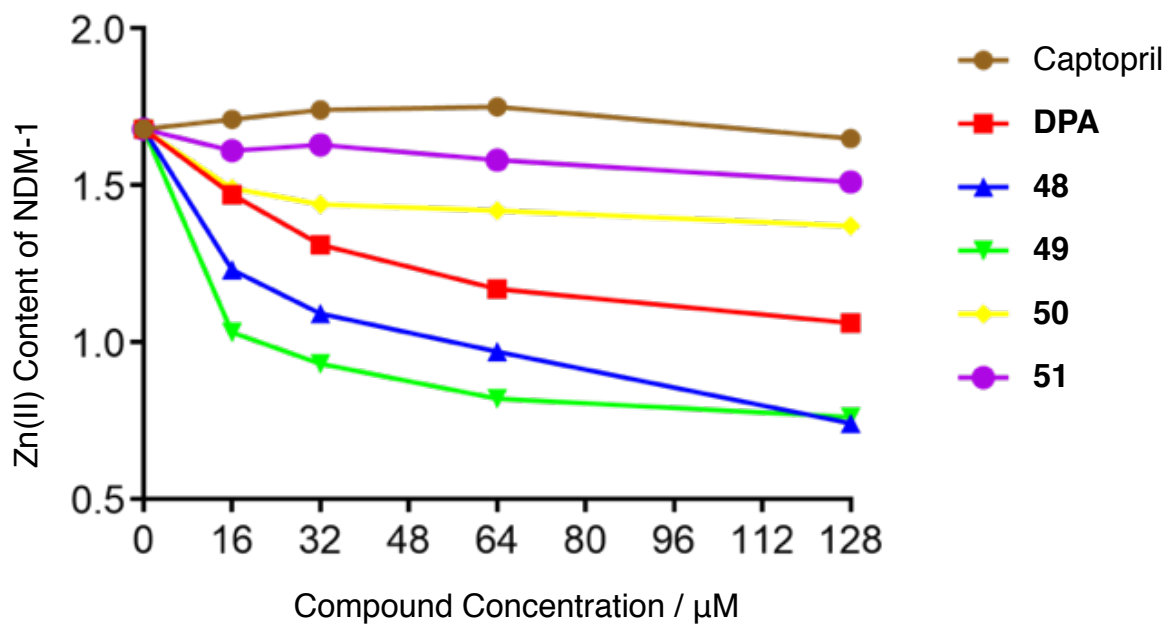


Figure 3-3. Zn(II) content of NDM-1 (8 μM) upon incubation with increasing concentrations of captopril, **DPA**, and **48** – **51** (16 μM – 128 μM).

UV-Visible Spectroscopy. As previously reported, UV-vis spectrophotometry of Co(II)-substituted NDM-1 can be used to probe inhibitor binding to the enzyme.⁸ The spectrum of di-Co(II) NDM-1 shows an intense peak between 320 – 350 nm, which has been assigned to a cysteine-to-Co(II) ligand-to-metal charge transfer band, and multiple peaks between 500 – 650 nm, which have been assigned to Co(II) ligand field bands (Figure 3-4A).¹³⁻¹⁴ The inclusion of captopril to the sample results in large changes in the ligand field transitions, and an increase in the LMCT band. These changes are consistent with the formation of a NDM-1:captopril ternary complex, with the captopril sulfur bridging the two Co(II) ions.¹⁵ Incubation of di-Co(II) NDM-1 with EDTA resulted in significant reduction of the LMCT and ligand field peaks, indicating that EDTA strips the metal from NDM-1.⁸ Incubation of di-Co(II) NDM-1 with compounds **48** – **51** and **DPA** resulted in a reduction of absorbance at 500 – 650 nm (Figure 3-4B), which indicates that Co(II) is being removed from the active site to varying degrees. Compound **49** appears to remove the most Co(II), followed by compound **48**, **DPA**, **50**, and then **51**. The findings with di-Co(II) NDM-1 are wholly consistent with the equilibrium dialysis results.

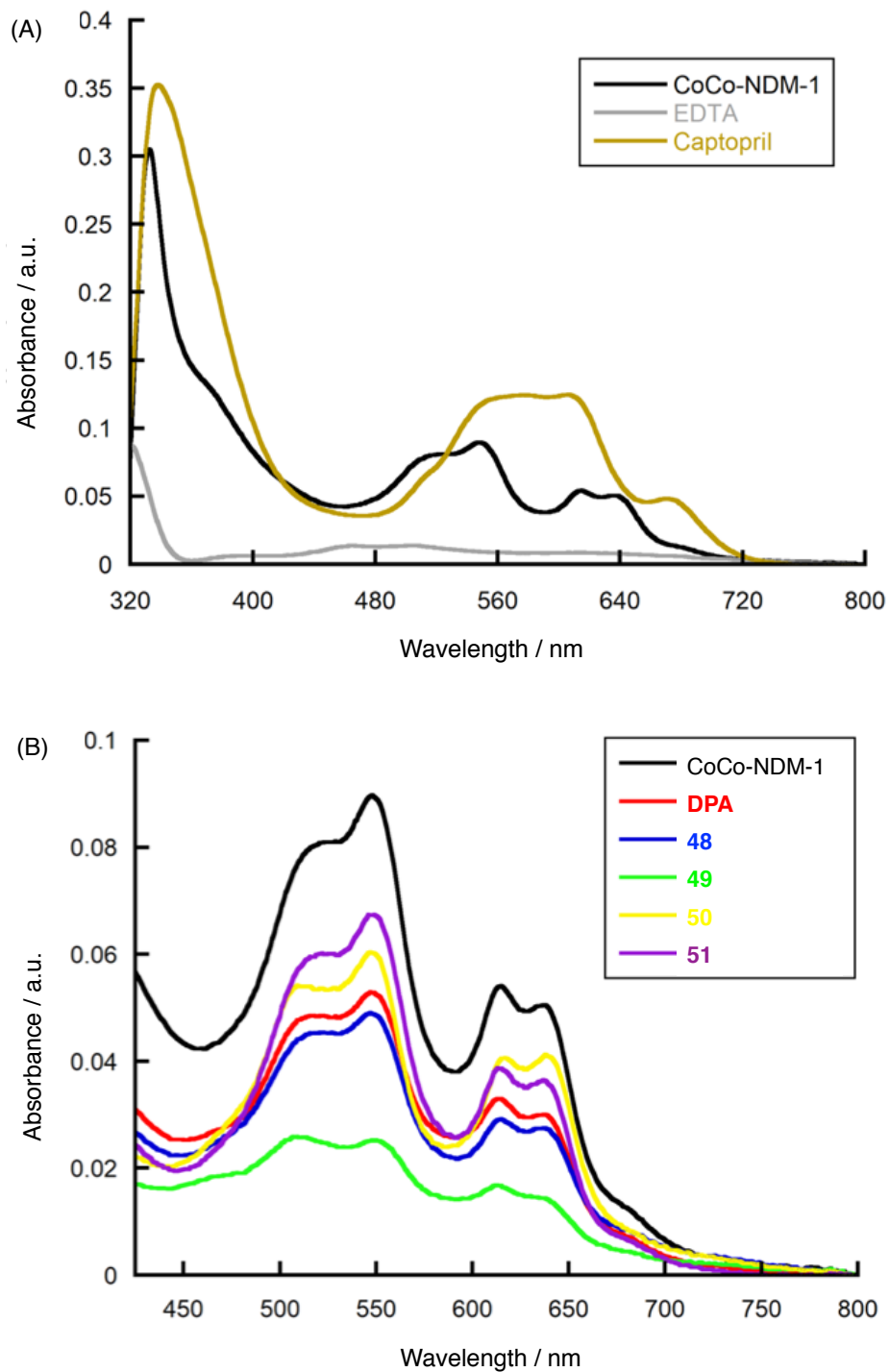


Figure 3-4. (A) UV-Vis spectrum of CoCo-NDM-1 with captopril and EDTA; (B) UV-Vis spectrum of CoCo-NDM-1 with **DPA** and isosteres **48 – 51**.

3.2.5 Derivatization of Isostere 49 (Sublibrary 5)

Although **49** was shown to remove Zn(II) from NDM-1, we sought to reduce the metal-chelation behavior via elaboration using a fragment growth strategy. We previously had success using this approach to optimize **DPA**.⁸ Also during the time of this study, a structure of **49** in complex with IMP-1 (PDB 5HH4) was reported.¹⁶ In this structure, the Zn₁ of IMP-1 is coordinated via residues His116, His118, His196, and a bridging hydroxide in a tetrahedral coordination geometry (Figure 3-5, standard BBL numbering). The bridging hydroxide also coordinates to Zn₂, which is further ligated by residues Asp120, Cys221, and His263, as well as by the pyridine nitrogen donor and carboxylate of **49** (in an overall octahedral coordination geometry). The phosphonic acid motif of **49** is shown to hydrogen bond with the bridging hydroxide ion and a nearby Ser80 residue. Guided by this crystallographic data and the homology of IMP-1 and NDM-1 enzymes, a small library of **49** derivatives (Sublibrary 5, **65a** – **65m**) were designed and synthesized to target the L3 of NDM-1.

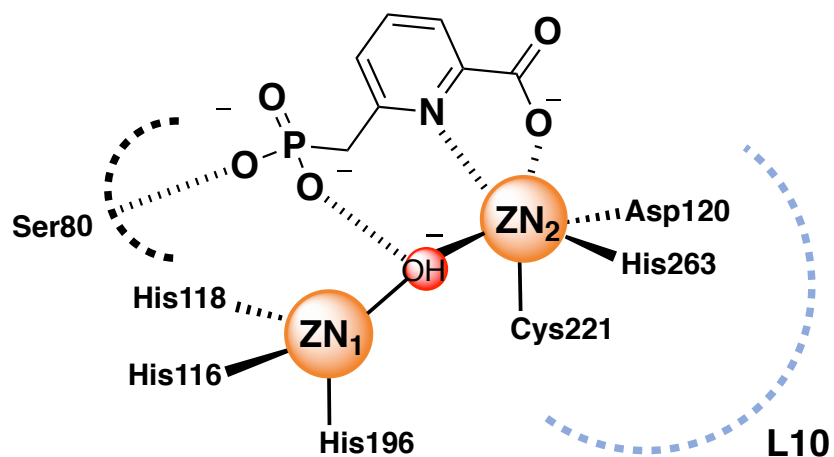
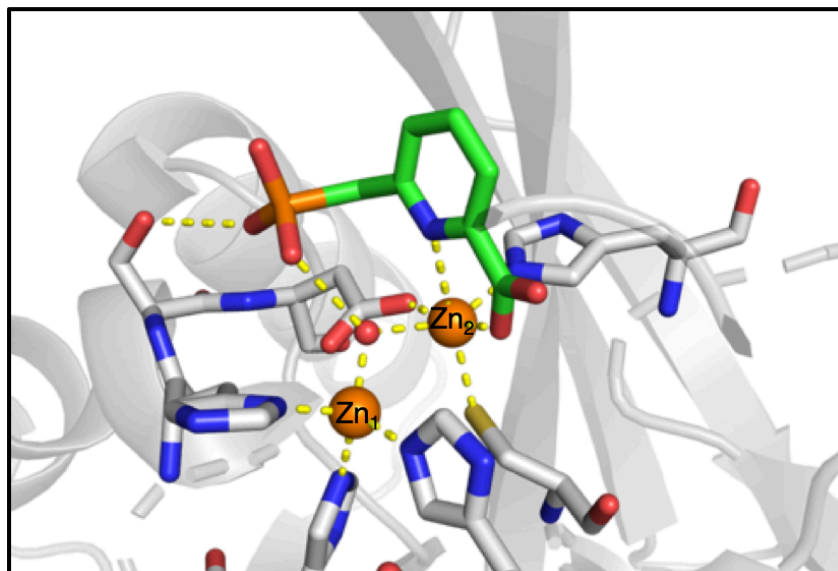
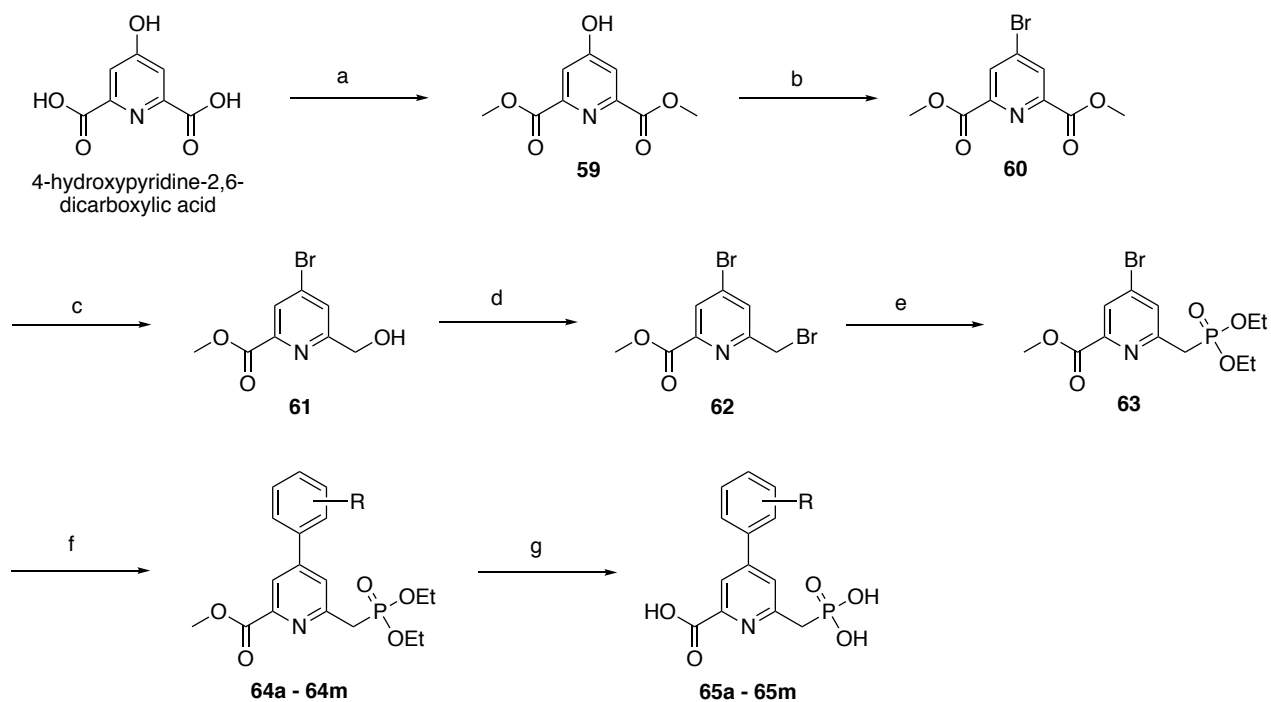


Figure 3-5. *Top:* Inhibitor **49** complexed with IMP-1 (PDB 5HH4).¹⁶ Figure was rendered with Pymol. *Bottom:* Chemical representation of the predicted binding of **49** with the NDM-1 active site. Zn(II) ions are shown as orange spheres and bridging hydroxide is shown as a red sphere.

The synthesis of **65a** – **65m** is presented in Scheme 3-4 and the IC₅₀ values, measured via NDM-1 catalyzed hydrolysis of meropenem, are reported in Table 3-4. This library consisted of simple aryl derivatives substituted at the 4-position of the pyridine ring. The aryl ring bears substituents (methoxy, hydroxyl, amine, and chlorine) in the *para*-, *ortho*-, and *meta*- position of the ring in an attempt to generate interactions with nearby residue side chains. To prepare these compounds, 4-hydroxypyridine-2,6-dicarboxylic acid was esterified to **59** with MeOH and catalytic H₂SO₄. Next, **59** was converted to **60** with tetrabutylammonium bromide and P₄O₁₀. Compound **60** was treated with NaBH₄ at 0 °C to obtain **61**, which was further converted to intermediate **62** via PBr₃. Compound **63** was obtained by heating **62** and triethyl phosphite in toluene at 140 °C for 22 h. Intermediates **64a** – **64m** were obtained via Suzuki cross-coupling procedures utilizing the corresponding boronic acid, Pd(PPh₃)₄, and K₃PO₄. Compounds **65a** – **65m** were obtained via hydrolysis.



Scheme 3-4. Synthesis of Sublibrary 5 (compounds **65a – 65**). Reagents and conditions: (a) MeOH, H₂SO₄ (cat.), 70 °C, overnight, 60%; (b) P₄O₁₀, tetrabutylammonium bromide, toluene, 100 °C, 3 h, 75%; (c) NaBH₄, MeOH/CH₂Cl₂, 0 °C, 1 h, 80%; (d) PBr₃, CHCl₃, 0 °C, 1 h, 68%; (e) P(OEt)₃, toluene, 140 °C, 22 h, 92%; (f) boronic acid, K₃O₄P, Pd(PPh₃)₄, 1,4-dioxanes, 80 °C, 18 h, 20 – 90%; (g) 6M HCl, 100 °C, 24 h, 29 – 97%.

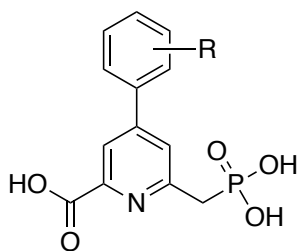
Compounds **65a** – **65m** did not yield greater inhibitory activity than that of **49** ($IC_{50} = 0.13 \pm 0.01 \mu\text{M}$). A simple aryl ring (**65a**), or an aryl ring with methoxy (**65b** – **65d**) or hydroxyl substituent (**65e** – **65g**) were generally well-tolerated, with $IC_{50} = 0.20 \pm 0.01$ – $0.48 \pm 0.01 \mu\text{M}$, but did not lead to a marked decrease IC_{50} value compared to that of **49**. Given the structural similarity of **65h** – **65j** (bearing the aniline substituent) to the previously reported inhibitor, **36**, no improvement in inhibition was observed compared to that of **49** ($IC_{50} = 0.24 \pm 0.01$ – $0.40 \pm 0.02 \mu\text{M}$). Notably, a chlorine substituent in the *ortho*- and *meta*- position of the aryl ring yields a 2- to 3-fold loss in potency. Due to the similarities between the observed inhibition values, no SAR could be obtained, and derivatives of **49** were not further pursued. Although isosteric replacement of the carboxylate group maintains the ability to bind metal ions, the relative positioning of attached substituents is likely altered, possibly due to changes in metal coordination geometries. In the case of **DPA** and NDM-1, this prevents a simple group-swapping approach and will necessitate re-optimization starting with the new isostere fragment.

To determine whether the derivatives have a reduced tendency to remove metal from the active site of NDM-1 (compare to the parent isostere **49**, Figure 3-2) to favor the formation of a NDM-1:Zn(II):inhibitor ternary complex, additional equilibrium dialysis studies were conducted (Figure 3-5). Compounds **65b** (which exhibited the lowest IC_{50} value) and **65i** (which resembled **36**) were incubated at varying concentrations against NDM-1. As previously described, the Zn(II) content of NDM-1 was significantly reduced when incubated with the metal chelator EDTA and isostere **49** (Figure 3-2). Incubation of NDM-1 with derivatives **65b** and **65i** (at $16 \mu\text{M}$) resulted in a minor loss of Zn(II)

content. Exposure to higher concentrations of these inhibitors (up to 128 μM) resulted in only minor reduction in Zn(II) content. These results show the conversion of a lead MBP (**49**), which inhibits via a metal stripping mechanism, to more lead-like compounds (**65b** and **65i**) that favor the formation of a ternary complex.

Despite similar overall protein fold and hydrolysis mechanism between NDM-1 and IMP-1, the sequence heterogeneity of residues at the binding pocket (specially the extended β -hairpin loop, L3) has contributed to a change in the active site pocket size and hydrophobicity.¹⁷ Compounds **65a** – **65m** were further screened against IMP-1 (Table 3-4); however, the obtained IC_{50} values (1.20 ± 0.05 – 4.1 ± 0.2 μM) did not reveal any informative SAR.

Table 3-4. Inhibitory activity of Sublibrary 5 (compounds **65a** – **65m**) against NDM-1. Inhibition values were obtained via monitoring the MBL-catalyzed hydrolysis of substrate meropenem.^[a]



R =	IC_{50} (μM)					
	<i>para</i>		<i>meta</i>		<i>ortho</i>	
---H	65a	0.41 ± 0.02	–		–	
---OCH_3	65b	0.20 ± 0.01	65c	0.42 ± 0.02	65d	0.30 ± 0.01
---OH	65e	0.48 ± 0.01	65f	0.28 ± 0.01	65g	0.28 ± 0.01
---NH_2	65h	0.30 ± 0.01	65i	0.40 ± 0.02	65j	0.24 ± 0.01
---Cl	65k	0.40 ± 0.01	65l	1.29 ± 0.07	65m	0.95 ± 0.05

^[a] Activity measurements were taken in triplicate using varying inhibitor concentrations that bracket each IC_{50} value, with fitting errors listed above.

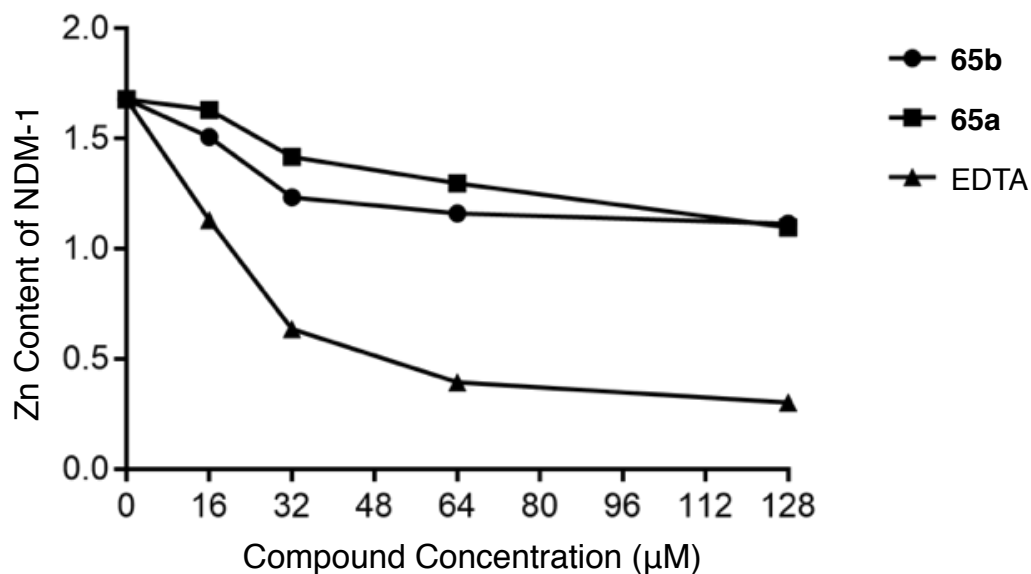


Figure 3-6. Zn(II) content of NDM-1 (8 μM) upon incubation with increasing concentrations of **65b**, **65i**, and EDTA (16 μM – 128 μM).

Table 3-5. Inhibitory activity of Sublibrary 5 (compounds **65a** – **65m**) against IMP-1. Inhibition values were obtained via monitoring the MBL-catalyzed hydrolysis of substrate meropenem.^[a]

Compound	IC ₅₀ (μM)	Compound	IC ₅₀ (μM)
65a	4.1 ± 0.2	65h	2.66 ± 0.09
65b	2.8 ± 0.2	65i	2.3 ± 0.1
65c	2.5 ± 0.1	65j	3.1 ± 0.1
65d	2.0 ± 0.1	65k	3.35 ± 0.09
65e	1.94 ± 0.06	65l	3.2 ± 0.1
65f	1.20 ± 0.05	65m	3.5 ± 0.2
65g	2.36 ± 0.08		

^[a] Activity measurements were taken in triplicate using varying inhibitor concentrations that bracket each IC₅₀ value, with fitting errors listed above.

3.3 Discussion

This chapter reports the isosteric replacement of the carboxylic acid group of **DPA** with various surrogate structures. Compounds **48** – **57** yield a range of chemical diversity (various acidic or metal-binding groups) and show that the choice of the carboxylate isostere not only impacts the IC_{50} value, but also the propensity for metal removal. Replacement of one carboxylic acid with a phosphonic substituent (**49**) results in a MBP with an extraordinarily low IC_{50} value, but also with a greater tendency for NDM-1 Zn(II) removal. Replacement of the carboxylic acid with a tetrazole motif (**51**) yields a higher IC_{50} value, but reduces NDM-1 Zn(II) removal. Equilibrium dialysis data, in conjunction with UV-vis spectroscopy of CoCoNDM-1, reveals differences in inhibition mechanism: inhibition by **49** occurs primarily via Zn(II) removal, likely forming the inactive mono-Zn(II) NDM-1, while inhibition by **51** is primarily via formation of a ternary complex at the dinuclear Zn(II) site. Because **51** forms a ternary complex at the active site, we can use IC_{50} and the Cheng-Prusoff relationship for competitive inhibitors to calculate a K_i of $2.2 \pm 0.5 \mu\text{M}$.¹⁸ It is important to note that calculating K_i values for metal-stripping inhibitors (such as **48** or **48**) is not appropriate because changes in IC_{50} may not reflect changes in binding affinity. Available data suggesting potential varying inhibition mechanisms between homologous MBLs and **49** (ternary complex formation with IMP-1,¹⁶ but metal-stripping with NDM-1) was unexpected. This difference may be due to a lower binding affinity for Zn(II) in the Zn_2 site of NDM-1 ($K_d = 2 \mu\text{M}$)¹¹ compared to that of IMP-1 ($K_d = 0.3 \mu\text{M}$),¹⁹⁻²⁰ resulting in more facile metal removal. Future

studies are required to elucidate and conclude the observed mechanistic differences of **49** against IMP-1 and NDM-1.

In an attempt to decrease the IC_{50} value and reduce the propensity to strip metal from the NDM-1 active site, a small set of derivatives of isostere **49** were synthesized. It was predicted that **65i**, bearing the same amine backbone as a reported inhibitor that uses **DPA** as a metal-binding group, would result in a decrease in the observed IC_{50} value. Unfortunately, **65i** (and other derivatives) did not yield a lower IC_{50} value than that of **49**, suggesting that the isosteres are not exactly equivalent substitutions of their parent fragment; however, equilibrium dialysis reveal **65i** (and **65b**) has a significantly reduced tendency for Zn(II) removal from the active site compared to that of **49**. This shows the potential to engineer a compound which inhibits via a metal-stripping mechanism (**49**) to one which inhibits via the formation of a ternary complex (albeit no reduction in the observed IC_{50} value).

Despite the understanding that compounds can inhibit MBLs via a number different mechanisms (covalent inhibition, metal-chelation, reversible competitive inhibition, allosteric inhibition, etc.), the mechanism of action of most reported MBL inhibitors is not well defined.²¹ Many current studies focus on achieving low IC_{50} values, with little consideration regarding the mechanism of action. Here, we clearly demonstrate how the mechanism of inhibition can significantly differ between similar isosteres and homologous enzymes and illustrate challenges to optimizing inhibitors with metal-stripping mechanisms. In the design of future MBL inhibitors, a loss of potency may be preferred when selecting compounds with a desired mechanism of

action for further optimization (i.e., selection of **51** over **49**). Additionally, compounds with confirmed metal stripping tendencies may be further developed to reduce metal removal (as seen in the transformation of **49** to **65b** and **65i**). Early-stage evaluation of how the inhibitor interacts with the active site will be crucial for accelerating NDM (and other MBLs) inhibitor development.

3.4 Conclusion

In summary, the synthesis and inhibitory activity of ten **DPA** isosteres and investigation of the mechanism of action of the most active compounds was reported. We show that the exchange of the carboxylic acid with other acidic isosteres not only drastically affects the IC_{50} value but can also modulate the mechanism of action. The compounds which showed the lowest IC_{50} were shown to act via a metal-stripping mechanism, while compounds that displayed poorer IC_{50} values formed a ternary complex with the enzyme. Preliminary data suggest differences in inhibition mechanism between homologous NDM-1 and IMP-1 and isostere **49**. This study demonstrates the importance of considering the inhibition mechanism and the utility of bioisosteric replacement for routinely-used metal-binding motifs (i.e., carboxylic acid) in NDM-1 inhibitor development. The additional design, synthesis and screening data of **51** derivatives, as well as the screening of 2-picolinic acid isosteres, as inhibitors against NDM-1 is presented in Chapter 5.

3.5 Experimental

All reagents and solvents were obtained from commercial sources and used without further purification. Corning UV-transparent 96-well microplates (3635), Corning black polystyrene round-bottom 96-well microplates (3792), CHAPS, HEPES, DMSO, L-captopril and fluorocillin green 495/525 β -lactamase substrate were purchased from ThermoFisher Scientific Inc. (Fair Lawn, NJ). All other reagents were purchased from Sigma-Aldrich Inc. (St. Louis, MO). Screening assays were performed on a PerkinElmer Victor3 V 1420 multilabel counter plate reader. Fluorescent assays were performed on a PerkinElmer Victor3 V fluorescent plate reader. Column chromatography was performed using a Teledyne ISCO CombiFlash Rf system with prepacked silica cartridges. All ^1H NMR and ^{13}C spectra were recorded at either ambient temperature or at 35 °C using Varian 400 Mercury Plus or Varian VX500 instrument located in the Department of Chemistry and Biochemistry at the University of California, San Diego. Mass spectrometry data were obtained from the University of California San Diego Chemistry and Biochemistry Mass Spectrometry Facility. The purity of all compounds used for screening was determined to be $\geq 95\%$ by high-performance liquid chromatography (HPLC).

Synthesis

6-Phosphonopicolinic acid (48). A solution of methyl 6-bromopicolinate (300 mg, 1.39 mmol), diethylphosphate (172.0 μL , 1.39 mmol), $\text{Pd}_2(\text{dba})_3$ (67 mg, 0.69 mmol), $\text{Pd}(\text{dppf})\text{Cl}_2$ (77 mg, 0.14 mmol), and trimethylamine (387.0 μL , 2.78 mmol) were

dissolved in toluene (10 mL), and heated to 90 °C for 20 h. EtOAc (20 mL) was added to the reaction mixture, and the solution was filtered through a pad of celite. The collected organic layers were concentrated in vacuo. The crude mixture was purified via flash column chromatography, with the intermediate eluting at 50% EtOAc in hexanes. The intermediate was heated under reflux conditions with 6M HCl (3 mL) for 20 h. The excess HCl was removed in vacuo, and co-evaporated with copious amounts of MeOH and water until a precipitate was observed. The product was collected via vacuum filtration as a white solid in 19% yield (54 mg, 0.27 mmol). ¹H NMR (400 MHz, MeOD-*d*₄): δ 8.26 (d, *J* = 7.7 Hz, 1H), 8.19 – 8.00 (m, 2H). ¹³C NMR (126 MHz, DMSO-*d*₆): δ 166.4, 156.2, 149.0, 138.0, 129.4, 126.1. ESI-MS(-) calculated for [C₆H₅NO₅P]⁻ *m/z* 202.10, found *m/z* 201.98 [M-H]⁻.

6-(Phosphonomethyl)picolinic acid (49). A solution of **58** (200 mg, 0.87 mmol) and P(OEt)₃ (1.6 g, 9.56 mmol) were heated in toluene (20 mL) at 140 °C for 2 h to give a clear liquid solution. Excess P(OEt)₃ and toluene were removed in vacuo, and the intermediate was purified via flash column chromatography eluting at 100% EtOAc in hexanes as a clear oil in 80% yield (200 mg, 0.70 mmol). ¹H NMR (400 MHz, CDCl₃-*d*): δ 8.02 (d, *J* = 8.0 Hz, 1H), 7.80 (td, *J* = 7.8, 2.1 Hz, 1H), 7.62 (d, *J* = 8.0 Hz, 1H), 4.13 – 4.06 (m, 4H), 3.99 (d, *J* = 2.0 Hz, 3H), 3.53 (d, *J* = 22.0 Hz, 2H), 1.31 – 1.25 (m, 6H). ESI-MS(+) calculated for [C₁₂H₁₉NO₅P]⁺ *m/z* 288.10, found *m/z* 288.29 [M+H]⁺.

The intermediate, methyl 6-((diethoxyphosphoryl)methyl)picolinate (200 mg, 0.70 mmol), was refluxed in 6M HCl (5 mL) for 27 h. The excess HCl was removed in vacuo

and co-evaporate with copious amounts of MeOH and water until a white precipitate was observed. Compound **49** was collected via vacuum filtration as a white solid in 86% yield (130 mg, 0.60 mmol). ^1H NMR (400 MHz, DMSO- d_6): δ 8.02 (t, J = 7.7 Hz, 1H), 7.95 (d, J = 7.5 Hz, 1H), 7.67 (d, J = 7.6 Hz, 1H), 3.38 (s, 1H), 3.32 (s, 1H). ^{13}C NMR (126 MHz, DMSO- d_6): δ 166.6, 155.4, 148.0, 137.9, 127.8, 122.8, 38.3. ESI-MS(-) calculated for $[\text{C}_7\text{H}_8\text{NO}_5\text{P}]^-$ m/z 217.01, found m/z 216.00 $[\text{M}-\text{H}]^-$.

6-(Carboxymethyl)picolinic acid (50). To a solution of **58** (2.5 g, 10.87 mmol) dissolved in THF (50 mL) was added a pre-dissolved solution of KCN (1.1 g, 16.30 mmol) in water (9 mL). All supplies in contact with KCN were quenched with 1M sodium thiosulfate prior to disposal. The mixture was stirred at 50 °C for 19 h and quenched with 1M sodium thiosulfate solution. The mixture was extracted with CH_2Cl_2 (25 mL \times 5). The combined organic layers were dried over MgSO_4 , filtered, and concentrated in vacuo. Intermediate methyl 6-(cyanomethyl)picolinate was purified via flash column chromatography, eluting at 58% EtOAc in hexanes to yield yellow crystals in 49% yield (941 mg, 5.34 mmol). ^1H NMR (400 MHz, DMSO- d_6): δ 8.09 – 7.95 (m, 2H), 7.68 (t, J = 5.5 Hz, 1H), 4.30 (s, 2H), 3.88 (s, 3H). ESI-MS(+) calculated for $[\text{C}_9\text{H}_9\text{N}_2\text{O}_2]^+$ m/z 177.06, found m/z 177.18 $[\text{M}+\text{H}]^+$.

The intermediate, methyl 6-(cyanomethyl)picolinate, was dissolved in 12M HCl and heated to 100 °C for 12 h. The solvent was removed in vacuo and the crude was hydrolyzed in 3 mL of 1M NaOH at 60 °C for 6 h. The solution was acidified with to pH 4, and product **50** was collected via vacuum filtration as a white solid in 30% yield

(37 mg, 0.20 mmol). ^1H NMR (400 MHz, $\text{DMSO-}d_6$): δ 7.98 – 7.86 (m, 2H), 7.56 (d, J = 6.3 Hz, 1H), 3.83 (s, 2H). ^{13}C NMR (126 MHz, $\text{DMSO-}d_6$): δ 172.1, 166.6, 155.8, 148.3, 138.3, 128.0, 123.4, 43.6. ESI-MS(+) calculated for $[\text{C}_8\text{H}_8\text{NO}_4]^+$ m/z 182.04, found m/z 182.25 $[\text{M}+\text{H}]^+$.

6-(1H-Tetrazol-5-yl)picolinic acid (51). Methyl 6-bromopicolinate (3.00 g, 13.89 mmol) and copper(I) cyanide (2.49 g, 27.77 mmol) were dissolved in pyridine (120 mL) and heated to 116 °C for 4 h. The reaction was monitored via TLC. Upon completion of the reaction, the mixture was filtered, and the filtrate was concentrated in vacuo. Aqueous NaHCO_3 (50 mL) and CH_2Cl_2 (50 mL) were added to the crude mixture. The aqueous layer was extracted with CH_2Cl_2 (50 mLX3), and the combined organic layers were dried over MgSO_4 , concentrated in vacuo, and purified with flash chromatography. Intermediate methyl 6-cyanopicolinate eluted 40% EtOAc in hexanes as a yellow solid in 20% yield (470 mg, 2.90 mmol). ^1H NMR (400 MHz, CDCl_3 - d): δ 8.34 (d, J = 7.9 Hz, 1H), 8.04 (t, J = 7.9 Hz, 1H), 7.88 (d, J = 7.8 Hz, 1H), 4.04 (s, 3H). ESI-MS(+) calculated for $[\text{C}_8\text{H}_7\text{N}_2\text{O}_2]^+$ m/z 163.05, found m/z 163.10 $[\text{M}+\text{H}]^+$.

In a round bottom flask, intermediate methyl 6-cyanopicolinate (200 mg, 1.23 mmol), sodium azide (408 mg, 6.29 mmol), and ammonia hydrochloride (336 mg, 6.29 mmol) were dissolved in anhydrous DMF (10 mL). The reaction was heated under N_2 at 130 °C for 20 h. After cooling, the inorganic salts were removed via vacuum filtration, and washed with hot DMF. The organic filtrate was concentrated in vacuo to yield a yellow solid. The solid was suspended in a solution of 2M HCl (3 mL), and stirred at

25 °C for 1 h. The precipitate was collected via vacuum filtration and washed with copious amounts of cold water to afford product **51** as a white solid in 98% yield (232 mg, 1.21 mmol). ¹H NMR (400 MHz, DMSO-*d*₆): δ 8.37 (d, *J* = 7.5 Hz, 1H), 8.26 – 8.13 (m, 2H). ¹³C NMR (126 MHz, DMSO-*d*₆): δ 165.2, 155.1, 149.1, 144.3, 140.3, 126.8, 126.2. ESI-MS(-) calculated for [C₇H₄N₅O₂]⁻ *m/z* 190.04, found *m/z* 189.25 [M-H]⁻.

6-(Sulfomethyl)picolinic acid (52). In a round bottom flask, **58** (200 mg, 0.87 mmol) and Na₂SO₃ (110 mg, 0.87 mmol) were dissolved in H₂O (10 mL) and heated to 100 °C for 16 h. The reaction was cooled to room temperature, and H₂O was removed in vacuo until it reached one-third of the original volume. The white precipitate was collected via vacuum filtration as the ester intermediate. The intermediate was hydrolyzed via stirring in 4M HCl at 100 °C for 16 h. The excess HCl was removed in vacuo, and the product was co-evaporated with copious amounts of MeOH and H₂O until white crystals were observed. The precipitate was collected via vacuum filtration to yield compound **52** as a white crystal in 41% yield (77.0 mg, 0.35 mmol). ¹H NMR (400 MHz, DMSO-*d*₆): δ 8.08 – 7.88 (m, 2H), 7.79 (d, *J* = 6.0 Hz, 1H), 4.06 (s, 2H). ¹³C NMR (126 MHz, DMSO-*d*₆): δ 164.7, 155.0, 145.2, 140.7, 129.9, 124.1, 57.6. ESI-MS(-) calculated for [C₇H₆NO₅S]⁻ *m/z* 216.10, found *m/z* 216.08 [M-H]⁻.

6-((Methylsulfonyl)methyl)picolinic acid (53). In a round bottom flask, **58** (300 mg, 1.30 mmol) and sodium methanesulfinate (266 mg, 2.61 mmol) were dissolved in DMF (15 mL). The solution was heated to 120 °C for 2 h. DMF was removed in vacuo, and

the crude product was purified via flash column chromatography eluting at 90% EtOAc in hexanes. The intermediate was hydrolyzed by stirring in 3:1 1M NaOH:THF at 70 °C for 3 h. The THF was removed in vacuo, and the solution was acidified with 4M HCl until pH 4. The aqueous layer was extracted with EtOAc (20 mLX3) to afford **53** a white solid in 43% yield over two steps (120 mg, 0.56 mmol). ¹H NMR (400 MHz, DMSO-*d*₆): δ 8.03 (s, 2H), 7.70 (t, *J* = 4.5 Hz, 1H), 4.75 (s, 2H), 3.08 (s, 3H). ¹³C NMR (126 MHz, DMSO-*d*₆): δ 166.3, 150.7, 149.2, 138.9, 129.3, 124.5, 61.5, 41.1. ESI-MS(-) calculated for [C₈H₈NO₄S]⁻ *m/z* 214.02, found *m/z* 214.16 [M-H]⁻.

6-(Methylsulfonamido)picolinic acid (54). Commercially available methyl 6-aminopicolinate (300 mg, 1.97 mmol) was dissolved in a solution of triethylamine (1 mL):CH₂Cl₂ (5 mL) and cooled to 0 °C. Next, methanesulfonyl chloride (168.0 μL, 2.17 mmol) was added drop-wise to the mixture. The reaction was stirred at room temperature for 16 h. The solvent was removed in vacuo, and the crude mixture was purified via flash column chromatography. The ester intermediate eluted at 62% EtOAc in hexanes as a white solid. The intermediate was hydrolyzed via stirring at room temperature for 16 h in 3:1 1M NaOH:THF (8 mL). The excess THF was removed in vacuo, and the solution was acidified to pH 4. The aqueous layer was extracted with EtOAc (10 mLX3), and the combined organic layers were dried over MgSO₄, filtered, and concentrated in vacuo to afford **54** as a white solid. ¹H NMR (400 MHz, MeOD-*d*₄): δ 7.89 (t, *J* = 7.9 Hz, 1H), 7.79 (d, *J* = 7.5 Hz, 1H), 7.28 (d, *J* = 8.3 Hz, 1H), 3.33 (s, 3H).

^{13}C NMR (126 MHz, $\text{DMSO-}d_6$): δ 166.2, 152.4, 147.1, 140.1, 119.5, 115.9, 42.5. ESI-MS(-) calculated for $[\text{C}_7\text{H}_7\text{N}_2\text{O}_4\text{S}]^-$ m/z 215.10, found m/z 215.05 $[\text{M-H}]^-$.

6-((N-Methylmethanesulfonamido)methyl)picolinic acid (55). In a round bottom flask, **58** (158 mg, 0.69 mmol), *N*-methylmethanesulfonamide (74 mg, 0.69 mmol), and potassium carbonate (48 mg, 0.34 mmol) were dissolved in acetonitrile (10 mL) and heated to 75 °C for 20 h. The solvent was removed in vacuo and the crude mixture was purified via flash column chromatography. The ester intermediate eluted at 3% MeOH in CH_2Cl_2 as a yellow oil. The intermediate was hydrolyzed by stirring in 1M NaOH at 70 °C for 3 h. The solution was then acidified to pH 4, and the aqueous layer was extracted with EtOAc (20 mLX4). The combined organic layers were dried over MgSO_4 , filtered, and concentrated in vacuo to afford **55** a pale solid in 55% yield over two steps (92 mg, 0.38 mmol). ^1H NMR (400 MHz, $\text{DMSO-}d_6$): δ 8.04 – 7.90 (m, 2H), 7.61 (d, J = 7.3 Hz, 1H), 4.46 (s, 2H), 3.08 (s, 3H), 2.75 (s, 3H). ^{13}C NMR (126 MHz, $\text{DMSO-}d_6$): δ 166.5, 157.4, 148.5, 138.9, 125.7, 124.1, 54.9, 36.7, 35.2. ESI-MS(-) calculated for $[\text{C}_9\text{H}_{11}\text{N}_2\text{O}_4\text{S}]^-$ m/z 243.04, found m/z 243.31 $[\text{M-H}]^-$.

6-(Thiazol-2-yl)picolinic acid (56). In a round bottom flask, methyl 6-bromopicolinate (300 mg, 1.39 mmol) and 2-(tributylstannyl)thiazole (624 mg, 1.67 mmol) were dissolved in anhydrous THF (15 mL). The solution was purged with N_2 for 15 min, followed by the addition of bis(triphenylphosphine)palladium(II) dichloride (97 mg, 0.14 mmol). The reaction was heated to 75 °C for 18 h. Upon completion, water (20 mL) and EtOAc (20

mL) were added to the brown slurry. The aqueous layer was extracted with EtOAc (20 mLX3), and the combined organic layers were dried over MgSO₄, filtered, and concentrated in vacuo. The ester intermediate was purified via column chromatography, eluting at 45% EtOAc in hexanes as a yellow solid. The intermediate was hydrolyzed in 3:1 1M NaOH:THF at 70 °C for 3 h. THF was removed in vacuo, and the aqueous layer was acidified to pH 4. The precipitate was collected via vacuum filtration to afford compound **56** as a tan solid in 74% yield (213 mg, 1.03 mmol). ¹H NMR (400 MHz, DMSO-*d*₆): δ 9.18 (s, 1H), 8.68 (s, 1H), 8.22 (d, *J* = 8.0 Hz, 1H), 8.05 (t, *J* = 7.8 Hz, 1H), 7.94 (d, *J* = 7.7 Hz, 1H). ¹³C NMR (126 MHz, DMSO-*d*₆): δ 166.1, 157.0, 150.5, 149.0, 142.3, 139.7, 139.1, 124.2, 123.4. ESI-MS(-) calculated for [C₉H₅N₂O₂S]⁻ *m/z* 205.01, found *m/z* 205.18 [M-H]⁻.

6-(Oxazol-2-yl)picolinic acid (57). In a round bottom flask, methyl 6-bromopicolinate (300 mg, 1.39 mmol) and 2-(tributylstannyl)oxazole (596 mg, 1.67 mmol) were dissolved in anhydrous THF (15 mL). The solution was purged with N₂ for 15 min, followed by the addition of bis(triphenylphosphine)palladium(II) dichloride (79 mg, 0.14 mmol). The solution was heated to 75 °C for 18 h. Upon completion, water (20 mL) and EtOAc (20 mL) were added to the slurry. The aqueous layer was extracted with EtOAc (20 mLX3), and the combined organic layers were dried over MgSO₄, filtered, and concentrated in vacuo. The ester intermediate was purified via column chromatography, eluting at 60% EtOAc in hexanes as a yellow solid. The intermediate was hydrolyzed in 3:1 1M NaOH:THF at 70 °C for 3 h. THF was removed in vacuo, and the aqueous layer was

acidified to pH 4. The aqueous layer was extracted with EtOAc (20 mLX3), and the combined organic layers were dried over MgSO₄, filtered, and concentrated in vacuo to yield **57** as a white solid in 8% yield (20 mg, 0.12 mmol). ¹H NMR (400 MHz, DMSO-*d*₆): δ 8.35 (s, 1H), 8.28 (dd, *J* = 6.4, 2.6 Hz, 1H), 8.16 – 8.10 (m, 2H), 7.49 (s, 1H). ¹³C NMR (126 MHz, DMSO-*d*₆): δ 166.2, 160.0, 149.4, 145.9, 142.0, 139.4, 129.4, 126.2, 125.3. ESI-MS(-) calculated for [C₉H₅N₂O₃]⁻ *m/z* 189.03, found *m/z* 189.20 [M-H]⁻.

Methyl 6-(bromomethyl)picolinate (58). To a solution of methyl 6-(hydroxymethyl)picolinate (1.0 g, 5.98 mmol) in chloroform (25 mL) at 0 °C was added PBr₃ (1.9 g, 7.18 mmol) dropwise over the course of 15 min. The reaction was stirred at room temperature for 3 h. The reaction mixture was quenched with saturated sodium carbonate in water and extracted with chloroform (20 mLX4). The combined organic layers were dried over MgSO₄, filtered, and concentrated in vacuo. The product was purified via flash column chromatography, eluting at 45% EtOAc in hexanes to afford **58** as a white crystal in 70% yield (95 mg, 4.14 mmol). ¹H NMR (400 MHz, CDCl₃-*d*): δ 8.06 (d, *J* = 7.8 Hz, 1 H), 7.86 (td, *J* = 7.8, 1.4 Hz), 7.68 (d, *J* = 7.8 Hz, 1 H), 4.64 (s, 2H), 4.01 (s, 3H). ESI-MS(+) calculated for [C₈H₉BrNO₂]⁺ *m/z* 229.98, found *m/z* 230.24 [M+H]⁺.

Dimethyl 4-hydroxypyridine-2,6-dicarboxylate (59). Commercially-available 4-hydroxypyridine-2,6-dicarboxylic acid (10.0 g, 55 mmol) was dissolved in MeOH (500 mL) and H₂SO₄ (cat.) was added. The reaction was stirred at 70 °C for 16 h. The

solvent was removed in vacuo, and the crude mixture was purified via column chromatography, eluting at 1% MeOH in CH₂Cl₂ as a yellow solid in 60% yield (7.0 g, 30 mmol). ¹H NMR (400 MHz, MeOD-*d*₄): δ 7.59 (s, 2H), 3.96 (s, 6H). ESI-MS(+) calculated for [C₉H₁₀NO₅]⁺ *m/z* 212.06, found *m/z* 212.07 [M+H]⁺.

Dimethyl 4-bromopyridine-2,6-dicarboxylate (60). Tetrabutylammonium bromide (28.623 g, 88.789 mmol) and P₄O₁₀ (12.6 g, 89 mmol) were dissolved in dry toluene (50 mL), and heated to 100 °C for 30 min under N₂. Compound **59** (7.5 g, 36 mmol) was added to the solution and the mixture was heated at 100 °C for 3 h. The toluene layer was decanted, and an additional 50 mL of toluene was added to the residual brown oil. The mixture was heated to 100 °C for an additional 30 min, and the toluene layer was decanted again. Addition and removal of toluene was repeated three times. The combined toluene layers were dried in vacuo, and the crude mixture was purified via column chromatography. Compound **60** eluted at 45% EtOAc in hexanes as yellow needles in 75% yield (7.3 g, 27 mmol). ¹H NMR (400 MHz, DMSO-*d*₆): δ 8.42 (s, 2H), 3.91 (s, 6H). ESI-MS(+) calculated for [C₉H₉BrNO₄]⁺ *m/z* 273.97, found *m/z* 274.26 and 275.25 [M+H]⁺.

Methyl 4-bromo-6-(hydroxymethyl)picolinate (61). In a round bottom flask, compound **60** (1.0 g, 3.65 mmol) was dissolved in a solution of MeOH:CH₂Cl₂ (16 mL:4 mL) and cooled to 0 °C. NaBH₄ (138 mg, 3.65 mmol) was added to the mixture and stirred at 0 °C for 1 h. The reaction was quenched with aqueous NaHCO₃ (10 mL). The

mixture was extracted with CH₂Cl₂ (10 mLX3), and the combined organic layers were dried in vacuo. The crude mixture was purified via column chromatography, with **61** eluting at 70% EtOAc in hexanes as white crystals in 80% yield (689 mg, 2.80 mmol). ¹H NMR (400 MHz, MeOD-*d*₄): δ 8.17 (s, 1H), 7.97 (s, 1H), 4.73 (s, 2H), 3.97 (s, 3H). ESI-MS(+) calculated for [C₈H₉BrNO₃]⁺ *m/z* 245.98, found *m/z* 246.16 and 248.09 [M+H]⁺.

Methyl 4-bromo-6-(bromomethyl)picolinate (62). Compound **61** (400 mg, 1.63 mmol) was dissolved in CHCl₃ (4 mL) and cooled to 0 °C. Next, PBr₃ (528 mg, 1.95 mmol) was added dropwise, and the reaction was stirred at 0 °C for 1 h. The reaction was tracked via TLC. Upon completion, the reaction mixture was quenched with aqueous Na₂CO₃ (40 mL), and the aqueous layer was extracted with chloroform (40 mLX4). The combined organic layers were dried over MgSO₄, filtered, and concentrated in vacuo to yield a yellow oil with white precipitate. The crude product was purified via flash column chromatography, with compound **62** eluting at 42% EtOAc in hexanes as a white solid in 68% yield (342 mg, 1.11 mmol). ¹H NMR (400 MHz, CDCl₃-*d*): δ 8.21 (s, 1H), 7.86 (s, 1H), 4.59 (s, 2H), 4.02 (s, 3H). ESI-MS(+) calculated for [C₈H₈Br₂NO₂]⁺ *m/z* 307.89, found *m/z* 308.07 and 310.00 [M+H]⁺.

Methyl 4-bromo-6-((diethoxyphosphoryl)methyl)picolinate (63). In a round bottom flask, **62** (3.5 g, 11.39 mmol) and triethyl phosphite (5.7 g, 34.16 mmol) were dissolved in toluene (30 mL). The reaction was heated at 140 °C for 22 h. Excess triethyl

phosphite and toluene were removed in vacuo, and the crude product was purified via flash column chromatography. Compound **63** eluted at 70% EtOAc in hexanes as a clear oil in 92% yield (3.9 g, 10.52 mmol). $^1\text{H NMR}$ (400 MHz, CDCl_3 -*d*): δ 8.17 (s, 1H), 7.78 (s, 1H), 4.12 (dq, $J = 10.2, 3.6$ Hz, 4H), 3.99 (s, 3H), 3.50 (d, $J = 22.0$ Hz, 2H), 1.29 (t, $J = 7.0$ Hz, 6H). ESI-MS(+) calculated for $[\text{C}_{12}\text{H}_{18}\text{BrNO}_5\text{P}]^+$ m/z 366.01, found m/z 366.03 $[\text{M}+\text{H}]^+$.

*General procedures for the synthesis of compounds **64a** – **64m***

In a round bottom flask, compound **63** (1 equivalent), the corresponding boronic acid (1.2 equivalents) and $\text{K}_3\text{O}_4\text{P}$ (2 equivalents) were dissolved in 1,4-dioxanes (5 mL). The solution was purged under N_2 for 20 min, followed by the addition of tetrakis(triphenylphosphine)palladium(0) (0.1 equivalents). The reaction was heated to 80 °C for 18 h under N_2 . The crude mixture was filtered through a pad of celite, washed with EtOAc, and the combined organic layers were concentrated in vacuo. The crude products were purified via flash column chromatography to afford derivatives **64a** – **64m**.

Methyl 6-((diethoxyphosphoryl)methyl)-4-phenylpicolinate (64a). Yield: 74% (59 mg, 0.16 mmol). $^1\text{H NMR}$ (400 MHz, MeOD -*d*₄): δ 8.26 (s, 1H), 7.90 (d, $J = 2.1$ Hz, 1H), 7.77 (d, $J = 6.5$ Hz, 2H), 7.65 – 7.31 (m, 3H), 4.28 – 4.07 (m, 4H), 3.65 (d, $J = 22.2$ Hz, 2H), 1.28 (t, $J = 7.0$ Hz, 6H). ESI-MS(+) calculated for $[\text{C}_{18}\text{H}_{23}\text{NO}_5\text{P}]^+$ m/z 364.13, found m/z 364.11 $[\text{M}+\text{H}]^+$.

Methyl 6-((diethoxyphosphoryl)methyl)-4-(4-methoxyphenyl)picolinate (64b). Yield: 79% (120 mg, 0.31 mmol). $^1\text{H NMR}$ (400 MHz, $\text{DMSO-}d_6$): δ 8.14 (s, 1H), 7.87 (s, 1H), 7.79 (d, $J = 7.3$ Hz, 2H), 7.10 (d, $J = 7.7$ Hz, 2H), 4.11 – 3.94 (m, 4H), 3.89 (s, 3H), 3.82 (s, 3H), 3.56 (d, $J = 21.7$ Hz, 2H), 1.18 (t, $J = 6.2$ Hz, 6H). ESI-MS(+) calculated for $[\text{C}_{19}\text{H}_{25}\text{NO}_6\text{P}]^+$ m/z 394.14, found m/z 394.28 $[\text{M}+\text{H}]^+$.

Methyl 6-((diethoxyphosphoryl)methyl)-4-(3-methoxyphenyl)picolinate (64c). Yield: 58% (86 mg, 0.22 mmol). $^1\text{H NMR}$ (400 MHz, $\text{MeOD-}d_4$): δ 8.26 (s, 1H), 7.90 (s, 1H), 7.45 (t, $J = 8.0$ Hz, 1H), 7.34 (d, $J = 7.8$ Hz, 1H), 7.30 (s, 1H), 7.07 (d, $J = 8.2$ Hz, 1H), 4.21 – 4.07 (m, 4H), 4.00 (s, 3H), 3.88 (s, 3H), 3.66 (d, $J = 22.2$ Hz, 2H), 1.29 (t, $J = 7.0$ Hz, 6H). ESI-MS(+) calculated for $[\text{C}_{19}\text{H}_{25}\text{NO}_6\text{P}]^+$ m/z 394.14, found m/z 416.13 $[\text{M}+\text{Na}]^+$.

Methyl 6-((diethoxyphosphoryl)methyl)-4-(2-methoxyphenyl)picolinate (64d). Yield: 87% (125 mg, 0.32 mmol). $^1\text{H NMR}$ (400 MHz, $\text{MeOD-}d_4$): δ 8.20 (s, 1H), 7.81 (s, 1H), 7.50 – 7.36 (m, 2H), 7.15 (d, $J = 8.4$ Hz, 1H), 7.09 (t, $J = 7.5$ Hz, 1H), 4.24 – 4.06 (m, 4H), 3.98 (s, 3H), 3.86 (s, 3H), 3.63 (d, $J = 22.2$ Hz, 2H), 1.28 (t, $J = 7.0$ Hz, 6H). ESI-MS(+) calculated for $[\text{C}_{19}\text{H}_{25}\text{NO}_6\text{P}]^+$ m/z 394.14, found m/z 416.13 $[\text{M}+\text{Na}]^+$.

Methyl 6-((diethoxyphosphoryl)methyl)-4-(4-hydroxyphenyl)picolinate (64e). Yield: 20% (27 mg, 0.07 mmol). $^1\text{H NMR}$ (400 MHz, $\text{MeOD-}d_4$): δ 8.21 (s, 1H), 7.83 (s, 1H), 7.65 (d, $J = 6.4$ Hz, 2H), 6.92 (d, $J = 6.7$ Hz, 2H), 4.31 – 4.04 (m, 4H), 3.99 (s, 3H), 3.61

(d, $J = 23.0$ Hz, 2H), 1.28 (t, $J = 7.0$ Hz, 7H). ESI-MS(+) calculated for $[C_{18}H_{23}NO_6P]^+$ m/z 380.12, found m/z 402.13 $[M+Na]^+$.

Methyl 6-((diethoxyphosphoryl)methyl)-4-(3-hydroxyphenyl)picolinate (64f). Yield: 90% (135 mg, 0.40 mmol). 1H NMR (400 MHz, MeOD- d_4): δ 8.23 (s, 1H), 7.86 (s, 1H), 7.35 (t, $J = 7.9$ Hz, 1H), 7.22 (d, $J = 7.9$ Hz, 1H), 7.16 (s, 1H), 6.92 (d, $J = 8.0$ Hz, 1H), 4.21 – 4.06 (m, 4H), 4.00 (s, 3H), 3.65 (d, $J = 20.8$ Hz, 2H), 1.29 (t, $J = 6.3$ Hz, 6H). ESI-MS(+) calculated for $[C_{18}H_{23}NO_6P]^+$ m/z 380.12, found m/z 402.13 $[M+Na]^+$.

Methyl 6-((diethoxyphosphoryl)methyl)-4-(2-hydroxyphenyl)picolinate (64g). Yield: 63% (91 mg, 0.24 mmol). 1H NMR (400 MHz, MeOD- d_4): δ 8.31 (s, 1H), 7.91 (s, 1H), 7.41 (d, $J = 7.4$ Hz, 1H), 7.28 (t, $J = 7.8$ Hz, 1H), 7.02 – 6.80 (m, 2H), 4.21 – 4.05 (m, 4H), 3.98 (s, 3H), 3.63 (d, $J = 22.1$ Hz, 2H), 1.28 (t, $J = 7.0$ Hz, 6H). ESI-MS(+) calculated for $[C_{18}H_{23}NO_6P]^+$ m/z 380.12, found m/z 402.13 $[M+Na]^+$.

Methyl 4-(4-acetamidophenyl)-6-((diethoxyphosphoryl)methyl)picolinate (64h)
Yield: 43% (72 mg, 0.170mmol). 1H NMR (400 MHz, MeOD- d_4): δ 8.36 (s, 1H), 8.02 (s, 1H), 7.87 – 7.72 (m, 4H), 4.23 – 4.09 (m, 4H), 4.03 (s, 3H), 3.72 (d, $J = 22.3$ Hz, 2H), 2.16 (s, 3H), 1.29 (t, $J = 7.0$ Hz, 6H). ESI-MS(+) calculated for $[C_{20}H_{26}N_2O_6P]^+$ m/z 421.15, found m/z 421.20 $[M+H]^+$.

Methyl 4-(3-acetamidophenyl)-6-((diethoxyphosphoryl)methyl)picolinate (64i).

Yield: 39% (60 mg, 0.14 mmol). $^1\text{H NMR}$ (400 MHz, CDCl_3-d): δ 8.22 (s, 1H), 8.16 (s, 1H), 7.85 (d, $J = 6.8$ Hz, 2H), 7.68 (d, $J = 7.0$ Hz, 1H), 7.43 – 7.32 (m, 2H), 4.28 – 4.05 (m, 4H), 4.00 (s, 3H), 3.67 (d, $J = 21.9$ Hz, 2H), 2.22 (s, 3H), 1.30 (t, $J = 7.1$ Hz, 6H). ESI-MS(+) calculated for $[\text{C}_{20}\text{H}_{26}\text{N}_2\text{O}_6\text{P}]^+$ m/z 421.15, found m/z 421.19 $[\text{M}+\text{H}]^+$.

Methyl 4-(2-acetamidophenyl)-6-((diethoxyphosphoryl)methyl)picolinate (64j).

Yield: 84% (136 mg, 0.32 mmol). $^1\text{H NMR}$ (400 MHz, $\text{MeOD}-d_4$): δ 8.17 (s, 1H), 7.80 (s, 1H), 7.64 – 7.29 (m, 4H), 4.32 – 4.08 (m, 4H), 4.02 (s, 3H), 3.74 (d, $J = 22.3$ Hz, 2H), 1.99 (s, 3H), 1.31 (t, $J = 7.0$ Hz, 6H). ESI-MS(+) calculated for $[\text{C}_{20}\text{H}_{26}\text{N}_2\text{O}_6\text{P}]^+$ m/z 421.15, found m/z 421.21 $[\text{M}+\text{H}]^+$.

Methyl 4-(4-chlorophenyl)-6-((diethoxyphosphoryl)methyl)picolinate (64k).

Yield: 60% (91 mg, 0.23 mmol). $^1\text{H NMR}$ (400 MHz, $\text{MeOD}-d_4$): δ 8.28 (s, 1H), 7.91 (s, 1H), 7.80 (d, $J = 8.7$ Hz, 2H), 7.55 (d, $J = 8.6$ Hz, 2H), 4.23 – 4.08 (m, 5H), 4.00 (s, 3H), 3.66 (d, $J = 22.2$ Hz, 2H), 1.28 (t, $J = 7.1$ Hz, 6H). ESI-MS(+) calculated for $[\text{C}_{18}\text{H}_{22}\text{ClNO}_5\text{P}]^+$ m/z 398.09, found m/z 398.24 $[\text{M}+\text{H}]^+$.

Methyl 4-(3-chlorophenyl)-6-((diethoxyphosphoryl)methyl)picolinate (64l).

Yield: 42% (63 mg, 0.16 mmol). $^1\text{H NMR}$ (400 MHz, $\text{MeOD}-d_4$): δ 8.28 (s, 1H), 7.93 (s, 1H), 7.84 (s, 1H), 7.78 – 7.68 (m, 1H), 7.61 – 7.47 (m, 2H), 4.24 – 4.08 (m, 4H), 4.01 (s, 3H),

3.67 (d, $J = 22.0$ Hz, 2H), 1.29 (t, $J = 6.8$ Hz, 6H). ESI-MS(+) calculated for $[\text{C}_{18}\text{H}_{22}\text{ClNO}_5\text{P}]^+$ m/z 398.09, found m/z 398.15 $[\text{M}+\text{H}]^+$.

Methyl 4-(2-chlorophenyl)-6-((diethoxyphosphoryl)methyl)picolinate (64m). Yield: 71% (114 mg, 0.29 mmol). ^1H NMR (400 MHz, $\text{MeOD-}d_4$): δ 8.11 (s, 1H), 7.74 (s, 1H), 7.61 – 7.40 (m, 4H), 4.23 – 4.07 (m, 4H), 3.99 (s, 3H), 3.67 (d, $J = 22.2$ Hz, 2H), 1.28 (t, $J = 7.1$ Hz, 6H). ESI-MS(+) calculated for $[\text{C}_{18}\text{H}_{22}\text{ClNO}_5\text{P}]^+$ m/z 398.09, found m/z 398.13 $[\text{M}+\text{H}]^+$.

General procedures for the synthesis of 65a – 65m.

Compounds **64a – 64m** were dissolved in a solution of 6M HCl and heated to 100 °C for 24 h. Excess HCl was removed in vacuo followed by co-evaporation with copious amounts of water and MeOH until precipitate was observed. The precipitate was collected via vacuum filtration and washed with cold water to afford products **65a – 65m**.

4-Phenyl-6-(phosphonomethyl)picolinic acid (65a). Yield: 29% (14 mg, 0.05 mmol). ^1H NMR (400 MHz, $\text{MeOD-}d_4$): δ 8.65 (s, 1H), 8.39 (s, 1H), 8.14 – 7.57 (m, 5H), 3.82 (d, $J = 22.3$ Hz, 2H). ESI-MS(-) calculated for $[\text{C}_{13}\text{H}_{11}\text{NO}_5\text{P}]^-$ m/z 292.03, found m/z 292.04 $[\text{M}-\text{H}]^-$.

4-(4-Methoxyphenyl)-6-(phosphonomethyl)picolinic acid (65b). Yield: 61% (48 mg, 0.15 mmol). ^1H NMR (400 MHz, $\text{DMSO-}d_6$): δ 8.08 (s, 1H), 7.82 (s, 1H), 7.75 (d, $J = 8.6$ Hz, 2H), 7.09 (d, $J = 8.5$ Hz, 2H), 3.81 (s, 3H), 3.30 (d, $J = 21.4$ Hz, 2H). ^{13}C NMR (126 MHz, $\text{DMSO-}d_6$): δ 166.7, 161.0, 156.2, 148.9, 148.3, 129.2, 128.7, 124.3, 119.6, 115.2, 55.8, 38.3. ESI-MS(-) calculated for $[\text{C}_{14}\text{H}_{13}\text{NO}_6\text{P}]^-$ m/z 322.05, found m/z 322.10 $[\text{M-H}]^-$.

4-(3-Methoxyphenyl)-6-(phosphonomethyl)picolinic acid (65c). Yield: 71% (50 mg, 0.15 mmol). ^1H NMR (400 MHz, $\text{MeOD-}d_4$): δ 8.33 (s, 1H), 8.01 (s, 1H), 7.53 – 7.31 (m, 3H), 7.09 (d, $J = 7.4$ Hz, 1H), 3.89 (s, 3H), 3.56 (d, $J = 21.8$ Hz, 2H). ^{13}C NMR (126 MHz, $\text{DMSO-}d_6$): δ 166.7, 160.4, 156.2, 149.4, 148.6, 138.8, 131.0, 125.3, 120.4, 119.6, 115.7, 112.7, 55.8, 38.4. ESI-MS(-) calculated for $[\text{C}_{14}\text{H}_{13}\text{NO}_6\text{P}]^-$ m/z 322.05, found m/z 322.02 $[\text{M-H}]^-$.

4-(2-Methoxyphenyl)-6-(phosphonomethyl)picolinic acid (65d). Yield: 67% (67 mg, 0.21 mmol). ^1H NMR (400 MHz, $\text{MeOD-}d_4$): δ 8.32 (s, 1H), 7.96 (s, 1H), 7.59 – 7.38 (m, 2H), 7.17 (d, $J = 8.2$ Hz, 1H), 7.11 (t, $J = 7.4$ Hz, 1H), 3.88 (s, 3H), 3.55 (d, $J = 21.7$ Hz, 2H). ^{13}C NMR (126 MHz, $\text{DMSO-}d_6$): δ 166.7, 156.7, 155.5, 147.9, 147.2, 131.2, 130.6, 127.7, 126.6, 123.3, 121.5, 112.5, 56.1, 38.3. ESI-MS(-) calculated for $[\text{C}_{14}\text{H}_{13}\text{NO}_6\text{P}]^-$ m/z 322.05, found m/z 322.04 $[\text{M-H}]^-$.

4-(4-Hydroxyphenyl)-6-(phosphonomethyl)picolinic acid (65e). Yield: 82% (16 mg, 0.06 mmol). ^1H NMR (400 MHz, MeOD- d_4): δ 8.38 (s, 1H), 8.08 (s, 1H), 7.81 (d, J = 8.2 Hz, 2H), 6.96 (d, J = 8.0 Hz, 2H), 3.56 (d, J = 21.4 Hz, 2H). ^{13}C NMR (126 MHz, DMSO- d_6): δ 166.7, 159.5, 155.9, 148.8, 148.7, 128.7, 127.5, 124.0, 119.4, 116.6, 38.2. ESI-MS(-) calculated for $[\text{C}_{13}\text{H}_{11}\text{NO}_6\text{P}]^-$ m/z 308.03, found m/z 308.02 $[\text{M-H}]^-$.

4-(3-Hydroxyphenyl)-6-(phosphonomethyl)picolinic acid (65f). Yield: 82% (77 mg, 0.30 mmol). ^1H NMR (400 MHz, MeOD- d_4): δ 8.47 (s, 1H), 8.21 (s, 1H), 7.48 – 7.33 (m, 2H), 7.29 (s, 1H), 7.01 (d, J = 7.4 Hz, 1H), 3.73 (d, J = 22.1 Hz, 2H). ^{13}C NMR (126 MHz, DMSO- d_6): δ 166.6, 158.6, 156.2, 148.9, 148.9, 138.5, 131.0, 125.0, 120.2, 118.0, 117.0, 113.9, 38.3. ESI-MS(-) calculated for $[\text{C}_{13}\text{H}_{11}\text{NO}_6\text{P}]^-$ m/z 308.03, found m/z 308.05 $[\text{M-H}]^-$.

4-(2-Hydroxyphenyl)-6-(phosphonomethyl)picolinic acid (65g). Yield: 76% (56 mg, 0.18 mmol). ^1H NMR (400 MHz, MeOD- d_4): δ 8.87 (s, 1H), 8.48 (s, 1H), 7.68 (d, J = 6.7 Hz, 1H), 7.45 (t, J = 7.1 Hz, 1H), 7.13 – 7.01 (m, 1H), 3.86 (d, J = 22.4 Hz, 2H). ^{13}C NMR (126 MHz, DMSO- d_6): δ 166.8, 155.5, 155.3, 147.8, 147.6, 130.9, 130.5, 127.2, 124.5, 123.1, 120.2, 116.8, 38.4. ESI-MS(-) calculated for $[\text{C}_{13}\text{H}_{11}\text{NO}_6\text{P}]^-$ m/z 308.03, found m/z 308.09 $[\text{M-H}]^-$.

4-(4-Aminophenyl)-6-(phosphonomethyl)picolinic acid (65h). Yield: 56% (14 mg, 0.05 mmol). ^1H NMR (400 MHz, MeOD- d_4): δ 8.68 (s, 1H), 8.43 (s, 1H), 8.14 (d, J =

8.2 Hz, 2H), 7.56 (d, $J = 8.2$ Hz, 2H), 3.86 (d, $J = 22.4$ Hz, 2H). ^{13}C NMR (126 MHz, DMSO- d_6): δ 166.6, 155.5, 151.1, 149.2, 148.6, 128.2, 123.1, 123.0, 118.5, 114.6, 38.0. ESI-MS(-) calculated for $[\text{C}_{13}\text{H}_{12}\text{N}_2\text{O}_5\text{P}]^-$ m/z 307.05, found m/z 307.09 $[\text{M-H}]^-$.

4-(3-Aminophenyl)-6-(phosphonomethyl)picolinic acid (65i). Yield: 96% (48 mg, 0.16 mmol). ^1H NMR (400 MHz, MeOD- d_4): δ 8.35 (s, 1H), 8.01 (s, 1H), 7.96 – 7.47 (m, 4H), 3.59 (d, $J = 21.9$ Hz, 2H). ESI-MS(-) calculated for $[\text{C}_{13}\text{H}_{12}\text{N}_2\text{O}_5\text{P}]^-$ m/z 307.05, found m/z 307.09 $[\text{M-H}]^-$.

4-(2-Aminophenyl)-6-(phosphonomethyl)picolinic acid (65j). yield: 60% (60 mg, 0.19 mmol). ^1H NMR (400 MHz, MeOD- d_4): δ 8.24 (s, 1H), 7.87 (s, 1H), 7.54 – 7.32 (m, 2H), 7.25 – 7.05 (m, 2H), 3.57 (d, $J = 21.7$ Hz, 2H). ^{13}C NMR (126 MHz, DMSO- d_6): δ 166.7, 155.8, 155.7, 148.9, 148.7, 145.9, 130.3, 127.2, 122.6, 122.1, 117.3, 116.3, 38.3. ESI-MS(-) calculated for $[\text{C}_{13}\text{H}_{12}\text{N}_2\text{O}_5\text{P}]^-$ m/z 307.05, found m/z 307.06 $[\text{M-H}]^-$.

4-(4-Chlorophenyl)-6-(phosphonomethyl)picolinic acid (65k). Yield: 97% (60 mg, 0.18 mmol). ^1H NMR (400 MHz, DMSO- d_6): δ 8.13 (s, 1H), 7.86 (s, 2H), 7.83 (d, $J = 8.1$ Hz, 3H), 7.62 (d, $J = 8.1$ Hz, 2H), 3.34 (d, $J = 21.5$ Hz, 2H). ^{13}C NMR (126 MHz, DMSO- d_6): δ 166.6, 156.3, 149.1, 147.5, 136.0, 135.0, 129.8, 129.2, 125.0, 120.2, 38.3. ESI-MS(-) calculated for $[\text{C}_{13}\text{H}_{10}\text{ClNO}_5\text{P}]^-$ m/z 326.00, found m/z 326.01 $[\text{M-H}]^-$.

4-(3-Chlorophenyl)-6-(phosphonomethyl)picolinic acid (65l). Yield: 90% (47 mg, 0.14 mmol). ^1H NMR (400 MHz, DMSO- d_6): δ 8.14 (s, 1H), 7.95 – 7.35 (m, 5H), 3.34 (d, $J = 21.5$ Hz, 2H). ^{13}C NMR (126 MHz, DMSO- d_6): δ 166.6, 156.4, 149.1, 147.2, 139.4, 134.6, 131.7, 129.8, 127.2, 126.2, 125.2, 120.4, 38.4. ESI-MS(-) calculated for $[\text{C}_{13}\text{H}_{10}\text{ClNO}_5\text{P}]^-$ m/z 326.00, found m/z 325.97 $[\text{M}-\text{H}]^-$.

4-(2-Chlorophenyl)-6-(phosphonomethyl)picolinic acid (65m). Yield: 72% (67 mg, 0.20 mmol). ^1H NMR (400 MHz, MeOD- d_4) δ 8.57 (s, 1H), 8.30 (s, 1H), 7.77 – 7.48 (m, 4H), 3.89 (d, $J = 22.5$ Hz, 2H). ^{13}C NMR (126 MHz, DMSO- d_6): δ 166.5, 155.8, 148.2, 147.5, 137.0, 131.7, 131.4, 131.2, 130.7, 128.4, 127.9, 123.2, 38.3. ESI-MS(-) calculated for $[\text{C}_{13}\text{H}_{10}\text{ClNO}_5\text{P}]^-$ m/z 326.00, found m/z 325.98 $[\text{M}-\text{H}]^-$.

Determination of IC_{50} values for MBL inhibition

NDM-1, IMP-1, and VIM-2 were over-expressed and purified as previously described.⁸ The IC_{50} values for which meropenem was used as a substrate is described. The decrease in absorption of meropenem at 300 nm (buffer: 50 mM HEPES, 2mM CHAPS, pH 7) was monitored in UV-transparent 96 well plates (Corning product #3635).¹¹ Briefly, 20 μL of each compound at various concentrations (final concentration 0 – 10 μM) was added to each well, followed by addition of 50 μL (final concentration NDM-1, 10 nM or IMP-1, 25 nM). The wells were incubated at 25 $^\circ\text{C}$ for 20 min. Next, 30 μL of meropenem (final concentration 180 μM) was added to each well to initiate the reaction. The plate was then centrifuged at 600 rpm for 30 s to

eliminate air bubbles, and placed into a Synergy H4 plate reader (BioTek). The absorbance was monitored at 300 nm over 5 min with 15 s intervals. The $\Delta\text{Abs}_{300\text{nm}}/\text{min}$ was calculated from each slope as described below, fixing the uninhibited value at 100%, and solving for both the IC_{50} and Hill coefficient values.⁸

The IC_{50} values for which fluorocillin was used as a substrate were determined as described previously,⁸ with minor modifications made to the volume of reagents used. Briefly, 20 μL of each compound at various concentrations (final concentration 0.001 – 10 μM) was added to each well, followed by addition of 50 μL enzyme (final concentration, NDM-1, 0.2 nM; IMP-1, 0.06 nM). Each plate was incubated for 20 min at 25 °C, followed by the addition of 30 μL fluorocillin (final concentration 87 nM). The hydrolysis of fluorocillin is monitored at $\lambda_{\text{ex/em}}$ of 495/525 nm. Plates were prepared in parallel to minimize any variability due to compound storage and handling. The rates of fluorescence increase are determined and IC_{50} values determined as described above for the chromogenic assay.

Equilibrium dialysis

ZnZn-NDM-1 (final concentration 8 μM) in 5 mL of 100 mM ammonium acetate, pH 7.5, was mixed with the compounds at concentrations of 0 – 128 μM . After incubation for 1 h, the solutions were dialyzed versus 500 mL of metal-free ammonium acetate, pH 7.5, overnight (dialysis tubing MWCO 6000–8000, Fisherbrand). The Zn(II) content in the resulting NDM-1 samples was determined using inductively coupled

plasma with atomic emission spectroscopy (ICP-AES, Perkin Elmer Optima 7300DV). The emission wavelength was set to 213.856 nm, as previously described.⁸

UV–Visible spectroscopy

To prepare Co(II)-substituted NDM-1, NDM-1 (150 μ M) was dialyzed twice against 2 mM EDTA, 50 mM HEPES, pH 6.8, containing 150 mM NaCl, and 2 mM EDTA, followed by three separate dialysis steps against 50 mM HEPES, pH 6.8, containing 150 mM NaCl, and 0.5 g/L Chelex resin. Buffers were exchanged at approximately 12 h intervals. Metal-free NDM-1 was diluted to 300 μ M with 50 mM HEPES, pH 6.8, containing 150 mM NaCl, 10% glycerol, and 2 mM TCEP (*tris*(2-carboxyethyl)phosphine). CoCl_2 (100 mM stock in water) was added to result in a protein with 2 molar equivalents of Co(II). The resulting CoCo-NDM-1 enzyme was separated into 500 μ L aliquots, and captopril, **DPA**, and **48 – 51** (stock solutions of 50 mM in DMSO) were added to result in samples with 2 molar equivalents of compound. The EDTA stock was dissolved in water. The samples were then incubated on ice for 5 min. The samples were added to a 500 μ L quartz cuvette, and UV–vis spectra were collected on a PerkinElmer Lambda 750 UV/vis/NIR spectrometer measuring absorbance between 300 and 800 nm at 25 °C. A blank spectrum of apo-NDM-1 (300 μ M) was used to generate difference spectra. All data were normalized at 800 nm.

3.6 Acknowledgements

Texts, schemes, and figures in Chapter 3 have been adapted from the materials published in the following paper: Allie Y. Chen, Pei W. Thomas, Zishuo Cheng, Nasa Y. Xu, David L. Tierney, Michael W. Crowder, Walter Fast, Seth M. Cohen, “Investigation of Dipicolinic Acid Isosteres for the Inhibition of Metallo- β -Lactamases” *ChemMedChem*, **2019**, *14*, 1271-1282. The dissertation author was the primary researcher and author and gratefully acknowledges the contributions of all co-authors. The permission to reproduce this paper was granted by John Wiley and Sons.

3.7 References

1. Kalgutkar, A. S.; Scott Daniels, J., Chapter 3 Carboxylic Acids and Their Bioisosteres. In *Metabolism, Pharmacokinetics and Toxicity of Functional Groups: Impact of Chemical Building Blocks on ADMET*, The Royal Society of Chemistry: 2010; pp 99-167.
2. Ballatore, C.; Huryn, D. M.; Smith, A. B., Carboxylic Acid (Bio)Isosteres in Drug Design. *ChemMedChem* **2013**, *8*, 385-395.
3. Lassalas, P.; Gay, B.; Lasfargeas, C.; James, M. J.; Tran, V.; Vijayendran, K. G.; Brunden, K. R.; Kozlowski, M. C.; Thomas, C. J.; Smith, A. B., 3rd; Huryn, D. M.; Ballatore, C., Structure Property Relationships of Carboxylic Acid Isosteres. *J. Med. Chem.* **2016**, *59*, 3183-3203.
4. Chen, A. Y.; Adamek, R. N.; Dick, B. L.; Credille, C. V.; Morrison, C. N.; Cohen, S. M., Targeting Metalloenzymes for Therapeutic Intervention. *Chem. Rev.* **2018**, *119*, 1323-1455.
5. Adamek, R. N.; Credille, C. V.; Dick, B. L.; Cohen, S. M., Isosteres of Hydroxypyridinethione as Drug-like Pharmacophores for Metalloenzyme Inhibition. *J. Biol. Inorg. Chem.* **2018**, *23*, 1129–1138.
6. Dick, B. L.; Cohen, S. M., Metal-Binding Isosteres as New Scaffolds for Metalloenzyme Inhibitors. *Inorg. Chem.* **2018**, *57*, 9538-9543.
7. Skagseth, S.; Akhter, S.; Paulsen, M. H.; Muhammad, Z.; Lauksund, S.; Samuelsen, O.; Leiros, H. S.; Bayer, A., Metallo-beta-lactamase inhibitors by bioisosteric replacement: Preparation, activity and binding. *Eur J Med Chem* **2017**, *135*, 159-173.
8. Chen, A. Y.; Thomas, P. W.; Stewart, A. C.; Bergstrom, A.; Cheng, Z. S.; Miller, C.; Bethel, C. R.; Marshal, S. H.; Credille, C. V.; Riley, C. L.; Page, R. C.; Bonomo, R. A.; Crowder, M. W.; Tierney, D. L.; Fast, W.; Cohen, S. M., Dipicolinic Acid Derivatives as Inhibitors of New Delhi Metallo-beta-Lactamase-1. *J. Med. Chem.* **2017**, *60*, 7267-7283.
9. Klingler, F. M.; Wichelhaus, T. A.; Frank, D.; Cuesta-Bernal, J.; El-Delik, J.; Muller, H. F.; Sjuts, H.; Gottig, S.; Koenigs, A.; Pos, K. M.; Pogoryelov, D.; Proschak, E., Approved Drugs Containing Thiols as Inhibitors of Metallo-beta-lactamases: Strategy To Combat Multidrug-Resistant Bacteria. *J. Med. Chem.* **2015**, *58*, 3626-3630.
10. Bergstrom, A.; Katko, A.; Adkins, Z.; Hill, J.; Cheng, Z.; Burnett, M.; Yang, H.; Aitha, M.; Mehaffey, M. R.; Brodbelt, J. S.; Tehrani, K.; Martin, N. I.; Bonomo, R. A.; Page, R. C.; Tierney, D. L.; Fast, W.; Wright, G. D.; Crowder, M. W., Probing the Interaction of Aspergillomarasmine A with Metallo-beta-lactamases NDM-1, VIM-2, and IMP-7. *ACS Infect. Dis.* **2018**, *4*, 135-145.

11. Thomas, P. W.; Zheng, M.; Wu, S.; Guo, H.; Liu, D.; Xu, D.; Fast, W., Characterization of Purified New Delhi Metallo-beta-Lactamase-1. *Biochemistry* **2011**, *50*, 10102-10113.
12. Brem, J.; van Berkel, S. S.; Zollman, D.; Lee, S. Y.; Gileadi, O.; McHugh, P. J.; Walsh, T. R.; McDonough, M. A.; Schofield, C. J., Structural Basis of Metallo-beta-Lactamase Inhibition by Captopril Stereoisomers. *Antimicrob. Agents. Chemother.* **2016**, *60*, 142-150.
13. Yang, H.; Aitha, M.; Marts, A. R.; Hetrick, A.; Bennett, B.; Crowder, M. W.; Tierney, D. L., Spectroscopic and Mechanistic Studies of Heterodimetallic Forms of Metallo-beta-Lactamase NDM-1. *J. Am. Chem. Soc.* **2014**, *136*, 7273-7285.
14. Cheng, Z.; Thomas, P. W.; Ju, L.; Bergstrom, A.; Mason, K.; Clayton, D.; Miller, C.; Bethel, C. R.; VanPelt, J.; Tierney, D. L.; Page, R. C.; Bonomo, R. A.; Fast, W.; Crowder, M. W., Evolution of New Delhi Metallo-beta-Lactamase (NDM) in the Clinic: Effects of NDM Mutations on Stability, Zinc Affinity, and Mono-Zinc Activity. *J. Biol. Chem.* **2018**, *293*, 12606-12618.
15. King, D. T.; Worrall, L. J.; Gruninger, R.; Strynadka, N. C., New Delhi Metallo-beta-lactamase: Structural Insights into beta-Lactam Recognition and Inhibition. *J. Am. Chem. Soc.* **2012**, *134*, 11362-11365.
16. Hinchliffe, P.; Tanner, C. A.; Krismanich, A. P.; Labbe, G.; Goodfellow, V. J.; Marrone, L.; Desoky, A. Y.; Calvopina, K.; Whittle, E. E.; Zeng, F.; Avison, M. B.; Bols, N. C.; Siemann, S.; Spencer, J.; Dmitrienko, G. I., Structural and Kinetic Studies of the Potent Inhibition of Metallo-beta-Lactamases by 6-Phosphonomethylpyridine-2-carboxylates. *Biochemistry* **2018**, *57*, 1880-1892.
17. Mojica, M. F.; Bonomo, R. A.; Fast, W., B1-Metallo-beta-Lactamases: Where Do We Stand? *Curr Drug Targets* **2016**, *17* (9), 1029-1050.
18. Cheng, Y.; Prusoff, W. H., Relationship Between the Inhibition Constant (K₁) and the Concentration of Inhibitor Which Causes 50 per cent Inhibition (I₅₀) of an Enzymatic Reaction. *Biochem. Pharmacol.* **1973**, *22*, 3099-3108.
19. Yamaguchi, Y.; Ding, S.; Murakami, E.; Imamura, K.; Fuchigami, S.; Hashiguchi, R.; Yutani, K.; Mori, H.; Suzuki, S.; Arakawa, Y.; Kurosaki, H., A Demetallation Method for IMP-1 Metallo-beta-Lactamase with Restored Enzymatic Activity Upon Addition of Metal Ion(s). *ChemBiochem* **2011**, *12*, 1979-1983.
20. Yamaguchi, Y.; Kuroki, T.; Yasuzawa, H.; Higashi, T.; Jin, W.; Kawanami, A.; Yamagata, Y.; Arakawa, Y.; Goto, M.; Kurosaki, H., Probing the Role of Asp-120(81) of Metallo-beta-Lactamase (IMP-1) by Site-directed Mutagenesis, Kinetic Studies, and X-ray Crystallography. *J. Biol. Chem.* **2005**, *280*, 20824-20832.

21. Ju, L. C.; Cheng, Z.; Fast, W.; Bonomo, R. A.; Crowder, M. W., The Continuing Challenge of Metallo-beta-Lactamase Inhibition: Mechanism Matters. *Trends Pharmacol. Sci.* **2018**, *39*, 635-647.

**Chapter 4. Iminodiacetic Acid as a Metal-binding Pharmacophore for New Delhi
Metallo- β -lactamase Inhibitor Development**

4.1 Introduction

There is growing interest in compounds bearing metal-chelating motifs as inhibitors for NDM-1.¹⁻⁶ Of these, the fungal natural product Aspergillomarasmine A (AMA, Figure 4-1), an aminopolycarboxylic acid, has gained attention due to its ability to restore meropenem activity in a mouse infected with NDM-1 expressing *Klebsiella pneumoniae*.^{5, 7} AMA inhibitor development has mainly focused on modification of the carboxylic acid functional groups through removal or conversion to an ester motif (Figure 4-1). These derivatives displayed weaker inhibition, validating the requirement of free carboxylic acids for enzyme inactivation and supporting the mechanism of action of AMA is via non-selective Zn(II) sequestration (similar to that of EDTA).⁸⁻⁹ The non-selective metal-chelating properties of AMA, along with difficult synthesis and derivatization routes for AMA has hindered the development of this motif for NDM-1 inhibitors.^{8, 10-12}

Structural comparison of AMA and EDTA reveals iminodiacetic acid (**IDA**) as a sub-scaffold that could be leveraged for NDM-1 inhibitor development (Figure 4-1, highlighted in bold). **IDA** is a strong tridentate metal chelator (via its *O,N,O*-donor atoms), as evidenced by its role in immobilized metal affinity chromatography (IMAC)¹³ and its development for the sequestration of Zn(II) in IDA-modified human lysozyme (IDA-hLys) against Zn(II)-mediated A β -aggregation for the treatment of Alzheimer's disease.¹⁴ Utilization of **IDA** for inhibitor development allows for greater synthetic accessibility of derivatives to probe the NDM-1 active site and to develop inhibitors that form stable ternary complexes. In addition, **IDA** bears structural resemblance to the

hydrolyzed antibiotic β -lactam ring (Figure 4-1), suggesting the potential for the development of transition-state analogue inhibitors. Notably, **IDA** is an aliphatic derivative of the previously investigated **DPA** MBP (Chapter 2 and Chapter 3), further justifying its use as a scaffold for novel NDM-1 Inhibitor development. Chapter 4 will report the utilization of **IDA** as a MBP for NDM-1 inhibitor development. Through FBDD, the **IDA** MBP ($IC_{50} = 122 \mu M$) was developed into the lead inhibitor **89f** ($IC_{50} = 8.6 \mu M$) against NDM-1. Protein thermal shift and native state electrospray ionization mass spectrometry (ESI-MS) experiments revealed **89f**, and related derivatives, inhibits NDM-1 via the formation of a stable ternary complex. This work demonstrates the potential of the **IDA** scaffold for NDM-1 inhibitor development and provides a roadmap for the future **IDA** derived lead compounds.

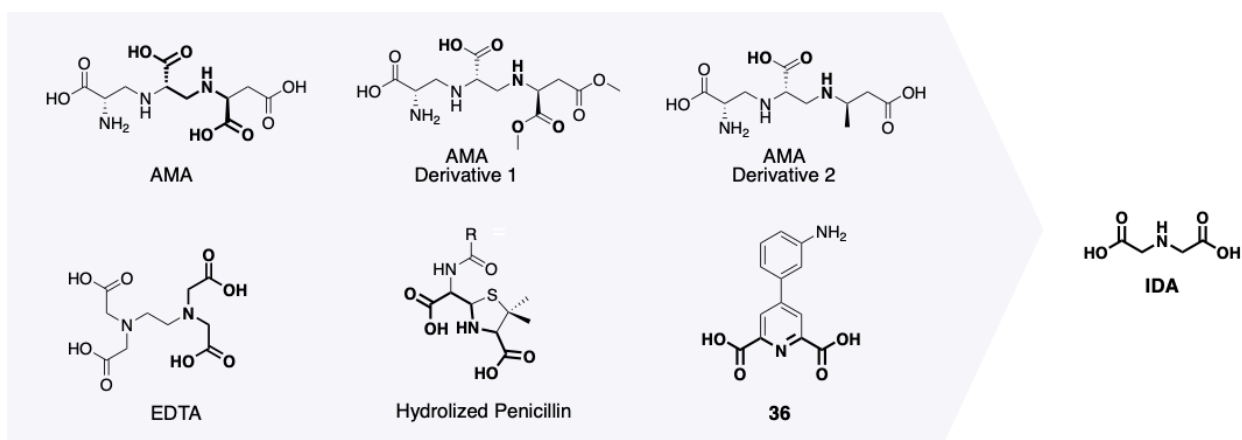


Figure 4-1. NDM-1 inhibitors and hydrolyzed penicillin bearing the **IDA** motif.

4.2 Results and Discussion

4.2.1 IDA MBP Design and Verification

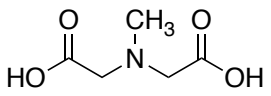
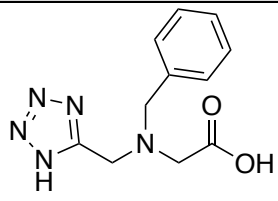
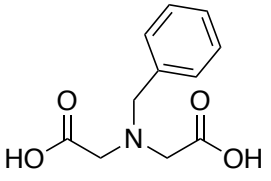
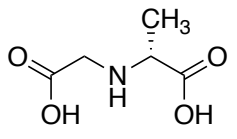
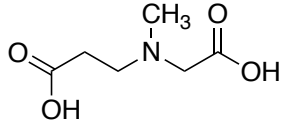
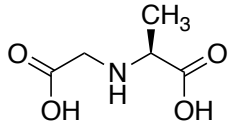
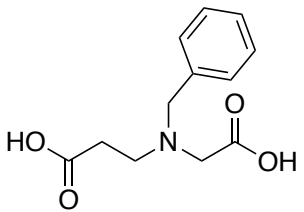
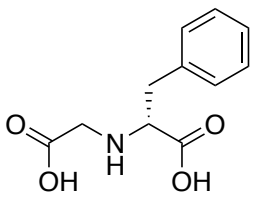
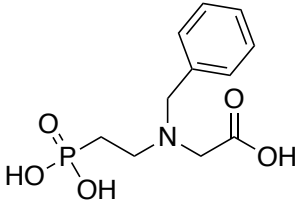
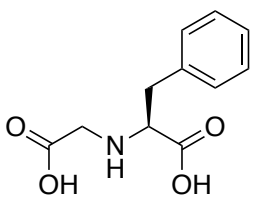
To verify **IDA** as a potential MBP lead for inhibitor design, a small library of compounds bearing structural similarity to **DPA** and **IDA** was assembled and their inhibitory activity against NDM-1 was assessed (Table 4-1). This library included compounds that have a nitrogen atom and a carboxylate functional group (*N,O*-donor atoms) for bidentate metal-binding. The *N*-donor atom in the MBP was either a secondary amine (**IDA**, **67** – **72**), a tertiary amine (**66**), or diazole (**73** – **75**). These MBPs were screened (at a concentration of 200 μ M) via an enzymatic assay monitoring the NDM-1 mediated hydrolysis of meropenem as the substrate.¹⁵ Evaluation of this library revealed **IDA** to be the only MBP with a secondary amine to yield significant inhibition activity (48% at 200 μ M). A methylated **IDA** derivative (**66**), was the most potent of this library, reaching 80% inhibition (at 200 μ M). MBPs bearing diazoles showed some inhibitory activity, with **73** displaying the second highest inhibition (57% at 200 μ M). Comparison of **72** and **73** reveals that the inhibitory activity arises from the diazole tautomerization. Data from this small set of MBPs suggests a preference for a tertiary or diazole *N*-donor atom. Based on these findings, MBP **66** was chosen for further investigation.

Table 4-1. Percent inhibition of MBPs and **IDA** derivatives (at 200 μ M) against NDM-1. Percent inhibition values were obtained via monitoring the MBL-catalyzed hydrolysis of substrate meropenem.

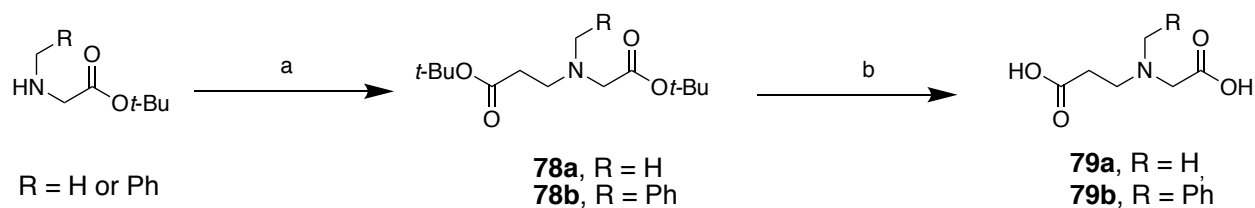
Compound	% Inhibition	Compound	% Inhibition
IDA	48 \pm 2	71	3 \pm 10
66	80 \pm 4	72	0
67	8 \pm 7	73	57 \pm 4
68	0	74	28 \pm 1
69	0	75	33 \pm 5
70	4 \pm 4		

Second round of **IDA** derivatives were synthesized according to Scheme 4-1 – Scheme 4-3). Compounds in this sublibrary incorporated a benzyl substituent, as aromatic rings have previously been shown to form favorable hydrophobic interactions with the NDM β -hairpin loop.¹⁶ **IDA** derivatives where one carboxylic acid was modified via bioisostere replacement (**79a**, **79b**, **81**, **83**, Table 4-2) were prepared to determine if both carboxylic acids were necessary for inhibition and if alternative MBPs could achieve increase potency. Compounds where the methyl- or benzyl-substituent (**85a** – **85d**) was placed at the α -carbon were explored as well. The compounds (at a concentration of 250 μ M) were screened against NDM-1 (Table 4-2). Methylated-**IDA** (**66**) exhibited the best inhibitory activity (90%). The benzylated-**IDA** (**77**) also exhibited appreciable inhibitory activity (65%). Although bioisosteres with a propionic acid motif (**79a** and **79b**) are most structurally similar to AMA, these compounds displayed a complete loss of activity. While the phosphate isostere (**82**) showed no significant inhibition against NDM, the less acidic tetrazole isostere (**83**) showed inhibition that was comparable to that of **77**. Derivatives **85a** – **85d** displayed inhibitory activity similar to that of **IDA** and **77**, but did not show any improved activity.

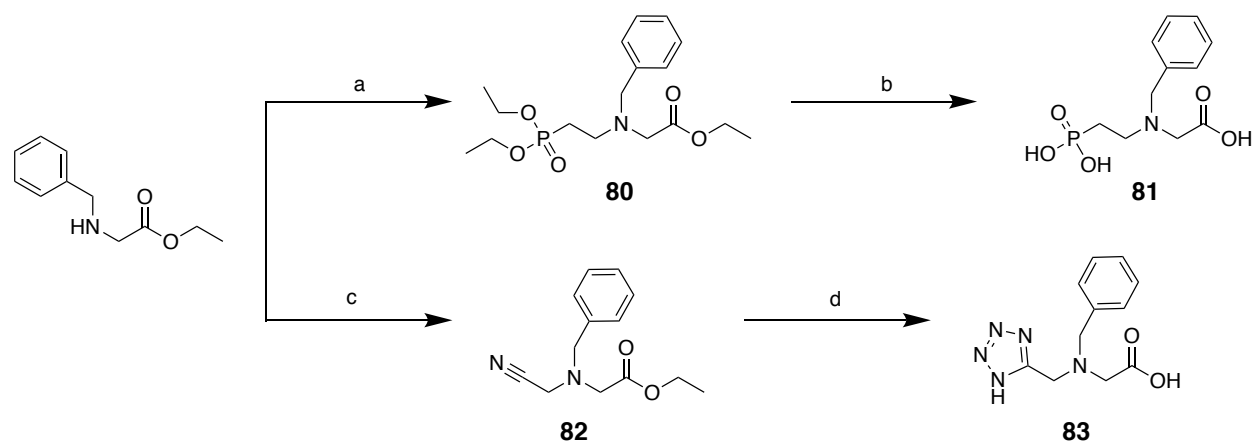
Table 4-2. Percent inhibition of **IDA** MBP derivatives at 250 μ M against NDM-1. Percent inhibition values were obtained via monitoring the MBL-catalyzed hydrolysis of substrate meropenem.^[a]

Compound	% Inhibition	Compound	% Inhibition
66 	90 \pm 1	83 	43 \pm 1
77 	65 \pm 1	85a 	53 \pm 3
79a 	0	85b 	51 \pm 1
79b 	0	85c 	54 \pm 1
81 	0	85d 	65 \pm 1

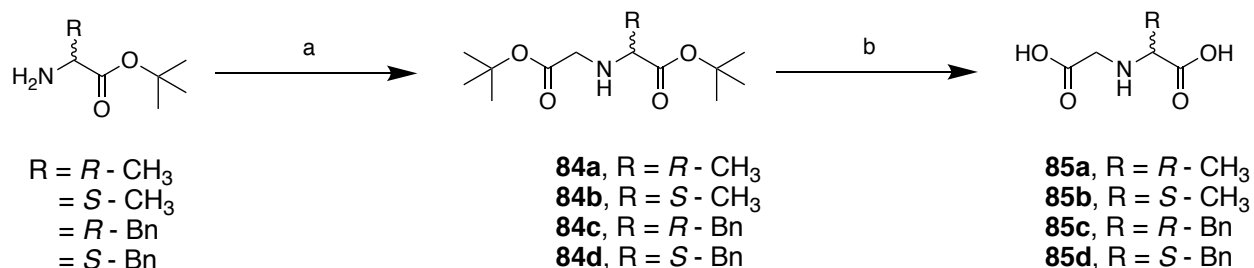
^[a] Activity measurements are reported as the average between two duplicate runs.



Scheme 4-1. Synthesis of **79a** and **79b**. Reagents and conditions: *tert*-butyl acrylate, TEA, EtOH, 65 °C, 16 h, 43 – 90%; (b) TFA:CH₂Cl₂, 25 °C, 16 h, ~99%.



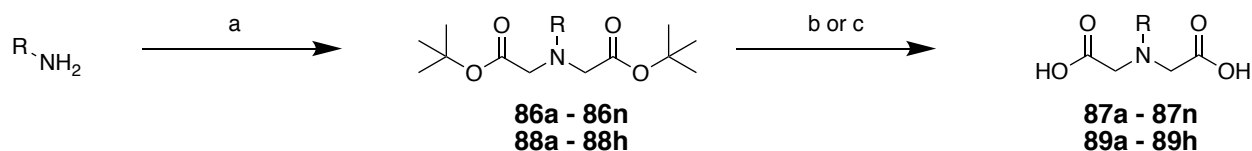
Scheme 4-2. Synthesis of IDA inhibitors **81** and **83**. Reagents and conditions: (a) diethyl (2-bromoethyl)phosphonate, K₂CO₃, KI, ACN, 82 °C, 16 h, 40%; (b) HCl, 100 °C, 16 h, 99%; (c) 2-bromocetonitrile, K₂CO₃, KI, ACN, 25 °C, 16 h, 74%; (d) NaN₃, NH₄Cl, DMF, 110 °C, 16 h; then 1:1:1 MeOH:THF:1M NaOH, 60 °C, 16 h; *two steps* 19%.



Scheme 4-3. Synthesis of **85a** – **85d**. Reagents and conditions: (a) *tert*-butyl 2-bromoacetate, TEA, DMF, 0 – 25 °C, 16 h, 40 – 54%; (b) TFA, CH₂Cl₂, 25 °C, 16 h, ~99%.

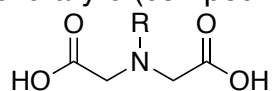
4.2.2 IDA Derivative Synthesis and Inhibitory Activity (Sublibrary 6 – Sublibrary 7)

Compounds **66** and **77** were selected as scaffolds for inhibitor development, and additional **IDA** derivatives with various substituents were prepared. This sublibrary was prepared using a double substitution reaction of various primary amines with *tert*-butyl 2-bromoacetate to yield compounds **87a** – **87n** (Scheme 4-4, **Table 4-3**). The sublibrary was screened at an inhibitor concentration of 250 μ M. While the majority of the compounds in this sublibrary inhibited NDM-1 at an appreciable level (\sim 60%), no clear SAR could be elucidated. Notably, compounds bearing a sulfonamide linker (**87k** and **87l**) displayed a complete loss of activity (most likely due to the reduced basicity of the central nitrogen); however, the substitution of the phenyl ring with a thiophene substituent (**87m** and **87n**) restored activity by \sim 20%. In addition, **87j** stood out as the most potent inhibitor of this sublibrary with almost complete inhibition against NDM-1 (\sim 99%). When the heterocyclic oxygen is swapped out for a sulfur (**87i**), the activity is reduced by 5-fold (64%), showing a preference for the furan substituent.



Scheme 4-4. Synthesis of **IDA** inhibitors Sublibrary 6 (compounds **87a** – **87n**) and Sublibrary 7 (compounds **89a** – **89h**). Reagents and conditions: (a) *tert*-butyl 2-bromoacetate, $KHCO_3$, THF, 25 $^{\circ}C$, 16 h, 25 – 98%; (b) TFA, CH_2Cl_2 , 25 $^{\circ}C$, 16 h or (c) MeOH:THF:1M NaOH, 100 $^{\circ}C$, 16 h, 29 – 99%.

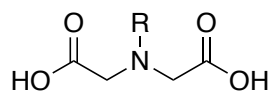
Table 4-3. Inhibitory activity of Sublibrary 6 (compounds **87a** – **87n**) against NDM-1.



Compound	IC ₅₀ (μM)	Compound	IC ₅₀ (μM)
87a	70±1	87h	67±2
87b	56±2	87i	64±2
87c	76±6	87j	99±7
87d	66±2	87k	0
87e	36±2	87l	0
87f	74±2	87m	20±5
87g	74±2	87n	21±8

To develop further inhibitors against NDM-1 and investigate the difference in inhibitory activity between the furan and thiophene substituents, an additional sublibrary bearing analogues of **87i** and **87j** was synthesized and evaluated (**89a** – **89h**, Table 4-4). In general, all derivatives bearing a furan motif exhibited a lower IC₅₀ value compared to that of the corresponding thiophene derivative. These results validate a preference for an oxygen heteroatom. While the 1,2-furan (**89b**, IC₅₀ = 21.6 μM) displayed a lowered IC₅₀ value compared to that of the 1,3-furan (**87j**, IC₅₀ = 32.2 μM), the introduction of a methyl substituent at the 5-position (**89d**, IC₅₀ = 47.2 μM) resulted in poorer activity. Extension from a methyl-linker (**89b**) to an ethyl-linker (**89f**, IC₅₀ = 8.6 μM) resulted in a 2.5-fold improvement in inhibitory activity and resulted in the most potent inhibitor of this sublibrary. It is predicted that the ethyl linker allows for the furan substituent to make more favorable interactions with the base of the L3 β-hairpin loop of NDM-1, as observed in the crystal structure of hydrolyzed antibiotic cefuroxime complexed with NDM-1 (PDB 5O2E);¹⁷ however, further experiments are required to confirm the specific ligand-protein interactions. The corresponding thiophene derivatives displayed similar trends, albeit with poorer inhibition values. Due to the strong affinity **IDA** has for Zn(II) ions ($K_d = 3.2 \times 10^{-5}$ M),¹⁸ we can assume that **89f** binds via coordination to the metal ions at the NDM-1 protein active site via a competitive mechanism of action. The Cheng–Prusoff relationship for competitive inhibitors allow for us to calculate a K_i of 2.6 ± 0.2 μM for **89f**.

Table 4-4. Inhibitory activity of Sublibrary 7 (compounds **89a** – **89h**) against NDM-1.



Compound		IC ₅₀ (μM)	Compound		IC ₅₀ (μM)
IDA		122.2±10.1	66		24.5±1.6
87i		171.6±7.5	87j		32.2±2.8
89a		66.2±3.1	89b		21.6±0.7
89c		91.2±8.2	89d		47.2±4.4
89e		50.7±2.4	89f		8.6±0.2
89g		31.9±1.9			
89h		46.2±2.0			

4.2.3 Thermal Shift Assay

Protein thermal shift assays can be utilized for hit identification and confirmation. Selected **IDA** derivatives were validated via thermal shift assay and their propensity to remove Zn(II) from the active site of NDM-1 was evaluated. In this assay, a fluorescent dye is utilized to monitor the difference in the unfolding temperature of the native protein versus the inhibitor-bound protein. The inhibitor-bound protein generally has greater stability and results in an increase in the observed melting temperature (positive ΔT_m , as observed with L-captopril, Table 4-5). In contrast, the removal of metal generally destabilizes the protein and results in a negative ΔT_m (as observed with **DPA**). It is important to note that while reported thermal shift data has revealed a good correlation between the observed IC_{50} value and ΔT_m ,¹⁹ this correlation has not been observed for inhibitors of NDM-1.²⁰⁻²¹ In the case of the compounds tested here, ΔT_m did not correlate well with IC_{50} values (Table 3). Compounds (**IDA**, **87i**, **87j**, **89a – 89h**) displayed a range of positive ΔT_m values, with **IDA**, **87i**, **89c**, and **89h** yielding ΔT_m on par with, or better than, that of L-captopril. This data provides evidence of NDM-1:inhibitor complex formation by the derivatives of interest.

Table 4-5. Protein thermal shift of compounds against NDM-1.

Compound	ΔT_m (°C)	Compound	ΔT_m (°C)
L-Captopril	4.61±0.07	DPA	-14.46±0.16
IDA	4.39±0.04	66	1.92±0.16
87i	4.43±0.07	87j	3.43±0.28
89a	3.12±0.12	89b	1.58±0.35
89c	5.22±0.13	89d	3.35±0.18
89e	1.67±0.16	89f	1.50±0.14
89g	2.98±0.25		
89h	4.19±0.19		

4.2.4 Native State Electrospray Ionization Mass Spectrometry

Native state electrospray ionization mass spectrometry was used to further investigate the formation of enzyme:inhibitor ternary complexes for derivatives **66** and **89c – 89f** against NDM-1 and VIM-2. The major advantage of ESI-MS is the ability to analyze for the formation of a ternary complex using near physiological concentrations of enzyme and inhibitor. Briefly, NDM-1 or VIM-2 (at 10 μM) were incubated for approximately 5 min with each inhibitor (50 μM) prior to analysis. The control spectra of NDM-1 revealed a dominant +9 peak at 2,821 m/z , corresponding to the mass of di-Zn(II) NDM-1 (25,385 Da, Figure 4-2A). In contrast, incubation of NDM-1 with **DPA** resulted in +9 peaks at 2,807 m/z , 2,814 m/z , and 2,821 m/z (dominant), corresponding to the presence of apo-Zn(II), mono-Zn(II) and di-Zn(II) NDM-1, respectively (Figure 4-2B). It is important to note that the current native MS experiment procedures do not generate quantitative results. Higher relative peak intensities (dominant peaks) do not indicate higher concentrations of the solution species, but rather the species that is best ionized by the mass analyzer.²²

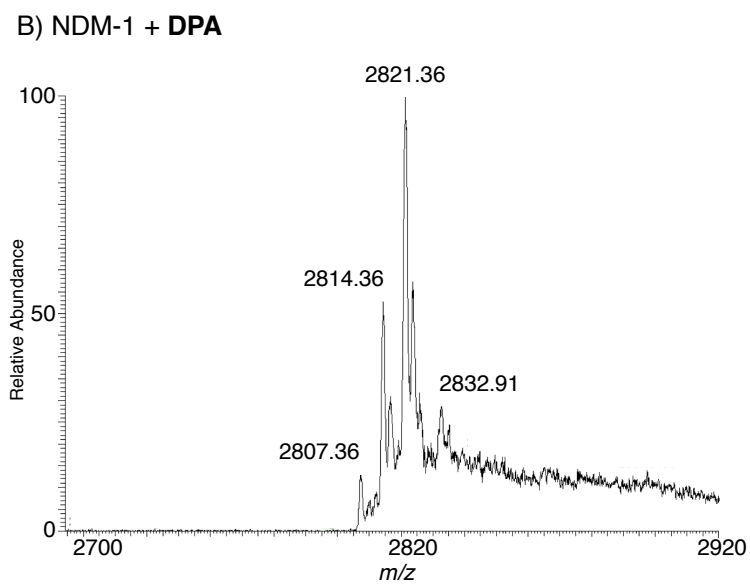
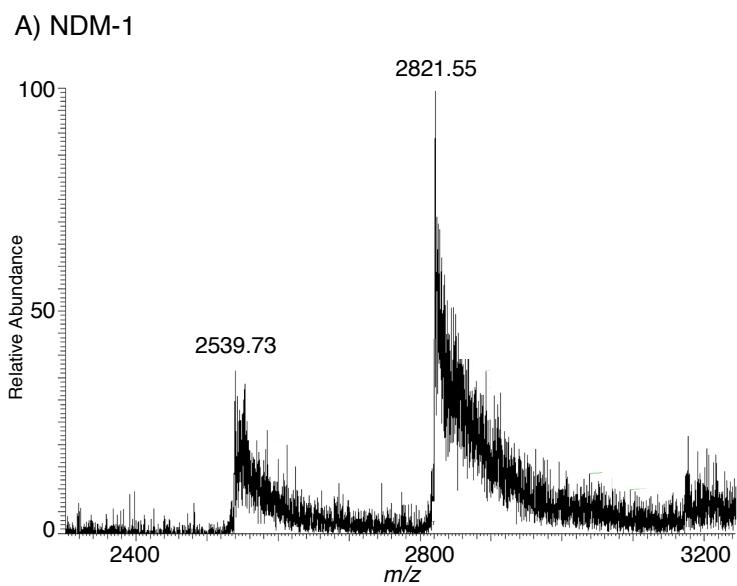


Figure 4-2. Control spectra of A) NDM-1 and B) NDM-1 incubated with **DPA**.

The spectra of NDM-1 incubated with inhibitors **66** and **89c – 89f** all showed the presence of ternary complexes, with the predicted and observed peaks summarized in Table 4-6. In all of these experiments, in addition to the dominant di-Zn(II) NDM-1 peak (+9 peak at 2,821 *m/z*, corresponding to 25,385 Da), peaks corresponding to the mass of di-Zn(II) NDM-1 plus inhibitor were observed. Protein incubation with derivative **66** revealed a less dominant di-Zn(II) NDM-1:**66** +9 peak at 2,836 *m/z* (25,532 Da). Incubation of protein with **89c** yielded +9 and +8 peaks at 2,849 *m/z* and 3,209 *m/z*, respectively, corresponding to the di-Zn(II) NDM-1:**89c** complex (25,628 Da). Similarly, incubation of protein with **89d** yielded +8 peak at 3,201 *m/z*, corresponding to the di-Zn(II) NDM-1:**89d** complex. Inhibitor **89e** produced a significantly less intense +9 peak at 2,847 *m/z*, corresponding to the di-Zn(II) NDM-1:**89e** complex (25,628 Da). Lastly, incubation of NDM-1 with lead inhibitor **89f** revealed a less intense +9 peak at 2,847 *m/z* and a more intense +8 peak at 3,201 *m/z*, both of which correspond to the mass of di-Zn(II) NDM-1:**89f** (25,612 Da).

Table 4-6. Summary of the native MS experimental results for NDM-1.^[a]

Sample	Inhibitor Molecular Weight (g/mol)	NDM-1 + Inhibitor Complex Weight (Da)	Peak Charge (+)	Predicted Peak (<i>m/z</i>)	Observed Peak (<i>m/z</i>)
NDM-1			9	2,821	2,821
			10	2,539	2,539
NDM-1 + DPA	167	25,255	9	2,807	2,807
	167	25,320	9	2,814	2,814
	167	25,385	9	2,821	2,821
NDM-1 + 66	147	25,532	9	2,838	2,837
NDM-1 + 89c	243	25,628	9	2,848	2,850
			8	3,204	3,210
NDM-1 + 89d	227	25,612	9	2,847	2,846
			8	3,202	3,202
NDM-1 + 89e	243	25,628	9	2,848	2,847
			8	3,204	3,205
NDM-1 + 89f	227	25,612	9	2,847	2,848
			8	3,202	3,201

^[a] Percent error was calculated by subtracting the expected peak value from the actual peak value, dividing by the expected peak value and multiplying by 100. All percent errors are <0.2.

Previous work has shown that different mechanisms of inhibition can be observed for the same inhibitors against varying MBLs (unpublished data). To verify that the **IDA** inhibitors are able to form ternary complexes with other MBLs, additional ESI-MS experiments were performed for inhibitors **66** and **89c – 89f** with VIM-2. Control spectra of VIM-2 revealed dominant +9 and +8 peaks at 2,886 *m/z* and 3,247 *m/z*, respectively, corresponding to the mass of di-Zn(II) VIM-2 (25,972 Da, Figure 4-3A). VIM-2 incubated with **DPA** revealed dominant +9 and +8 peaks at 2,891 *m/z* and 3,253 *m/z*, respectively, corresponding most closely with the mass of apo-VIM-2 with 1 equivalent of DPA bound (26,009 Da, Figure 4-3B).

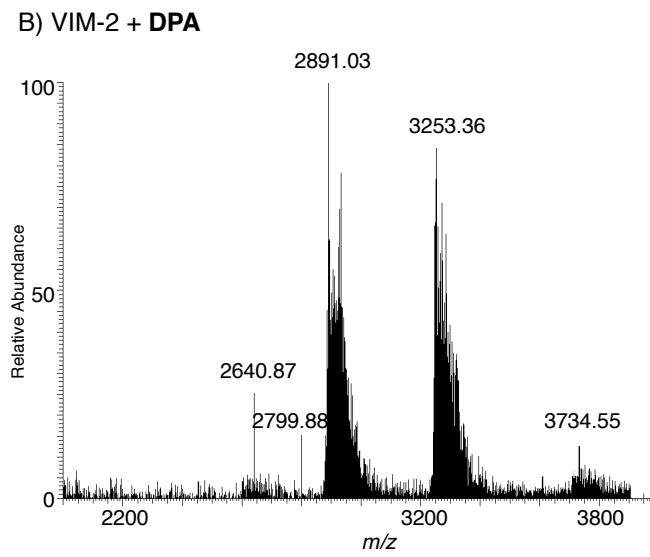
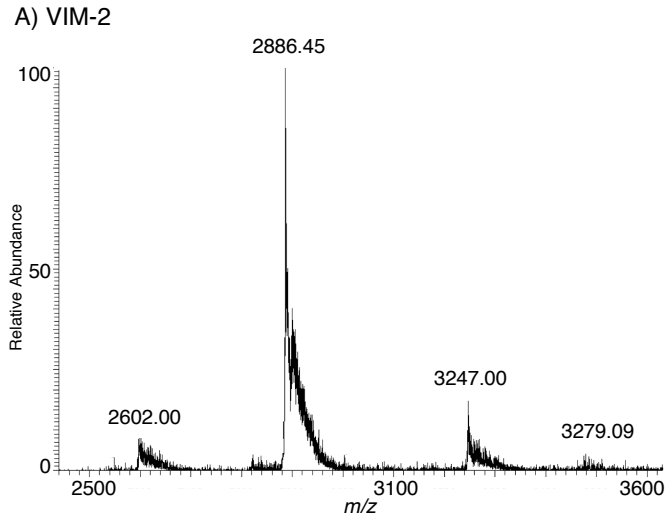


Figure 4-3. Control spectra of A) VIM-2 and B) VIM-2 incubated with **DPA**.

Similar to the previously reported NDM-1:inhibitor complexes, spectra of VIM-2 incubated with inhibitors **66** and **89c – 89f** all revealed the presence of ternary complexes. In addition to the dominant di-Zn(II) VIM-2 peak, additional di-Zn(II) VIM-2:inhibitor peaks were observed. The predicted and observed peaks are summarized in Table 4-7. Incubation of VIM-2 with **66** revealed a less dominant +9 peak at 2,902 *m/z*, corresponding to di-Zn(II) VIM-2:**66** complex (26,119 Da). The native MS of VIM-2 incubated with inhibitors **89c – 89f** displayed similar secondary peaks at 3,277 *m/z* (26,215 Da), 3,276 *m/z* (26,199 Da), 2,913 *m/z* (26,215 Da), and 3,278 *m/z* (26,199 Da) representing the formation of the di-Zn(II) VIM-2: **89c**, di-Zn(II) VIM-2: **89d**, di-Zn(II) VIM-2:**89e**, and di-Zn(II) VIM-2: **9f** ternary complex, respectively.

Table 4-7. Summary of the native MS experimental results for VIM-2.^[a]

Sample	Inhibitor Molecular Weight (g/mol)	VIM-2 + Inhibitor Complex Weight (Da)	Peak Charge (+)	Predicted Peak (<i>m/z</i>)	Observed Peak (<i>m/z</i>)
VIM-2			9	2,887	2,886
			8	3,247	3,247
VIM-2 + DPA	167	26,010	9	2,891	2,891
		26,010	8	3,252	3,253
VIM-2 + 1	147	26,119	9	2,903	2,902
VIM-2 + 89c	243	26,215	8	3,278	3,277
VIM-2 + 89d	227	26,199	8	3,276	3,276
VIM-2 + 89e	243	26,215	8	3,278	3,277
VIM-2 + 89f	227	26,199	8	3,276	3,278

^[a] Percent error was calculated by subtracting the expected peak value from the actual peak value, dividing by the expected peak value and multiplying by 100. All percent errors are <0.07.

4.3 Conclusion

Since the discovery of AMA as an effective inhibitor against NDM-1 ($IC_{50} = 4 \mu\text{M}$) there has been interest in the synthesis and development of this compound into a more potent and selective inhibitor.^{5, 10-11} AMA is a non-competitive inhibitor that deactivates NDM-1 via active site Zn(II) metal sequestration.⁷ Inhibitor development of AMA through modification of one of the four carboxylic acid functional groups has been unsuccessful, as this motif is necessary for metal chelation.⁸ Herein, we report the FBDD of **IDA** as a novel MBP for NDM-1 inhibitor development. **IDA** is a simplified analogue of AMA and EDTA, allowing for more facile inhibitor derivatization to probe the NDM-1 active site pocket. From a preliminary screen of a small library of MBPs, **IDA** and **66** were verified as novel hits for inhibitor development. Upon rounds of library design and synthesis, **IDA** ($IC_{50} = 122 \mu\text{M}$) was developed into inhibitor **89f** ($IC_{50} = 8.6 \mu\text{M}$). To study the mode of inhibition, protein thermal shift and native state electrospray ionization mass spectrometry (ESI-MS) were utilized. Both experiments revealed **89f** and related derivatives inhibited NDM-1 via the formation of stable ternary complexes and additional studies are currently underway to elucidate the precise protein-inhibitor binding interactions. This work represents the benefit of performing mechanistic analysis hand-in-hand with inhibitor derivation for the development of inhibitors with a favorable mode of inhibition. By utilizing a novel **IDA** MBP scaffold, traditional metal chelators (such as AMA and EDTA) not viewed as candidates for inhibitor development can be elaborated into potent inhibitors that form favorable enzyme:inhibitor ternary complexes.

4.4 Experimental

Inhibitors **66** – **75**, **IDA**, reagents, and solvents were obtained from commercial sources and used without further purification. All reactions, unless otherwise stated, were performed at room temperature under a nitrogen atmosphere. Flash column chromatography was performed using a Teledyne ISCO CombiFlash Rf system using hexanes, ethyl acetate, dichloromethane, and methanol as eluents with prepacked silica cartridges. Reverse phase column chromatography was performed on the same instrument using methanol and water (w/ 0.1% formic acid) as eluents with high-performance Gold C18 columns. Column separation was monitored via Teledyne ISCO RF+ Purlon ESI-MS. ^1H and ^{13}C NMR spectra were recorded at ambient temperature on a 400 Varian Mercury Plus or 500 Varian VX NMR instrument located in the Department of Chemistry and Biochemistry at the University of California, San Diego. Mass spectra were obtained at the Molecular Mass Spectrometry Facility (MMSF) in the Department of Chemistry and Biochemistry at the University of California, San Diego. The purity of all compounds used in assays was determined to be $\geq 95\%$ by high-performance liquid chromatography. Enzymatic assays were performed via monitoring the hydrolysis of substrate meropenem on Synergy H4 Hybrid Microplate Reader using 96-well UV-transparent microplates #3635 (Corning) according to previously published procedures. Thermal shift assays were performed on QuantStudio 3 real-time PCR machines (Applied Biosystems) using 96-well 0.2 mL optical MicroAmp thermocycler plates and SYPRO orange Thermal Shift dye (ThermoFisher). Native state electrospray

ionization mass spectrometry experiments were performed on a LTQ Orbitrap XL hybrid ion trap-orbitrap mass spectrometer (ThermoScientific).

Synthesis

***tert*-Butyl 3-((2-(*tert*-butoxy)-2-Oxoethyl)(methyl)amino)propanoate (78a).**

Commercially available *tert*-butyl methylglycinate HCl (500 mg, 2.75 mmol), *tert*-butyl acrylate (529 mg, 4.13 mmol), and TEA (0.43 mL, 3.12 mmol) were dissolved in ethanol (5 mL) and stirred at 65 °C for 16 h. The reaction was monitored via TLC. Upon completion, the solvent was removed in vacuo and purified via flash column chromatography to yield the title compound as a colorless oil in 90% yield (676 mg, 2.47 mmol). ¹H NMR (400 MHz, CDCl₃-*d*): δ 3.22 (s, 2H), 2.88 (t, *J* = 7.1 Hz, 2H), 2.50 – 2.38 (m, 5H), 1.46 (d, *J* = 10.6 Hz, 18H). ESI-MS(+) calculated for [C₁₄H₂₈NO₄]⁺ *m/z* 274.20, found *m/z* 274.06 [M+H]⁺.

3-((Carboxymethyl)(methyl)amino)propanoic acid (79a). Compound **78a** (109 mg, 0.40 mmol) was dissolved in TFA:CH₂Cl₃ (4:1 mL) and the reaction mixture was stirred at 25 °C for 16 h. The solvent was removed under reduced pressure and the excess TFA was removed via co-evaporation with excess MeOH. The compound was lyophilized under reduced pressure to yield the title compound as a TFA salt in quantitative yield (102 mg, 0.40 mmol). ¹H NMR (400 MHz, D₂O): δ 3.83 (s, 2H), 3.39 (s, 2H), 2.87 – 2.72 (m, 5H). ¹³C NMR (126 MHz, DMSO-*d*₆): δ 172.30, 168.40, 56.57,

51.94, 41.26, 29.51. ESI-MS(+) calculated for $[C_6H_{12}NO_4]^+$ m/z 162.08, found m/z 162.08 $[M+H]^+$.

***tert*-Butyl 3-(benzyl(2-(*tert*-butoxy)-2-oxoethyl)amino)propanoate (78b).**

Commercially available *tert*-butyl benzylglycinate (350.0 mg, 1.58 mmol), *tert*-butyl acrylate (405.4 mg, 3.16 mmol), and TEA (0.44 mL, 3.16 mmol) were dissolved in ethanol (5 mL) and stirred at 65 °C for 16 h. The reaction was monitored via TLC. Upon completion, the solvent was removed in vacuo and purified via flash column chromatography to yield the title compound as a colorless oil in 43% yield (239 mg, 0.67 mmol). 1H NMR (400 MHz, CD_3OD-d_4): δ 7.38 – 7.19 (m, 5H), 3.77 (s, 2H), 3.18 (s, 2H), 2.95 (t, $J = 6.6$ Hz, 2H), 2.40 (t, $J = 7.0$ Hz, 2H), 1.45 (d, $J = 8.3$ Hz, 18H). ESI-MS(+) calculated for $[C_{20}H_{32}NO_4]^+$ m/z 350.23, found m/z 350.09 $[M+H]^+$.

3-(Benzyl(carboxymethyl)amino)propanoic acid (79b). Compound **78b** (171 mg, 0.47 mmol) was dissolved in TFA: CH_2Cl_3 (4:1 mL) and the reaction mixture was stirred at 25°C for 16 h. The solvent was removed under reduced pressure and the excess TFA was removed via co-evaporation with excess MeOH. The compound was lyophilized under reduced pressure to yield the title compound as a TFA salt in quantitative yield (168 mg, 0.47 mmol). 1H NMR (400 MHz, D_2O): δ 7.48 – 7.29 (m, 5H), 4.34 (s, 2H), 3.78 (s, 2H), 3.41 (t, $J = 6.7$ Hz, 2H), 2.76 (t, $J = 6.6$ Hz, 2H). ^{13}C NMR (126 MHz, $DMSO-d_6$): δ 172.09, 168.31, 137.15, 129.28, 129.10, 127.33, 55.27,

53.77, 49.85, 29.81.ESI-MS(-) calculated for $[C_{12}H_{14}NO_4]^-$ m/z 236.09, found m/z 236.12 $[M-H]^-$.

Ethyl *N*-benzyl-*N*-(2-(diethoxyphosphoryl)ethyl)glycinate (80). To a stirred solution of ethyl benzylglycinate (200 mg, 1.03 mmol), KI (34 mg, 0.21 mmol), K_2CO_3 (172 mg, 1.24 mmol) in ACN (10 mL) was added diethyl (2-bromoethyl)phosphonate (279 mg, 1.14 mmol), and the reaction mixture was heated to 82 °C for 16 h. After completion of the reaction, the salts were removed via vacuum filtration. The collected filtrate was concentrated in vacuo and the residue was purified via flash column chromatograph using ethyl acetate in hexanes as eluent to afford the desired product in 40% yield as a clear oil (150 mg, 0.42 mmol). 1H NMR (400 MHz, CD_3OD-d_4): δ = 7.40 – 7.21 (m, 5H), 4.21 – 3.97 (m, 6H), 3.78 (s, 2H), 3.35 (s, 2H), 2.99 – 2.86 (m, 2H), 2.10 – 1.98 (m, 2H), 1.36 – 1.22 (m, 9H). ESI-MS(+) calculated for $[C_{17}H_{29}NO_5P]^+$ m/z 358.18, found m/z 358.22 $[M+H]^+$.

***N*-Benzyl-*N*-(2-phosphonoethyl)glycine (81).** Compound **80** (150.0 mg, 0.42 mmol) was dissolved in 6M HCl and heated to 100 °C for 16 h. Excess HCl was removed under reduced pressure and co-evaporated with copious amounts of H_2O to yield the title product as a white solid in 99% yield (114 mg, 0.42 mmol). 1H NMR (400 MHz, CD_3OD-d_4): δ = 7.66 – 7.42 (m, 5H), 4.53 (s, 2H), 4.14 (s, 2H), 3.52 (m, 2H), 2.37 – 2.20 (m, 2H). ESI-MS(-) calculated for $[C_{11}H_{15}NO_5P]^-$ m/z 272.07, found m/z 272.23 $[M-H]^-$.

Ethyl *N*-benzyl-*N*-(cyanomethyl)glycinate (82). A solution of ethyl benzylglycinate (500 mg, 2.59 mmol), 2-bromoacetonitrile (341 mg, 2.85 mmol), KI (86 mg, 0.52 mmol), K₂CO₃ (429 mg, 3.10 mmol) was dissolved in ACN (10 mL) and stirred at 25 °C for 16 h. After completion of the reaction, the salts were removed via vacuum filtration. The collected filtrate was concentrated in vacuo and the residue was purified via flash column chromatograph to afford the title product in 74% yield as a clear oil (447 mg, 1.92 mmol). ¹H NMR (400 MHz, CD₃OD-*d*₄): δ 7.45 – 7.24 (m, 5H), 4.17 (q, *J* = 7.1 Hz, 2H), 3.77 (s, 2H), 3.72 (s, 2H), 3.41 (s, 2H), 1.26 (t, *J* = 7.1 Hz, 3H). ESI-MS(+) calculated for [C₁₃H₁₇N₂O₂]⁺ *m/z* 233.13, found *m/z* 233.19 [M+H]⁺.

Ethyl *N*-((1*H*-tetrazol-5-yl)methyl)-*N*-benzylglycinate (83). Compound **82** (200 mg, 0.86 mmol), NaN₃ (168 mg, 2.58 mmol), and NH₄Cl (138 mg, 2.58 mmol) were dissolved in DMF (10 mL), and the reaction mixture was allowed to stir at 110 °C for 16 h. DMF was concentrated to one-third of the original volume under reduced pressure followed by the addition of water (40 mL). The aqueous layer was washed three times with ethyl acetate. The aqueous layer was carefully acidified with 1M HCl to pH 3 and extracted three times with ethyl acetate. The combined organic layers were dried over MgSO₄, filtered and concentrated in vacuo to yield a yellow oil. The product was purified via reverse phase column chromatography with MeOH in H₂O (w/ 0.1% formic acid) to afford the intermediate as a clear oil. The intermediate was dissolved in a solution of MeOH:THF:6M NaOH (1:1:1 mL), and the reaction mixture was allowed to stir at 60 °C for 16 h. The organic solvents were removed in vacuo and the aqueous

solution was acidified to pH 5. The aqueous mixture was extracted three times with ethyl acetate. The combined organic layers were dried over MgSO₄, filtered and concentrated in vacuo to afford the product in 18% yield as a yellow solid (40.0 mg, 0.16 mmol). ¹H NMR (500 MHz, DMSO-*d*₆): δ 7.38 – 7.20 (m, 5H), 4.18 (s, 2H), 3.77 (s, 2H), 3.28 (s, 2H). ESI-MS(-) calculated for [C₁₁H₁₂N₅O₂]⁻ *m/z* 246.10, found *m/z* 246.20 [M-H]⁻.

General procedures for the synthesis of 85a – 85d.

To a solution of the corresponding amine (1.1 equivalents) and TEA (2 equivalents) in DMF (10 mL) was added *tert*-butyl 2-bromoacetate (1 equivalent) dropwise at 0°C. The reaction was allowed to warm to 25 °C and stirred for additional 16 h. After completion of the reaction, the salts were removed via vacuum filtration. The collected filtrate was concentrated in vacuo and the residue was purified via flash column chromatograph to afford the desired intermediates **84a – 84d**. Intermediates were dissolved in TFA:CH₂Cl₂ (4:1 mL) and the reaction mixture was stirred at 25 °C for 16 h. The excess TFA removed via co-evaporation with copious amounts of MeOH under reduced pressure. The product was purified via reverse phase column chromatography using MeOH in H₂O (w/ 0.1% formic acid) as eluent to afford the title compounds **85a – 85d**.

***tert*-Butyl (2-(*tert*-butoxy)-2-oxoethyl)-D-alaninate (84a).** Yield: 40% (175 mg, 0.68 mmol). ¹H NMR (500 MHz, CD₃OD-*d*₄): δ 3.33 – 3.21 (m, 3H), 1.48 (s, 18H), 1.27 (d, *J*

= 6.9 Hz, 3H). ESI-MS(+) calculated for $[C_{13}H_{26}NO_4]^+$ m/z 260.18, found m/z 260.01 $[M+H]^+$.

(Carboxymethyl)-D-alanine (85a). Yield: 99% (93 mg, 0.63 mmol). 1H NMR (400 MHz, DMSO- d_6): δ 3.92 (q, J = 7.0 Hz, 1H), 3.87 – 3.72 (m, 2H), 1.41 (d, J = 7.2 Hz, 3H). ^{13}C NMR (126 MHz, DMSO- d_6): δ 171.41, 168.69, 54.72, 45.86, 14.56. ESI-MS(+) calculated for $[C_5H_8NO_4]^-$ m/z 146.04, found m/z 146.15 $[M-H]^-$.

***tert*-Butyl (2-(*tert*-butoxy)-2-oxoethyl)-L-alaninate (84b).** Yield: 40% (176 mg, 0.68 mmol). 1H NMR (500 MHz, CD_3OD-d_4): δ 3.35 – 3.19 (m, 3H), 1.49 (s, 18H), 1.27 (d, J = 7.0 Hz, 3H). ESI-MS(+) calculated for $[C_{13}H_{26}NO_4]^+$ m/z 260.18, found m/z 260.00 $[M+H]^+$.

(Carboxymethyl)-L-alanine (85b). Yield: 99% (72 mg, 0.49 mmol). 1H NMR (400 MHz, DMSO- d_6): δ 4.07 – 3.83 (m, 3H), 1.43 (d, J = 7.1 Hz, 3H). ^{13}C NMR (126 MHz, DMSO- d_6): δ = 175.87, 173.22, 59.19, 50.27, 19.02. ESI-MS(+) calculated for $[C_5H_8NO_4]^-$ m/z 146.04, found m/z 146.16 $[M-H]^-$.

***tert*-Butyl (2-(*tert*-butoxy)-2-oxoethyl)-D-phenylalaninate (84c).** Yield: 52% (296 mg, 0.88 mmol). 1H NMR (400 MHz, CD_3OD-d_4): δ 7.35 – 7.13 (m, 5H), 3.49 (dd, J = 7.9, 6.4 Hz, 1H), 3.32 – 3.16 (m, 2H), 3.01 – 2.83 (m, 2H), 1.45 (s, 9H), 1.33 (s, 9H). ESI-MS(+) calculated for $[C_{19}H_{30}NO_4]^+$ m/z 336.22, found m/z 335.99 $[M+H]^+$.

(Carboxymethyl)-D-phenylalanine (85c). Yield: 98% (116 mg, 0.52 mmol). ^1H NMR (400 MHz, DMSO- d_6): δ 7.40 – 7.10 (m, 5H), 3.93 (t, J = 6.8 Hz, 1H), 3.62 (s, 2H), 3.07 (d, J = 62.0 Hz, 2H). ^{13}C NMR (126 MHz, DMSO- d_6): δ 171.91, 170.27, 136.68, 129.75, 128.81, 127.26, 60.94, 47.40, 36.55. ESI-MS(-) calculated for $[\text{C}_{11}\text{H}_{12}\text{NO}_4]^-$ m/z 222.08, found m/z 222.22 $[\text{M}-\text{H}]^-$.

***tert*-Butyl (2-(*tert*-butoxy)-2-oxoethyl)-L-phenylalaninate (84d).** Yield: 54% (308 mg, 0.92 mmol). ^1H NMR (500 MHz, $\text{CD}_3\text{OD}-d_4$): δ 7.33 – 7.16 (m, 5H), 3.50 (dd, J = 7.9, 6.4 Hz, 1H), 3.30 – 3.19 (m, 2H), 3.01 – 2.86 (m, 2H), 1.46 (s, 9H), 1.34 (s, 9H). ESI-MS(+) calculated for $[\text{C}_{19}\text{H}_{30}\text{NO}_4]^+$ m/z 336.22, found m/z 335.99 $[\text{M}+\text{H}]^+$.

(Carboxymethyl)-L-phenylalanine (85d). Yield: 98% (110 mg, 0.49 mmol). ^1H NMR (500 MHz, DMSO- d_6): δ 7.33 – 7.19 (m, 5H), 3.79 (t, J = 6.7 Hz, 1H), 3.50 (s, 2H), 3.05 – 2.96 (m, 2H). ^{13}C NMR (126 MHz, DMSO- d_6): δ 172.97, 171.28, 137.35, 129.73, 128.72, 127.05, 61.30, 48.00, 37.34. ESI-MS(-) calculated for $[\text{C}_{11}\text{H}_{12}\text{NO}_4]^-$ m/z 222.08, found m/z 222.23 $[\text{M}-\text{H}]^-$.

General procedures for the synthesis of 87a – 87n and 89a – 89h.

To a solution of the corresponding amine (1 equivalent) and KHCO_3 (4 equivalents) in THF or DMF (10 mL) was added *tert*-butyl 2-bromoacetate (2.25 equivalents), and the reaction was stirred at 25 °C for 16 h. After completion of the reaction, as indicated by TLC, the salts were removed via vacuum filtration. The

collected filtrate was concentrated in vacuo and the residue was purified via flash column chromatograph using hexane/ethyl acetate as eluent to afford the desired intermediates **86a – 86n** and **88a – 88h**. Compounds **87a – 87n** and **89a – 89h** were obtained through the following deprotection procedures: A) Intermediate was dissolved in a mixture of TFA:CH₂Cl₃ (4:1 mL) and the reaction was stirred at 25 °C for 16 h. The excess TFA was removed under reduced pressure and co-evaporated with copious amounts of MeOH. The acid product was purified via reverse phase column chromatography with MeOH and H₂O (w/ 0.1% formic acid) as eluent to afford the desired products; or B) Intermediate was dissolved in 1M NaOH:THF:MeOH (3:1:1 mL) and the reaction mixture was stirred at 65 °C for 16 h. THF and MeOH was removed under reduced pressure and the aqueous solution was acidified to pH 5 with 4M HCl. The precipitate was collected via vacuum filtration.

Di-*tert*-butyl 2,2'-(phenethylazanediy)diacetate (86a). Yield: 84% (708 mg, 2.03 mmol). ¹H NMR (400 MHz, CDCl₃-*d*): δ 7.34 – 7.14 (m, 5H), 3.49 (s, 4H), 3.01 – 2.74 (m, 4H), 1.46 (s, 18H). ESI-MS(+) calculated for [C₂₀H₃₂NO₄]⁺ *m/z* 350.23, found *m/z* 350.08 [M+H]⁺.

2,2'-(Phenethylazanediy)diacetic acid (87a). Deprotection procedure A. Yield: 99% (104 mg, 0.44 mmol). ¹H NMR (400 MHz, DMSO-*d*₆): δ 7.40 – 7.15 (m, 5H), 3.97 (s, 4H), 3.22 (t, *J* = 7.7 Hz, 2H), 2.89 (t, *J* = 8.2 Hz, 2H). ¹³C NMR (126 MHz, DMSO-*d*₆): δ

169.64, 137.98, 129.21, 129.00, 127.05, 57.07, 54.87, 31.19. ESI-MS(-) calculated for $[C_{12}H_{14}NO_4]^-$ m/z 236.09, found m/z 236.18 $[M-H]^-$.

Di-*tert*-butyl 2,2'-([1,1'-biphenyl]-4-ylmethyl)azanediyl)diacetate (86b). Yield: 69% (680 mg, 1.65 mmol). 1H NMR (400 MHz, CD_3OD-d_4): δ 7.67 – 7.38 (m, 8H), 7.32 (t, J = 7.3 Hz, 1H), 3.90 (s, 2H), 3.42 (s, 4H), 1.47 (s, 18H). ESI-MS(+) calculated for $[C_{25}H_{34}NO_4]^+$ m/z 412.25, found m/z 412.03 $[M+H]^+$.

2,2'-([1,1'-Biphenyl]-4-ylmethyl)azanediyl)diacetic acid (87b). Deprotection procedure A. Yield: 99% (72 mg, 0.24 mmol). 1H NMR (400 MHz, $DMSO-d_6$): δ 7.67 (d, J = 7.0 Hz, 4H), 7.56 – 7.41 (m, 4H), 7.36 (t, J = 7.4 Hz, 1H), 4.05 (s, 2H), 3.65 (s, 4H). ^{13}C NMR (126 MHz, $DMSO-d_6$): δ 170.96, 140.28, 140.14, 140.07, 130.82, 129.42, 128.02, 127.13, 127.10, 57.76, 54.00. ESI-MS(-) calculated for $[C_{17}H_{16}NO_4]^-$ m/z 298.11, found m/z 298.19 $[M-H]^-$.

Di-*tert*-butyl 2,2'-([1,1'-biphenyl]-3-ylmethyl)azanediyl)diacetate (86c). Yield: 98% (967 mg, 2.35 mmol). 1H NMR (400 MHz, CD_3OD-d_4): δ 7.68 – 7.26 (m, 9H), 3.91 (s, 2H), 3.41 (s, 4H), 1.44 (s, 18H). ESI-MS(+) calculated for $[C_{25}H_{34}NO_4]^+$ m/z 412.25, found m/z 412.07 $[M+H]^+$.

2,2'-([1,1'-Biphenyl]-3-ylmethyl)azanediyl)diacetic acid (21c). Deprotection procedure A. Yield: 98% (141 mg, 0.47 mmol). 1H NMR (400 MHz, $DMSO-d_6$): δ 7.74

(s, 1H), 7.70 – 7.33 (m, 8H), 4.15 (s, 2H), 3.74 (s, 4H). ESI-MS(-) calculated for $[C_{17}H_{16}NO_4]^-$ m/z 298.11, found m/z 298.26 $[M-H]^-$.

Di-*tert*-butyl 2,2'-((4-hydroxybenzyl)azanediyl)diacetate (86d). Yield: 63% (530 mg, 1.51 mmol). 1H NMR (400 MHz, CD_3OD-d_4): δ 7.15 (d, $J = 8.6$ Hz, 2H), 6.72 (d, $J = 8.5$ Hz, 2H), 3.73 (s, 2H), 3.35 (s, 4H), 1.46 (s, 18H). ESI-MS(+) calculated for $[C_{19}H_{30}NO_5]^+$ m/z 352.21, found m/z 352.14 $[M+H]^+$.

2,2'-((4-Hydroxybenzyl)azanediyl)diacetic acid (87d). Deprotection procedure A. Yield: 99% (105 mg, 0.44 mmol). 1H NMR (400 MHz, CD_3OD-d_4): δ 7.32 (d, $J = 8.3$ Hz, 2H), 6.85 (d, $J = 8.2$ Hz, 2H), 4.41 (s, 2H), 4.01 (s, 4H). ^{13}C NMR (126 MHz, $DMSO-d_6$): δ 169.65, 168.38, 158.35, 132.53, 115.73, 58.29, 53.66. ESI-MS(-) calculated for $[C_{11}H_{12}NO_5]^-$ m/z 238.07, found m/z 238.17 $[M-H]^-$.

Di-*tert*-butyl 2,2'-((4-chlorobenzyl)azanediyl)diacetate (86e). Yield: 82% (727 mg, 1.97 mmol). 1H NMR (400 MHz, CD_3OD-d_4): δ 7.36 (d, $J = 8.3$ Hz, 2H), 7.30 (d, $J = 8.5$ Hz, 2H), 3.84 (d, $J = 2.5$ Hz, 2H), 3.37 (s, 4H), 1.46 (d, $J = 2.6$ Hz, 18H). ESI-MS(+) calculated for $[C_{19}H_{29}ClNO_4]^+$ m/z 370.18, found m/z 370.02 $[M+H]^+$.

2,2'-((4-Chlorobenzyl)azanediyl)diacetic acid (87e). Deprotection procedure A. Yield: 98% (120 mg, 0.48 mmol). 1H NMR (400 MHz, $DMSO-d_6$): δ 7.42 (d, $J = 3.4$ Hz, 4H), 4.00 (s, 2H), 3.63 (s, 4H). ^{13}C NMR (126 MHz, $DMSO-d_6$): δ 172.46, 161.39,

132.82, 131.69, 128.78, 57.19, 54.08. ESI-MS(-) calculated for $[C_{11}H_{11}ClNO_4]^-$ m/z 256.04, found m/z 256.17 $[M-H]^-$.

Di-*tert*-butyl 2,2'-((benzo[*d*][1,3]dioxol-5-ylmethyl)azanediyl)diacetate (86f). Yield: 25% (230 mg, 0.61 mmol). 1H NMR (400 MHz, CD_3OD-d_4): δ 6.92 (s, 1H), 6.82 – 6.69 (m, 2H), 5.92 (s, 2H), 3.75 (s, 2H), 3.36 (s, 4H), 1.46 (s, 18H). ESI-MS(+) calculated for $[C_{20}H_{30}NO_6]^+$ m/z 380.21, found m/z 379.99 $[M+H]^+$.

2,2'-((Benzo[*d*][1,3]dioxol-5-ylmethyl)azanediyl)diacetic acid (87f). Yield: 29% (57 mg, 0.21 mmol). 1H NMR (400 MHz, D_2O): δ 6.86 (d, $J = 9.4$ Hz, 2H), 6.82 – 6.75 (m, 1H), 5.88 (s, 2H), 4.27 (s, 2H), 3.78 (s, 4H). ^{13}C NMR (126 MHz, D_2O): $\delta = 169.54, 148.75, 147.74, 125.75, 121.97, 110.93, 108.79, 101.61, 59.03, 55.14$. ESI-MS(-) calculated for $[C_{12}H_{12}NO_6]^-$ m/z 266.07, found m/z 266.12 $[M-H]^-$.

Di-*tert*-butyl 2,2'-((4-cyanobenzyl)azanediyl)diacetate (86g). Yield: 75% (1.30 g, 3.60 mmol). 1H NMR (400 MHz, CD_3OD-d_4): δ 7.88 – 7.51 (m, 4H), 3.95 (s, 2H), 3.40 (s, 4H), 1.46 (s, 18H). ESI-MS(+) calculated for $[C_{20}H_{29}N_2O_4]^+$ m/z 361.21, found m/z 361.07 $[M+H]^+$.

2,2'-((4-Cyanobenzyl)azanediyl)diacetic acid (87g). Yield: 94% (67 mg, 0.27 mmol). 1H NMR (400 MHz, $DMSO-d_6$): δ 7.81 (d, $J = 8.2$ Hz, 2H), 7.59 (d, $J = 6.5$ Hz, 2H), 3.97 (s, 2H), 3.49 (s, 4H). ^{13}C NMR (126 MHz, $DMSO-d_6$): δ 172.14, 144.47, 132.67,

130.15, 119.35, 110.51, 57.35, 54.27. ESI-MS(-) calculated for $[C_{12}H_{11}N_2O_4]^-$ m/z 247.07, found m/z 247.17 $[M-H]^-$.

Di-*tert*-butyl 2,2'-((4-(1*H*-tetrazol-5-yl)benzyl)azanediyl)diacetate (86h). Yield: 46% (130 mg, 0.32 mmol). 1H NMR (400 MHz, CD_3OD-d_4): δ 7.99 (d, $J = 7.9$ Hz, 2H), 7.62 (d, $J = 7.9$ Hz, 2H), 3.97 (s, 2H), 3.44 (s, 4H), 1.47 (s, 18H). ESI-MS(+) calculated for $[C_{20}H_{30}N_5O_4]^+$ m/z 404.23, found m/z 404.05 $[M+H]^+$.

2,2'-((4-(1*H*-Tetrazol-5-yl)benzyl)azanediyl)diacetic acid (87h). Deprotection procedure B. Yield: 54% (50 mg, 0.17 mmol). 1H NMR (400 MHz, $DMSO-d_6$): δ 8.00 (d, $J = 7.6$ Hz, 2H), 7.55 (d, $J = 7.8$ Hz, 2H), 3.89 (s, 2H), 3.42 (s, 4H). ^{13}C NMR (126 MHz, $DMSO-d_6$): δ 172.79, 149.23, 142.75, 129.88, 127.33, 123.67, 57.20, 54.19. ESI-MS(-) calculated for $[C_{12}H_{12}N_5O_4]^-$ m/z 290.09, found m/z 290.27 $[M-H]^-$.

Di-*tert*-butyl 2,2'-((thiophen-3-ylmethyl)azanediyl)diacetate (86i). Yield: 62% (506 mg, 1.48 mmol). 1H NMR (400 MHz, CD_3OD-d_4): δ 7.45 – 7.06 (m, 3H), 3.88 (s, 2H), 3.37 (s, 4H), 1.46 (s, 18H). ESI-MS(+) calculated for $[C_{17}H_{28}NO_4S]^+$ m/z 342.17, found m/z 342.07 $[M+H]^+$.

2,2'-((Thiophen-3-ylmethyl)azanediyl)diacetic acid (87i). Deprotection procedure A. Yield: 80% (118 mg, 0.52 mmol). 1H NMR (400 MHz, $DMSO-d_6$): δ 7.58 – 7.52 (m, 1H), 7.51 (s, 1H), 7.14 (d, $J = 4.8$ Hz, 1H), 4.06 (s, 2H), 3.65 (s, 4H). ^{13}C NMR (126

MHz, DMSO-*d*₆) δ 170.87, 135.97, 129.34, 127.10, 126.10, 53.89, 52.91. ESI-MS(-) calculated for [C₉H₁₀NO₄S]⁻ *m/z* 228.03, found *m/z* 228.21 [M-H]⁻.

Di-*tert*-butyl 2,2'-((furan-3-ylmethyl)azanediyl)diacetate (86j). Yield: 29% (230 mg, 0.71 mmol). ¹H NMR (400 MHz, CD₃OD-*d*₄): δ 7.53 – 7.32 (m, 2H), 6.46 (s, 1H), 3.73 (s, 2H), 3.38 (s, 4H), 1.46 (s, 18H). ESI-MS(+) calculated for [C₁₇H₂₆NO₅]⁺ *m/z* 326.20, found *m/z* 326.14 [M+H]⁺.

2,2'-((Furan-3-ylmethyl)azanediyl)diacetic acid (87j). Deprotection procedure A. Yield: 99% (179 mg, 0.84 mmol). ¹H NMR (400 MHz, DMSO-*d*₆): δ 7.74 (s, 1H), 7.67 (s, 1H), 6.55 (s, 1H), 4.01 (s, 2H), 3.74 (s, 4H). ¹³C NMR (126 MHz, DMSO-*d*₆): δ 170.23, 144.36, 143.66, 117.97, 112.17, 53.79, 49.08. ESI-MS(-) calculated for [C₉H₁₀NO₅]⁻ *m/z* 212.06, found *m/z* 212.16 [M-H]⁻.

Di-*tert*-butyl 2,2'-((phenylsulfonyl)azanediyl)diacetate (86k). Yield: 70% (273 mg, 0.71 mmol). ¹H NMR (400 MHz, CD₃OD-*d*₄): δ 7.84 (d, *J* = 8.2 Hz, 2H), 7.73 – 7.51 (m, 3H), 4.07 (s, 4H), 1.38 (s, 18H). ESI-MS(+) calculated for [C₁₈H₂₈NO₆S]⁺ *m/z* 386.16, found *m/z* 408.05 [M+Na]⁺.

2,2'-((Phenylsulfonyl)azanediyl)diacetic acid (87k). Deprotection Procedure A. Yield: 100% (115 mg, 0.42 mmol). ¹H NMR (400 MHz, DMSO-*d*₆): δ = 7.80 (d, *J* = 7.8 Hz, 2H), 7.64 (t, *J* = 7.3 Hz, 1H), 7.55 (t, *J* = 7.6 Hz, 2H), 4.05 (s, 4H). ¹³C NMR (126

MHz, DMSO- d_6): δ = 170.42, 140.06, 133.29, 129.54, 127.38, 48.75. ESI-MS(-) calculated for $[C_{10}H_{10}NO_6S]^-$ m/z 272.02, found m/z 272.10 $[M-H]^-$.

Di-*tert*-butyl 2,2'-((benzylsulfonyl)azanediyl)diacetate (86l). Yield: 76% (310 mg, 0.78 mmol). 1H NMR (400 MHz, CD_3OD-d_4): δ 7.62 – 7.28 (m, 5H), 4.47 (s, 2H), 3.93 – 3.83 (m, 4H), 1.48 (s, 18H). ESI-MS(+) calculated for $[C_{19}H_{30}NO_6S]^+$ m/z 400.18, found m/z 422.09 $[M+Na]^+$.

2,2'-((Benzylsulfonyl)azanediyl)diacetic acid (87l). Deprotection Procedure A. Yield: 99% (90 mg, 0.31 mmol). 1H NMR (400 MHz, DMSO- d_6): δ 7.49 – 7.41 (m, 2H), 7.38 – 7.33 (m, 3H), 4.50 (s, 2H), 3.94 (s, 4H). ^{13}C NMR (126 MHz, DMSO- d_6): δ =171.20, 131.47, 129.97, 128.78, 128.69, 58.51, 49.63. ESI-MS(-) calculated for $[C_{11}H_{12}NO_6S]^-$ m/z 286.04, found m/z 286.09 $[M-H]^-$.

Di-*tert*-butyl 2,2'-((thiophen-2-ylsulfonyl)azanediyl)diacetate (86m). Yield: 77% (308 mg, 0.79 mmol). 1H NMR (400 MHz, CD_3OD-d_4): δ 7.80 (d, J = 5.0 Hz, 1H), 7.63 (d, J = 3.8 Hz, 1H), 7.25 – 7.08 (m, 1H), 4.09 (s, 4H), 1.41 (s, 18H). ESI-MS(+) calculated for $[C_{16}H_{25}NO_6S_2]^+$ m/z 392.12, found m/z 413.98 $[M+Na]^+$.

2,2'-((Thiophen-2-ylsulfonyl)azanediyl)diacetic acid (87m). Deprotection Procedure A. Yield: 90% (105 mg, 0.38 mmol). 1H NMR (400 MHz, DMSO- d_6): δ 8.04 – 7.87 (m, 1H), 7.77 – 7.64 (m, 1H), 7.27 – 7.12 (m, 1H), 4.07 (s, 4H). ^{13}C NMR (126 MHz,

DMSO-*d*₆): δ 170.27, 140.06, 133.74, 132.96, 128.29, 48.99. ESI-MS(-) calculated for [C₈H₈NO₆S₂]⁻ *m/z* 277.98, found *m/z* 278.06 [M-H]⁻.

Di-*tert*-butyl 2,2'-((benzo[*b*]thiophen-2-ylsulfonyl)azanediyl)diacetate (86n). Yield: 70% (312 mg, 0.71 mmol). ¹H NMR (400 MHz, CD₃OD-*d*₄): δ 8.04 – 7.87 (m, 3H), 7.58 – 7.42 (m, 2H), 4.15 (s, 4H), 1.33 (s, 18H). ESI-MS(+) calculated for [C₂₀H₂₈NO₆S₂]⁺ *m/z* 442.14, found *m/z* 464.01 [M+Na]⁺.

2,2'-((Benzo[*b*]thiophen-2-ylsulfonyl)azanediyl)diacetic acid (87n). Deprotection Procedure A. Yield: 99% (101 mg, 0.31 mmol). ¹H NMR (400 MHz, DMSO-*d*₆): δ 8.16 – 7.96 (m, 3H), 7.60 – 7.39 (m, 2H), 4.13 (s, 4H). ¹³C NMR (126 MHz, DMSO-*d*₆): δ 170.18, 141.32, 140.42, 138.10, 129.82, 127.73, 126.40, 125.93, 123.50, 49.16. ESI-MS(-) calculated for [C₁₂H₁₀NO₆S₂]⁻ *m/z* 327.99, found *m/z* 327.99 [M-H]⁻.

Di-*tert*-butyl 2,2'-((thiophen-2-ylmethyl)azanediyl)diacetate (88a). Yield: 87% (717 mg, 2.10 mmol). ¹H NMR (400 MHz, CD₃OD-*d*₄): δ 7.32 (dd, *J* = 4.4, 2.1 Hz, 1H), 7.08 – 6.84 (m, 2H), 4.08 (s, 2H), 3.40 (s, 4H), 1.46 (s, 18H). ESI-MS(+) calculated for [C₁₇H₂₈NO₄S]⁺ *m/z* 342.17, found *m/z* 341.96 [M+H]⁺.

2,2'-((Thiophen-2-ylmethyl)azanediyl)diacetic acid (89a). Deprotection Procedure A. Yield: 70% (130 mg, 0.57 mmol). ¹H NMR (400 MHz, D₂O): δ = 7.50 (dd, *J* = 5.2, 1.3 Hz, 1H), 7.21 (dd, *J* = 3.8, 1.3 Hz, 1H), 7.01 (dd, *J* = 5.2, 3.6 Hz, 1H), 4.64 (d, *J* = 2.2

Hz, 2H), 3.94 (s, 4H). ^{13}C NMR (126 MHz, $\text{D}_2\text{O}-d_2$): δ 168.73, 133.19, 130.09, 128.44, 127.83, 54.17, 52.84. ESI-MS(-) calculated for $[\text{C}_9\text{H}_{10}\text{NO}_4\text{S}]^-$ m/z 228.03, found m/z 228.12 $[\text{M}-\text{H}]^-$.

Di-*tert*-butyl 2,2'-((furan-2-ylmethyl)azanediyl)diacetate (88b). Yield: 82% (646 mg, 1.99 mmol). ^1H NMR (400 MHz, $\text{CD}_3\text{OD}-d_4$): δ 7.48 – 7.42 (m, 1H), 6.38 – 6.30 (m, 1H), 6.26 (d, $J = 3.1$ Hz, 1H), 3.90 (s, 2H), 3.38 (s, 4H), 1.46 (s, 18H). ESI-MS(+) calculated for $[\text{C}_{17}\text{H}_{28}\text{NO}_5]^+$ m/z 326.20, found m/z 326.09 $[\text{M}+\text{H}]^+$.

2,2'-((Furan-2-ylmethyl)azanediyl)diacetic acid (89b). Deprotection Procedure A. Yield: 99% (160 mg, 0.75 mmol). ^1H NMR (400 MHz, D_2O): δ 7.48 (s, 1H), 6.48 (d, $J = 93.7$ Hz, 2H), 4.47 (s, 2H), 3.97 (s, 4H). ^{13}C NMR (126 MHz, $\text{DMSO}-d_6$): δ 171.02, 158.62, 158.34, 143.96, 111.05, 53.88, 50.24. ESI-MS(-) calculated for $[\text{C}_9\text{H}_{10}\text{NO}_5]^-$ m/z 212.06, found m/z 212.18 $[\text{M}-\text{H}]^-$.

Di-*tert*-butyl 2,2'-(((5-methylthiophen-2-yl)methyl)azanediyl)diacetate (88c). Yield: 82% (700 mg, 1.97 mmol). ^1H NMR (400 MHz, $\text{CD}_3\text{OD}-d_4$): δ 6.74 – 6.55 (m, 2H), 3.98 (s, 2H), 3.39 (s, 4H), 2.43 (s, 3H), 1.46 (s, 18H). ESI-MS(+) calculated for $[\text{C}_{18}\text{H}_{30}\text{NO}_4\text{S}]^+$ m/z 356.19, found m/z 356.05 $[\text{M}+\text{H}]^+$.

2,2'-(((5-Methylthiophen-2-yl)methyl)azanediyl)diacetic acid (89c). Deprotection Procedure A. Yield: 97% (113 mg, 0.46 mmol). ^1H NMR (400 MHz, $\text{DMSO}-d_6$): δ 6.81

(s, 1H), 6.65 (s, 1H), 4.08 (s, 2H), 3.87 (s, 4H), 2.39 (s, 3H). ^{13}C NMR (126 MHz, DMSO- d_6): δ 171.39, 168.38, 149.25, 128.47, 125.34, 53.40, 46.96, 15.53. ESI-MS(-) calculated for $[\text{C}_{10}\text{H}_{12}\text{NO}_4\text{S}]^-$ m/z 242.05, found m/z 242.18 $[\text{M}-\text{H}]^-$.

Di-*tert*-butyl 2,2'-(((5-methylfuran-2-yl)methyl)azanediyl)diacetate (88d). Yield: 64% (522 mg, 1.54 mmol). ^1H NMR (400 MHz, $\text{CD}_3\text{OD}-d_4$): δ 6.11 (d, $J = 3.0$ Hz, 1H), 5.92 (d, $J = 2.9$ Hz, 1H), 3.82 (s, 2H), 3.37 (s, 4H), 2.25 (s, 3H), 1.46 (s, 18H). ESI-MS(+) calculated for $[\text{C}_{18}\text{H}_{30}\text{NO}_5]^+$ m/z 340.21, found m/z 340.03 $[\text{M}+\text{H}]^+$.

2,2'-(((5-Methylfuran-2-yl)methyl)azanediyl)diacetic acid (89d). Deprotection Procedure B. Yield: 53% (70 mg, 0.31 mmol). ^1H NMR (400 MHz, $\text{CD}_3\text{OD}-d_4$): δ 6.45 (s, 1H), 6.05 (s, 1H), 4.32 (s, 2H), 3.74 (s, 4H), 2.30 (s, 3H). ^{13}C NMR (126 MHz, $\text{CD}_3\text{OD}-d_4$): δ 169.28, 156.39, 149.61, 114.30, 106.55, 54.16, 50.11, 12.10. ESI-MS(-) calculated for $[\text{C}_{10}\text{H}_{12}\text{NO}_5]^-$ m/z 226.07, found m/z 226.27 $[\text{M}-\text{H}]^-$.

Di-*tert*-butyl 2,2'-((2-(thiophen-2-yl)ethyl)azanediyl)diacetate (88e). Yield: 85% (726 mg, 2.04 mmol). ^1H NMR (400 MHz, $\text{CD}_3\text{OD}-d_4$): δ 7.17 (dd, $J = 5.2, 1.2$ Hz, 1H), 6.95 – 6.77 (m, 2H), 3.44 (s, 4H), 3.02 – 2.91 (m, 4H), 1.47 (s, 18H). ESI-MS(+) calculated for $[\text{C}_{18}\text{H}_{30}\text{NO}_4\text{S}]^+$ m/z 356.19, found m/z 356.00 $[\text{M}+\text{H}]^+$.

2,2'-((2-(Thiophen-2-yl)ethyl)azanediyl)diacetic acid (89e). Deprotection Procedure A. Yield: 75% (109 mg, 0.45 mmol). ^1H NMR (400 MHz, $\text{CD}_3\text{OD}-d_4$): $\delta = 7.26$ (dd, $J =$

3.8, 2.5 Hz, 1H), 7.05 – 6.86 (m, 2H), 3.90 (s, 4H), 3.42 (t, $J = 8.2$ Hz, 2H), 3.29 – 3.19 (m, 2H). ^{13}C NMR (126 MHz, DMSO- d_6): $\delta = 172.87, 142.52, 127.24, 125.38, 124.27, 56.07, 54.84, 28.50$. ESI-MS(-) calculated for $[\text{C}_{10}\text{H}_{12}\text{NO}_4\text{S}]^-$ m/z 242.05, found m/z 242.20 $[\text{M}-\text{H}]^-$.

Di-*tert*-butyl 2,2'-((2-(furan-2-yl)ethyl)azanediyl)diacetate (88f). Yield: 84% (683 mg, 2.01 mmol). ^1H NMR (400 MHz, $\text{CD}_3\text{OD}-d_4$): δ 7.47 – 7.25 (m, 1H), 6.37 – 6.22 (m, 1H), 6.16 – 5.94 (m, 1H), 3.42 (s, 4H), 2.97 (t, $J = 7.8$ Hz, 2H), 2.80 (t, $J = 7.4$ Hz, 2H), 1.46 (s, 18H). ESI-MS(+) calculated for $[\text{C}_{18}\text{H}_{30}\text{NO}_5]^+$ m/z 340.21, found m/z 340.09 $[\text{M}+\text{H}]^+$.

2,2'-((2-(Furan-2-yl)ethyl)azanediyl)diacetic acid (89f). Deprotection Procedure A. Yield: 33% (24 mg, 0.11 mmol). ^1H NMR (400 MHz, DMSO- d_6): δ 7.47 (s, 1H), 6.38 – 6.27 (m, 1H), 6.18 – 6.08 (m, 1H), 3.42 (s, 4H), 2.89 (t, $J = 7.7$ Hz, 2H), 2.72 (t, $J = 7.5$ Hz, 2H). ^{13}C NMR (126 MHz, DMSO- d_6): δ 172.97, 154.03, 141.74, 110.83, 106.08, 54.90, 52.64, 26.84. ESI-MS(-) calculated for $[\text{C}_{10}\text{H}_{12}\text{NO}_5]^-$ m/z 226.07, found m/z 226.31 $[\text{M}-\text{H}]^-$.

Di-*tert*-butyl 2,2'-(((5-bromothiophen-2-yl)methyl)azanediyl)diacetate (88g). Yield: 90% (908 mg, 2.16 mmol). ^1H NMR (400 MHz, $\text{CD}_3\text{OD}-d_4$): δ 6.92 (d, $J = 3.6$ Hz, 1H), 6.74 (d, $J = 3.7$ Hz, 1H), 4.02 (s, 2H), 3.41 (s, 4H), 1.46 (s, 18H). ESI-MS(+) calculated for $[\text{C}_{17}\text{H}_{27}\text{BrNO}_4\text{S}]^+$ m/z 420.08, found m/z 419.92 $[\text{M}+\text{H}]^+$.

2,2'-(((5-Bromothiophen-2-yl)methyl)azanediyl)diacetic acid (89g). Deprotection Procedure A. Yield: 98% (108 mg, 350 μ mol). ^1H NMR (400 MHz, $\text{CD}_3\text{OD}-d_4$): δ 7.02 (s, 1H), 6.91 (s, 1H), 4.31 (s, 2H), 3.75 (s, 4H). ^{13}C NMR (126 MHz, $\text{DMSO}-d_6$) δ 172.58, 145.96, 130.12, 127.00, 111.09, 53.76, 52.67. ESI-MS(-) calculated for $[\text{C}_9\text{H}_9\text{BrNO}_4\text{S}]^-$ m/z 305.94, found m/z 306.19 $[\text{M}-\text{H}]^-$.

Di-*tert*-butyl 2,2'-(((5-chlorothiophen-2-yl)methyl)azanediyl)diacetate (88h). Yield: 80% (510 mg, 1.36 mmol). ^1H NMR (400 MHz, $\text{CD}_3\text{OD}-d_4$): δ 6.78 (dd, $J = 7.9, 2.1$ Hz, 2H), 4.00 (s, 2H), 3.42 (s, 4H), 1.46 (s, 18H). ESI-MS(+) calculated for $[\text{C}_{17}\text{H}_{27}\text{ClNO}_4\text{S}]^+$ m/z 376.13, found m/z 375.97 $[\text{M}+\text{H}]^+$.

2,2'-(((5-Chlorothiophen-2-yl)methyl)azanediyl)diacetic acid (89h). Deprotection Procedure A. Yield: 98% (107 mg, 0.41 mmol). ^1H NMR (400 MHz, $\text{DMSO}-d_6$): δ 6.95 (d, $J = 3.8$ Hz, 1H), 6.88 (d, $J = 3.8$ Hz, 1H), 4.05 (s, 2H), 3.53 (s, 4H). ^{13}C NMR (126 MHz, $\text{DMSO}-d_6$) δ 171.69, 149.32, 141.54, 128.66, 126.73, 53.64, 52.89. ESI-MS(-) calculated for $[\text{C}_9\text{H}_9\text{ClNO}_4\text{S}]^-$ m/z 261.99, found m/z 262.14 $[\text{M}-\text{H}]^-$.

Inhibition Screening and IC_{50} Determination

A soluble truncation of NDM-1 was over-expressed and purified as described previously.⁴ IC_{50} values were determined using 11 concentrations of compound that span the IC_{50} value, and were assayed using meropenem as described previously¹⁵ except that total assay volumes were increased to 200 μL . Final DMSO concentrations

(derived from compound stock solutions) were 1% (v/v). For initial screening of compounds, the percent inhibition at 200 μ M and 250 μ M for each compound was determined using a similar procedure. Briefly, each compound (357 μ M) was incubated with NDM-1 (3.6 nM) for 20 min at 25 °C and diluted upon addition of the meropenem substrate to initiate the reaction with final concentrations as: NDM-1 (2.5 nM), compound (200 μ M and 250 μ M), meropenem (180 μ M), CHAPS (2 mM), HEPES (50 mM), DMSO (0.5 %) at pH 7. Assays were completed as described for the IC₅₀ determinations above.

Thermal Shift Assay

To each well of a 96-well 0.2 mL optical MicroAmp (ThermoFisher) thermocycler plate was added 9.5 μ L of buffer (50 mM HEPES pH 7.5), 4 μ L of NDM-1 in buffer (25 μ M), 4 μ L of inhibitor in buffer (1 mM), and 2.5 μ L of SYPRO orange thermal shift dye (ThermoFisher) in buffer. Each well contained a final concentration of 5 μ M NDM-1 and 200 μ M inhibitor. Thermocycler plate wells were sealed prior to analysis, and the plate was then heated in a thermocycler from 25 to 99 °C at a ramp rate of 0.05 °C/sec. Each thermal shift measurement was taken in six replicates. Fluorescence was read using the ROX filter channel ($\lambda_x = 580$ nm; $\lambda_{em} = 623$ nm), and the fluorescence signal was fitted to a first derivative curve to identify T_M . Native NDM-1 was observed to melt with a $T_M = 56 - 57$ °C.

Native state electrospray ionization mass spectrometry

NanoESI-MS was used to analyze the mechanism of inhibition of some of the inhibitors in this study. Samples (50 μ M VIM-2 and NDM-1) were incubated for 1 h and dialyzed overnight against 100 mM ammonium acetate, pH 7.5, after addition of *tris*(2-carboxyethyl) phosphine hydrochloride (TCEP, final concentration 2 mM) and 3 equivalents (VIM-2) or 2 equivalents (NDM-1) of Zn(II) (from a 0.1 M ZnCl₂ stock). To analyze samples, a nano-electrospray ionization (n-ESI) probe (ThermoFisher Scientific, San Jose, CA, USA) with positive mode protein detection was used on a Thermo Scientific LTQ Orbitrap XL™ hybrid ion trap-orbitrap mass spectrometer. The major parameters were set as follows: capillary temperature, 180 °C; sheath gas, 0; auxiliary gas, 0; sweep gas, 0; spray voltage, 1.1-1.9kV; tube-lens, 150 V; capillary voltage, 35 V; full scan ranging 1000-4000 (m/z); and resolution set to 30,000. The automated gain control was set as follows: full scan, 3×10^4 ; SIM, 1×10^4 ; and MSⁿ 1×10^5 for Fourier-transform. Making slight modifications, the nESI source was equipped with an offline unite (Cat# ES260) which was constructed based on previously- published material.²³ To construct the source, a platinum wire (0.25 mm diameter) was inserted into the center of the offline unit. The glass capillaries (inner tip diameter 0.8 mm, outer tip diameter 1.5 mm) were produced in-house using a micropipette puller (model P-87 Flaming/Brown Micropipette Puller, Sutter Instrument Inc., USA), 5 μ L of sample was loaded into the pulled glass capillary. The platinum wire was inserted into the capillary and the capillary position was adjusted approximately 3 mm from the MS inlet.

4.5 Acknowledgements

Chapter 4 is in preparation for publication. The manuscript in preparation is authored by the following: Allie Y. Chen, Caitlyn Thomas, Pei W. Thomas, Walter Fast, Michael W. Crowder, and Seth M. Cohen with a planned title of “Iminodiacetic Acid as a Metal-binding Pharmacophore for New Delhi Metallo- β -lactamase Inhibitor Development.” The dissertation author was the primary researcher and the co-authors listed above also participated in the research.

4.6 References

1. Zhang, E.; Wang, M. M.; Huang, S. C.; Xu, S. M.; Cui, D. Y.; Bo, Y. L.; Bai, P. Y.; Hua, Y. G.; Xiao, C. L.; Qin, S., NOTA Analogue: A First Dithiocarbamate Inhibitor of Metallo-beta-Lactamases. *Bioorg. Med. Chem. Lett.* **2018**, *28* (2), 214-221.
2. Schnaars, C.; Kildahl-Andersen, G.; Prandina, A.; Popal, R.; Radix, S.; Le Borgne, M.; Gjoen, T.; Andresen, A. M. S.; Heikal, A.; Okstad, O. A.; Frohlich, C.; Samuelsen, O.; Lauksund, S.; Jordheim, L. P.; Rongved, P.; Astrand, O. A. H., Synthesis and Preclinical Evaluation of TPA-Based Zinc Chelators as Metallo-beta-lactamase Inhibitors. *ACS Infect. Dis.* **2018**, *4* (9), 1407-1422.
3. Yu, Z. J.; Liu, S.; Zhou, S.; Li, H.; Yang, F.; Yang, L. L.; Wu, Y.; Guo, L.; Li, G. B., Virtual Target Screening Reveals Rosmarinic Acid and Salvianolic Acid A Inhibiting Metallo- and Serine-beta-Lactamases. *Bioorg. Med. Chem. Lett.* **2018**, *28* (6), 1037-1042.
4. Chen, A. Y.; Thomas, P. W.; Stewart, A. C.; Bergstrom, A.; Cheng, Z. S.; Miller, C.; Bethel, C. R.; Marshal, S. H.; Credille, C. V.; Riley, C. L.; Page, R. C.; Bonomo, R. A.; Crowder, M. W.; Tierney, D. L.; Fast, W.; Cohen, S. M., Dipicolinic Acid Derivatives as Inhibitors of New Delhi Metallo-beta-Lactamase-1. *J. Med. Chem.* **2017**, *60*, 7267-7283.
5. King, A. M.; Reid-Yu, S. A.; Wang, W.; King, D. T.; De Pascale, G.; Strynadka, N. C.; Walsh, T. R.; Coombes, B. K.; Wright, G. D., Aspergillomarasmine A Overcomes Metallo-beta-lactamase Antibiotic Resistance. *Nature* **2014**, *510* (7506), 503-506.
6. Liu, S.; Zhou, Y.; Niu, X.; Wang, T.; Li, J.; Liu, Z.; Wang, J.; Tang, S.; Wang, Y.; Deng, X., Magnolol Restores the Activity of Meropenem Against NDM-1-Producing *Escherichia coli* by Inhibiting the Activity of Metallo-beta-Lactamase. *Cell Death Discov.* **2018**, *4*, 28.
7. Bergstrom, A.; Katko, A.; Adkins, Z.; Hill, J.; Cheng, Z.; Burnett, M.; Yang, H.; Aitha, M.; Mehaffey, M. R.; Brodbelt, J. S.; Tehrani, K.; Martin, N. I.; Bonomo, R. A.; Page, R. C.; Tierney, D. L.; Fast, W.; Wright, G. D.; Crowder, M. W., Probing the Interaction of Aspergillomarasmine A with Metallo-beta-lactamases NDM-1, VIM-2, and IMP-7. *ACS Infect. Dis.* **2018**, *4* (2), 135-145.
8. Albu, S. A.; Koteva, K.; King, A. M.; Al-Karmi, S.; Wright, G. D.; Capretta, A., Total Synthesis of Aspergillomarasmine A and Related Compounds: A Sulfamidate Approach Enables Exploration of Structure-Activity Relationships. *Angew. Chem., Int. Ed. Engl.* **2016**, *55* (42), 13259-13262.
9. Zhang, J.; Wang, S.; Wei, Q.; Guo, Q.; Bai, Y.; Yang, S.; Song, F.; Zhang, L.; Lei, X., Synthesis and Biological Evaluation of Aspergillomarasmine A Derivatives as Novel NDM-1 Inhibitor to Overcome Antibiotics Resistance. *Bioorg. Med. Chem.* **2017**, *25* (19), 5133-5141.

10. Liao, D.; Yang, S.; Wang, J.; Zhang, J.; Hong, B.; Wu, F.; Lei, X., Total Synthesis and Structural Reassignment of Aspergillomarasmine A. *Angew. Chem., Int. Ed. Engl.* **2016**, *55* (13), 4291-4295.
11. Koteva, K.; King, A. M.; Capretta, A.; Wright, G. D., Total Synthesis and Activity of the Metallo-beta-lactamase Inhibitor Aspergillomarasmine A. *Angew. Chem., Int. Ed. Engl.* **2016**, *55* (6), 2210-2212.
12. Zhang, J.; Wang, S.; Bai, Y.; Guo, Q.; Zhou, J.; Lei, X., Total Syntheses of Natural Metallophores Staphylopine and Aspergillomarasmine A. *J. Org. Chem.* **2017**, *82* (24), 13643-13648.
13. Ni, L. B.; Zhang, R. H.; Liu, Q. X.; Xia, W. S.; Wang, H.; Zhou, Z. H., pH- and mol-Ratio Dependent Formation of Zinc(II) Coordination Polymers with Iminodiacetic Acid: Synthesis, Spectroscopic, Crystal Structure and Thermal Studies. *J. Solid State Chem.* **2009**, *182* (10), 2698-2706.
14. Li, X.; Xie, B.; Dong, X.; Sun, Y., Bifunctionality of Iminodiacetic Acid-Modified Lysozyme on Inhibiting Zn(2+)-Mediated Amyloid beta-Protein Aggregation. *Langmuir* **2018**, *34* (17), 5106-5115.
15. Chen, A. Y.; Thomas, P. W.; Cheng, Z.; Xu, N. Y.; Tierney, D. L.; Crowder, M. W.; Fast, W.; Cohen, S. M., Investigation of Dipicolinic Acid Isosteres for the Inhibition of Metallo-beta-Lactamases. *ChemMedChem* **2019**, *14* (13), 1271-1282.
16. Linciano, P.; Cendron, L.; Gianquinto, E.; Spyrakis, F.; Tondi, D., Ten Years with New Delhi Metallo-beta-Lactamase-1 (NDM-1): From Structural Insights to Inhibitor Design. *ACS Infect. Dis.* **2018**, *5* (1), 9-34.
17. Raczynska, J. E.; Shabalin, I. G.; Minor, W.; Wlodawer, A.; Jaskolski, M., A Close Look onto Structural Models and Primary Ligands of Metallo-beta-Lactamases. *Drug Resist. Updat.* **2018**, *40*, 1-12.
18. Krezel, A.; Maret, W., The Biological Inorganic Chemistry of Zinc Ions. *Arch. Biochem. Biophys.* **2016**, *611*, 3-19.
19. Credille, C. V.; Morrison, C. N.; Stokes, R. W.; Dick, B. L.; Feng, Y.; Sun, J.; Chen, Y.; Cohen, S. M., SAR Exploration of Tight-Binding Inhibitors of Influenza Virus PA Endonuclease. *J Med Chem* **2019**, *62* (21), 9438-9449.
20. Klingler, F. M.; Wichelhaus, T. A.; Frank, D.; Cuesta-Bernal, J.; El-Delik, J.; Muller, H. F.; Sjuts, H.; Gottig, S.; Koenigs, A.; Pos, K. M.; Pogoryelov, D.; Proschak, E., Approved Drugs Containing Thiols as Inhibitors of Metallo-beta-lactamases: Strategy To Combat Multidrug-Resistant Bacteria. *J Med Chem* **2015**, *58* (8), 3626-3630.
21. Lo, M. C.; Aulabaugh, A.; Jin, G.; Cowling, R.; Bard, J.; Malamas, M.; Ellestad, G., Evaluation of fluorescence-based thermal shift assays for hit identification in drug discovery. *Anal Biochem* **2004**, *332* (1), 153-159.

22. Stokvis, E.; Rosing, H.; Beijnen, J. H., Stable isotopically labeled internal standards in quantitative bioanalysis using liquid chromatography/mass spectrometry: necessity or not? *Rapid Commun. Mass Spectrom.* **2005**, *19* (3), 401-407.
23. Harvey, S. R.; Porrini, M.; Stachl, C.; MacMillan, D.; Zinzalla, G.; Barran, P. E., Small-molecule Inhibition of c-MYC:MAX Leucine Zipper Formation is Revealed by Ion Mobility Mass Spectrometry. *J. Am. Chem. Soc.* **2012**, *134* (47), 19384-19392.

**Chapter 5. Alternative DPA Libraries and the Future of NDM-1 Inhibitor
Development**

5.1 Introduction

During the FBDD of NDM-1 inhibitors (as described in Chapter 2, Chapter 3, and Chapter 4 of this dissertation), alternative compound sublibraries were synthesized and evaluated. These sublibraries focused on either inhibitor backbone development (where the backbones targeted the various NDM-1 active site pockets, Figure 5-1) or MBP development (where the MBP was modified via isosteric replacement). While these sublibraries did not yield meaningful SAR and were not further pursued, they provide valuable information for future inhibitor development. In Section 5.2, *meta*-substituted **DPA** inhibitors (Sublibrary 8) were explored to probe the L5 binding pocket of NDM-1. The synthesis and evaluation of Sublibrary 9 is described in Section 5.3, where triazole substituents were appended to the *para*- position of the **DPA** MBP. An extension of Chapter 3 of this dissertation, Section 5.4 will discuss the synthesis and evaluation of 6-(1*H*-tetrazol-5-yl)picolinic acid (**51**) derivatives (Sublibrary 10) and picolinic acid isosteres for the identification of NMEs for NDM-1 inhibitor development. Finally, the synthesis of fungal natural product Aspergillomarasmine A and its preliminary assessment as a non-specific metal-chelator is presented in section 5.5. Section 5.6 is dedicated to a perspective on the future of NDM inhibitor development.

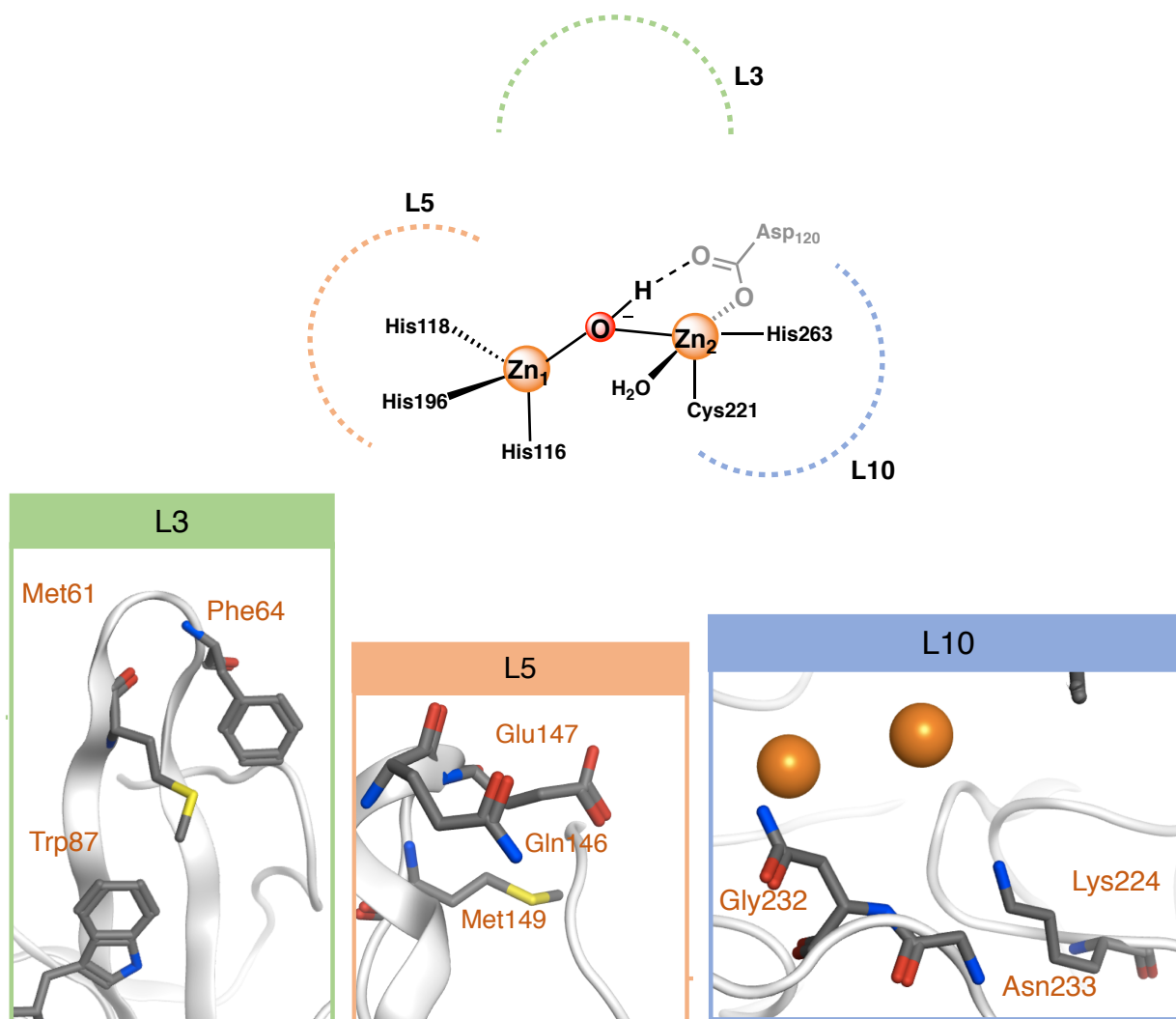


Figure 5-1. The NDM active site pockets available for inhibitor development (standard BBL numbering)

5.2 *meta*-Substituted DPA Derivatives (Sublibrary 8)

Metalloenzymes previously targeted by the Cohen lab (such as RNA-dependent RNA polymerase PA N-terminal endonuclease, PA_N endonuclease, and Glyoxalase1) possess narrow active sites with distinct binding pockets.¹⁻² This has allowed for small modifications in the inhibitor backbone to yield notable changes in inhibitory activity and provide meaningful SAR. Unfortunately, this same FBDD methodology for the development of NDM-1 inhibitors has yielded less than optimal results. As previously described, NDM-1 bears an open, dynamic active site pocket staged by a large hydrophobic wall (the β -hairpin loop, L3, Figure 5-1). In fact, the cavity of the active site of NDM has a volume of 591 Å³, which is nearly 2-fold larger compared to that of IMP (303 Å³) and 13-fold larger compared to that of VIM (45 Å³).³ In addition, this pocket bears few residues available for inhibitor-protein binding, making it difficult to identify key protein residues. Due to these factors, previous development of MBP-bearing “small” molecules has been met with limited success and the design of “large” compounds where the backbone extends beyond the cavity is needed.

As described in Chapter 1, cyclic boronates inhibitors (Figure 5-2) displayed potent inhibitory activity (IC₅₀ = 4 – 29 nM) against NDM-1. A crystal structure of **Cyclic Boronate Inhibitor 2** complexed with VIM-2 revealed the inhibitor forming a bicyclic phenyl-boronate ring interaction with the active site Zn(II) ions and the terminal primary amine of the inhibitor H-bonding with L5 residues.⁴ Although no crystal structure with NDM-1 complexed with this inhibitor is present, SAR analysis predicts the terminal primary amine of **Cyclic Boronate Inhibitor 5** to be H-bonding with L5 of NDM-1.

Recently, this hypothesis was supported by the crystal structure of VNRX-5133 complexed with NDM-1.⁵ In this crystal structure, VNRX-5133 displayed a “morphed” cyclic boronate intermediate with the terminal the side amine chain pointing towards the L5 of NDM-1. The earlier report for cyclic boronate inhibitors inspired the design of a *meta*-substituted **DPA** inhibitors (Sublibrary 8).

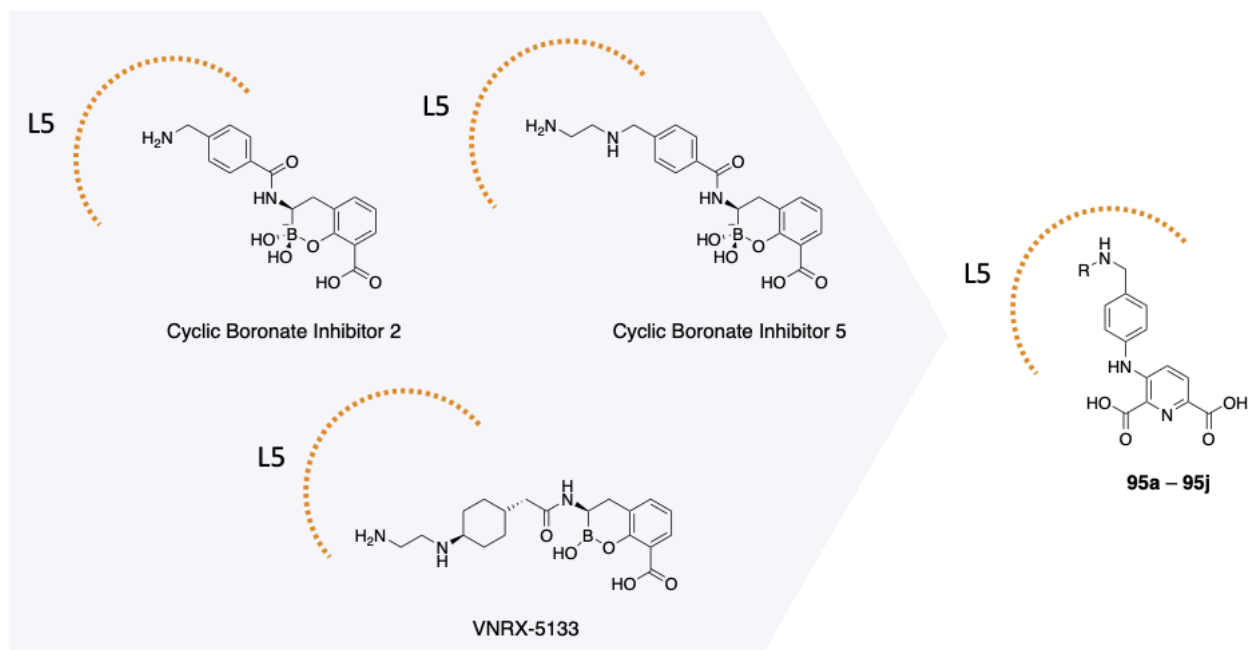


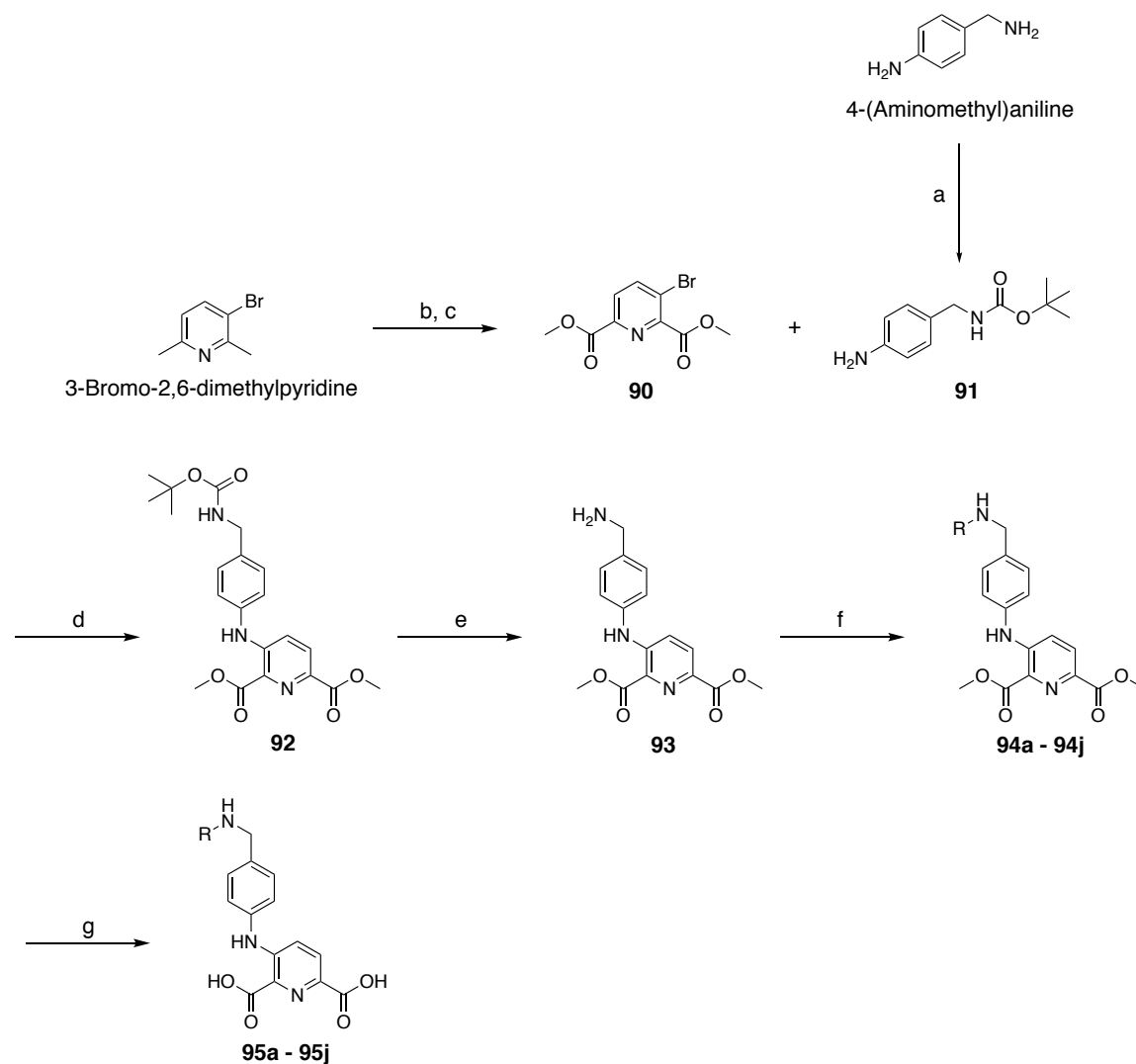
Figure 5-2. Cyclic boronate inhibitors previously reported against MBLs.

5.2.1 Synthesis and Evaluation of Sublibrary 8

Guided by the crystal structure of cyclic boronate inhibitor **5** complexed to VIM-2, *meta*-substituted **DPA** derivatives were designed to yield Sublibrary 8 (Scheme 5-1, **95a** – **95j**). This sublibrary contained a phenyl ring appended via a nitrogen linker at the *meta*-position of **DPA**. The phenyl ring is decorated with an amide functional group bearing various substituents, including terminal primary amines, secondary amines, cyclic motifs, and a methyl-sulfonamide. Briefly, commercially available 3-bromo-2,6-dimethylpyridine was oxidized with KMnO_4 to yield 3-bromopyridine-2,6-dicarboxylic acid, which was then esterified via an acid catalyzed transesterification to result in intermediate **90**. The Buchwald-Hartwig cross-coupling reaction of intermediates **90** and **91** yielded **92**, which was deprotection with TFA to provide intermediate **93**. The amine **93** was converted to the corresponding amide of interest (**94a** – **94j**) via *N,N'*-dicyclohexylcarbodiimide (DCC) coupling. Final compounds **95a** – **95j** were obtained from the saponification of **94a** – **94j**.

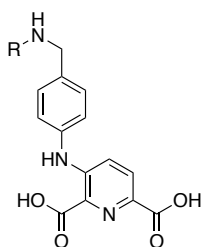
Sublibrary 8 inhibitors were evaluated via monitoring the NDM-1 catalyzed hydrolysis of substrate meropenem and the IC_{50} values are presented in Table 5-1. In general, most of the compounds in Sublibrary 8 exhibited lower inhibitory values than that of the parent **DPA** ($\text{IC}_{50} = 564$ nM). Inhibitors where the terminal amine was extended (**95a** – **95c**) revealed the ethyl-linker (**95b**, $\text{IC}_{50} = 297$ nM) to be slightly more favorable than the methyl-linker (**95a**, $\text{IC}_{50} = 332$ nM) and ~2.5-fold better than the propyl-linker (**95c**, $\text{IC}_{50} = 791$ nM). Unfortunately, inhibitors bearing a piperidine (**95d** – **95e**), aromatic (**95f** and **95g**), acidic (**95h**), or sulfonamide (**95i** and **95j**) motif did not

provide clear SAR. From this data, it can be concluded that the major binding interaction stems from the common phenyl ring appended via a nitrogen linker at the *meta*-position of **DPA**. Future inhibitor development would be necessary to determine how the amide substituents affect inhibitor values.



Scheme 5-1. Synthetic procedures for Sublibrary 8 (compounds **95a** – **95j**). Reagents and conditions: (a) di-*tert*-butyl dicarbonate, CH₂Cl₂, 25 °C, 3 h, 36%; (b) KMnO₄, H₂O, 70 – 90 °C, 10 h; then (c) MeOH, H₂SO₄ (cat.), 70 °C, 24 h; *two steps* 48%; (d) Pd₂(dba)₃ (cat.), Cs₂CO₃, X-Phos, toluene, 100 °C, 17 h, 87%; (e) TFA, CH₂Cl₂, quantitative; (f) corresponding boc-amides, DCC, CH₂Cl₂, 25 °C, 1 h; then trimethylamine, 25 °C, 1 h; *two steps* 58 – 92% (g) 1M NaOH:THF, 25 °C, 12 h, then TFA: CH₂Cl₂, 25 °C, 12 h; *two steps* 77 – 98 %.

Table 5-1. Inhibitory activity of Sublibrary 8 (compounds **95a** – **95j**) against NDM-1. Inhibition values were obtained via monitoring the MBL-catalyzed hydrolysis of substrate meropenem.



Compound		IC ₅₀
DPA		564.3±2.1
95a		332.4±1.7
95b		297.0±3.1
95c		790.9±2.5
95d		633.7±1.3
95e		338.3±2.0
95f		349.3±5.2
95g		490.4±2.3
95h		314.2±0.7
95i		513.0±3.8
95j		396.0±4.2

5.2.2 Discussion

The design of Sublibrary 8 was inspired by previously published cyclic boronate inhibitors. This series contained a phenyl ring appended via a nitrogen linker at the *meta*-position of **DPA** and varied in the amide functional group. The amide linkers included terminal primary amines, secondary amines, cyclic motifs, and methyl-sulfonamides. Compounds in Sublibrary 8 yielded inhibitory activity better than, or on par with, that of the parent **DPA** MBP. While little SAR could be established from the sublibrary, it is believed that there is value in investigating alternative amide linkers. Substituents found in various β -lactam antibiotics (such as thiophene and furans), additional acidic or basic motifs, and aromatic substituents could be utilized to generate larger molecules that bind at the NDM-1 L5 pocket. Notably, the flat SAR obtained from this sublibrary could be attributed to the substrate utilized in the enzymatic assay. Previous work (as described in Chapter 2 and Chapter 3) revealed substrates such as meropenem and chromacef to have a high $K_{M\text{-NDM-1}}$ and low relative absorbance. Due to these factors, a large substrate concentration ($[S]$) is required in the enzymatic assay and leads to higher observed IC_{50} values and a reduction in assay sensitivity. It is believed that the plateaued IC_{50} values observed for this sublibrary could be mitigated by using an alternative substrate with a lower $K_{M\text{-NDM-1}}$ and higher sensitivity (such as fluorocillin). Hence, future development of Sublibrary 8 should include a rescreen utilizing fluorocillin to gain more accurate SAR before further inhibitor design and synthesis.

5.2.3 Experimental

Inhibitory activity of inhibitors against NDM-1 was obtained via monitoring the NDM-1-catalyzed hydrolysis of substrate meropenem or fluorocillin according to previously described methods. All reagents were purchased according to previously detailed sources and used without further purification.

Synthesis

Dimethyl 3-bromopyridine-2,6-dicarboxylate (90). To a solution of 3-bromo-2,6-dimethylpyridine (10.0 g, 53.8 mmol) in H₂O (120 mL) was added KMnO₄ (84.9 g, 537.5 mmol) portion-wise. The first half was added in 1 h intervals at 70 °C, followed by the second half added in 1 h intervals at 90 °C. The reaction was monitored via TLC. After the addition of all 10 equivalents over the course of 10 h, the brown-purple slurry was filtered through a pad of celite and washed with copious amounts of H₂O. The collected aqueous solution was reduced to 1/3 of the volume and acidified with 4M HCl to pH 4. The aqueous layer was extracted with EtOAc (5 × 100mL). The combined organic layers were dried over MgSO₄, filtered and concentrated in vacuo. The crude intermediate **89** was esterified by dissolving in MeOH (600 mL) with catalytic amounts of H₂SO₄ and heated 70 °C for 24 h. The MeOH was removed under reduced pressure and the crude mixture was purified via flash column chromatography to yield the title compound as a white solid in 48 % yield over two steps (7.0 g, 25.5 mmol). ¹H NMR (400 MHz, CDCl₃-*d*): δ 8.15 (d, *J* = 8.8 Hz, 1H), 8.07 (d, *J* = 7.7 Hz, 1H), 4.01 (s, 6H).

ESI-MS(+) calculated for $[\text{C}_9\text{H}_9\text{BrNO}_4]^+$ m/z 275.97, found m/z 276.05 $[\text{M}+\text{H}]^+$ and 290.81 $[\text{M}+\text{NH}_4]^+$.

***tert*-Butyl (4-aminobenzyl)carbamate (91).** In a round bottom flask, 4-(aminomethyl)aniline (1.1 g, 8.8 mmol) was added to a solution of di-*tert*-butyl dicarbonate (1.9 g, 8.8 mmol) in CH_2Cl_2 . The reaction mixture was stirred at 25 °C for 3 h. The solvent was removed in vacuo, and the product was purified via flash column chromatography to yield a yellow solid in 36% yield (700 mg, 3.2 mmol). ^1H NMR (400 MHz, $\text{DMSO}-d_6$): δ 7.13 (s, 1H), 6.87 (d, $J = 7.9$ Hz, 2H), 6.47 (d, $J = 8.0$ Hz, 2H), 4.90 (s, 2H), 3.91 (d, $J = 6.0$ Hz, 2H), 1.36 (s, 9H). ESI-MS(+) calculated for $[\text{C}_{12}\text{H}_{19}\text{N}_2\text{O}_2]^+$ m/z 223.14, found m/z 223.03 $[\text{M}+\text{H}]^+$ and 245.10 $[\text{M}+\text{Na}]^+$.

Dimethyl-3-((4-(((*tert*-butoxycarbonyl)amino)methyl)phenyl)amino)pyridine-2,6-dicarboxylate (92). In a round bottom flask, **90** (150 mg, 0.55 mmol), **91** (145 mg, 0.66 mmol), cesium carbonate (249 mg, 0.77 mmol), $\text{Pd}_2(\text{dba})_3$ (50 mg, 0.05 mmol), and X-Phos (52 mg, 0.11 mmol) were dissolved in toluene (25 mL) and the solution was purged with N_2 for 30 min. The reaction was then heated at 100 °C for 17 h under vigorous stirring. Upon completion, the mixture was filtered through a pad of celite and the celite was washed with toluene (3 \times 25mL). The combined filtrate was concentrated under reduced pressure and the crude product was purified via flash column chromatography, eluting at ~40% EtOAc in hexanes as yellow crystals in 87% yield (197 mg, 0.47 mmol). ^1H NMR (400 MHz, CDCl_3-d): δ 9.81 (s, 1H), 8.03 (d, $J = 9.2$ Hz, 1H),

7.52 (d, $J = 9.1$ Hz, 1H), 7.33 (d, $J = 8.2$ Hz, 2H), 7.21 (d, $J = 6.0$ Hz, 2H), 4.93 (s, 1H), 4.32 (s, 2H), 4.01 (s, 3H), 3.96 (s, 3H), 1.46 (s, 9H). ESI-MS(+) calculated for $[\text{C}_{21}\text{H}_{26}\text{N}_3\text{O}_6]^+$ m/z 416.18, found m/z 438.18 $[\text{M}+\text{Na}]^+$.

Dimethyl 3-((4-(aminomethyl)phenyl)amino)pyridine-2,6-dicarboxylate (93).

Compound **92** (450 mg, 1.08 mmol) was dissolved in a solution of TFA: CH_2Cl_2 (1:5 mL) and stirred at 25 °C for 3 h. Ninhydrin stain and TLC were utilized to monitor the reaction. Excess TFA was removed under reduced pressure and product was co-evaporated with copious amount of toluene to yield the title compound as an orange oil in quantitative yield (342 mg, 1.07 mmol). ^1H NMR (400 MHz, $\text{DMSO}-d_6$): δ 9.62 (s, 1H), 8.15 (s, 2H), 8.04 (d, $J = 9.0$ Hz, 1H), 7.59 (d, $J = 9.0$ Hz, 1H), 7.49 (d, $J = 8.5$ Hz, 2H), 7.38 (d, $J = 8.5$ Hz, 2H), 4.03 (d, $J = 6.0$ Hz, 2H), 3.90 (s, 3H), 3.84 (s, 3H). ESI-MS(+) calculated for $[\text{C}_{16}\text{H}_{18}\text{N}_3\text{O}_4]^+$ m/z 316.13, found m/z 316.15 $[\text{M}+\text{H}]^+$.

Dimethyl-3-((4-((2-((*tert*-butoxycarbonyl)amino)acetamido)methyl)phenyl) amino)-pyridine-2,6-dicarboxylate (94a)

In a round bottom flask, (*tert*-butoxycarbonyl)glycine (330 mg, 1.88 mmol) and DCC (194 mg, 0.94 mmol) were dissolved in CH_2Cl_2 (10 mL) and stirred at 25 °C for 1 h. The white precipitate (dicyclohexylurea, DCU) was removed via vacuum filtration and compound **93** (150 mg, 0.48 mmol) was added directly to the filtrate. TEA (2 mL) was added to the mixture and stirred at 25 °C for an additional 2 h. The solvent was removed in vacuo and the product was purified via flash column chromatography, eluting at 78% EtOAc in hexanes as a yellow powder in 57.8%

yield (130 mg, 0.28 mmol). $^1\text{H NMR}$ (400 MHz, CDCl_3 -*d*): δ 9.82 (s, 1H), 8.03 (d, $J = 8.8$ Hz, 1H), 7.52 (d, $J = 9.0$ Hz, 1H), 7.32 (d, $J = 8.3$ Hz, 2H), 7.20 (d, $J = 8.4$ Hz, 2H), 6.66 (s, 1H), 5.23 (s, 1H), 4.47 (d, $J = 6.3$ Hz, 2H), 4.01 (s, 3H), 3.96 (s, 3H), 3.85 (d, $J = 5.7$ Hz, 2H), 1.43 (s, 9H). ESI-MS(+) calculated for $[\text{C}_{23}\text{H}_{29}\text{N}_4\text{O}_7]^+$ m/z 473.20, found m/z 495.09 $[\text{M}+\text{H}]^+$.

Dimethyl-3-((4-((3-((*tert*-butoxycarbonyl)amino)propanamido)methyl)phenyl)amino)pyridine-2,6-dicarboxylate (94b). In a round bottom flask, 3-((*tert*-butoxycarbonyl)amino)propanoic acid (400 mg, 2.11 mmol) and DCC (218 mg, 1.06 mmol) were dissolved in dichloromethane (10 mL) and the mixture was stirred at 25 °C for 1 h. The white precipitate (DCU) removed via vacuum filtration, and compound **93** (150 mg, 0.48 mmol) was added directly to the filtrate. TEA (2 mL) was added to the mixture and allowed to stir at 25 °C for an additional 2 h. The solvent was removed in vacuo and the product was purified via flash column chromatography, eluting at 78% EtOAc in hexanes as a white solid in 92% yield (213 mg, 0.44 mmol). $^1\text{H NMR}$ (400 MHz, CDCl_3 -*d*): δ 9.81 (s, 1H), 8.02 (d, $J = 8.9$ Hz, 1H), 7.52 (d, $J = 9.0$ Hz, 1H), 7.31 (d, $J = 8.2$ Hz, 2H), 7.19 (d, $J = 8.5$ Hz, 2H), 6.46 (s, 1H), 4.43 (d, $J = 5.7$ Hz, 2H), 4.00 (s, 3H), 3.95 (s, 3H), 3.42 (t, $J = 6.0$ Hz, 2H), 2.48 (t, $J = 6.0$ Hz, 2H), 1.40 (s, 9H). ESI-MS(+) calculated for $[\text{C}_{24}\text{H}_{31}\text{N}_4\text{O}_7]^+$ m/z 487.21, found m/z 487.05 $[\text{M}+\text{H}]^+$.

Dimethyl-3-((4-((4-((*tert*-butoxycarbonyl)amino)butanamido)methyl)phenyl)amino)-pyridine-2,6-dicarboxylate (94c). In a round bottom flask, 4-((*tert*-

butoxycarbonyl)amino)butanoic acid (400 mg, 1.97 mmol) and DCC (203 mg, 0.98 mmol) were dissolved in CH₂Cl₂ (10 mL) and the reaction mixture was stirred at 25 °C for 1 h. The white precipitate (DCU) removed via vacuum filtration and compound **93** (150 mg, 0.48 mmol) was added directly to the filtrate. TEA (2 mL) was added to the reaction mixture and allowed to stir at 25 °C for an additional 2 h. The solvent was removed in vacuo and the product was purified via flash column chromatography, eluting at 90% EtOAc in hexanes as a pale solid in 64% yield (153 mg, 0.31 mmol). ¹H NMR (400 MHz, CDCl₃-d): δ 9.83 (s, 1H), 8.04 (d, *J* = 9.1 Hz, 1H), 7.65 – 7.51 (m, 1H), 7.45 – 7.29 (m, 2H), 7.27 – 7.14 (m, 2H), 6.85 (s, 1H), 4.76 (d, *J* = 6.4 Hz, 1H), 4.47 (d, *J* = 5.5 Hz, 2H), 4.02 (s, 3H), 3.97 (s, 3H), 3.19 (t, *J* = 6.6 Hz, 2H), 2.37 – 2.27 (m, 2H), 1.91 – 1.80 (m, 2H), 1.44 (s, 9H). ESI-MS(+) calculated for [C₂₅H₃₃N₄O₇]⁺ *m/z* 501.23, found *m/z* 501.06 [M+H]⁺.

Dimethyl-3-((4-((1-(*tert*-butoxycarbonyl)piperidine-4-carboxamido)methyl) phenyl)-amino)pyridine-2,6-dicarboxylate (94d). In a round bottom flask, 1-(*tert*-butoxycarbonyl)piperidine-4-carboxylic acid (218 mg, 0.95 mmol) and DCC (98 mg, 0.48 mmol) were dissolved in CH₂Cl₂ (10 mL) and the reaction mixture was stirred at 25 °C for 1 h. The white precipitate (DCU) removed via vacuum filtration and compound **93** (100 mg, 0.32 mmol) was added directly to the filtrate. TEA (2 mL) was added to the reaction mixture and allowed to stir at 25 °C for an additional 2 h. The solvent was removed in vacuo and the product was purified via flash column chromatography, eluting at 80% EtOAc in hexanes as a yellow solid in 66% yield (110 mg, 0.21 mmol). ¹H NMR

(400 MHz, MeOD- d_4): δ 8.01 (d, J = 9.0 Hz, 1H), 7.58 (d, J = 9.0 Hz, 1H), 7.35 (d, J = 8.4 Hz, 2H), 7.26 (d, J = 8.4 Hz, 2H), 4.38 (s, 2H), 4.11 (d, J = 13.5 Hz, 2H), 3.98 (s, 3H), 3.92 (s, 3H), 2.81 (s, 2H), 2.53 – 2.37 (m, 1H), 1.90 – 1.71 (m, 2H), 1.68 – 1.53 (m, 2H), 1.46 (s, 9H). ESI-MS(+) calculated for $[\text{C}_{27}\text{H}_{35}\text{N}_4\text{O}_7]^+$ m/z 527.25, found m/z 549.21 $[\text{M}+\text{Na}]^+$.

Dimethyl-3-((4-((2-(1-(*tert*-butoxycarbonyl)piperidin-4-yl)acetamido)methyl)-phenyl)amino)pyridine-2,6-dicarboxylate (94e). In a round bottom flask, 2-(1-(*tert*-butoxycarbonyl)piperidin-4-yl)acetic acid (231 mg, 0.95 mmol) and DCC (98 mg, 0.48 mmol) were dissolved in CH_2Cl_2 (10 mL) and stirred at 25 °C for 1 h. The white precipitate (DCU) removed via vacuum filtration and compound **93** (100 mg, 0.32 mmol) was added directly to the filtrate. TEA (2 mL) was added to the reaction mixture and allowed to stir at 25 °C for an additional 2 h. The solvent was removed in vacuo and the product was purified via flash column chromatography, eluting at 95% EtOAc in hexanes as a yellow solid in 41 % yield (70 mg, 0.13 mmol). ^1H NMR (400 MHz, MeOD- d_4): δ 8.02 (d, J = 9.0 Hz, 1H), 7.58 (d, J = 9.0 Hz, 1H), 7.37 (d, J = 8.5 Hz, 2H), 7.27 (d, J = 8.4 Hz, 2H), 4.38 (s, 2H), 4.04 (d, J = 13.5 Hz, 2H), 3.98 (s, 3H), 3.92 (s, 3H), 2.76 (s, 2H), 2.18 (d, J = 7.3 Hz, 2H), 1.96 (s, 1H), 1.73 – 1.62 (m, 2H), 1.44 (s, 9H), 1.16 – 1.07 (m, 2H). ESI-MS(+) calculated for $[\text{C}_{28}\text{H}_{37}\text{N}_4\text{O}_7]^+$ m/z 541.27, found m/z 563.23 $[\text{M}+\text{Na}]^+$.

3-((4-((2-Aminoacetamido)methyl)phenyl)amino)pyridine-2,6-dicarboxylic acid TFA (95a). In a round bottom flask, **94a** (127 mg, 0.27 mmol) was dissolved in a

solution of 1M NaOH:THF (3:1 mL) and stirred at 25 °C for 16 h. THF was removed in vacuo. The aqueous solution was cooled to 0 °C and acidified with 4M HCl until pH 4. The precipitate was collected via vacuum filtration and washed with copious amounts of water. The intermediate was dissolved in a solution of CH₂Cl₂:TFA (5:1 mL) and stirred at 25 °C overnight. Excess TFA was removed via co-evaporation with MeOH and water to yield the title compound as an orange oil in 77.0 % yield (95 mg, 0.21 mmol). ¹H NMR (400 MHz, MeOD-*d*₄): δ 8.06 (d, *J* = 9.0 Hz, 1H), 7.62 (d, *J* = 9.0 Hz, 1H), 7.40 (d, *J* = 8.1 Hz, 2H), 7.29 (d, *J* = 8.2 Hz, 2H), 4.46 (s, 2H), 3.73 (s, 2H). ESI-MS(+) calculated for [C₁₆H₁₇N₄O₅]⁺ *m/z* 345.12, found *m/z* 344.99 [M+H]⁺.

3-((4-((3-Aminopropanamido)methyl)phenyl)amino)pyridine-2,6-dicarboxylic acid TFA (95b). In a round bottom flask, **94a** (137 mg, 0.28 mmol) was dissolved in a solution of 1M NaOH:THF (3:1 mL) and stirred at 25 °C for 16 h. THF was removed in vacuo. The aqueous solution was cooled to 0 °C and acidified with 4M HCl until pH 4. The precipitate was collected via vacuum filtration and washed with copious amounts of water. The intermediate was dissolved in a solution of CH₂Cl₂:TFA (5:1 mL) and stirred at 25 °C overnight. Excess TFA was removed via co-evaporation with MeOH and water to yield the title compound as an orange oil in 98 % yield (131 mg, 0.28 mmol). ¹H NMR (400 MHz, MeOD-*d*₄): δ 8.07 (d, *J* = 9.0 Hz, 1H), 7.62 (d, *J* = 9.0 Hz, 1H), 7.40 (d, *J* = 8.5 Hz, 2H), 7.29 (d, *J* = 8.4 Hz, 2H), 4.42 (s, 2H), 3.22 (t, *J* = 6.5 Hz, 2H), 2.67 (t, *J* = 6.5 Hz, 2H). ESI-MS(+) calculated for [C₁₇H₁₉N₄O₅]⁺ *m/z* 349.14, found *m/z* 349.06 [M+H]⁺.

3-((4-((4-Aminobutanamido)methyl)phenyl)amino)pyridine-2,6-dicarboxylic acid TFA (95c). In a round bottom flask, **94c** (122 mg, 0.24 mmol) was dissolved in a solution of 1M NaOH:THF (3:1 mL) and stirred at 25 °C for 16 h. THF was removed in vacuo. The aqueous solution was cooled to 0 °C and acidified with 4M HCl until pH 4. The precipitate was collected via vacuum filtration and washed with copious amounts of water. The intermediate was dissolved in a solution of CH₂Cl₂:TFA (5:1 mL) and stirred at 25 °C overnight. Excess TFA was removed via co-evaporation with MeOH and water to yield the title compound as an orange oil in 80 % yield (95 mg, 0.20 mmol). ¹H NMR (400 MHz, MeOD-*d*₄): δ 8.07 (d, *J* = 9.0 Hz, 1H), 7.62 (d, *J* = 9.0 Hz, 1H), 7.38 (d, *J* = 9.0 Hz, 2H), 7.30 (d, *J* = 2.7 Hz, 2H), 4.39 (s, 2H), 2.98 (t, *J* = 7.6 Hz, 2H), 2.42 (t, *J* = 7.2 Hz, 2H), 2.01 – 1.87 (m, 2H). ESI-MS(+) calculated for [C₁₈H₂₁N₄O₅]⁺ *m/z* 373.15, found *m/z* 373.08 [M+H]⁺.

3-((4-((Piperidine-4-carboxamido)methyl)phenyl)amino)pyridine-2,6-dicarboxylic acid TFA (95d). In a round bottom flask, **94d** (111 mg, 0.21 mmol) was dissolved in a solution of 1M NaOH:THF (3:1 mL) and stirred at 25 °C for 16 h. THF was removed in vacuo. The aqueous solution was cooled to 0 °C and acidified with 4M HCl until pH 4. The precipitate was collected via vacuum filtration and washed with copious amounts of water. The intermediate was dissolved in a solution of CH₂Cl₂:TFA (5:1 mL) and stirred at 25 °C overnight. Excess TFA was removed via co-evaporation with MeOH and water to yield the title compound as an orange oil in 88 % yield (95 mg, 0.19 mmol). ¹H NMR (400 MHz, MeOD-*d*₄): δ 8.00 (d, *J* = 8.9 Hz, 1H), 7.56 (d, *J* = 9.0 Hz, 1H), 7.32 (d, *J* =

7.5 Hz, 2H), 7.22 (d, $J = 8.1$ Hz, 2H), 4.34 (s, 2H), 3.93 (s, 1H), 3.40 (d, $J = 13.2$ Hz, 2H), 3.26 (dd, $J = 3.3, 1.7$ Hz, 1H), 3.05 – 2.93 (m, 2H), 2.65 – 2.51 (m, 1H), 2.05 – 1.94 (m, 2H), 1.95 – 1.81 (m, 2H). ESI-MS(+) calculated for $[C_{20}H_{23}N_4O_5]^+$ m/z 399.17, found m/z 399.06 $[M+H]^+$.

3-((4-((2-(Piperidin-4-yl)acetamido)methyl)phenyl)amino)pyridine-2,6-dicarboxylic acid TFA (95e). In a round bottom flask, **94e** (122 mg, 0.23 mmol) was dissolved in a solution of 1M NaOH:THF (3:1 mL) and stirred at 25 °C for 16 h. THF was removed in vacuo. The aqueous solution was cooled to 0 °C and acidified with 4M HCl until pH 4. The precipitate was collected via vacuum filtration and washed with copious amounts of water. The intermediate was dissolved in a solution of CH_2Cl_2 :TFA (5:1 mL) and stirred at 25 °C overnight. Excess TFA was removed via co-evaporation with MeOH and water to yield the title compound as an orange oil in 97 % yield (90 mg, 0.22 mmol). 1H NMR (400 MHz, MeOD- d_4): δ 8.05 (d, $J = 9.2$ Hz, 1H), 7.61 (d, $J = 9.2$ Hz, 1H), 7.37 (d, $J = 8.1$ Hz, 2H), 7.27 (d, $J = 8.3$ Hz, 2H), 4.38 (s, 2H), 3.98 (s, 1H), 3.31 (s, 1H), 3.08 – 2.90 (m, 2H), 2.26 (d, $J = 6.8$ Hz, 2H), 2.11 (s, 1H), 1.94 (d, $J = 14.0$ Hz, 2H), 1.49 (t, $J = 13.1$ Hz, 2H). ESI-MS(+) calculated for $[C_{21}H_{25}N_4O_5]^+$ m/z 413.18, found m/z 413.11 $[M+H]^+$.

3-((4-((2-(Thiophen-2-yl)acetamido)methyl)phenyl)amino)pyridine-2,6-dicarboxylic acid (95f). In a round bottom flask, **93** (223 mg, 0.74 mmol) was dissolved in a mixture of TEA (1 mL) and anhydrous CH_2Cl_2 (5 mL). Next, 2-(thiophen-2-yl)acetyl chloride (1.11 mmol, 137 μ L) was added dropwise to the mixture and the reaction was stirred at

25 °C for 16 h. The solvent was removed in vacuo and the crude mixture was purified via flash column chromatography to yield **94f** as a dark orange solid. The intermediate was hydrolyzed by stirring in solution of 1M NaOH:THF (3:1 mL) at 25 °C for 16 h. The THF was removed under reduced pressure and the aqueous solution was then acidified with 4M HCl to pH 4 at 0 °C. The precipitate was collect via vacuum filtration and the isolated solid was purified via reverse-phase flash column chromatography, eluting at 80% MeOH in water as beige solid in 19 % yield (57 mg, 0.14 mmol). ¹H NMR (400 MHz, DMSO-*d*₆): δ 8.62 (s, 1H), 7.95 (d, *J* = 8.7 Hz, 1H), 7.61 (d, *J* = 8.9 Hz, 1H), 7.38 – 7.22 (m, 4H), 6.93 (d, *J* = 11.1 Hz, 2H), 4.28 (s, 2H), 3.71 (s, 2H). ESI-MS(-) calculated for [C₂₀H₁₆N₃O₅S]⁻ *m/z* 410.08, found *m/z* 410.03 [M-H]⁻.

3-((4-(Benzamidomethyl)phenyl)amino)pyridine-2,6-dicarboxylic acid (95g). In a round bottom flask, **93** (223 mg, 0.74 mmol) was dissolved in a mixture of TEA (1 mL) and anhydrous CH₂Cl₂ (5 mL). Next, benzoyl chloride (1.48 mmol, 172 μL) was added dropwise and the reaction was stirred at 25 °C for 16 h. The solvent was removed in vacuo and the crude mixture was purified via flash column chromatography to yield **94g** as a dark orange solid. The intermediate was hydrolyzed by stirring in solution of 1M NaOH:THF (3:1 mL) at 25 °C for 16 h. The solution was then acidified with 4M HCl to pH 4 at 0 °C and the precipitate was collect via vacuum filtration to the title compound as a yellow solid in 16% yield (47 mg, 0.12 mmol). No further purification was required. ¹H NMR (400 MHz, MeOD-*d*₄): δ 8.00 (d, *J* = 8.9 Hz, 1H), 7.86 (d, *J* = 7.3 Hz, 2H), 7.68 (d, *J* = 8.9 Hz, 1H), 7.53 (d, *J* = 7.1 Hz, 1H), 7.51 – 7.38 (m, 4H), 7.28 (d, *J* = 8.1 Hz,

2H), 4.59 (s, 2H). ESI-MS(-) calculated for $[C_{21}H_{16}N_3O_5]^-$ m/z 390.11, found m/z 390.08 $[M-H]^-$.

3-((4-((3-Carboxypropanamido)methyl)phenyl)amino)pyridine-2,6-dicarboxylic

acid (95h). In a round bottom flask, **93** (210 mg, 0.70 mmol) was dissolved in a mixture of TEA (1 mL) and anhydrous CH_2Cl_2 (5 mL). Next, methyl 4-chloro-4-oxobutanoate (1.39 mmol, 172 μ L) was added drop-wise to the mixture and the reaction was stirred at 25 °C for 4 h. The solvent was removed in vacuo and the crude mixture was purified via flash column chromatography to afford **94h** as a yellow solid. The intermediate was hydrolyzed by stirring in solution of 1M NaOH:THF (3:1 mL) at 25 °C for 16 h. The solution was then acidified with 4M HCl to pH 4 at 0 °C. The precipitate was collect via vacuum filtration to yield compound **8** as a yellow solid in 37% yield (99 mg, 0.26 mmol). No further purification. 1H NMR (400 MHz, MeOD- d_4): δ 8.05 (d, J = 9.0 Hz, 1H), 7.62 (d, J = 9.0 Hz, 1H), 7.38 (d, J = 7.9 Hz, 2H), 7.27 (d, J = 8.1 Hz, 2H), 4.39 (s, 2H), 2.63 (t, J = 6.8 Hz, 2H), 2.54 (t, J = 6.8 Hz, 2H). ESI-MS(-) calculated for $[C_{18}H_{16}N_3O_7]^-$ m/z 386.10, found m/z 386.08 $[M-H]^-$.

3-((4-(Methylsulfonamidomethyl)phenyl)amino)pyridine-2,6-dicarboxylic acid (95i).

In a round bottom flask, **93** (100 mg, 0.32 mmol) was dissolved in a mixture of TEA: CH_2Cl_2 (1 mL:5 mL) and the reaction was cooled to 0 °C. Methanesulfonyl chloride (0.35 mmol, 27.0 μ L) was added dropwise to the reaction mixture and allowed to stir at 25 °C for 2.5 h. The solvent was removed in vacuo and the crude mixture was purified via flash column chromatography. The intermediate **94i** was hydrolyzed by stirring in

solution of 1M NaOH:THF (3:1 mL) at 25 °C for 16 h. The solution was then acidified with 4M HCl to pH 4 at 0 °C. The precipitate was collect via vacuum filtration to yield compound the title compound as a yellow solid in 41% yield (47 mg, 0.13 mmol). No further purification. ¹H NMR (400 MHz, MeOD-*d*₄): δ 8.06 (d, *J* = 9.0 Hz, 1H), 7.65 (d, *J* = 8.9 Hz, 1H), 7.46 (d, *J* = 8.5 Hz, 2H), 7.31 (d, *J* = 8.4 Hz, 2H), 4.27 (s, 2H), 2.90 (s, 3H). ESI-MS(-) calculated for [C₁₅H₁₄N₃O₆S]⁻ *m/z* 364.06, found *m/z* 363.99 [M-H]⁻.

3-((4-(Methylsulfonamidomethyl)phenyl)amino)pyridine-2,6-dicarboxylic acid (95j).

In a round bottom flask, **93** (150 mg, 0.48 mmol) was dissolved in a mixture of TEA:CH₂Cl₂ (1 mL:5 mL) and the reaction was cooled to 0 °C. Pyridine-3-sulfonyl chloride (1.43 mmol, 174 μL) was added dropwise and the reaction was stirred at 25 °C for 16 h. The solvent was removed in vacuo and the crude mixture was purified via flash column chromatography. The intermediate **94j** was hydrolyzed by stirring in solution of 1M NaOH:THF (3:1 mL) at 25 °C for 16 h. The solution was then acidified with 4M HCl to pH 4 at 0 °C and the precipitate was collect via vacuum filtration to afford the title compound as a pale-yellow solid in 14% yield (29 mg, 0.07 mmol). No further purification was required. ¹H NMR (400 MHz, MeOD-*d*₄): δ 8.88 (s, 1H), 8.70 (d, *J* = 4.9 Hz, 1H), 8.18 (d, *J* = 8.2 Hz, 1H), 8.09 (d, *J* = 9.0 Hz, 1H), 7.64 – 7.48 (m, 2H), 7.28 (d, *J* = 8.3 Hz, 2H), 7.18 (d, *J* = 8.2 Hz, 2H), 4.19 (s, 2H). ESI-MS(-) calculated for [C₁₉H₁₅N₄O₆S]⁻ *m/z* 427.07, found *m/z* 326.99 [M-H]⁻.

5.3 Tetrazole DPA Derivatives (Sublibrary 9)

Triazoles are five-membered heterocyclic compounds bearing three nitrogen and two carbon atoms in either a 1,2,3- or 1,2,4-isomeric form. This functional group is widely utilized as a pharmacophore for drug development, as demonstrated by its occurrence in a span of therapeutic drugs (including antimicrobial, anti-inflammatory, antimalarial, antiviral, anticancer, and many others).⁶ Triazoles are able to form H-bonds, exhibit strong dipole-dipole forces and generate π - π stacking interactions, making it an excellent bioisostere for amide and ester bonds, as well as carboxylic acid, olefin, and heterocycle motifs.⁷⁻⁸ Reported inhibitors of NDM-1 have routinely incorporated phenyl groups (as seen in inhibitor **36** and **Cyclic Boronate Inhibitor 5**, Figure 5-3) to make hydrophobic or π - π stacking interactions with the base of the β -hairpin loop (L3) of NDM-1. Herein, we report the substitution of the phenyl ring with a tetrazole heterocycle for NDM-1 inhibitor development. The tetrazole motif not only maintains the predicted π - π stacking interactions with the β -hairpin loop of NDM-1 but also reduces the overall occupied volume and generates a strong dipole moment.

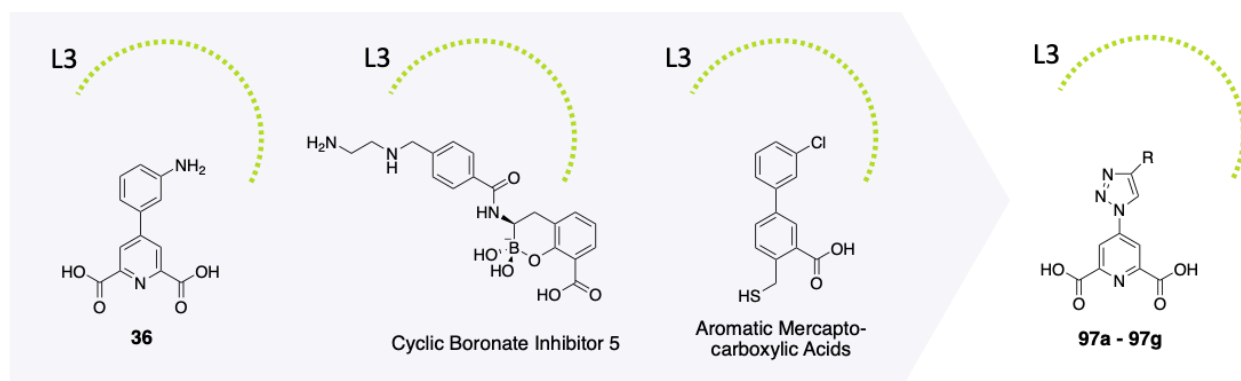
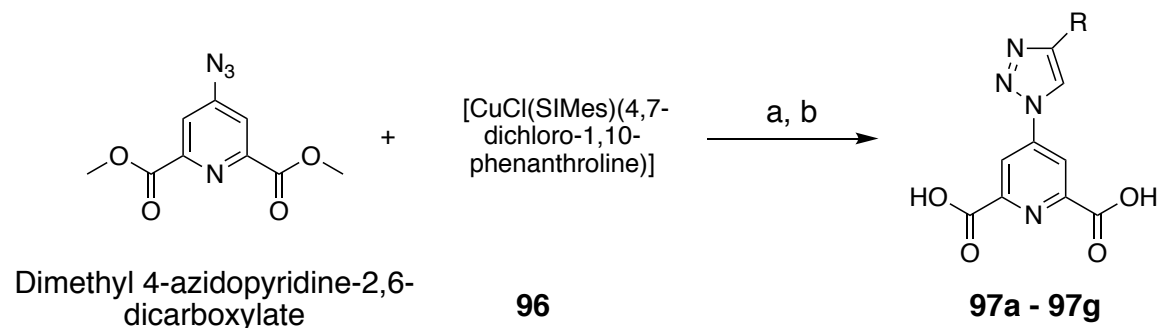


Figure 5-3. Substitution of the phenyl ring with a tetrazole heterocycle for NDM-1 inhibitor development.

5.3.1 Synthesis and Evaluation of Sublibrary 9

Sublibrary 9 includes various 1,2,3-tetrazole derivatives appended at the *para*-position of **DPA**. Various hydrophobic, basic and acidic substituents occupy the 4-position of the appended tetrazole. The synthesis of this sublibrary was achieved through copper-catalyzed azide-alkyne cycloaddition (CuAAC, Scheme 5-2). Briefly, commercially available dimethyl 4-azidopyridine-2,6-dicarboxylate was reacted with various alkynes in the presence of copper catalyst (**96**) to yield the corresponding diester intermediates. Final compounds **97a – 97g** were obtained via the saponification of the obtained intermediates.

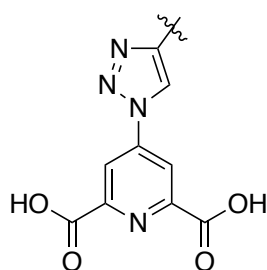


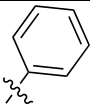
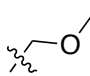
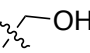
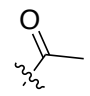
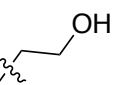
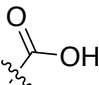
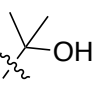
Scheme 5-2. Synthetic route for compounds in Sublibrary 9 (compounds **97a – 97g**). Reagents and conditions: (a) **96** (cat.), MeOH, corresponding alkyne, 25 °C, 16 h; (b) 3:1 1M NaOH:THF, 25 °C, 16 h; then 4M HCl to pH 4; *two steps*: 48 – 79%.

Sublibrary 9 inhibitors were evaluated via monitoring the NDM-1 catalyzed hydrolysis of substrates meropenem and fluorocillin and presented in Table 5-2. Initial dose response screening via substrate meropenem yielded IC_{50} values $>10 \mu\text{M}$. The percent inhibition at $10 \mu\text{M}$ for Sublibrary 9 compounds are reported. A secondary screen utilizing substrate fluorocillin provided IC_{50} values. The inhibitory values

observed for both substrates followed the same trends, with **97d** showing the best inhibitory activity (36%, $IC_{50} = 2.73 \mu\text{M}$) and **97a** and **94b** showing the weakest inhibitory activity (8 – 18%, $IC_{50} = 4.09 - 6.71 \mu\text{M}$). Unfortunately, due to the small number of substituents investigated and high error in the observed IC_{50} values, no meaningful SAR could be established for this series of inhibitors.

Table 5-2. Inhibitory activity against NDM-1 of Sublibrary 9 (**97a – 97g**).^[a]



Compound	Percent Inhibition	IC_{50} (μM)	Compound	Percent Inhibition	IC_{50} (μM)
97a 	18%	6.71 ± 5.41	97e 	29%	3.08 ± 0.86
97b 	8%	4.09 ± 2.69	97f 	19%	3.19 ± 1.63
97c 	25%	3.67 ± 0.58	97g 	26%	3.12 ± 0.51
97d 	36%	2.73 ± 1.37			

^[a] Percent inhibition at inhibitor concentration of $10 \mu\text{M}$ is reported utilizing substrate meropenem and reported values are average of duplicate runs. A secondary assay was utilizing substrate fluorocillin provided the IC_{50} values. Inhibitors were screened in triplicates.

5.3.2 Discussion

The utilization of a tetrazole motif for *para*-**DPA** derivation was investigated. The tetrazole motif was of interest due to its precedent as a bioisostere for amide and ester bonds, as well as carboxylic acid, olefin, and heterocycle motifs. It was hypothesized that a tetrazole substituent would provide better binding interactions compared to that of the routinely used phenyl motif. Unfortunately, none of the compounds in this sublibrary yielded better potency when compared to that of **DPA** or any of the 4-phenylpyridine-2,6-dicarboxylic acid derivatives (**33** – **47**) reported in Chapter 2. Thus, it was concluded that a tetrazole could not replace a phenyl motif and this sublibrary was not further pursued for inhibitor development.

5.3.3 Experimental

Inhibitory activity of inhibitors against NDM-1 was obtained via monitoring the NDM-1-catalyzed hydrolysis of substrate meropenem or fluorocillin according to previously described methods. All reagents were purchased according to previously detailed sources and used without further purification.

Synthesis

[CuCl(SiMes)(4,7-dichloro-1,10-phenanthroline)] (96): Catalyst [CuCl(SiMes)(4,7-dichloro-1,10-phenanthroline)] was synthesized according to literature reported procedures.⁹ Briefly, [CuCl-(SiMes)] (200 mg, 0.50 mmol, 1 equivalent) was dissolved in dichloromethane (5 mL) followed by the addition of 4,7-dichloro-1,10-phenanthroline (1.4 equivalents). Pentane (25 mL) was added drop-wise over the course of 20 min and the reaction was stirred at 25 °C for an additional 1 h. The precipitate was filtered, washed with pentane, and dried under vacuum to yield a dark purple crystalline solid. Yield: 48% (158 mg, 0.24 mmol). No characterization was obtained.

General procedures for the synthesis of compounds 97a –97g.

CuAAC reactions were performed in accordance to literature reported procedures.¹⁰ Dimethyl 4-azidopyridine-2,6-dicarboxylate (150 mg, 0.64 mmol, unless otherwise stated, 1.0 equivalent), the corresponding alkyne (1.5 equivalents), and **96** (2 mol% equivalent) were suspended in MeOH (7 mL). The suspension was stirred at 25 °C for 16 h. The precipitate was collected via vacuum filtration and washed with

copious amounts of cold MeOH. The di-ester intermediate was collected and hydrolyzed in 3:1 1M NaOH:THF at 25 °C for 16 h. The reaction was monitored via TLC. The organic solvent was removed under reduced pressure and the aqueous solution was acidified with 4M HCl to pH 4 to afford the title compounds.

4-(4-Phenyl-1H-1,2,3-triazol-1-yl)pyridine-2,6-dicarboxylic acid (97a). Dimethyl 4-azidopyridine-2,6-dicarboxylate (236 mg, 1.00 mmol). Light yellow powder, yield: 79% (245 mg, 0.79 mmol). ¹H NMR (400 MHz, DMSO-*d*₆): δ 9.82 (s, 1H), 8.78 (d, *J* = 4.3 Hz, 2H), 7.98 (s, 2H), 7.52 (s, 2H), 7.41 (s, 1H). ESI-MS(-) calculated for [C₁₅H₉N₄O₄]⁻ *m/z* 309.06, found *m/z* 309.11 [M-H]⁻.

4-(4-(Hydroxymethyl)-1H-1,2,3-triazol-1-yl)pyridine-2,6-dicarboxylic acid (97b). White powder, yield: 64% (108 mg, 0.41 mmol). ¹H NMR (400 MHz, DMSO-*d*₆): δ 8.99 (s, 1H), 8.78 (d, *J* = 5.4 Hz, 1H), 8.50 (s, 1H), 8.09 (s, 1H), 4.62 (s, 2H). ESI-MS(-) calculated for [C₁₀H₇N₄O₅]⁻ *m/z* 263.04, found *m/z* 263.00 [M-H]⁻.

4-(4-(2-Hydroxyethyl)-1H-1,2,3-triazol-1-yl)pyridine-2,6-dicarboxylic acid (97c). White powder, yield: 65% (114 mg, 0.41 mmol). ¹H NMR (400 MHz, D₂O-*d*₂): δ 8.39 (s, 1H), 8.29 (d, *J* = 3.1 Hz, 1H), 3.78 (t, *J* = 6.3 Hz, 2H), 2.90 (t, *J* = 6.2 Hz, 2H). ESI-MS(-) calculated for [C₁₁H₉N₄O₅]⁻ *m/z* 277.06, found *m/z* 276.86 [M-H]⁻.

4-(4-(2-Hydroxypropan-2-yl)-1H-1,2,3-triazol-1-yl)pyridine-2,6-dicarboxylic acid

(97d). White powder, yield: 70% (130 mg, 0.45 mmol). ^1H NMR (400 MHz, MeOD- d_4): δ 8.83 (s, 2H), 8.78 (s, 1H), 1.66 (s, 6H). ESI-MS(-) calculated for $[\text{C}_{12}\text{H}_{11}\text{N}_4\text{O}_5]^-$ m/z 291.07, found m/z 290.98 $[\text{M}-\text{H}]^-$.

4-(4-(Methoxymethyl)-1H-1,2,3-triazol-1-yl)pyridine-2,6-dicarboxylic acid (97e).

White powder, yield: 52% (91 mg, 0.33 mmol). ^1H NMR (400 MHz, MeOD- d_4): δ 8.94 (s, 1H), 8.84 (s, 2H), 4.65 (d, $J = 0.7$ Hz, 2H), 3.44 (s, 3H). ESI-MS(-) calculated for $[\text{C}_{11}\text{H}_9\text{N}_4\text{O}_5]^-$ m/z 277.06, found m/z 277.04 $[\text{M}-\text{H}]^-$.

4-(4-Acetyl-1H-1,2,3-triazol-1-yl)pyridine-2,6-dicarboxylic acid (97f).

White powder, yield: 54% (95 mg, 0.34 mmol). ^1H NMR (400 MHz, DMSO- d_6): δ 9.96 (s, 1H), 8.76 (s, 2H), 2.62 (s, 3H). ESI-MS(-) calculated for $[\text{C}_{11}\text{H}_7\text{N}_4\text{O}_5]^-$ m/z 275.04, found m/z 274.98 $[\text{M}-\text{H}]^-$.

4-(4-Carboxy-1H-1,2,3-triazol-1-yl)pyridine-2,6-dicarboxylic acid (97g).

White powder, yield: 48% (85 mg, 0.31 mmol). ^1H NMR (400 MHz, DMSO- d_6): δ 9.81 (s, 1H), 8.72 (s, 2H). ESI-MS(-) calculated for $[\text{C}_{10}\text{H}_5\text{N}_4\text{O}_6]^-$ m/z 277.02, found m/z 276.92 $[\text{M}-\text{H}]^-$.

5.4 Alternative Isosteres for Inhibitor Development (Sublibrary 10)

In Chapter 3 of this dissertation, compound **51** was identified as a NME for NDM-1 (and related MBL) inhibitor development.¹¹ Isostere **51** displayed a reduced propensity to remove Zn(II) from the active site of NDM-1 when compared to that of **DPA**, the ability to form a stable ternary complex, and exhibited an IC_{50} of 2.2 – 7.0 μ M (depending on the substrate utilized in the enzymatic assay). In an attempt to probe the metal-binding interactions, additional **51** derivatives (Sublibrary 10) were explored (**51a** – **51d**, Figure 5-4). Compounds where the tetrazole (**51a**) or carboxylic acid (**51b**) motif were moved to the β -carbon, as well as derivatives where the pyridine nitrogen is removed (**51c**) or replaced (**51d**) was synthesized. In addition, the inhibitory activity of 24 picolinic acid isosteres (metal-binding isosteres, MBIs, Figure 5-5)¹² were evaluated to identify alternative isosteres.

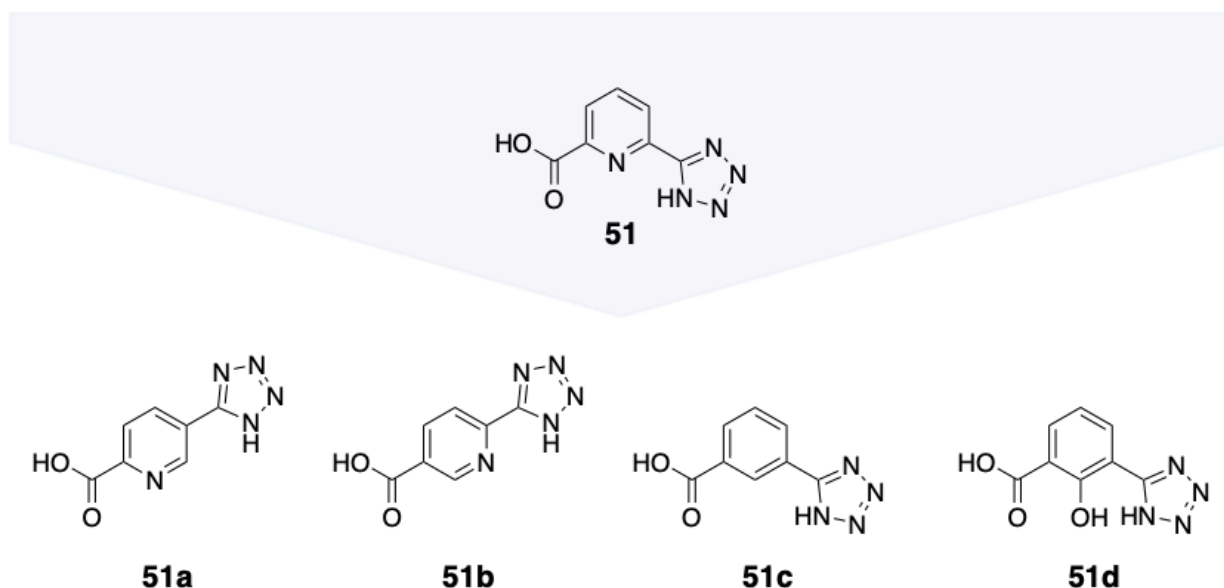


Figure 5-4. Derivatives of **51** that were screened against NDM-1.

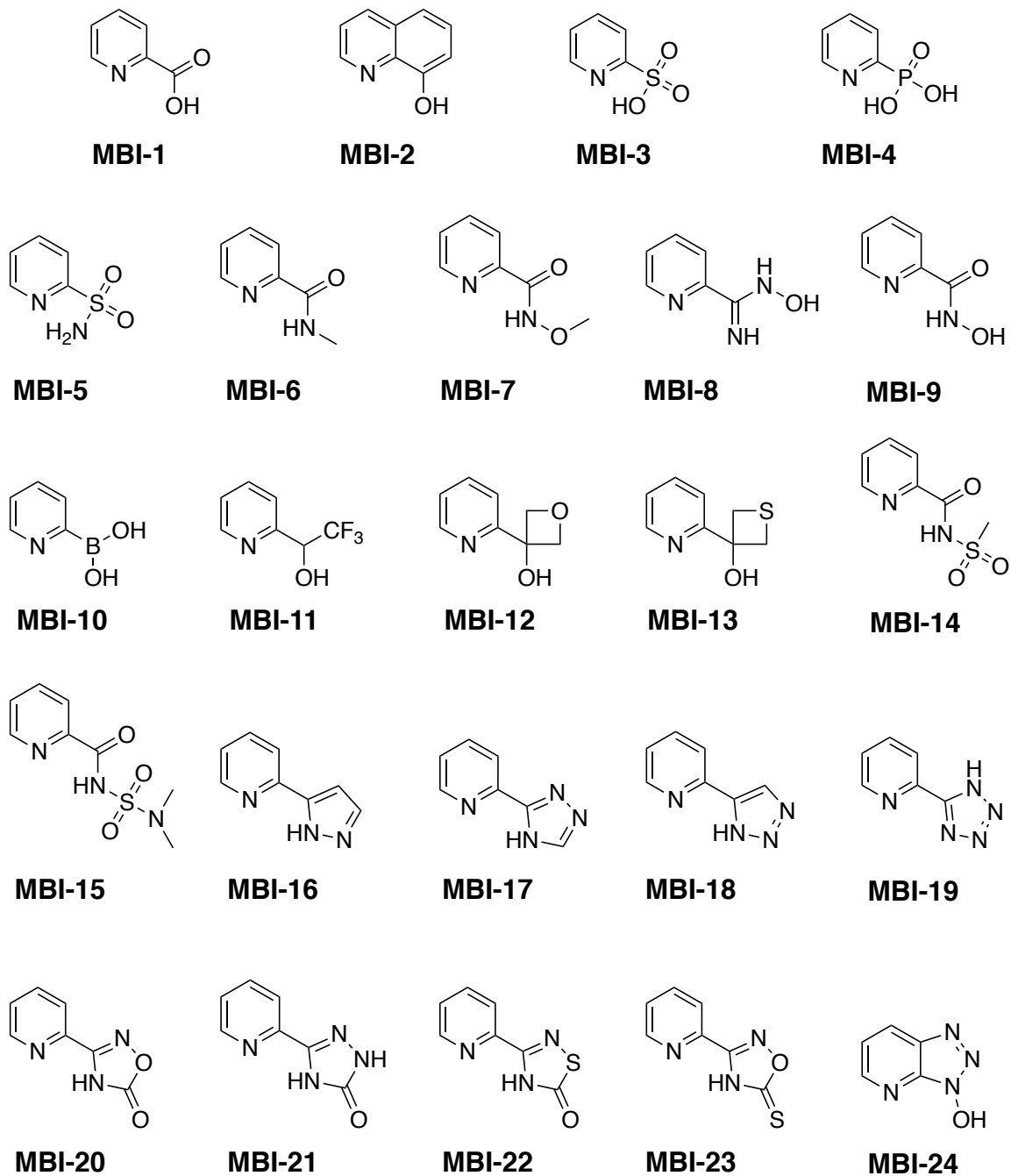


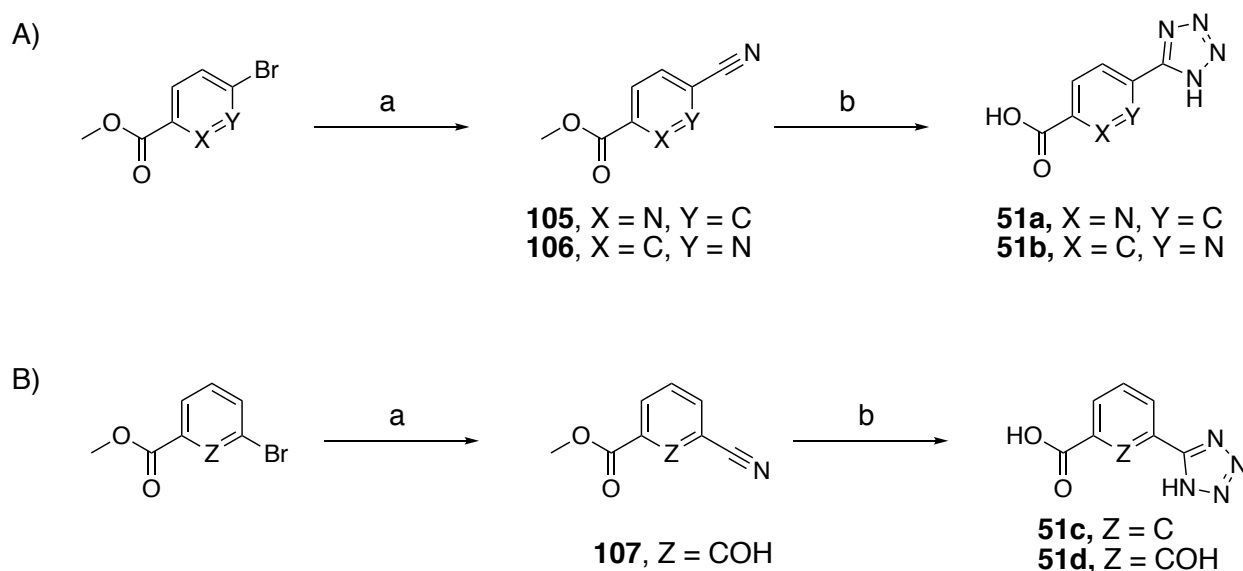
Figure 5-5. MBI library screened against NDM-1 in an attempt to discover new isostere leads.

5.4.1 Synthesis and Evaluation of Sublibrary 10

The synthesis of compounds **51a** – **51d** is described in Scheme 5-3. Briefly, the Pd(II)-catalyzed cyanation of commercially available aryl-bromides with $\text{Zn}(\text{CN})_2$ yield aryl-nitrile intermediates **105** – **107**. In the presence of NaN_3 , the nitrile substituents in **105** – **107** were transformed into a tetrazole through an azide–nitrile cycloaddition. Saponification of the isolated intermediates yielded final inhibitors **51a** – **51d**. The preparation of **MBI-1** – **MBI-24** was previously reported.¹²

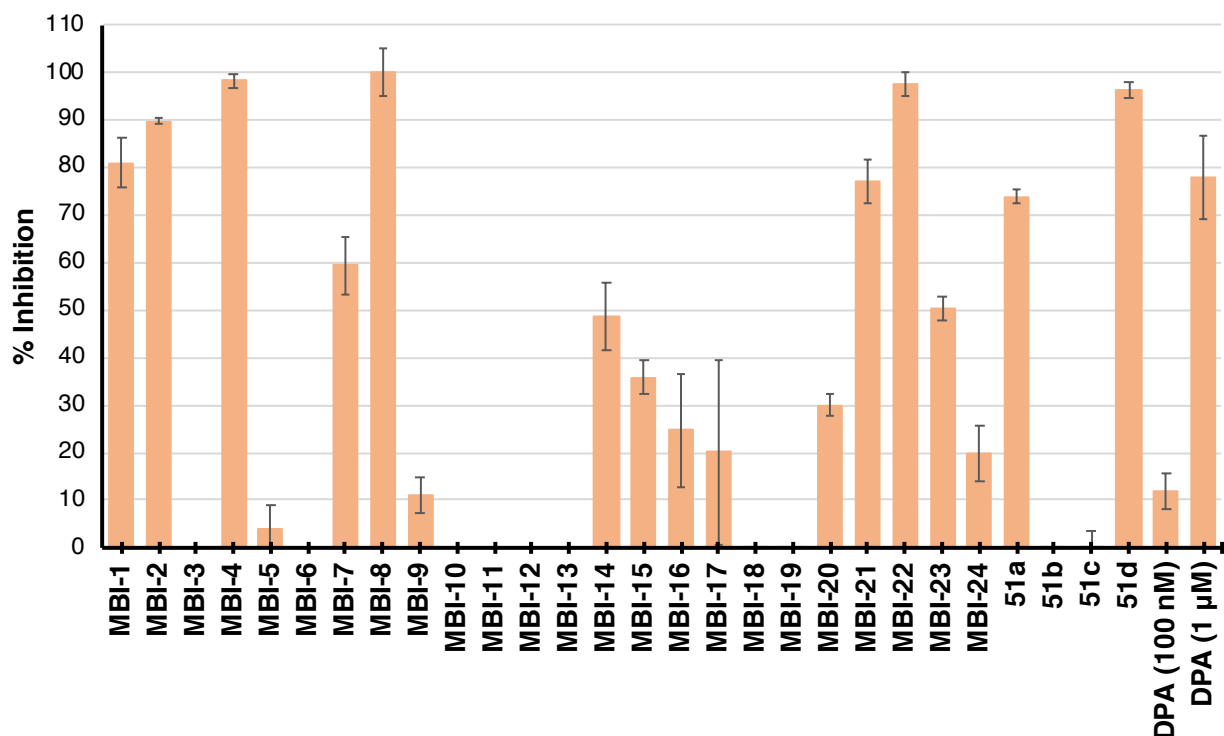
Compounds of Sublibrary 10 were evaluated via monitoring the NDM-1 catalyzed hydrolysis of substrate meropenem at an inhibitor concentration of 100 μM (Figure 5-6). **MBI-1** and **MBI-2** (which were hits in the MBP library screen) displayed inhibition of 80% and 90%, respectively. **MBI-4**, which included a phosphate isostere identical to that of **48**, displayed full inhibition. *N*-Hydroxypicolinimidamide (**MBI-8**), also displayed 100% inhibition; however, the mode of metal-binding was not determined. Several other MBIs, including *N*-methoxyacetamide (**MBI-7**), sulfonyl-acetamides (**MBI-14** and **MBI-15**) and imidazole (**MBI-16**), displayed moderate inhibitory activity (20% – 50%). **MBI-17** is most likely a false hit, as other members in the same family did not display any significant inhibition and the error obtained was large. Interesting, oxadiazole isostere (**MBI-20**) and its related members (**MBI-21** – **MBI-23**) were potent NDM-1 inhibitors, with **MBI-22** displaying potency on par with **MBI-4** and **MBI-8** (near 100%). Derivative **51a** displayed moderate inhibition (73%), while **51b** and **51c** displayed no inhibitory activity against NDM. Surprisingly, **51d** (where the pyridine nitrogen was replaced with a phenol motif) restored potency and exhibited near 100% inhibition.

IC₅₀ values were obtained for selected compounds and reported in Table 5-3. Unfortunately, other than **51d** (IC₅₀ = 9.5 μM), no derivative exhibited IC₅₀ under 36 μM. MBP **51** (IC₅₀ = 2.2 μM) was 4-fold more potent than **51d**, validating the need for a tetrazole and carboxylate motif to be in the α-position of the pyridine ring. The inhibitory activity of **51d** is predicted to be achieved by displacement of the bridging hydroxide by the phenol substituent; however, additional derivatives (ones where the phenol is blocked or substituted with another basic group) and mechanism of action studies are required for further SAR analysis.



Scheme 5-3. Synthetic procedures for Sublibrary 10 (compounds **51a** – **51d**). Reagents and conditions: (a) Pd(Ph₃)₄, ZnCN₂, DMF, 80 °C, 16 h, 51 – 84%; (b) NaN₃, NH₄Cl, 120 °C, 2.5 – 16 h, then 3:1 mL 1M NaOH:THF, 25 °C, 16 h; *two steps*: 32 – 92%.

Figure 5-6. Percent Inhibition of MBIs and Sublibrary 10 at 100 μM against NDM-1 with substrate meropenem.^[a]



^[a] Each inhibitor was tested in six replicates. Inhibitors which displayed $<0\%$ inhibition are shown as 0% inhibition. **DPA** at concentrations of 100 nM and 1 μM (11% and 77% inhibition, respectively) were used as controls.

Table 5-3. Inhibitory activity of compounds **51**, **51a** – **51b**, **MBI-1** and **MBI-20** against NDM-1. Inhibition values were obtained via monitoring the MBL-catalyzed hydrolysis of substrate meropenem.

Compound	IC_{50} (μM)
51	2.2 \pm 0.6
51a	>36
51b	>36
51c	>36
51d	9.5 \pm 1.3
MBI-1	>36
MBI-20	>36

5.4.2 Discussion

Replacement of the carboxylic acid of **DPA** with various surrogate structures is a vital step in the discovery of new MBPs for NDM-1 inhibitor development. In continuation of our findings from Chapter 3, several **51** derivatives were synthesized. It was discovered that while **51a** and **51d** both displayed notable inhibition when screened at an inhibitor concentration of 100 μM against NDM-1, only **51d** resulted in IC_{50} close to the parent **51** MBP. Replacement of the phenol of **51d** with other motifs could yield insight to the mode of inhibition and whether the phenol is displacing the bridging hydroxide ion. In addition, 24 MBIs were evaluated to reveal several new isosteres motifs for **DPA** inhibitor development. The most notable includes **MBI20** – **MBI24**, which bear a heterocycle appended to the α -position of the pyridine ring. Future development of **DPA** inhibitors can utilize the motifs found in **MBI20** – **MBI24** for isosteric replacement. In addition, previous research has solely focused on replacing one carboxylic acid of **DPA**; hence, to reveal additional and more complex NMEs, combinations of isosteres can be used for the double-replacement of carboxylate groups.

5.4.3 Experimental

Inhibitory activity of inhibitors against NDM-1 was obtained via monitoring the NDM-1-catalyzed hydrolysis of substrate meropenem or fluorocillin according to previously described methods. All reagents were purchased according to previously detailed sources and used without further purification.

Synthesis

Methyl 5-cyanopicolinate (105). In a round bottom flask, methyl 5-bromopicolinate (500 mg, 2.3 mmol) and ZnCN_2 (408 mg, 3.5 mmol) were dissolved in DMF (5 mL) and the solution was purged with N_2 for 30 min. Next, $\text{Pd}(\text{Ph}_3)_4$ (10 mol%) was added and the mixture was purged with N_2 for an additional 10 min. The reaction was heated to 80 °C for 16 h. The mixture was filtered through a pad of celite and the filtrate was concentrated in vacuo. The compound was purified via flash column chromatography to yield the title compound in 60% yield (225 mg, 1.39 mmol). ^1H NMR (400 MHz, $\text{MeOD-}d_4$): δ 9.02 (s, 1H), 8.39 (d, $J = 8.1$ Hz, 1H), 8.28 (d, $J = 1.0$ Hz, 1H), 4.00 (s, 3H). ESI-MS(+) calculated for $[\text{C}_8\text{H}_7\text{N}_2\text{O}_2]^+$ m/z 163.05, found m/z 163.14 $[\text{M}+\text{H}]^+$.

5-(1*H*-Tetrazol-5-yl)picolinic acid (51a). In a round bottom flask, compound **105** (200 mg, 1.23 mmol), NaN_3 (321 mg, 4.93 mmol), and NH_4Cl (264 mg, 4.93 mmol) were dissolved in DMF (10 mL). The reaction was heated to 130 °C for 16 h. The reaction was cooled to 25 °C and the precipitation was collected via vacuum filtration. The isolated solid was suspended in acidic water (pH 3) and the precipitate was collected

via vacuum filtration. The collected white solid was dissolved in 1M NaOH (5 mL) and the aqueous layer was washed with EtOAc (3×5mL). The aqueous layer was then acidified with 4M HCl to pH 1 and placed in freezer for 2 h. The precipitate was collected to yield the title compound as a white solid in 32% yield (75 mg, 0.39 mmol). ¹H NMR (400 MHz, MeOD-*d*₄): δ 9.35 (s, 1H), 8.64 (dd, *J* = 8.2, 2.2 Hz, 1H), 8.34 (d, *J* = 8.1 Hz, 1H). ESI-MS(-) calculated for [C₇H₄N₅O₂]⁻ *m/z* 190.04, found *m/z* 190.12 [M+H]⁺.

Methyl 6-cyanonicotinate (106). In a round bottom flask, methyl 6-bromonicotinate (500 mg, 2.31 mmol) and ZnCN₂ (408 mg, 3.47 mmol) were dissolved in DMF (5 mL) and the solution was purged with N₂ for 30 min. Next, Pd(Ph₃)₄ (10 mol%) was added and the mixture was purged with N₂ for an additional 10 min. The reaction was heated to 80 °C for 16 h. The mixture was filtered through a pad of celite and the filtrate was concentrated in vacuo. The compound was purified via flash column chromatography to yield the title compound in 51% yield as a white solid (193 mg, 1.19 mmol). ¹H NMR (400 MHz, MeOD-*d*₄): δ 9.23 (s, 1H), 8.52 (d, *J* = 8.1 Hz, 1H), 8.00 (d, *J* = 8.1 Hz, 1H), 3.99 (s, 3H). ESI-MS(+) calculated for [C₈H₇N₂O₂]⁺ *m/z* 163.05, found *m/z* 163.22 [M+H]⁺.

6-(1*H*-Tetrazol-5-yl)nicotinic acid (51b). In a round bottom flask, compound **106** (150 mg, 0.93 mmol), NaN₃ (241 mg, 3.70 mmol), and NH₄Cl (198 mg, 3.70 mmol) were dissolved in DMF (10 mL). The reaction was heated to 120 °C for 16 h. The reaction

was cooled to 25 °C and concentrated in vacuo. The crude solid was dissolved in 1M NaOH (10 mL). The aqueous layer was washed with EtOAc (3×10mL) and heated to 50 °C for 3 h under vigorous stirring. The aqueous layer was then acidified with 4M HCl to pH 1 and the precipitate was collected to yield the title compound as a white solid in 92% yield (162 mg, 0.85 mmol). ¹H NMR (400 MHz, MeOD-*d*₄): δ 9.31 (s, 1H), 8.59 (s, 1H), 8.37 (s, 1H). ESI-MS(-) calculated for [C₇H₄N₅O₂]⁻ *m/z* 190.03, found *m/z* 190.07 [M-H]⁻.

3-(1*H*-Tetrazol-5-yl)benzoic acid (51c). In a round bottom flask, methyl 3-cyanobenzoate (500 mg, 3.10 mmol), NaN₃ (807 mg, 12.4 mmol), and NH₄Cl (664 mg, 12.4 mmol) were dissolved in DMF (10 mL). The reaction was heated to 120 °C for 2.5 h. The DMF solution was cooled to 0 °C and poured over H₂O (30 mL). NaNO₃ (800 mg) was added to the mixture and stirred vigorously for 5 min to destroy excess NaN₃. The aqueous mixture was washed with EtOAc (30 mL) and subsequently acidified with 4M HCl to pH 2. The white solid was collected via vacuum filtration. The solid was dissolved in 1M NaOH (5 mL) and stirred at 25 °C for 16 h. The aqueous layer was acidified with 4M HCl to pH 4 and the white precipitate was collected via vacuum filtration to afford the title compound in 75% yield (444 mg, 2.33 mmol). ¹H NMR (400 MHz, MeOD-*d*₄): δ 8.70 (s, 1H), 8.27 (d, *J* = 7.7 Hz, 1H), 8.22 (d, *J* = 7.6 Hz, 1H), 7.71 (t, *J* = 7.8 Hz, 1H). ESI-MS(-) calculated for [C₈H₅N₄O₂]⁻ *m/z* 189.04, found *m/z* 188.97 [M-H]⁻.

Methyl 3-cyano-2-hydroxybenzoate (107). In a round bottom flask, methyl 3-bromo-2-hydroxybenzoate (500 mg, 2.16 mmol) and ZnCN₂ (762 mg, 6.49 mmol) were dissolved in DMF (5 mL) and the solution was purged with N₂ for 30 min. Next, Pd(Ph₃)₄ (10 mol%) was added and the mixture was purged with N₂ for an additional 10 min. The reaction was heated to 80 °C for 16 h. The mixture was filtered through a pad of celite and the filtrate was concentrated in vacuo. The compound was purified via flash column chromatography to yield the title compound in 84% yield as a white solid (320 mg, 1.81 mmol). ¹H NMR (400 MHz, MeOD-*d*₄): δ 8.14 (d, *J* = 8.0 Hz, 1H), 7.85 (d, *J* = 7.7 Hz, 1H), 7.07 (t, *J* = 7.9 Hz, 1H), 4.00 (s, 3H). ESI-MS(-) calculated for [C₉H₆NO₃]⁻ *m/z* 176.03, found *m/z* 175.98 [M-H]⁻.

2-Hydroxy-3-(1*H*-tetrazol-5-yl)benzoic acid (51d). In a round bottom flask, compound **107** (200 mg, 1.13 mmol), NaN₃ (294 mg, 4.52 mmol), and NH₄Cl (242 mg, 4.52 mmol) were dissolved in DMF (10 mL). The reaction was heated to 120 °C for 16 h. The DMF solution was cooled to 0 °C and poured over H₂O (30 mL). The mixture was heated to 120 °C for 1 h under vigorous stirring. NaNO₃ (800 mg) was added to the mixture and stirred vigorously for 5 min to destroy excess NaN₃. Next, 6M NaOH was added dropwise to the aqueous mixture until pH 10 and the aqueous layer was washed with EtOAc (30 mL). The mixture was concentrated under reduced pressure and subsequently acidified with 4M HCl to pH 3 to yield a beige solid which was collected via vacuum filtration as the title compound in 68% yield (159 mg, 0.77 mmol). ¹H NMR (400 MHz, MeOD-*d*₄): δ 8.37 (d, *J* = 7.8 Hz, 1H), 8.10 (d, *J* = 7.8 Hz, 1H), 7.13 (t, *J* =

7.9 Hz, 1H). ESI-MS(-) calculated for $[\text{C}_8\text{H}_5\text{N}_4\text{O}_3]^-$ m/z 205.03, found m/z 205.15
[M+H]⁺.

5.5 Synthesis and Evaluation of Aspergillomarasmine A

The fungal secondary metabolite, Aspergillomarasmine A (AMA, Figure 5-7) has been reported as a potent inhibitor of NDM-1 ($IC_{50}=4.0\pm 0.1\mu M$).¹³ AMA was a promising lead for inhibitor development due to its in vivo therapeutic potential in a mouse model infected with NDM-1 expressing Gram-negative bacteria;¹³ however, it was not until later that the absolute configuration at the 3-, 6- and 9-position of AMA was confirmed. A reported 9-step synthetic procedure for various AMA diastereomers confirmed the structural configuration of the natural product as LLL-AMA ($IC_{50}= 8.1\mu M$).¹⁴ These results were validated by other similar studies.¹⁵

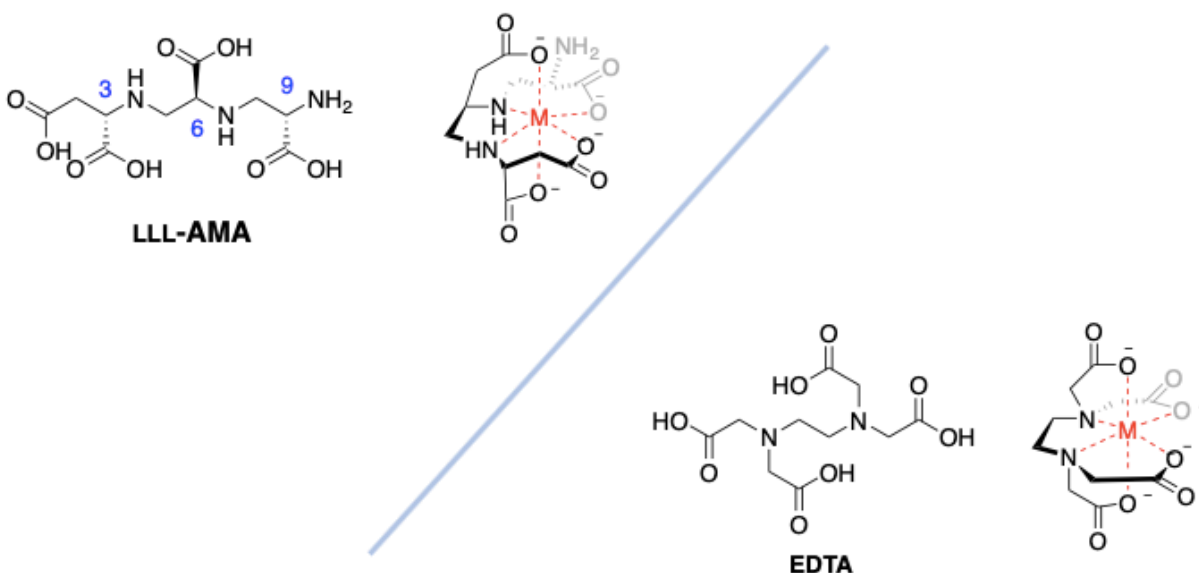


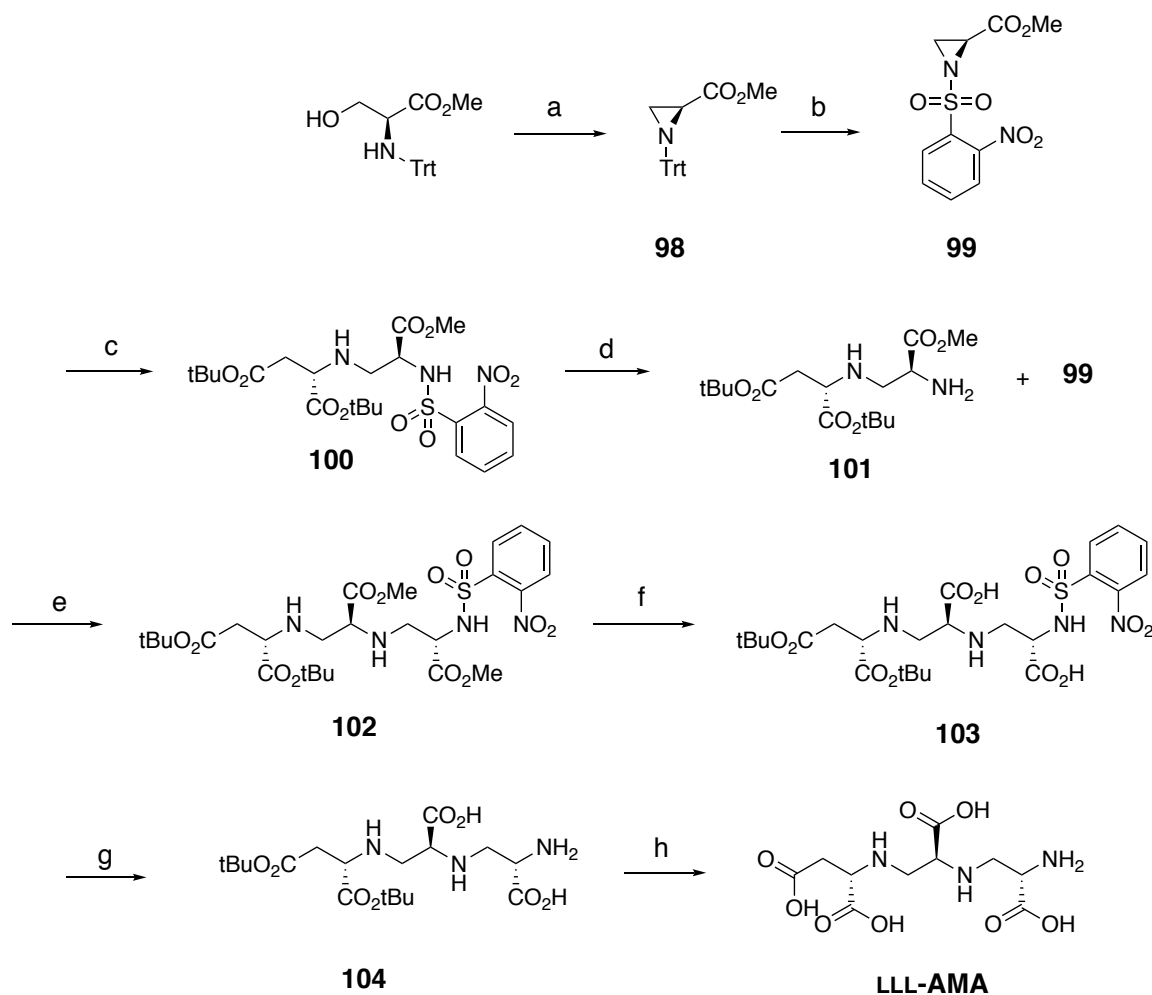
Figure 5-7. Predicted AMA chelation (*left*) in comparison with known EDTA chelation (*right*).

AMA gained interest as a lead for drug development, as demonstrated by the numerous publications for the synthesis of AMA and its derivatives; however, the

potential for AMA acting as a metal chelator similar to that of EDTA was overlooked. AMA and EDTA both bear N,O-donor atoms capable of forming a hexadentate ligand for metal chelation (Figure 5-7). The SAR of AMA and AMA derived compounds investigated by the Wright laboratory confirmed the four free carboxylate groups to be essential for enzyme inhibition and suggested AMA inhibited NDM-1 through sequestration of the catalytic Zn(II) ions.¹⁶ In Section 5.6, we hoped to validate AMA inhibits via a non-specific metal chelation mechanism of action. The total synthesis of AMA was carried out according to literature reported procedures,¹⁵ and the inhibition of AMA against a panel of Zn(II)-dependent metalloenzymes (hCAII, HDAC1, and MMPs) was evaluated.

5.5.1 Synthesis and Evaluation of AMA

The synthesis of LLL-AMA was carried out according to literature procedures with minor modifications reported in Section 5.6.3 (Scheme 5-4).¹⁵ The inhibitory activity of AMA and EDTA against Zn(II)-dependent metalloenzymes was determined according to previously reported procedures¹⁷ and reported in Table 5-4. The IC₅₀ for AMA against MMP-2 and MMP-12 was observed to be 158 μ M and 1.1 mM, respectively; however, no inhibition of MMP-2 and MMP-12 was found for EDTA (at inhibitor concentration up to 1.5 mM). It is suspected that EDTA chelation to the calcium ions in the assay buffer (CaCl₂ = 10 mM) resulted in depletion of available EDTA for enzyme inhibition. Although both AMA and EDTA are both hexadentate ligands, the identity of the N-donor atoms, chelation ring size, and resulting ring geometry differ and effects the formation of metal chelate complexes. The same results were observed when EDTA was screened against HDAC-1. No inhibition was observed at an EDTA concentration of up to 1 mM. This is likely due to the 1 mM MgCl₂ present in the assay buffer. AMA was not tested against HDAC-1. Lastly, AMA and EDTA were screened against hCAII at a single concentration of 1 mM. hCAII was a suitable alternative metalloenzyme due to the absence of excess metal in the assay buffer. AMA and EDTA both yielded minimal inhibitory activity (2 – 3%) against hCAII.



Scheme 5-4. Synthesis of LLL-AMA according to reported procedures.¹⁵ Reagents and conditions: (a) MsCl, TEA, THF, 65 °C, 46 h, 76%; (b) TFA, 0 °C, 30 min; *o*-NsCl, 25 °C, 24 h, 70%; (c) L-aspartic acid di-*tert*-butyl ester, THF, 25 °C, 16 h, 72%; (d) PhSH, DIPEA, ACN, 25 °C, 2.5 h, 83%; (e) THF, TEA, 25 °C, 24 h, 57%; (f) Me₃SnOH, DCE, 84 °C, 3 h, 99%; (g) PhSH, DIPEA, ACN, 25 °C, 4 h, 94%; (h) TfOH, anisol, CH₂Cl₂, 4 °C, 3 h, 41%.

Table 5-4. AMA and EDTA screened against a panel of Zn(II)-dependent metalloenzymes.

	MMP-2	MMP-12	HDAC-1	hCAII
AMA	IC ₅₀ = 157.6 ± 1.2 μM	IC ₅₀ = 1.1 ± 0.3 mM	N/A	3% inhibition (1 mM)
EDTA	IC ₅₀ = >1.5 mM	IC ₅₀ = >1.5 mM	IC ₅₀ = > 1mM	2% inhibition (1 mM)

5.5.2 Discussion

The synthesis of LLL-AMA and an attempt to compare its non-selective metal chelating ability with that of EDTA is reported. The synthesis of AMA was carried out successfully; unfortunately, the addition of metal ions in various assay buffers resulted in poor and unreliable assay results. While moderate inhibition was observed for AMA against MMP-2 and MMP-12, no enzyme inhibition was observed for EDTA at concentrations up to 1.5 mM. It was unclear whether the results were due to the inherent inactivity of the inhibitor or the chelation of the exogenous metals in the buffer. Assay buffer for hCAII did not contain exogenous metals and minor, but similar, inhibition values were observed for the two compounds of interest (2 – 3%) at a concentration of 1 mM. Unfortunately, conducting enzymatic assays in the absence of metals is not possible, as the exogenous di-valent ions (commonly from MgCl₂, ZnSO₄, and MnCl₂) ensures full metal occupancy of the metalloenzyme active site required for catalysis. This makes the evaluation of strong metal chelators difficult. To further study AMA, we had wished to synthesize, crystallize, and characterize various AMA transition metal complexes; however, due to the lengthy synthesis of the AMA and re-prioritization of projects, this study was no longer pursued.

5.5.3 Experimental

Inhibitory activity of AMA and EDTA against metalloenzymes were performed according to procedures reported in Chapter 2. All reagents were purchased according to previously detailed sources and used without further purification.

Methyl (S)-1-tritylaziridine-2-carboxylate (98). Commercially available methyl trityl-L-serinate (9.0 g, 24.9 mmol) was dissolved in THF (70 mL). Next, TEA (7.64 mL) was added in portion-wise and the mixture was cooled to 0 °C. Methanesulfonyl chloride (1.96 mL, 25.1 mmol) was added drop-wise to the solution over a period of 15 min to keep the reaction temperature under 20 °C. The reaction was stirred at 25 °C for an additional 30 min and then heated to 65 °C for 46 h. Upon completion, THF was removed under reduced pressure. The crude product was purified via flash column chromatography to afford the title compound in 76% yield as a white crystalline solid (6.5 g, 18.9 mmol). ¹H NMR (400 MHz, CDCl₃-d): δ 7.58 – 7.51 (m, 6H), 7.31 (dd, *J* = 8.1, 6.2 Hz, 7H), 7.25 (s, 2H), 3.79 (s, 3H), 2.30 (dd, *J* = 2.7, 1.6 Hz, 1H), 1.94 (dd, *J* = 6.1, 2.7 Hz, 1H), 1.46 (dd, *J* = 6.2, 1.6 Hz, 1H). ESI-MS(+) calculated for [C₂₃H₂₂NO₂]⁺ *m/z* 344.17, found *m/z* 366.17 [M+Na]⁺.

Methyl (S)-1-((2-nitrophenyl)sulfonyl)aziridine-2-carboxylate (99). Compound **98** (2.0 g, 5.82 mmol) was dissolved in a mixture of 1:1 CH₂Cl₂: MeOH (11:11 mL) and cooled to 0 °C. Next, TFA (11 mL, 143 mmol) was added drop-wise over the course of 30 min at 0 °C. The reaction was stirred for an additional 1 h while warming to 25 °C.

The solvents were removed under reduced pressure and excess TFA was removed via co-evaporation with MeOH. The residue was portioned between diethyl ether (75 mL) and water (75 mL). The organic layer was extracted with water (3×20mL) and the combined aqueous layers were treated with NaHCO₃ until pH 8 at 0 °C. Next, EtOAc (100 mL) was added to the aqueous fraction and 2-nitrobenzenesulfonyl chloride (1.2 g, 5.41 mmol) dissolved in EtOAc (4mL) was added while maintaining the temperature at 0 °C. The mixture was stirred vigorously at 25 °C for 24 h. Upon completion, the organic layer was decanted and the aqueous layer was further extracted with EtOAc (30 mL×3). The combined organic layers were dried over MgSO₄, filtered, and concentrated in vacuo. The crude product was purified via flash column chromatography to yield the title compound in 70% yield as an orange oil (1.17 g, 4.1 mmol). ¹H NMR (400 MHz, CDCl₃-*d*): δ 8.26 (d, *J* = 6.5 Hz, 1H), 7.83 – 7.74 (m, 3H), 3.80 (s, 3H), 3.62 (dd, *J* = 7.3, 4.2 Hz, 1H), 3.08 (d, *J* = 7.1 Hz, 1H), 2.80 (d, *J* = 4.4 Hz, 1H). ESI-MS(-) calculated for [C₁₀H₉N₂O₆S]⁻ *m/z* 285.02, found *m/z* 366.17 [M+MeOH-H]⁻.

Di-*tert*-butyl ((S)-3-methoxy-2-((2-nitrophenyl)sulfonamido)-3-oxopropyl)-L-aspartate (100). Di-*tert*-butyl-L-aspartate hydrochloride (2.95 g, 10.5 mmol) and TEA (1.75 mL, 12.6 mmol) in THF were stirred at 25 °C for 1.5 h to result in a cloudy white solution. The salt was removed via vacuum filtration and compound **99** (1.5 g, 5.24 mmol) was added directly to the filtrate. The reaction mixture was stirred at 25 °C for 16 h. Upon completion, the solvent was removed under reduced pressure. The crude product was purified via flash column chromatography to yield the title compound in

72% yield as a yellow oil (2.0 g, 3.8 mmol). ¹H NMR (400 MHz, CDCl₃-*d*): δ 8.09 (dd, *J* = 6.0, 3.4 Hz, 1H), 7.88 (d, *J* = 5.8 Hz, 1H), 7.76 – 7.67 (m, 2H), 3.51 (s, 3H), 3.41 – 3.34 (m, 2H), 2.81 – 2.76 (m, 1H), 2.63 – 2.55 (m, 1H), 2.50 (d, *J* = 7.2 Hz, 1H), 1.46 – 1.44 (m, 18H). ESI-MS(+) calculated for [C₂₂H₃₄N₃O₁₀S]⁺ *m/z* 532.20, found *m/z* 531.95 [M+H]⁺.

Di-*tert*-butyl ((*S*)-2-amino-3-methoxy-3-oxopropyl)-L-aspartate (101). In a small vial, compound **100** (834 mg, 1.6 mmol) and DIPA (0.89 mL) were added to dry ACN (5 mL). The mixture was purged with N₂ gas for 15 min, followed by the subsequent addition of benzenethiol (0.803 mL, 7.8 mmol). The mixture was stirred at 25 °C for 2.5 h to yield a light-yellow precipitate. The solvent was removed in vacuo and the product was purified via flash column chromatography to afford the title compound in 83% yield as a yellow oil (0.45 g, 1.30 mmol). ¹H NMR (400 MHz, CDCl₃-*d*): δ 3.72 (s, 3H), 3.60 – 3.55 (m, 1H), 3.48 (s, 1H), 3.00 (dd, *J* = 12.2, 6.8 Hz, 1H), 2.82 (dd, *J* = 12.2, 4.2 Hz, 1H), 2.73 – 2.64 (m, 1H), 2.46 (dd, *J* = 15.9, 7.7 Hz, 1H), 1.45 (s, 9H), 1.44 (s, 9H). ESI-MS(+) calculated for [C₁₆H₃₁N₂O₆]⁺ *m/z* 347.22, found *m/z* 346.98 [M+H]⁺.

Di-*tert*-butyl-(((*S*)-3-methoxy-2-(((*S*)-3-methoxy-2-((2-nitrophenyl) sulfonamido)-3-oxopropyl)amino)-3-oxopropyl)-L-aspartate (102). In a round bottom flask, compound **99** (317 mg, 1.11 mmol) and **101** (422 mg, 1.22 mmol) were dissolved in THF (6 mL). TEA (0.031 mL, 0.22 mmol) was added to the mixture and the reaction was stirred at 25 °C for 24 h. The solvent removed under reduced pressure and the

product was purified via flash column chromatography to afford the title compound in 57% yield as a yellow oil (374 mg, 0.63 mmol). ^1H NMR (400 MHz, CDCl_3 -*d*): δ 8.16 – 8.12 (m, 1H), 7.91 – 7.87 (m, 1H), 7.73 – 7.70 (m, 2H), 4.30 (t, $J = 4.7$ Hz, 1H), 3.72 (s, 3H), 3.70 (s, 1H), 3.57 (s, 3H), 3.29 (dd, $J = 12.8, 5.0$ Hz, 2H), 2.97 (s, 2H), 2.86 (dd, $J = 12.8, 4.4$ Hz, 2H), 2.71 (d, $J = 5.4$ Hz, 1H), 1.46 (d, $J = 4.6$ Hz, 18H). ESI-MS(-) calculated for $[\text{C}_{26}\text{H}_{39}\text{N}_4\text{O}_{12}\text{S}]^-$ m/z 631.23, found m/z 631.22 $[\text{M}-\text{H}]^-$.

(S)-3-(((S)-1-Carboxy-2-(((S)-1,4-di-*tert*-butoxy-1,4-dioxobutan-2-yl)amino)ethyl)amino)-2-((2-nitrophenyl)sulfonamido)propanoic acid (103). To a solution of **102** (397 mg, 0.63 mmol) in anhydrous DCE (4 mL) was added trimethylstannanol (681 mg, 3.77 mmol). The reaction was heated at 84 °C for 3 h. The solvent was removed under reduced pressure and the product was purified via reverse phase flash column chromatography, eluting at 50% MeOH in H_2O (w/ 0.1% TFA) as a white powder in 99% yield (375 mg, 0.62 mmol). ^1H NMR (400 MHz, $\text{MeOD}-d_4$): δ 8.16 (d, $J = 4.4$ Hz, 1H), 7.98 – 7.92 (m, 1H), 7.86 – 7.79 (m, 2H), 4.19 (s, 1H), 3.84 (s, 1H), 3.64 (s, 1H), 3.48 (s, 1H), 3.29 – 3.14 (m, 3H), 2.74 (t, $J = 6.2$ Hz, 2H), 1.49 (s, 9H), 1.46 (s, 9H). ESI-MS(+) calculated for $[\text{C}_{24}\text{H}_{37}\text{N}_4\text{O}_{12}\text{S}]^+$ m/z 605.21, found m/z 605.10 $[\text{M}+\text{H}]^+$.

(S)-2-Amino-3-(((S)-1-carboxy-2-(((S)-1,4-di-*tert*-butoxy-1,4-dioxobutan-2-yl)amino)ethyl)amino)propanoic acid (104). A solution of **103** (200 mg, 0.33 mmol) in dry ACN (2 mL) was added DIPA (0.187 mL, 1.32 mmol) and benzenethiol (169 mg,

1.65 mmol). The reaction was stirred at 25 °C for 5 h to result in a yellow mixture with white precipitate. The solvent was removed in vacuo and the product was purified via reverse phase flash column chromatography, eluting at 50% ACN (w/ 0.1% TFA) in H₂O (w/ 0.1% TFA) as a clear oil in 94% yield (130 mg, 0.31 mmol). ¹H NMR (400 MHz, D₂O-*d*₂): δ 3.99 – 3.92 (m, 1H), 3.87 – 3.80 (m, 1H), 3.59 (t, *J* = 6.5 Hz, 1H), 3.33 (dd, *J* = 12.8, 5.1 Hz, 1H), 3.20 (t, *J* = 7.0 Hz, 2H), 3.10 (dd, *J* = 13.0, 6.7 Hz, 1H), 2.94 – 2.77 (m, 2H), 1.34 (s, 8H), 1.32 (s, 9H). ESI-MS(-) calculated for [C₁₈H₃₂N₃O₈]⁻ *m/z* 418.22, found *m/z* 418.25 [M-H]⁻.

((S)-2-(((S)-2-Amino-2-carboxyethyl)amino)-2-carboxyethyl)-L-aspartic acid (LLL-AMA). At 0 °C, **104** (50 mg, 0.12 mmol) in CH₂Cl₂ (8 mL) was added anisole (0.065 mL, 0.60 mmol) and trifluoromethanesulfonic acid (0.053 mL, 0.60 mmol). The reaction was stirred at 0 °C for 30 min and 25 °C for an additional 3 h. Sodium bicarbonate (65 mg, 0.78 mmol) in H₂O (16 mL) was added to the mixture and allowed to stir for an additional for 1 h at 0 °C. The aqueous layer was washed with CH₂Cl₂ (3×10mL) and concentrated in vacuo to afford the desired product in the salt form. Next, the salt was dissolved in 1:3 H₂O: MeOH (10 mL) and acetic acid (0.095 mL, 1.66 mmol) was added dropwise. The mixture was placed in the -20 °C freezer for 30 min until a precipitate was observed. The solid was collected via vacuum filtration to afford the title compound as a white powder in 41% yield (15 mg, 0.05 mmol). ¹H NMR (500 MHz, D₂O-ND₄OD-*d*₇): δ 3.79 (t, *J* = 5.9 Hz, 1H), 3.74 – 3.67 (m, 1H), 3.47 – 3.42 (m, 1H), 3.20 – 3.09 (m, 2H), 3.02 – 2.90 (m, 2H), 2.79 (dd, *J* = 16.3, 4.3 Hz, 1H), 2.62 (dd, *J* = 16.2, 8.9 Hz,

1H). HR-MS-TOFMS(-) calculated for $[C_{10}H_{16}N_3O_8]^-$ m/z 306.09, found m/z 306.09 [M-H]⁻.

5.6 Outlook and Perspective on Future NDM-1 Inhibitor Development

Chapter 5 presents additional **DPA** sublibraries investigated for NDM-1 inhibitor development. In Section 5.2, large hydrophobic *meta*-substituted **DPA** inhibitors (Sublibrary 8) were explored in an attempt to probe the L5 binding pocket of NDM-1. The synthesis and evaluation of Sublibrary 9, where triazole substituents were appended to the *para*- position of the **DPA** MBP, is described in Section 5.3. The carboxylic acid of **DPA** was further explored via isosteric replacement and discussed in Section 5.4 (Sublibrary 10). While these sublibraries did not yield desirable nanomolar inhibitors, they provide an important foundation for future NDM-1 inhibitor development.

One sublibrary that warrants additional development includes Sublibrary 8 in Section 5.2. As previously stated, the majority of reported NDM-1 inhibitors are smaller compounds incapable of reaching into the L5 binding pocket of NDM-1. The compounds in Sublibrary 8 are larger with the potential to make binding interactions with L5. The mid-nanomolar inhibitory values obtained are a large improvement compared to the typical observed micromolar inhibitory values (with substrate meropenem) and suggest the potential to develop inhibitors reaching the low-nanomolar range. With established synthetic procedures, it is possible to access a wide variety of derivatives and establish needed SAR.

Another direction in NDM-1 inhibitor development that warrants attention includes the identification of alternative MBPs. Work reported in this dissertation showed that the isosteric replacement of one carboxylic acid of the **DPA** yielded alternative MBPs with a more favorable mechanism of action. Alternative mono- or di-carboxylic acid

substituted **DPA** derivatives should be developed. Upon investigation and understanding of the MBP mode of binding, new MBPs could undergo FBDD to yield full-length NDM-1 inhibitors. The development of new **DPA** isosteres MBPs is of high value, as synthesized NMEs can be screened against other targets of interest and contribute to the development of other metalloenzyme inhibitors.

An obstacle that has hindered the progress of NDM-1 inhibitor development includes the lack of consistency and reliability in the enzymatic assays utilized for inhibitor evaluation. Between research laboratories, several chromogenic (nitrocefin, CENTA, chromacef, imipenem, and meropenem) and fluorogenic (fluorocillin, FC5) reporter substrates have been applied.¹⁸⁻¹⁹ While both classes of substrates generate a signal upon β -lactam ring cleavage (either absorbance or fluorescence), the degree of substrate recognition by the enzyme and varying assay conditions (such as the concentration of substrate and buffer reagents) have led to different absolute inhibition values. The use of chromogenic substrates is more wide-spread compared to that of fluorogenic substrates; however, the high substrate concentration required for a reliable readout has made it difficult to detect inhibitors with low inhibitory values (typically under 1 μ M). While the high sensitivity of fluorogenic substrates has allowed for the detection of nanomolar inhibitors, the use of this substrate is limited likely due to the low commercial availability. FC5,²⁰ the reporter substrate for the promising cyclic boronate inhibitors (Figure 5-2), must be synthesized. While fluorocillin can be purchased, the two enzymatic turnovers required to liberate the fluorescein may complicate the determination of substrate turnover and not viewed by other labs as an ideal substrate

candidate.²¹ These complications have led to the use of a variety of reporter substrates, have made it difficult for the comparison of NDM-1 inhibitors from different laboratories, and have impeded protein-inhibitor SAR analysis. In line with the diversity of reporter substrates used for NDM-1 inhibitor development, different substrates are also used amongst different MBLs for the evaluation of pan-MBL inhibitors. This increases the difficulty for the evaluation of pan-MBL inhibitors and the utilization of a single suitable reporter substrate is of urgent need. Additionally, during our work obtaining dose-response measurements of developed inhibitors, we occasionally observed an enzymatic spike in activity that is greater than 100%. This activity shows up between the sigmoidal curve and asymptote and has been observed in assays utilizing both chromogenic and fluorogenic reporter substrates. We have investigated how different inhibitor motifs, buffer components, screening products (pipette tips, 96-well plates, eppendorf tubes), and assay conditions may lead to this phenomenon; however, all have been met with limited success. This has been observed in both the Walter Fast laboratory at the University of Texas at Austin and Seth Cohen laboratory at the University of California San Diego but never reported in the literature. Understanding the cause for this activity may provide crucial information regarding the Zn(II):substrate:inhibitor:enzyme interaction and aid in the development of future substrates.

Due to these factors, it is proposed that an orthogonal screening technique be utilized for inhibitor evaluation. Our lab has led the effort in utilizing a thermal shift assay as a secondary method to validate inhibitory activity. Although the observed

inhibitory data did not correlate with the thermal shift values, the mode of inhibitor binding (metal-stripping or formation of a ternary complex) can be elucidated. Additional screening methods such as protein NMR, MS, X-ray crystallography and isothermal titration calorimetry should be used in tandem with enzymatic assays to not only allow for the hit-to-lead verification of NDM-1 inhibitors but also provide insight regarding the mechanism of action. In conclusion, the future of NDM-1 inhibitor development should focus on 1) the FBDD of large inhibitors capable of reaching to the L5 loop or the channel flanked between the L3 and L10; 2) development of alternative MBPs for di-Zn(II) binding; 3) investigation and utilization of a single reporter substrate that is sensitive for low-nanomolar pan-MBL inhibitor detection; and 4) exploration of orthogonal/secondary screening methods for hit validation and mechanism of inhibition studies.

5.7 References

1. Perez, C.; Barkley-Levenson, A. M.; Dick, B. L.; Glatt, P. F.; Martinez, Y.; Siegel, D.; Momper, J. D.; Palmer, A. A.; Cohen, S. M., Metal-Binding Pharmacophore Library Yields the Discovery of a Glyoxalase 1 Inhibitor. *J. Med. Chem.* **2019**, *62* (3), 1609-1625.
2. Credille, C. V.; Chen, Y.; Cohen, S. M., Fragment-Based Identification of Influenza Endonuclease Inhibitors. *J. Med. Chem.* **2016**, *59* (13), 6444-6454.
3. Kim, Y.; Tesar, C.; Mire, J.; Jedrzejczak, R.; Binkowski, A.; Babnigg, G.; Sacchettini, J.; Joachimiak, A., Structure of Apo- and Monometalated Forms of NDM-1--a Highly Potent Carbapenem-hydrolyzing Metallo-beta-Lactamase. *PLoS One* **2011**, *6* (9), e24621.
4. Brem, J.; Cain, R.; Cahill, S.; McDonough, M. A.; Clifton, I. J.; Jimenez-Castellanos, J. C.; Avison, M. B.; Spencer, J.; Fishwick, C. W.; Schofield, C. J., Structural Basis of Metallo-beta-lactamase, Serine-beta-lactamase and Penicillin-binding Protein Inhibition by Cyclic Boronates. *Nat. Commun.* **2016**, *7*, 12406.
5. Krajnc, A.; Brem, J.; Hinchliffe, P.; Calvopina, K.; Panduwawala, T. D.; Lang, P. A.; Kamps, J.; Tyrrell, J. M.; Widlake, E.; Seward, B. G.; Walsh, T. R.; Spencer, J.; Schofield, C. J., Bicyclic Boronate VNRX-5133 Inhibits Metallo- and Serine-beta-Lactamases. *J. Med. Chem.* **2019**, *62* (18), 8544-8556.
6. Kharb, R.; Sharma, P. C.; Yar, M. S., Pharmacological Significance of Triazole Scaffold. *J. Enzyme Inhib. Med. Chem.* **2011**, *26* (1), 1-21.
7. Bonandi, E.; Christodoulou, M. S.; Fumagalli, G.; Perdicchia, D.; Rastelli, G.; Passarella, D., The 1,2,3-Triazole Ring as a Bioisostere in Medicinal Chemistry. *Drug Discovery Today* **2017**, *22* (10), 1572-1581.
8. Dheer, D.; Singh, V.; Shankar, R., Medicinal Attributes of 1,2,3-triazoles: Current developments. *Bioorg. Chem.* **2017**, *71*, 30-54.
9. Teyssot, M.-L.; Nauton, L.; Canet, J.-L.; Cisnetti, F.; Chevry, A.; Gautier, A., Aromatic Nitrogen Donors for Efficient Copper(I)-NHC CuAAC under Reductant-Free Conditions. *Eur. J. Org. Chem.* **2010**, *2010* (18), 3507-3515.
10. Chamas Zel, A.; Guo, X.; Canet, J. L.; Gautier, A.; Boyer, D.; Mahiou, R., Clicked Dipicolinic Antennae for Lanthanide Luminescent Probes. *Dalton Trans.* **2010**, *39* (30), 7091-7097.
11. Chen, A. Y.; Thomas, P. W.; Cheng, Z.; Xu, N. Y.; Tierney, D. L.; Crowder, M. W.; Fast, W.; Cohen, S. M., Investigation of Dipicolinic Acid Isosteres for the Inhibition of Metallo-beta-Lactamases. *ChemMedChem* **2019**, *14* (13), 1271-1282.

12. Dick, B. L.; Cohen, S. M., Metal-Binding Isosteres as New Scaffolds for Metalloenzyme Inhibitors. *Inorg. Chem.* **2018**, *57*, 9538-9543.
13. King, A. M.; Reid-Yu, S. A.; Wang, W.; King, D. T.; De Pascale, G.; Strynadka, N. C.; Walsh, T. R.; Coombes, B. K.; Wright, G. D., Aspergillomarasmine A Overcomes Metallo-beta-lactamase Antibiotic Resistance. *Nature* **2014**, *510* (7506), 503-506.
14. Liao, D.; Yang, S.; Wang, J.; Zhang, J.; Hong, B.; Wu, F.; Lei, X., Total Synthesis and Structural Reassignment of Aspergillomarasmine A. *Angew. Chem., Int. Ed. Engl.* **2016**, *55* (13), 4291-4295.
15. Koteva, K.; King, A. M.; Capretta, A.; Wright, G. D., Total Synthesis and Activity of the Metallo-beta-lactamase Inhibitor Aspergillomarasmine A. *Angew. Chem., Int. Ed. Engl.* **2016**, *55* (6), 2210-2212.
16. Albu, S. A.; Koteva, K.; King, A. M.; Al-Karmi, S.; Wright, G. D.; Capretta, A., Total Synthesis of Aspergillomarasmine A and Related Compounds: A Sulfamidate Approach Enables Exploration of Structure-Activity Relationships. *Angew. Chem., Int. Ed. Engl.* **2016**, *55* (42), 13259-13262.
17. Chen, A. Y.; Thomas, P. W.; Stewart, A. C.; Bergstrom, A.; Cheng, Z. S.; Miller, C.; Bethel, C. R.; Marshal, S. H.; Credille, C. V.; Riley, C. L.; Page, R. C.; Bonomo, R. A.; Crowder, M. W.; Tierney, D. L.; Fast, W.; Cohen, S. M., Dipicolinic Acid Derivatives as Inhibitors of New Delhi Metallo-beta-Lactamase-1. *J. Med. Chem.* **2017**, *60*, 7267-7283.
18. Fast, W.; Sutton, L. D., Metallo-beta-lactamase: inhibitors and reporter substrates. *Biochim Biophys Acta* **2013**, *1834* (8), 1648-1659.
19. van Berkel, S. S.; Brem, J.; Rydzik, A. M.; Salimraj, R.; Cain, R.; Verma, A.; Owens, R. J.; Fishwick, C. W.; Spencer, J.; Schofield, C. J., Assay platform for clinically relevant metallo-beta-lactamases. *J Med Chem* **2013**, *56* (17), 6945-6953.
20. Van Berkel, S. S.; Brem, J.; Rydzik, A. M.; Salimraj, R.; Cain, R.; Verma, A.; Owens, R. J.; Fishwick, C. W.; Spencer, J.; Schofield, C. J., Assay Platform for Clinically Relevant Metallo-beta-Lactamases. *J. Med. Chem.* **2013**, *56* (17), 6945-6953.
21. Rukavishnikov, A.; Gee, K. R.; Johnson, I.; Corry, S., Fluorogenic Cephalosporin Substrates for beta-Lactamase TEM-1. *Anal. Biochem.* **2011**, *419* (1), 9-16.